Decruz, Aloysius (2016) Development and integration of a green roof model within whole building energy simulation. PhD thesis, University of Nottingham.

**CENTRE FOR SUSTAINABLE
ENERGY TECHNOLOGIES**

**FACULTY OF SCIENCE AND
ENGINEERING**

DEVELOPMENT AND INTEGRATION OF A GREEN ROOF MODEL WITHIN WHOLE BUILDING ENERGY SIMULATION

Aloysius Decruz, MS.

Thesis submitted to the University of Nottingham

For the degree of Doctor of Philosophy

March 2016

Abstract

Green roofs are increasingly being employed as a sustainability feature of buildings. The sustainability approach in building designs requires reducing energy consumption and adopting low carbon energy sources without compromising the increasing expectations of comfort and health levels. Given the wide range of building designs, climates and green roof types, it is desirable to evaluate at the design stage the energy saving impact and other potential benefits from the application of green roofs. Currently, the abilities of building simulation programs to simulate the influences of green roofs are limited. For example, they have limitations in representing dynamic inter-layer interactions and moisture infiltration mechanisms. This research aims to develop a new model for the simulation of green roofs based on the control volume approach and to integrate the model within a whole building energy simulation program. The green roof elements consist of special layers such as plants and soil for which the control volume approach is capable of capturing their special characteristics with regards to the thermal and moisture exchanges.

The model has been integrated within the ESP-r whole building energy simulation program. Within the ESP-r, the new green roof model alters the boundary condition of a roof surface on which green roof is constructed. The model development is carried out by a series of steps which include a careful selection of governing equations that describe the thermal and moisture balances in various layers of green roof, the numerical implementation for a simultaneous solution of the governing equations for the whole green roof, algorithm and code development and finally developing the interface with ESP-r. After successful integration, the model results were validated on an experimental test cell, which consists of an approximately 2 m^2 planted medium on an insulated box with facilities for thermal, moisture and drainage measurements. The results for the thermal validation were promising with the significant boundary temperature values within a root mean square deviation (RMSD) in the vicinity of 0.5 K, whereas the moisture validation results are found to depend on initial conditions, the lower layers showing an RMSD of approximately 0.05 m^3/m^3 and the top layer nearly 0.12 [m^3/m^3]. The model is also able to predict the slowing down of water run-off. A methodology for collecting soil and plant properties which are required to be used along with the program has also been described. Based on the current state of the model and also considering the new developments in green roofs, some suggestions are proposed at the end of the thesis as a continuation of this research.

iii

List of Publications

1. DECRUZ, A., KOKOGIANNAKIS, G., DARKWA, J., STRACHAN, P. & HONG, J. 2012. A theoretical framework for the integration of a green roof model in ESP-r. ASim2012. Shanghai, China: International Building Performance Simulation Association.

2. DECRUZ, A., KOKOGIANNAKIS, J. & DARKWA, J. 2013. The State-of-the-art in Green Roof Simulation and a Proposal for a New Model. 2013 Nanjing World Green Roof Congress. Nanjing, China: International Rooftop Landscaping Association.

3. DECRUZ, A., KOKOGIANNAKIS, G., DARKWA, J., YUAN, K. & STRACHAN, P. 2014. Development of Databases for Facilitating Green Roof Energy Simulation Assessments. ASim2014. Nagoya, Japan: International Building Performance Simulation Association.

Acknowledgement

I would like to express my sincere gratitude to my two supervisors Prof Jo Darkwa and Dr. Georgios Kokogiannakis for their continuous support of my PhD. study and related research, and for their patience and motivation. Dr. Georgios had gone to great lengths in helping me to complete this research by identifying problems at key stages of the research and helping me to solve them. Prof Jo was instrumental in his overall guidance and support throughout the course of the research.

I would like to thank Kate Yuan and Fred Guan of CSET lab for helping with the experiments and data collections. I also place on record, my sincere thanks to all my PhD mates at CSET and FOSE.

I am also grateful to many academic staffs at UNNC who helped me throughout my PhD study, particularly to Dr. James Griffiths, FOSE, for helping with the soil moisture instruments, to Dr. Lynda O'Brien, ASU, for coordinating thesis writing group and supporting us in the writing-up and to Dr. Christopher Hallsworth, CELE, for giving advices on mathematic matters.

I wish to thank my employer, Universiti Kuala Lumpur for granting me study leave under the UniKL further study scheme to complete this PhD study.

I would like to thank my wife Juno and daughter Shalini, without whose helps this PhD study would not have been completed. I dedicate this work to my late father, Joachim Decruz and to my mother Celine Decruz, both of whom taught me to work hard.

Table of Contents

List of Figures

List of Tables

Glossary of Notation
EQUATION SYMBOLS

Symbol	Description	Units
a11, a12, etc.	Thermal side future time coefficients	$[\text{Wm}^{-2}\text{K}^{-1}]$
b11, b12, etc.	Thermal side present time coefficients	$[\text{Wm}^{-2}\text{K}^{-1}]$
c1,c2,etc.	Thermal side flux coefficients	$[\text{Wm}^{-2}]$
CC	Canopy cover	[-]
C_p	Specific heat of air	$[\text{Jkg}^{-1}\text{K}^{-1}]$
C_{s1}	Volumetric specific heat of soil	$[\text{Jm}^{-3}\text{K}^{-1}]$
Cp_{min}	Specific heat of soil minerals	$[\text{Jkg}^{-1}\text{K}^{-1}]$
Cp_{org}	Specific heat of soil organic matter	$[\text{Jkg}^{-1}\text{K}^{-1}]$
Cp_{wat}	Specific heat of soil water	$[\text{Jkg}^{-1}\text{K}^{-1}]$
C_{soil}	Net specific heat of soil	$[\text{Jkg}^{-1}\text{K}^{-1}]$
CV1, etc.	Control volume 1 through 7	
C_θ	Specific water content/ capillary capacity of soil	$[\text{m}^{-1}]$
d	Plant leaf thickness	[m]
e_{ca}	Vapour pressure of canopy air	[Pa]
e_α	Vapour pressure of ambient air	[Pa]
e_p	Saturated vapour pressure at plant temperature	[Pa]
e_{s1}	Soil surface vapour pressure	[Pa]
Ev	Evaporation from soil surface	$[\text{m}^3\text{m}^{-2}\text{s}^{-1}]$
$h_{r,p\text{-}s1}$	Linearized radiation transfer coefficient, between plant and soil	$[\text{Wm}^{-2}\text{K}^{-1}]$
$h_{r,s1}$	Linearized radiation transfer coefficient, between plant and soil	$[\text{Wm}^{-2}\text{K}^{-1}]$
$h_{r,sky}$	Linearized radiation transfer coefficient, between plant and sky	$[\text{Wm}^{-2}\text{K}^{-1}]$
$h_{r,sky\text{-}s1}$	Linearized radiation transfer coefficient, between sky and soil	$[\text{Wm}^{-2}\text{K}^{-1}]$
k_l	coefficient of extinction for long wave radiation	[-]
$K_{L,T}$	Thermal liquid conductivity	$[\text{m}^2\text{s}^{-1}\text{K}^{-1}]$
$K_{L,\psi}$	Isothermal liquid conductivity	$[\text{ms}^{-1}]$
k_s	coefficient of extinction for short wave	[-]
KT	Combined liquid vapour conductivity, thermal	$[\text{kgm}^{-1}\text{s}^{-1}\text{K}^{-1}]$
$K_{v,T}$	Thermal vapour conductivity (in volume units for moisture coefficients)	$[\text{m}^2\text{s}^{-1}\text{K}]$
$K_{v,\psi}$	Isothermal vapour conductivity (in volume units for moisture coefficients)	$[\text{ms}^{-1}]$
K_{vT_m}	Thermal vapour conductivity (in mass units for thermal coefficients)	$[\text{kgm}^{-1}\text{s}^{-1}\text{K}^{-1}]$
$K_{v\psi\_m}$	Isothermal vapour conductivity(in mass units for thermal coefficients)	$[\text{kgm}^{-2}\text{s}^{-1}]$

KΨ	Combined liquid vapour conductivity, iso-thermal	[kgm^{-2}s^{-1}]
l	Canopy height	[m]
L	Latent heat of water	[Jkg^{-1}]
LAI	Leaf Area Index	[m^{2}m^{-2}]
m11, m12, etc.	Moisture side future time coefficients	[s^{-1}]
MF	Mineral fraction of soil	[m^{3}m^{-3}]
n	soil pore size distribution factor (for VG relation)	[-]
n11, n12, etc.	Moisture side present time coefficients	[s^{-1}]
OF	Organic fraction of soil	[m^{3}m^{-3}]
P0	Precipitation at soil surface	[m^{3}m^{-2}s^{-1}]
q1,q2,etc.	Moisture side flux coefficients	[ms^{-1}]
r_e	Aerodynamic resistance to heat/mass transfer within canopy	[sm^{-1}]
$r_{e\alpha}$	Aerodynamic resistance to heat/mass transfer above canopy	[sm^{-1}]
r_i	Stomatal resistance at plant level	[PaK^{-1}]
r_s	Surface resistance to heat/mass transfer at soil surface	[sm^{-1}]
r_{s1-ca}	Aerodynamic resistance to heat/mass transfer soil to canopy air	[sm^{-1}]
S	Root moisture uptake	[m^{3}m^{-3}s^{-1}]
S1 , etc.	Soil layer height 1 through 5	[m]
S1S2, etc.	Soil interlayer distances between the centres of the numbered layers	[m]
S5X	Half thickness of lowest soil layer (layer 5)	[m]
T_{ca}	Canopy air temperature	[K]
T_{s1} , etc.	Temperature of soil layer as numbered	[K]
T_{sky}	Sky temperature (for longwave radiation)	[K]
T_x	Temperature at the lower end of green roof	[K]
T_α	Ambient air temperature	[K]
T_p	Temperature of plant leaves	[K]
t	Time step	[s]
z	Vertical dimension in soil	[m]
α	implicit/explicit weighting index for numerical solver	[-]
α1	soil retention curve factor (for VG relation)	[m^{-1}]
γ	Psychometric constant gamma	[PaK^{-1}]
ε_p	Radiation emissivity, plant surface	[-]
ε_{p-s1}	Radiation emissivity, plant to soil exchange	[-]
ε_{s1}	Radiation emissivity, soil surface	[-]
θ	Soil moisture content	[m^{3}m^{-3}]
θ_r	Residual moisture content of soil type	[m^{3}m^{-3}]

Symbol	Description	Units
θ_s	Saturated moisture content of soil type	[m^{3}m^{-3}]
λ	Thermal conductivity (with appropriate subscripts)	[Wm^{-1}K^{-1}]
ρ_{ca}	Canopy air density	[kgm^{-3}]
ρ_p	Plant leaf density	[kgm^{-3}]
ρr_g	Ground reflectance	[-]
ρr_α	Canopy bulk reflectance	[-]
ρ_α	Ambient air density	[kgm^{-3}]
ρ_{min}	Density of soil minerals	[kgm^{-3}]
ρ_{org}	Density of soil organic matter	[kgm^{-3}]
ρ_{wat}	Density of soil water	[kgm^{-3}]
σ	Stefan Boltzmann constant	[Wm^{-2}K^{-4}]
σ_f	Fractional vegetation coverage	[-]
τ_l	Canopy transmittance for long wave radiation	[-]
τ_s	Canopy transmittance for short wave radiation	[-]
$\phi_{cond,s1\text{-}s2}$, etc.	Conduction heat transfer between the numbered soil layers	[Wm^{-2}]
$\phi_{conv,ca\text{-}s1}$	Convection heat transfer from canopy air to soil	[Wm^{-2}]
$\phi_{conv,p\text{-}ca}$	Convection heat transfer from plant to canopy air	[Wm^{-2}]
$\phi_{conv,\alpha\text{-}p}$	Convection heat transfer from ambient to plant	[Wm^{-2}]
$\phi_{evap,s1\text{-}ca}$	Evaporation heat loss at soil (soil to canopy air vapour exchange)	[Wm^{-2}]
$\phi_{lw,p\text{-}s1}$	Long wave radiation exchange between plant and soil	[Wm^{-2}]
$\phi_{lw,sky\text{-}s1}$	Long wave radiation exchange between sky and soil	[Wm^{-2}]
$\phi_{rad,long}$	Long wave radiation absorbed by plant canopy	[Wm^{-2}]
$\phi_{rad,sol}$	Solar radiation absorbed by plant canopy	[Wm^{-2}]
ϕ_s	Global horizontal solar radiation	[Wm^{-2}]
$\phi_{s,s1}$	Solar radiation received at the soil surface	[Wm^{-2}]
$\phi_{transp\text{-}ca}$	Transpiration heat loss from plant to canopy air	[Wm^{-2}]
$\phi_{vap,p\text{-}ca}$	Vapour exchange rate between plant and canopy air	[kgm^{-2}s^{-1}]
$\phi_{vap,s1\text{-}ca}$	Vapour exchange rate between soil and canopy air	[kgm^{-2}s^{-1}]
$\phi_{vap,s2\text{-}s1}$,etc.	Heat transfer due to vapour flow between the numbered layers	[Wm^{-2}]
$\phi_{vap,\alpha\text{-}ca}$	Vapour exchange rate between ambient air and canopy air	[kgm^{-2}s^{-1}]
ψ	soil matric potential	[m]

OTHER ABBREVIATIONS

BREEAM	Building Research Establishment Environmental Assessment Methodology
CTF	Conduction Transfer Function
CV	Control volume
DPM	Damp proof membrane
FAO	Food and Agriculture Organization of the United Nations
LEED	Leadership in Energy and Environmental Design green building rating
PAR	Photo synthetically active radiation
PTC	Positive temperature coefficient type temperature sensor
RMSD	Root Mean Square Deviation
RMSE	Root Mean Square Error
SVAT	Soil Vegetation Atmosphere Transfer models
VG	van Genuchten model for soil moisture
WOFOST	World Food Studies, Wageningen University
XPS	Extruded Polystyrene insulation

CHAPTER 1

INTRODUCTION

1. Introduction

1.0 Research background

Intentionally planted roofs are called green roofs or vegetated roofs. Although this architectural feature in buildings has been practiced from as early as 6th century BC, the time of the hanging garden of Babylon, much emphasis as a sustainable feature of building is evident in the last decade [1]. A Green roof could offer several benefits such as: reduced building energy consumption, contribution to storm-water management, reduced urban heat island effect, contribution to building aesthetic quality, contribution to urban ecological diversity and protection to roof's water proof membrane [2]. However the benefits could come in some cases at a cost of an increase in the building's construction budget in terms of additional structural strength required for the roof and green roof cost itself which may include initial construction cost and on-going maintenance cost. Thus it is important to predict the performance of green roofs in the context of building's overall design. In addition, green building rating systems such as LEED [3] and BREEAM [4] require buildings' performance parameters to be predicted, typically over a period of one year. Green roof are considered within these standards as a method for potentially improving the buildings sustainability rating.

The subject of modelling a green roof is a complex matter considering the energy and moisture flow processes involved. The thermal flows include short wave and long wave radiation exchanges, convection and conduction exchanges with outside and among the components of green roof. Moisture flows include precipitation and irrigation infiltration, evaporation, plant transpiration and drainage. Currently there are some stand-alone models [5] available for green roofs which simulate the green roof performance as being independent of the building. On the other hand, models that are part of a whole building energy simulation are rare. There is only one such public domain simulation tool available, the 'eco-roof' in EnergyPlus [6]. There are also some recent published models available in commercial domains, such as TRNSYS [7]. A new green roof simulation model is developed within the ESP-r's whole building simulation program to overcome some of the short comings of these models.

1.1 Aim and Objectives of research

The aim of this research is to develop a computer simulation model for predicting the energy characteristics and water retention capabilities of green roofs. This is to enable the thermal and moisture characteristics of green roofs to be simulated using ESP-r whole building energy simulation program.

The specific objectives of the research are:

1. To develop a numerical finite volume model, for assessing the energy and comfort benefits from green roofs, in which the dynamic thermal and moisture flows and the interaction between these flows are accounted for at various layers of green roofs.
2. To integrate the model in a whole building energy simulation environment for allowing assessments of green roofs in combination and simultaneously with the rest of the building components.
3. To experimentally validate the new green roof simulation model

1.2 Research contributions:

The following features of the developed model are the contribution of the research in green roof simulation studies:

- Green roof benefit assessment: The model serves as a valuable tool for energy and carbon performance assessment of green roofs.
- Integrated model: The integration of a green roof model into a whole building simulation serves the above evaluation in the context of other features of the building. Some of the existing models are stand-alone programs, simulating only green roofs, without taking into account the rest of the built environments' characteristics. There is only one known public domain green roof simulation model that is working with a whole building energy simulation program, the 'eco-roof' module of EnergyPlus. The CTF (conduction transfer function) scheme with which this model works has limited facility to accommodate time varying properties of plants and soil media. The proposed finite volume

method is flexible and is more suited to simulate the complex thermo-physical interactions occurring in plant and soil media.

- Simulations of soil moisture migration include vapour and liquid phases which are highlighted in the literature as of significant contribution to the thermal and moisture exchanges [8].

- Rain water run-off is evaluated as part of soil moisture dynamics, allowing the predictions of storm water run-off.

- The model is developed with a generic structure which makes it adaptable to any whole building simulation programs.

- The model is a useful tool for green building rating systems and building regulations that consider green roofs as an essential sustainable feature in buildings.

In summary, for the first time there is a green roof model in a whole building simulation program that is able to quantify the storm water retention and thermal buffering capabilities of green roofs by accommodating for the interactions between the thermal and moisture domains and without ignoring the dynamic physical characteristics of plants and soil.

1.3 Research Questions

The research questions are explicitly stated as:

1. Which are the variables affecting the heat flux through a green roof? What are the mathematical equations that are representing the dynamic relations between these variables?

2. What are the temperatures at various components of a green roof, which can be associated to a building simulation program and what is the procedure to determine these temperatures?

3. Which equations can describe the moisture retention characteristics of the green roof substrate and how is it related to the overall moisture balance within green roof?

4. How to integrate this procedure in a whole building energy simulation environment?

5. How close are the simulation results to measurements carried out with a scaled down test cell of a green roof?

1.4 Research Challenges:

The complex interactions between thermal and moisture flows within green roof layers are a significant challenge for this research. The thermal and moisture exchanges across the soil and canopy layers need to be coupled in the model so as to account for their interactions occurring within each layer and, in some cases, across the layers.

Time varying properties of soil and canopy layers pose as another challenge to be resolved. As some of the properties are dependent on the state variables (for example, soil thermal conductivity on soil moisture content and plant stomatal resistance on air vapour pressure), they need to be updated in successive time steps. The implementation of this issue, which calls for updates of coefficients of the equations being solved in the numerical procedure (along with the state variables, namely, temperatures and vapour pressures), need to be studied and resolved in a manner that is feasible within the ESP-r.

Integration of the model into whole building simulation analysis with the whole building energy simulation program is a critical task to be resolved. Substantial work is needed to enable the green roof model to be used in tandem with the rest of the building simulation domains. The model will be solving the characteristics equations simultaneously (at the same time-step) with the rest of the equations in ESP-r.

Establishing standardised validation techniques for the model are essential to establish its reliability. The model validation requires to be done by way of experimental procedures and capturing the relevant moisture and heat fluxes with measurements is not a trivial task.

1.5 Methodology

A control volume numerical model of the green roof needs to be developed to represent the heat and moisture flows within the green roof. The model will be developed for the plant and soil layers. The steps involved in the current research are briefed below:

1. The finite volume approach to building modelling requires the identification of typical control volumes. Two layers of green roofs are considered for analysis: the vegetation layer and soil layer, as shown in figure 1.1.

2. For each of the control volumes, energy and moisture balance equations need to be formulated. These equations are in the form of partial differential equations (PDE) of key variables: Temperature for thermal exchanges and vapour pressure or matric potential for mass (water) transfer.

3. The state variables (i.e. temperatures and soil matric potentials) are determined in the energy simulation program by solving a set of linear equations, which can be expressed in a matrix equation set. Green roof module needs two sets of coefficients, one for temperature and another for moisture.

4. Having formulated the coefficients for each control volume, the set of linearized equations are solved by successive iterations

5. Model validation with experimental measurements and model revisions performed in several stages
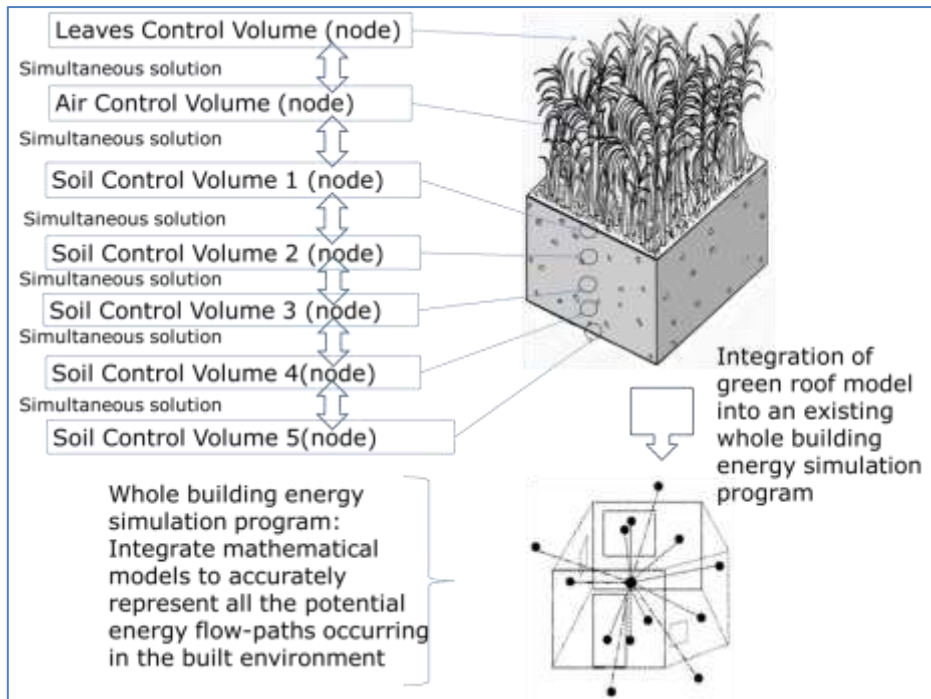
Figure 1-1 Control volume modelling approach for green roof

1.6 Thesis structure

The currently available green roof models are reviewed in chapter 2, with particular emphasis on models with which this research is compared with. A general review of building energy simulation methods is provided in chapter 2, where the control volume method as applied in ESP-r is also explained briefly. A brief literature review on related soil-vegetation-atmosphere -transfer (SVAT) models is also presented in chapter 2.

Chapter 3 discusses mainly the theoretical formulation of the proposed green roof model. The formulation of energy and mass balances in the control volumes of green roof are explained in detail. It also describes the coefficient table, the governing equations and their time-discretised forms which make up the model. The method of model integration with ESP-r is also described in chapter 3

The proposed model requires a large number of inputs. The sources and methods for obtaining the inputs of plants and soil are described in chapter 4. Experimental

methods for determining some of these inputs are described and the literature sources for other inputs are identified in order to create a database for the inputs that could be used with the model. An illustration of data on plant's varying properties such as LAI and canopy cover is presented in chapter 4. Chapter 4 also includes a section presenting a simple sensitivity analysis performed on the model to rank its input variables in the order of their influence on the models' output.

The experimental validations and model results are described in chapter 5, where details of thermal and moisture domain validation methods are presented.

Finally in chapter 6, the findings are summarized and conclusions are drawn on this research. Chapter 6 also includes potential directions in which the research could be continued towards.

CHAPTER 2
LITERATURE REVIEW

2. Literature Review

2.0 Introduction

The objective of this chapter is to present a review of the state of the art in modelling green roofs, thus to establish the gap in research which the proposed model is expected to cover and to review the ESP-r's structure which makes it a suitable host program for the model development. Prior to the models review, a general introduction of green roof's benefits and its construction, as a review from literature, is given in section 2.1. A chronological list of selected green roof models and their salient features are listed in table A.1 in appendix 1 and summarized in this chapter. Important stand-alone models, where green roofs are modelled independent from the building, are reviewed in section 2.2. Of particular interest to this research is a model published by Del Barrio [9] which is discussed in section 2.2.1. Three models are known to work with other whole building simulation programs, which are briefed in section 2.3. The research gap is explicitly identified in section 2.4 and justification is given for the significance of this research. A very brief review of the structure of the building energy simulation program, ESP-r, as is relevant to the new green roof model's development, is presented in section 2.5. Some soil-vegetation-atmosphere-transfer (SVAT) models, which include many features similar to the green roof models, are reviewed in section 2.6.

2.1 Green roofs' benefits and construction

Green roofs are intentionally vegetated roofs which contribute significantly to the enrichment of biodiversity and storm-water enhancement[10]. The benefits of green roofs include: reduction in building's thermal load with a resultant indirect reduction in carbon emissions, moderating urban heat island effect by reducing the heat reflection from roof surfaces, slowing down of storm water run-off through storage in the growing medium, promoting bio-diversity, providing aesthetically pleasing appearance for the building and providing additional sound attenuation

Types of green roof are [11] extensive type which is of light weight construction with often less than 15cm soil substrate supporting sedum types of plants and generally not

requiring irrigation. An intensive type is of heavier construction with variety of plants, with substrate height more than 20cm and generally requiring irrigation and maintenance[12].

A typical extensive green roof consists of several layers: a plant layer, a soil layer, a filter layer, a drainage layer, a moisture barrier and insulation [13]. A typical construction drawing is shown in figure 2.1.
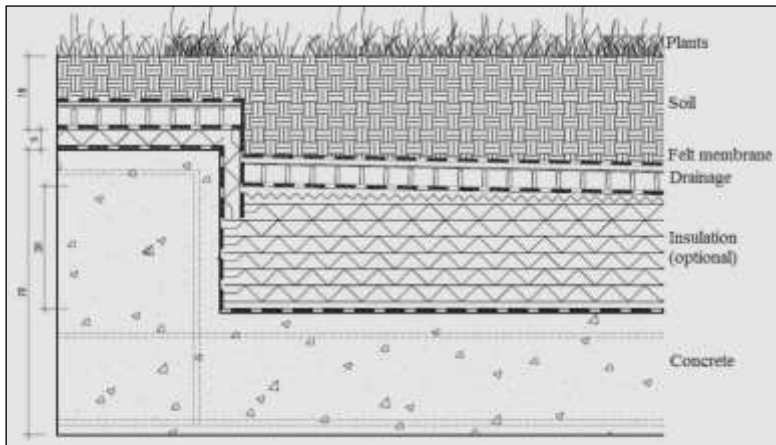
Figure 2-1: Typical green roof construction showing various layers

A research study published at the University of Nottingham Ningbo China [14] concluded that green roofs provide significant energy savings for buildings, especially for those without roof insulation. Hui [15] reports the development of technical guidelines for subtropical location of Hong Kong. Saadatian [16]provide an extensive review of benefits of green roofs and constructional details.

2.2 Stand-alone models

Alexandri et al [17] described a model of green roof with thermal and moisture coupling and experimentally verified some choice of equations such as that for convection heat transfer. Although the study justifies the use of some rule-of-thumb relations, such as:

$$LAI = 24\,h \tag{2-1}$$

(h=plant height) in the context of limited plant type of clipped grass, some excellent observations are provided. The study highlights, through experimental observations, the advantage of working with convection heat transfer coefficients based on analytical methods involving non-dimensional groups such as Reynolds, Prandtl, Grashof and Nusselt numbers over simplified relations (e.g.: h=5.6+18.6U for U<5m/s and h=7.2U$^{0.78}$ for U>5m/s, U being the wind speed) used in building heat transfer calculations. Another notable observation is the choice of equation for calculating stomatal resistance as given in Pielke [18] for convergence with the experimental measurements. The model (Alexandri et al) is derived on the finite difference method with several nodes located along layers of air, canopy, soil and structural part. In this model two sets of one dimensional vertical array of nodes are used, one representing thermal exchange and the other moisture exchange. The model is illustrated in figure 2.2, (adapted from Alexandri et al [17]) below.
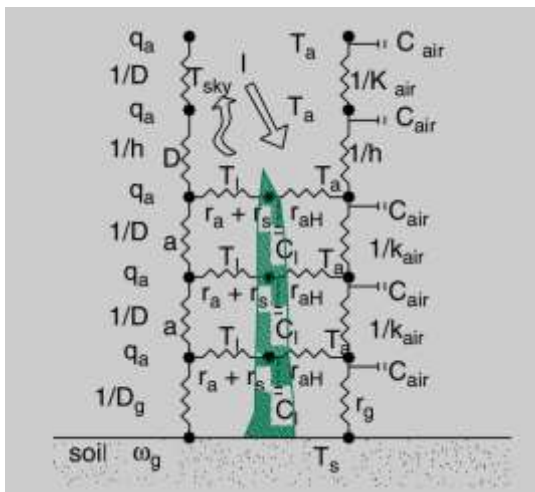
Figure 2-2 Heat and mass transfer model for plant and air [17]

Thermal capacitances C, temperatures T and thermal resistances (r_g for soil surface, $1/k_{air}$ for canopy air, $1/h$ for upper boundary of the canopy, and $1/K_{air}$ for ambient air above, between respective node points) form the thermal nodes network (right-side links). Moisture contents q, vapour pressures 'qa' and moisture transfer resistances $1/D$, form the moisture transfer nodes network (left-side links). Thermal leaf properties are C_l, and T_l linking to the air nodes on the right side by resistances r_{aH}. For the moisture exchange links, leaf surface vapour pressures are considered as saturated, and

12

are linked to air node vapour pressures by combined stomatal and air resistances, r_a+r_s. K and k represent thermal conductivities, h convection heat transfer coefficient and D diffusion coefficient. It is to be noted that the plant (leaf) nodes serve as coupling link between the thermal and moisture arrays. Similar type of arrangement is found to be used in a number of notable studies which are explained in later part of this study (Sellers et al [19], Bittelli et al [8]). It is ascertained that the assumption of a constant thermal conductivity, as is used in the domain of porous building materials heat transfer calculations, cannot be used in the soil medium as it is strongly dependent on the water content and temperature. Also notable is the observation that the surface radiation optical properties such as albedo, which are generally considered constant for a material, actually varies according to the incident radiation. However the study does not provide any indication of the degree of error brought in by such assumption. A noted draw back of the model is that it does not take into account moisture addition by precipitation or irrigation. The study does not provide any clue of the method of obtaining results from the set of differential equations. In general the study provides some useful insights for the choice of equations and some guiding to areas where attention to details are necessary in the modelling process. However the study does not indicate implementation of model in a whole building energy simulation program.

Takebayashi [20] provides a comparative study of various roofs (concrete roof with various paints, roof with bare soil and roof with planted soil) with the objective of identifying the effects of roof on the mitigation of urban heat island effect. While the study does not provide much added information towards formulation of a green roof model, the method adapted provides some useful hints towards identifying interesting procedures for experimentally verifying green roof equations and models. The heat budget at the top surface of roofs provides balances between (a) Incoming radiation heat, (b) downward conduction heat, (c) upward sensible heat and (d) upward latent heat. The method involves measuring all variables for calculating, as stated above, (a), (b) and (d) and determining (c), as [(a)- (b)-(d)]. The mixed experimental/modelling process is illustrated in the figure below, which is adapted from [20].
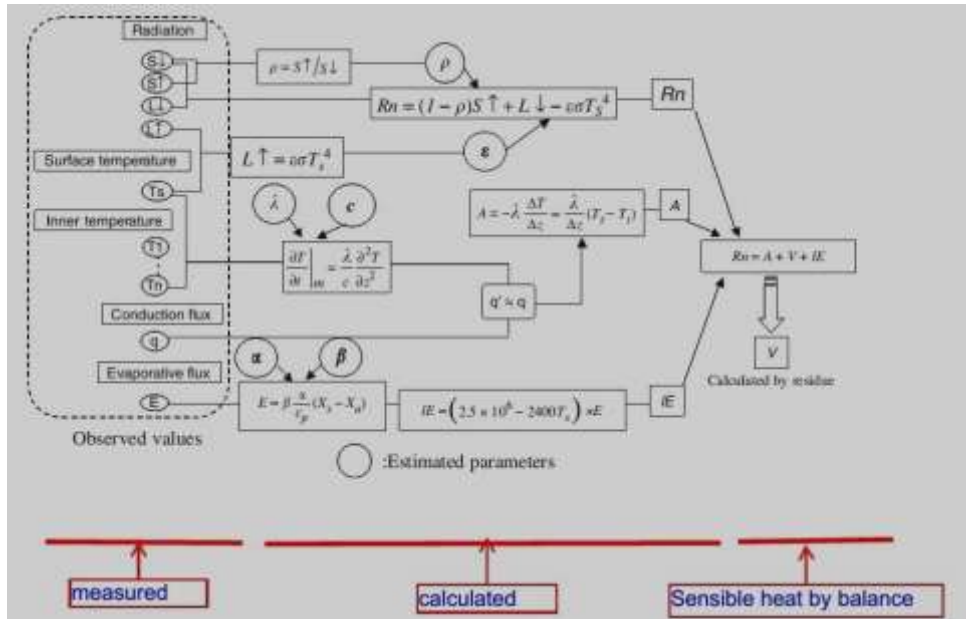
Figure 2-3 Heat budget analysis of combined modelling and measurement [20]

The variables mentioned here are: Rn - net radiation (W/m^2), A – conduction heat flux (W/m^2), V - sensible heat flux (W/m^2), lE - latent heat flux (W/m^2), λ - thermal conductivity (W/mK), α - convective heat transfer coefficient (W/m^{2}K), Ts - surface temperature (°C and K for radiation calculations),Ta - air temperature (°C), β - evaporative efficiency (-), Cp - Specific heat of air (J/kgK), Xs - saturated humidity (kg/kg) and Xa – air absolute humidity (kg/kg). A notable observation of the authors is the caution towards the determination of evaporation by measurement of soil moisture content, without considering the detailed distribution of water.

Santamouris et al [21] provided a brief description of experimental verification of energy benefits of a green roof system installed in a nursery school building in Athens (37°58'N, 23°44'E) where a reduction of summer cooling load up to 49% for a building of 0.47 aspect ratio (height/width) is observed. It was found that there was no effect on heating load during winter. The study reports simulation work in TRNSYS, but no details were given. From the reporting of results it is inferred that green roof is treated just as an additional insulation layer, because a reduced heat transmittance (U-value) is used in the energy calculations for green roof. An earlier published work by Niachou et al [22] reported a similar finding, but the tests were conducted in a hotel building in the extended Athens basin region.

A research report by Center for Climate Systems Research of Columbia University and Goddard Institute for Space Studies of NASA [23] explores the development of green roofs in New York City (40°45'N, 73°59'W). Research output on energy use, urban heat island effect, and storm-water runoff of specifically light-weight extensive green roof types are reported. Within the energy domain research, steady state simulations of rooftop energy balance model are reported. The energy balances were considered as algebraic sum of shortwave radiation downwards; shortwave radiation reflected upwards; long-wave radiation downwards; long-wave radiation emitted upwards; sensible heat loss or gain; latent heat loss; and heat conduction downwards or upwards from the room below the roof. Of interest are some specific results such as average day-time surface temperature on green roof was 19°C lower as compared to standard roof in summer and 8°C higher at night.

A PhD study conducted by Yu [24] in Singapore (1°22'N, 103°48'E) introduced a new concept of 'green sol-air temperature' which gives a combined effect of convection and radiation heat transfers and can be used as a single temperature in much simplified ETTV (Envelope Thermal Transfer Value) calculation of cooling load for Buildings. The study is based on the concept of surface energy budget as in Santamouris [25] . Although this concept is a simplified approach (treating green roof as a reduced transmittance value) in the context of a dynamic energy simulation scheme of the current research (considering the evolution of a set of variables across various layers), some excellent 'macro (climate) level' and 'micro (building) level' studies conducted in Singapore as part of the research are notable. A database for the leaf area index (LAI) of plants was developed as part of the above study and it is a valuable source, which can be further developed into a broader range of plants applicable for other regions as well.

In a previous study, conducted at the National University of Singapore, Wong et al [26] report results of experimental investigation of thermal performance of a green roof. A reduced roof top ambient air temperature of up to 4.2°C due to plants and a reduced upward irradiation due to plants by up to 109 W/m^2 were observed. Wong also reports in another study [27] the effects of roof top garden in a commercial building in Singapore investigated by using the DOE-2 building energy simulation[28]. The effect of a green roof is treated as an added insulation thermal resistance, determined by field

measurements of turfs, shrubs and trees. The objective was to determine if the roof thermal transfer value (RTTV) falls within a regulatory limit.

Some recent studies from Pennsylvania State University by Tabares-Velasco et al [29] and [30] report of a 'Cold Plate' (as is called by the authors) experimental set-up, located inside an environmental chamber, enabling isolation from random outdoor conditions. The model considers heat and mass transfer processes between ambient air, plants, and substrate. An interesting part of the outcome is a list of equations of which some are newly proposed and verified by way of experimental data, viz. substrate thermal conductivity for green roofs, substrate moisture resistance to calculate green roof soil evaporation, and stomatal resistance functions to calculate transpiration. The validation which has been provided in detail, established the accuracy of most of the formulae, except for those involving evapotranspiration rates. Various equations of the above study can be used as alternatives in the current research. However it is noted that, the accuracy of the equations needs to be further verified because the components of the equations are determined by experimental observations in the 'cold plate' apparatus and it is likely that the relations may not be valid in a different composition of soil.

Of interest are also two prior studies from the Pennsylvania State University; Tabares-Velasco et al [31] describing specifically laboratory set up details for green roof and Ayata et al [31] evaluating sensible heat flux to and from vegetated roof assembly. The latter study addresses a relatively complex part of green roof model, the convective heat transfer. Applications of various convective heat transfer correlations in the green roof assembly were established by experimental measurements in a green roof test bench, for various wind velocities creating free and forced convection conditions.

2.2.1 Finite volume green roof model

The most relevant source to this research is an earlier published work from Del Barrio [9] in which energy and moisture balance equations of canopy, soil and roof support layers and the boundary conditions coupling these layers were systematically developed. The simulations were done in MATLAB and parametric studies were provided, the results of which give an indication of which areas need close scrutiny in

both model development and simulation in the current research. For example on the canopy side, short wave extinction coefficient (k_s), long wave extinction coefficient (k_l) and LAI were found to have a strong influence on the transmitted solar radiation, but negligible effect on the canopy air temperature. On the soil side, the soil moisture content and the density of the soil were found to have a strong influence on the heat flux through green roof. A few disadvantages were also noted with regard to this study. There was no experimental validation of the model reported and the sensitivity analysis is of limited nature with regard to the lack of information on the influence of LAI, k_l and k_s on the green roof net heat flux, possibly due to the fact that there are numerous variables involved and that the focus of Del Barrio[9] was on theoretical formulation. Some of the data used in the plant canopy model are also of too specific nature (external aerodynamic resistance of leaves refers to tomatoes), which can only be used as a reference in the current research. However, the study provides an overall valuable information for the development of green roof models. The approach to model development is systematic, with formulation of the problem layer by layer, clearly defining the assumptions, expanding sub components, simplifying some equations and defining boundary conditions for each layer. However the model remains as a stand-alone type for green roof as it is not associated to a whole building energy simulation.

The modelling approach of Del Barrio [9] is used as a basis in this research to further develop a green roof model based on control volume method, which has definite advantages compared to the existing models in building simulation programs.

2.3 Models in whole building simulation programs

2.3.1 City-scale model

A recent city scale model called TEB GREENROOF [32] has been developed at Météo-France which predicts the influence of green roof on local climate. It combines an atmospheric model called ISBA (Interaction between Soil Biosphere and Atmosphere) [33] with the TEB (Town Energy Balance) [34] operating within a much larger land surface modelling platform domain called SURFEX (*External Surface*) [35]. The vegetation, substrate (three layer model) and drainage (two layer model) fall

within the ISBA scheme whereas the insulation layers are dealt within TEB domain. The hydrological characteristics of soil and drain are calibrated as per a case study in Nancy, France. The thermal moisture exchanges within this model are as illustrated in figure 2.4 which is from de Munck 2013 [32]. The model's published configuration is limited to extensive green roofs with two types of plants, sedum and grass and standard soil height of 100 mm and drainage layer height of 50 mm are assumed. The drainage is calculated as the vertical water flux, when the drainage layer moisture content exceeds saturation. Evapotranspiration is divided into three parts, soil top evaporation, plant transpiration and evaporation of intercepted rain water at canopy. The stomatal resistance calculation form the minimum stomatal resistance, makes use of root distribution profile and hydrological status of each node, which appears to be an ISBA feature. Thermal coupling between ISBA and TEB are done with both temperature and heat flux. No hydrological coupling is required at the ISBA-TEB interface, justifiably, as the water proof membrane prevents water from going down into TEB components and the drainage becomes a lower boundary condition. The model requires specific soil characteristics which are obtained from calibration exercises and advices against the use of pedotransfer properties according to texture classification. The model uses Clapp and Hornberger [36] relation for moisture retention characteristic of soil as against van Genuchten [37]. These are alternative empirical relations widely used in soil moisture models. The hydrological characteristics of the drainage layer which is assumed to be expanded clay granules (2-10mm) and consisting of micro and macro pores are compared to three types of material: organic matter, sand and clay. A statistical procedure is used for finding the best fit and organic matter was found to be the closest match. However the limitation of choice for green roof material (organic matter, sand or clay) is a short-coming of the model. It is stated that the building level implementation of the green roof model is in planning.

The model has several advantages with the main one being that it uses a set of well researched base facilities such as TEB, ISBA and SURFEX which have been validated in their respective domains at city scale, building scale and atmospheric scale respectively. The thermal coupling between the green roof and the structural part of the building is done by both temperature and heat flux which could allow for better simulations of the dynamics of thermal exchanges at times of heat flow direction

changes. Strengths of the model also include that the substrate definition consists of soil and drainage layers and that the drainage rate is calculated when the soil moisture content reaches saturation value.

Model limitations include its limited configurations (extensive green roof, two plant types, etc.) and that it is integrated to a city scale model and not to a building level simulation. The use of the model requires the knowledge of components such as ISBA, which are basically environmental models and have a variety of input outside the interest of building simulation practitioners. As the model use specific soil characteristics, local calibration is needed to specify some input parameters such as porosity and coefficient of water retention curve.
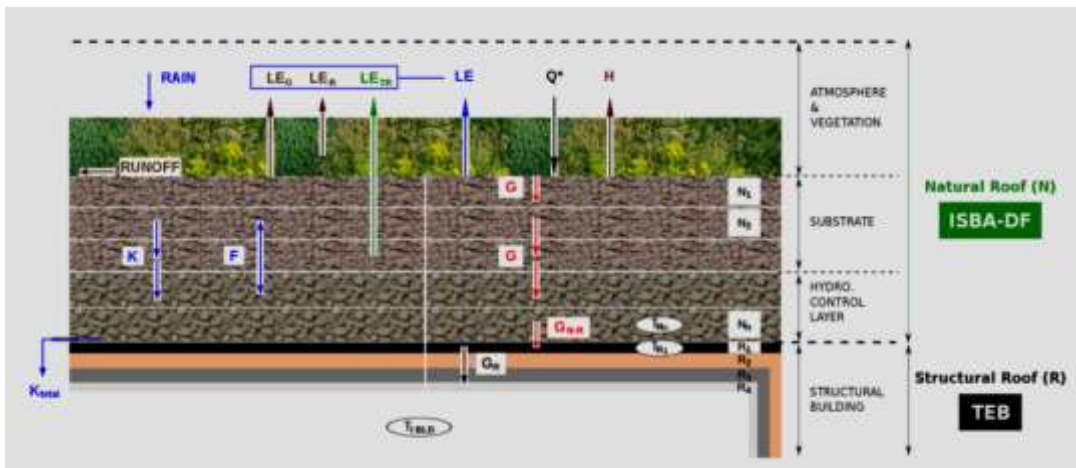
Figure 2-4 TAB GREENROOF model components [32]

2.3.2 EnergyPlus ecoroof model

Currently the ecoroof model in EnergyPlus [6]is the only existing model of green roof integrated to a public domain whole building energy simulation program. The model expresses in two equations the energy balance (for predicting the foliage temperature, equation 2.2 as stated below and the soil temperature, equation 2.3). The EnergyPlus (CTF) conduction transfer function scheme is used in this model and a recent improvement of the program takes into account moisture fluctuation and couples the thermal and moisture simulation domains[38]. Canopy air temperature and mixing ratio (or specific humidity which is the ratio of mass of water vapour to that of dry air) are defined as weighted average of the properties of ground and ambient air. In the time response factor method (or the so called conduction transfer function, CTF

method) that is used in the eco-roof model, the intermediate temperatures of a composite construction are not available, for model verification. Moreover the CTF model is unable to account for time varying thermal properties. This justifies the need to implement a model based on a numerical control volume (CV) approach where layer by layer variables are available for analysis, verification and further refinement of the model. Within the canopy, plants and air are treated as separate control volumes. The space discretisation into control volumes could also be modified if necessary (combining existing CVs or further subdividing them) in this method as a model refinement. As in a green roof the thermal and moisture exchanges are strongly inter-dependent and the phase change in evapotranspiration is a strong contributor for the cooling effect of green roofs, in a numerical model, precise calculations involving the related variables are necessary. By using the CV method all of variables (temperatures and moisture contents) of various layers are updated in each time step, so the results of simulation are expected to be reflecting the true dynamics.

The EnergyPlus ecoroof model requires data from weather file and a set of user inputs. The user inputs are: height of plants, leaf area index, leaf reflectivity, leaf emissivity, minimum stomatal resistance, soil roughness, soil thickness, soil conductivity, soil density, soil specific heat and soil absorption coefficients. All of these and the related state parameters are used in the definition of two linearized equations.

Foliage energy balance equation is of the form:

$$C_{1,f} + C_{2,f}\, T_g + C_{3,f}\, T_f = 0 \tag{2-2}$$

Soil energy balance equation is of the form:

$$C_{1,g} + C_{2,g}\, T_g + C_{3,g}\, T_f = 0 \tag{2-3}$$

Where C_1, C_2 and C_3 are the equation coefficients with additional subscript f representing those of plant and g representing those of soil. These equations are solved simultaneously to obtain T_g and T_f at every time step. The conduction terms $C_{1,g}$ and $C_{2,g}$ are obtained by inverting the Conduction Transfer Functions (CTF) from within the EnergyPlus. In the CTF approach, the heat flux at one side of a construction

element is obtained as a function of finite series of past temperatures at both bounding sides. This method has inherent limitations in dealing with complexities of multi-layers models where moisture and thermal interactions occur at different levels in different manner. A finite control volume approach on the other hand is capable of handling such intricacies. The differences between these two methods are summarized in table 2.1 below [39].

Table 2-1: Difference between CTF and CV methods

	Conduction Transfer Function	**Finite Control Volume**
Definition	Define the inner and outer wall surface heat flux at the current time as a function of the inner and outer surface temperature and the surface heat flux at a set of previous times	Based on an approximation of governing partial differential equations as applied to discretised control volumes followed by the establishment of a nodal equation-set, which is then solved simultaneously to obtain the distribution of the state variables.
Comparison	Involves summing the responses, determined independently of the system's component parts. If parts are strongly interacting then this will lead to an inherent inaccuracy because the parts are decoupled	Well suited to the integration challenge because they can be used to handle problems of almost any degree of complexity.

The ecoroof model has many advantages:

- It has been calibrated and validated in various locations[38] representing different climate zones in the USA.
- It is the most commonly used green roof model within building energy simulation[40], because it is the only available option for whole building energy simulation.

Model limitations include:

- The model is CTF implemented and as a result representations of dynamic interlayer interactions in green roofs are not explicitly defined.

- Although the moisture content of growing medium is represented in the model, no moisture flow is modelled across the green roof elements.

- The model treats the energy balance equations of foliage and soil as quasi steady state equations for each time step. There is no time derivative within the equations which is an indicator of internal dynamics. The absence of thermal storage term ($\rho C \frac{dT}{dt}$) for soil, indicates that thermal inertia are neglected.

- Also much simplified model assumptions are used for canopy air properties (temperature and vapour pressure) whereby they are taken as arbitrary weighted averages between the properties of the plant and the ambient air.

2.3.3 TRNSYS-VegEnvelope model

A new TRNSYS type called VegEnvelope [7], has just been developed at University of La Rochelle, France and is designed to work with TRNSYS multi-zone building component type 56. This model is developed at the same time as the current research which shows the significance of interests in building simulation community for green roof and green wall models. VegEnvelope is a green envelope model for representing green walls and green roofs. It has foliage and soil energy budgets similar to ecoroof model [6], but with thermal inertia accounted for and it is in finite difference formulation. Moisture content of soil is calculated by way of a moisture budget calculation of the format:

$$\rho_w \Delta z \frac{\partial \omega_g}{\partial t} = P + A - D - E \qquad \text{(2-4)}$$

Where ρ_w is the water density [kg/m^3], ω_g is the soil moisture content [m^3/m^3], Δz soil depth [m], P precipitation [kg/m^2], A irrigation [kg/m^2], D drainage [kg/m^2]and E evapotranspiration [kg/m^2]. The heat transfer across the drainage layer is also

specifically determined by using a thermal resistance across air layer and a mean coefficient for vapour transfer from air layer to ambience. The water flux along the substrate depth is not modelled and thus drainage is not determined. Evapotranspiration is taken as the total of latent heat exchanges (converted to mass units by latent heat of evaporation) in the foliage and soil. Within the moisture flux domain neither the moisture gradient along the substrate depth nor the root-uptake is accounted for. This model's [7] validation is based on green wall configuration and the substrate is maintained near saturation state by frequent watering. It was established, in the result analysis of the model validation that substrate layer thickness has an effect on thermal inertia and canopy's shading influences the diurnal peaks of temperature. The flow chart of the integration into TRNSYS of the Python scripted module is shown in figure[7] below.
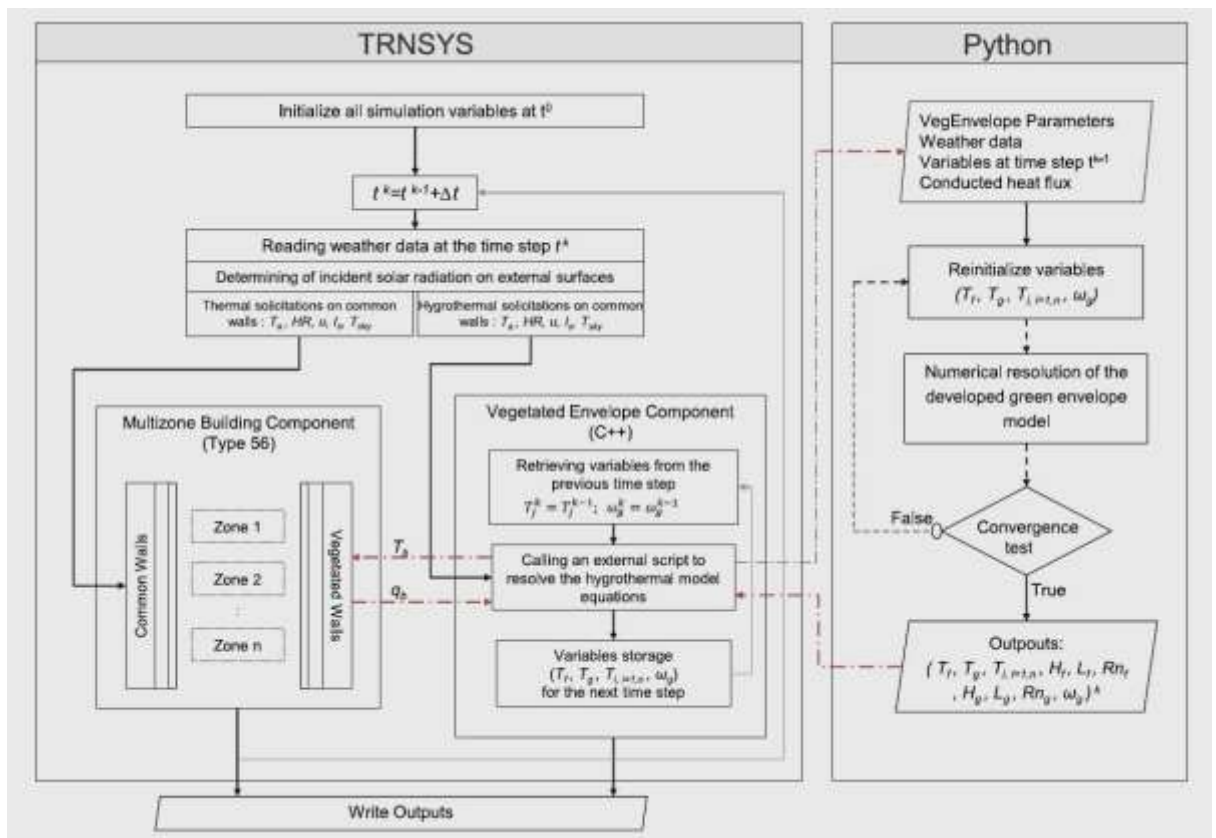
Figure 2-5: TRNSYS integration of the model VegEnvelop [7]

The symbols used in this model are: T- temperature, ω - moisture content, subscript f – foliage, subscript g- soil, H- sensible heat, L – latent heat, HR- relative humidity, u

23

wind velocity, Is- solar short wave radiation, Tsky-sky temperature, Ta – ambient temperature.

A previous research [41] details the configuration of the above green roof model. Implementation in TRNSYS was earlier reported in another research conducted at University of La Rochelle [42] which is a much simpler model with quasi steady state equations for foliage and soil energy budget and no moisture coupling was present in the model. Another research [43] also uses quasi-steady state equations for energy balances, but moisture flux is considered by way of Richard's equation [44] . This model uses the Penman-Monteith equation for evapotranspiration [45], which is given by equation 2.5:

$$ET_o = \frac{1}{\lambda}\left[\frac{\Delta(R_n - G)}{\Delta + \gamma\left(1 + \frac{r_c}{r_a}\right)} + \frac{\frac{\rho\,c_p}{r_a}(e_a - e_d)}{\Delta + \gamma\left(1 + \frac{r_c}{r_a}\right)}\right] \tag{2-5}$$

λ is the latent heat of vaporization[J/kg], Δ is the slope of saturation vapour pressure curve [Pa/°C], e_a is the saturation vapour pressure of air [Pa], e_d is the air vapour pressure [Pa], r_c is the crop-canopy resistance [s m^{-1}], r_a is the aerodynamic resistance [s m^{-1}], γ is the thermodynamic constant gamma [Pa/°C], cp is the specific heat of moist air, ρ is the density of moist air, Rn is the solar radiation [W/m^2] and G is the conduction heat down ward at soil surface [W/m^2]

However the implementation is in Matlab as a stand-alone program, i.e., not integrated to a building energy simulation program. For the above models the advantages and shortcomings can be summarized as below.

Models' advantages include implementation of finite difference method which can simulate closely the dynamic nature of thermal balances across the different green roof layers. Thermal moisture coupling is also implemented in this model.

Models have shortcomings in its moisture domain whereby no moisture gradient or moisture flux along substrate depth is simulated; consequently the drainage rate is also

not calculated. As the models are not available in public domain their access are limited. Finally, the models' literature does not indicate a possibility of using time varying inputs such as plant properties as model inputs.

2.4 Research gap in green roof modelling

From the afore-mentioned discussions it can be identified that following specific lacks exist in current models as a whole which this research is addressing.

1. A control volume approach, which can represent the dynamics of interlayer and inter phase interactions of green roof layers, is not available within a public domain building simulation program.

2. Vertical water flux along green roof substrate is not represented in the existing models which have been integrated with building energy simulation programs. As a consequence the models are unable to assess for the storm water retention capabilities of green roofs.

3. Thermal/moisture coupling has limited scope in current public domain models because they are not implemented in finite difference formulation.

4. Root uptakes of plants are not modelled in building scale simulations, limiting their capability to represent the dynamic nature of plants evapotranspiration process which varies according to environmental conditions.

5. The possibility of scheduled variations of properties such as plant LAI, height etc., as model inputs is not available in the existing models.

Thus far in this chapter, a review of existing green roof models has been presented. In the following section, a concise review of ESP-r's structure is provided.

2.5 Simulation method of ESP-r

ESP-r is an open source whole building energy simulation program [46] which has since its inception in 1974 [47] gone through many stages of developments. There are many references which explain the theoretical basis and developments of many features of ESP-r, such as Clarke [46], Beausoleil-Morrison [48], Kelly [49] and

Macdonald [50]. The objective of this section is to highlight the features of the program that is important to the development of the new green roof model. Some of the salient features of this program include its control volume approach of modelling, integrated whole building simulation capable of modeling a wide range of building's energy and environmental parameters and the use of optimized numerical technique to solve systems of simultaneous equations. Currently simulation domains include thermal exchanges, moisture transfer, and air flows within and across zones, HVAC plants, electrical distribution and piping networks. The building geometry and fabric are represented by control volumes and so are the zones. The energy sub systems which include air conditioning plant, air distribution and piping distribution are linked to these control volumes as attributes. These systems' representations along with the conditions set forth by the occupancy behaviour, control actions and climatic data forms the complete building model. Although integrated there is an opportunity to treat each simulation exercise to the degree of complexity it requires, starting from simple models and adding progressively the details. In ESP-r, control volume principle is applied to all elements of the building, such as the building fabric construction elements, plant equipment, water/air/electricity distribution networks, etc. In all of the control volumes, the conservation of mass, energy and momentum is applied. The conservation equations according to their nature are grouped and solved by customized solvers. This means that the resolution of accuracy and the required levels of details can be customized in the different elements of the building. When dealing with complex features, the user can assign uncertainty to input parameters, so the model will run many simulations to cover the range of uncertainty. There are many statistical methods to go about this sensitivity analysis seeking the effect of a particular kind of variation on the chosen parameters.

The program consists of several modules which are evoked form a 'Project Manager' interface; figure 2.6 shows a view of the Project Manager opened in an x11 interface in Linux.
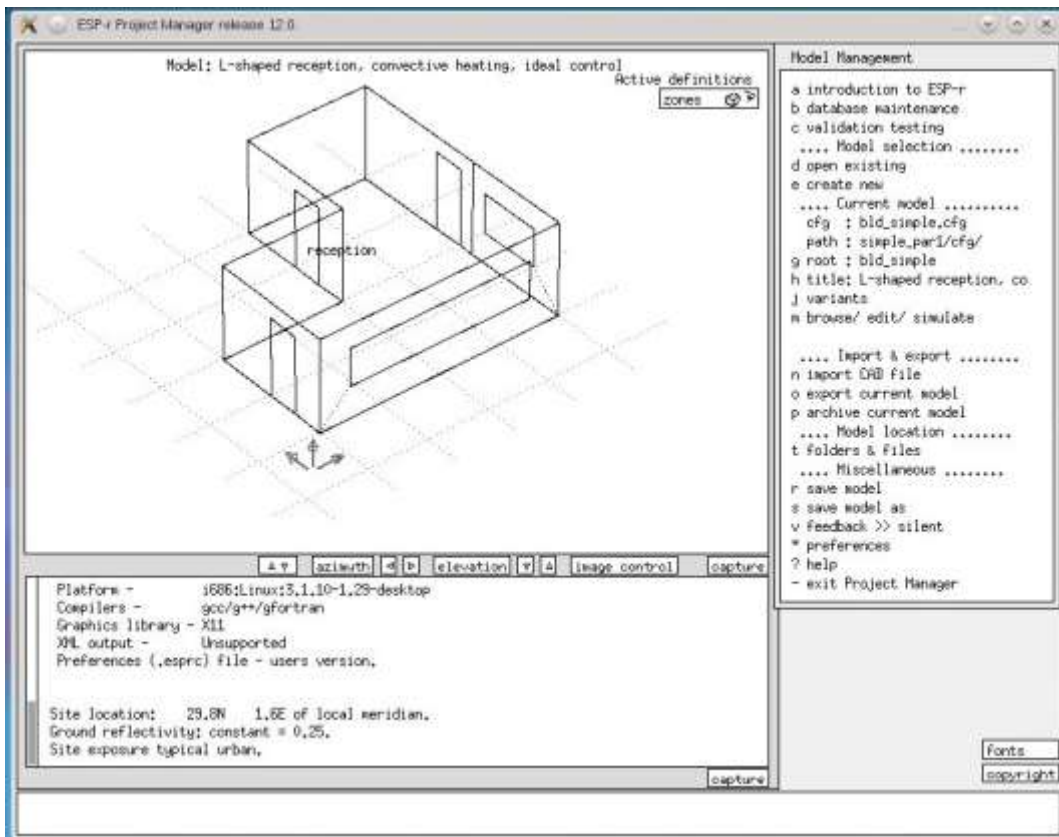
Figure 2-6: ESP-r Project Manager to activate various modules

The iterative solution approach of ESP-r involving handshaking with subsystems is shown in figure 2.7, which is reproduced from Clarke 2007 [47]. It can be summarized that the mass and energy balance equations at the building level control volumes along with heat injections of the plant systems are used to form a set of linear equations and are simultaneously solved in each time step by a matrix solving process.
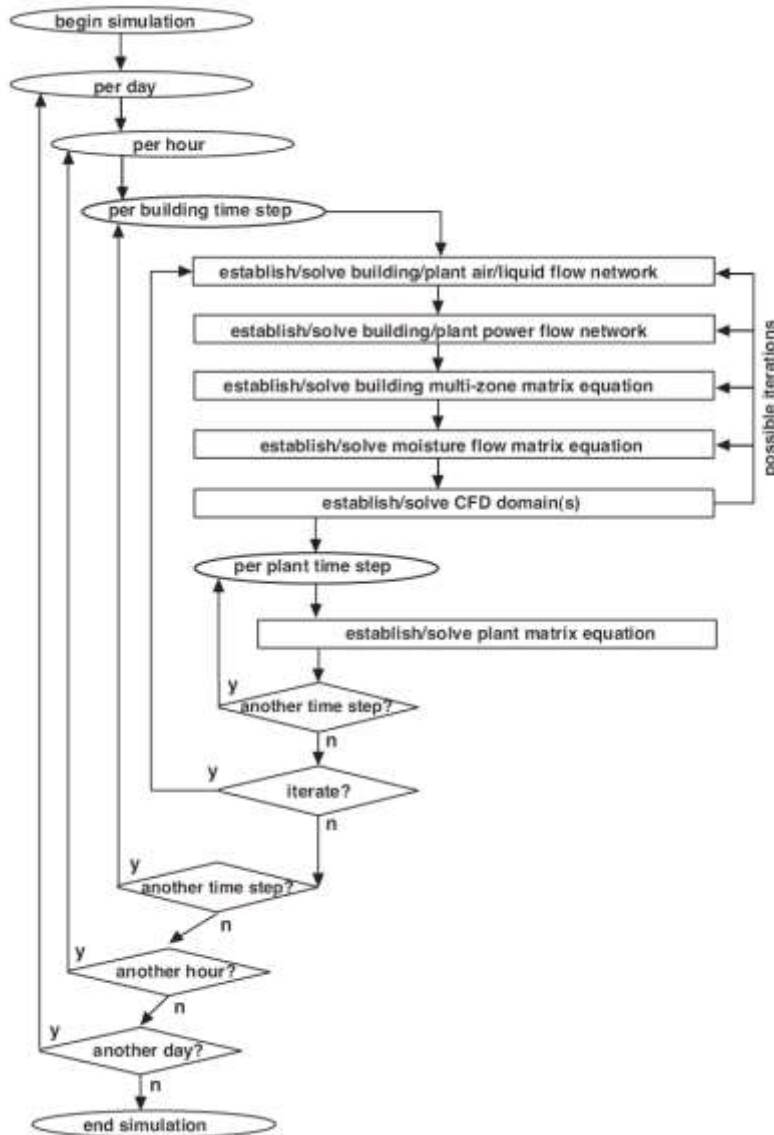
Figure 2-7: Nested domain loops of ESP-r's organization[47].

2.6 Soil vegetation models

There are several models in environmental and agricultural domain dealing with
thermal and moisture interactions of earth to predict hydrological processes of land,
meteorological effects of these interactions or crop transpiration and water
requirement [51] [52] [53]. Several components of these models are relevant for the
green roof simulations, although careful adaptations are needed, especially in the cases
of the boundary conditions in the roof-top non-natural environments of green roofs. In
a recent extensive literature review study [54] conducted on the thermal performance
of green façades, it is highlighted that the green façade simulation domain is currently

28

lacking input from biology, ecology and soil sciences. The objective of this section is to present a review of such environmental models which are relevant to the simulation of green roofs.

A well-documented soil physics research [8] published a model to compute soil top evaporation based on a coupled thermal moisture model in bare soil. The study makes use of an established knowledgebase in soil physics by Campbell [55]. The numerical model is based on nodal exchanges of thermal flux and liquid flu**x** as shown in the equations 2.6 and 2.7:

$$q_h = \lambda \frac{dT}{dz} + Lq_v \tag{2-6}$$

$$\frac{\partial \theta}{\partial t} = \frac{d}{dz}\left(K(\psi)\left[\frac{d\psi}{dz} + gz\right]\right) \tag{2-7}$$

where q_h is the net heat flux [W/m^2], λ - thermal conductivity [W/m/K], T temperature [K], z is the height [m], L is the latent heat [J/kg], q_v is the vapour flux [kg/s/m^2], θ is the moisture content [m^3/m^3], ψ is the matric potential [J/kg], K is the hydraulic conductivity [kg/m^2/s] and g is the acceleration due to gravity [m/s^2]. The state variables in the heat flux, liquid flux and vapour flux, namely temperature, T, matric potential ψ and concentration C, with their respective conductivities, λ, K and K_v, are connected by their nodal positions in a manner as shown in figure 2.7 [8] to form three sets of computational grid of equations. The coupling is ensured by the interdependency of variables as shown within parenthesis along each state variables in figure 2.8. The model uses Campbell's relation (equation 2.8) to calculate moisture content from matric potential as against the more recent van Genutchen which is used in this research.

$$\theta = \theta_s \left(\frac{\psi_m}{\psi_e}\right)^{-b} \tag{2-8}$$

where θ is the moisture content [m^3/m^3], θ_s is the saturated moisture content [m^3/m^3], ψ_m is the matric potential [J/kg], ψ_e is the air entry potential [J/kg] and b is a soil texture shape parameter.

It is highlighted among the findings that vapour transport plays an important role in mass and energy transfer in soils. In the validation study[8] it was also found that the vapour flow caused a sinusoidal variation of soil surface moisture content.
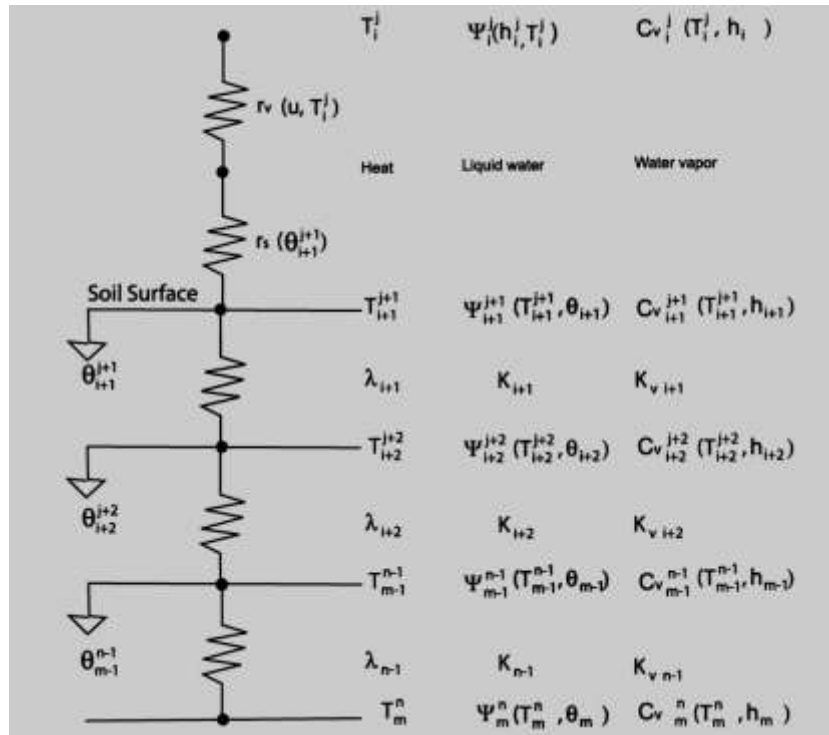
Figure 2-8: Illustration of nodal state variables for thermal, liquid and vapour exchanges in reference model [8].

In the validation studies [8] soil surface evaporation E is measured indirectly by measuring all of the following components of a surface heat budget equation:

$$LE = R_n - G - H \tag{2-9}$$

where Rn is the incoming solar radiation [W/m^2], G is the conduction heat into the soil [W/m^2] and H is the sensible (convection) heat from soil to air. An interesting part of this study is the measurement of H by a method called surface renewal method which uses high frequency temperature measurements. The model is implemented in Excel. One drawback of the model is that there is no plant involved in the energy exchange and it is a purely soil model.

In an earlier study on a soil model[56], a surface energy balance is developed to determine bare soil's surface temperature and heat flux. The model is numerically implemented by using the semi-implicit Crank Nicolson method, in which

simultaneous solving for state variables is executed by Gauss elimination. The steps are repeated in successive iterations performed using the Newton-Raphson method for convergence. The model's validation is done by measuring the thermal variables at a desert site. The model reports of getting negative evaporation in early morning which is treated as condensation from air to soil. This model also did not include plants in the thermal energy exchange calculations.

Among the atmospheric models the SiB2 (Simple Biosphere), which is a large scale model [19] is interesting because it incorporates many details of moisture and heat exchanges similar to those for a green roof. SiB2 is a land surface parametrization model for atmospheric transfer simulation. SiB2 uses satellite data for deriving vegetation properties such as LAI specific to the region of interest for its climate studies. The aerodynamic resistances at canopy air space, below canopy and above canopy (turbulent transition layer) are defined in detail. On the thermal side, the model uses three sets of equations (2.10 -12) to define the canopy (subscript c), soil surface (subscript g) and deep soil (subscript d) temperatures.

$$C_c \frac{\partial T_c}{\partial t} = Rn_c - H_c - L\,E_c - \xi_c \tag{2-10}$$

$$C_g \frac{\partial T_g}{\partial t} = Rn_g - H_g - L\,E_g - \frac{2\pi C_d \left(T_g - T_d\right)}{\tau_d} - \xi_g \tag{2-11}$$

$$C_d \frac{\partial T_d}{\partial t} = \frac{1}{2(365\pi)^{1/2}} (Rn_g - H_g - L\,E_g) \tag{2-12}$$

where C- effective heat capacities [J/m^2/K], T temperature [K], t -time (s), Rn - absorbed net radiation [W/m^2], H-sensible heat flux [W/m^2], E- evapotranspiration rates [kg/m^2/s], τ_d- day length [s] and ξ - energy transfer due to phase changes of water vapour. It was observed in the numerical solution of these prognostic equations that the heat capacity terms (C's) are small compared to the energy flux terms (Rn's, E's and H's) which has an effect of making these equations as fast responding thus requiring shorter time steps in simulations. A notable feature is the implementation of offline calculation of vegetation variables like LAI and use them in an array to be called by the program during simulation. The SiB2 model also includes a detailed precipitation interception model. In addition, the plant to canopy air resistances for thermal and mass exchanges are treated differently; i.e., heat flow as occurring at both sides of the leaves has a resistance half of that for transpiration vapour flow which is modelled as occurring only on the front surface. The model is composed of many sub

models to perform separate vegetation and soil functions and has gone through a few cycles of revisions and upgrading. The main disadvantage of the SiB2 model is its complexity, as it deals with a multitude of domains such as hydrology, atmospheric studies, etc.

Another published study by Noilhan [57] of French National Centre for Meteorological Research(CNRM), treats many processes in a much simplified manner although it is also a large scale meteorological land surface model and report that the soil moisture coefficients of the mass balance equations are strongly dependent on the texture class of soil. In this model, soil heat flux for areas completely covered by vegetation is considered zero. The model proposes a function for calculating the stomatal resistance of plant, as given in equation 2.13

$$Rs = \frac{Rs_{min}}{LAI} F_1 F_2^{-1} F_3^{-1} F_4^{-1}$$ (2-13)

where Rs is the canopy level stomatal resistance, Rs_{min} is the minimum stomata resistance specific to the plant, F_1, F_2, F_3 and F_4 are dimensionless coefficients for existing photo synthetically active radiation (PAR), root-level soil moisture content, air vapour pressure and air temperature respectively.

A research conducted at Wageningen Agricultural University [58]published details of the SWAP (Soil-Water-Atmosphere-Plant), an extensive multi-faceted domain open access model. SWAP is a implemented as a fully implicit backward finite difference numerical model. There are extensive drainage functions for various field drain configurations and they account for the dynamic pressure heads which drive the drainage rate. The inter-nodal hydraulic conductivities calculated either as arithmetic mean or geometric mean of those of the nodal locations, depending on the grid spacing. Node spacing and time steps themselves are self-adjusted variables according to the dynamics of the simulation, which optimises the computational time for simulations. A mixed mode implementation of moisture balance equation (both moisture content and matric potentials are present in one equation, as shown in equation 2.14) and a feature to remove the uncertainty of specific water capacity make the model stable in both saturated and unsaturated states of soil.

$$C_i^{j+1,p-1}\left(h_i^{j+1,p} - h_i^{j+1,p-1}\right) + \theta_i^{j+1,p-1} - \theta_i^j \qquad \text{(2-14)}$$

$$= \frac{\Delta t^j}{\Delta z_i}\left[K^j_{i-\left(\frac{1}{2}\right)}\left(\frac{h_{i-1}^{j+1,p} - h_i^{j+1,p}}{\Delta z_u}\right) + K^j_{i-\left(\frac{1}{2}\right)}\right.$$

$$\left. - K^j_{i+\left(\frac{1}{2}\right)}\left(\frac{h_i^{j+1,p} - h_{i+1}^{j+1,p}}{\Delta z_l}\right) - K^j_{i+\left(\frac{1}{2}\right)}\right] - \Delta t^j S_i^j$$

where subscript i is the node number, superscript j is the time step and superscript p is the iteration number within each time step. θ is the moisture content [m^3/m^3], h is the matric potential [m], C is the specific water capacity [m^{-1}], t is time[s], z is height[m], K is hydraulic conductivity [m/s] and S is the root uptake [m^3/m^3/s]. As the iterations move to convergence, the terms $h_i^{j+1,p}$ and $h_i^{j+1,p-1}$ become closer, thus the first term in the above equation (2.12) vanishes, making the solution stable. The model includes dynamic crop characteristics simulated within another program, WOFOST [59]. One main drawback of this model is that it does not account for the vapour flow within the soil and its effect on the thermal exchange.

Apart from SWAP, the most notable development in this sector is another open source program called HYDRUS 1D [60]. HYDRUS 1D is a fully coupled soil-plant model and it incorporates vapour fluxes and thermal driven liquid fluxes, in addition to other usual elements of mass transfer. In addition, CO_2 production and transport are simulated within the model. A specific feature of the model is its dynamic nature of boundary conditions; i.e., the lower boundary condition changes according to the seepage condition. When the lower layer soil is unsaturated, the lower boundary condition is set to zero water flux (flux boundary condition) while when it is saturated, the drain starts and the lower boundary condition is changed to zero matric potential (potential boundary condition). A lysimeter (which is a measurement collection tank placed below the soil being tested) type of drainage profile is available, which is similar to green roof's drainage construction.

2.7 Conclusion

Green roof simulation is a subject that involves many domains. In this chapter of literature review three main areas have been reviewed. Firstly, a review of the current state of research of models for green roofs, which falls into two categories, the stands alone models and the models integrated to building energy simulation programs, is

presented. This has led to an explicit set of statements of research gap that this research aims to address. Secondly, as the research is aimed to integrate a new model for green roofs to a whole building energy simulation program, the ESP-r, the relevant features of this program is highlighted. Finally, as the soil vegetation atmosphere models provide detailed relevant theoretical background knowledge required for the green roof simulations, a review of some key models has been presented. The new model from this research, which combines many features of the models discussed in this chapter, is presented in the next chapter.

CHAPTER 3

DEVELOPMENT OF A GREEN ROOF MODEL
AND ITS INTEGRATION INTO THE ESP-r

3. Development of a green roof model and its integration into the ESP-r

3.0 Introduction

The objective of this chapter is to describe the theoretical formulation of the green roof model which is used in the building simulation. The chapter starts with an explicit listing of model assumptions followed by an explanation of the control volumes approach to the modelling which includes the model's mass and energy balance equations. The solution process to establish the two types of state variables namely temperatures of control volumes and matric potential of soil layers is explained. The chapter concludes with the description of details of integration of the newly developed model into ESP-r simulation.

3.1 Model Assumptions

The model represents the dynamic characteristics of green roofs. To be able to model the physical system a set of assumptions are employed, which are a necessary compromise to the complexity of the system but sufficiently addressing the physical variables within the required accuracy[61]. These assumptions are summarized below:

1. The thermal and moisture fluxes are considered one dimensional, in a vertical direction. The area of roof is usually large enough so that sideways advection flux can be neglected. The roof is horizontal, which is generally the case for green roofs[11]

2. At the interface between the lowest soil layer and structural roof, where the drainage layer is located, heat exchange is purely conduction. This is required as the design variations in green roofs differ so much. Adaptation of a single type of geometry for the air gap at this interface is not going to be representative of most green roof types. Moreover as this drainage space is often traversed by water, it is reasonable to assume uniform temperature within this space.

3. Physical properties within a control volume are uniform. This is also true for the plant layer where a definite leaf area index represents a uniform canopy distribution.

4. For the soil's moisture retention characteristics a uniform retention curve is assumed. Hysteresis effects on drying and wetting directions of the curves are neglected.

5. Phase changes due to evaporation and transpiration are assumed to occur only from the top soil surface and at leaves' surface.

6. Wind profile over the green roof plants is assumed logarithmic extending to a 2m height above the vegetation [62].

7. Plant leaves are considered as a control volume and they are actively contributing in the thermal and moisture exchanges. No heat exchange occurs through plant stems to ground.

8. Plant stomata openings on plant leaves are uniform on front and rear surfaces and respond in a similar manner to environmental stimulants. Moreover for heat exchange, the same air resistance is assumed for both sides of the leaves.

9. Plant roots are assumed to be evenly distributed across the soil layers. There are different types of plant-specific root profiles that are used in soil vegetation models. However in an artificial planting medium of limited size in green roofs, it is reasonable to assume that roots will grow densely thus justifying the assumption of even root density. Moreover, any specific profile assumption and additional calculations and user data requirements are not justified as the data are not available for the types of plants used in green roofs.

The above assumptions are applied to different elements of the model and for the reasons that are outlined above.

3.2 Discretisation of green roof components as control volumes

The construction details of a typical green roof is reviewed below which forms the basis of the control volume formulation of the green roof model. The physical components of a green roof can be considered as consisting of three layers: a plant canopy layer, a planting medium layer and an interface layer linking to the roof structure. The plants are selected vegetation types, usually natively adapted to the

building location thus requiring little maintenance and upkeep. The planting medium substrate is usually soil, but it can also be synthetic material or blends with specific moisture retention properties adapted to the local climate. Considerations in the selection of substrate include its ability to provide for the biological requirements of the plants, having sufficient strength as a building component and having a moisture retention characteristic suitable for the plant. Below the substrate/soil layer, there are some layers which vary according to the green roof's construction types (lighter extensive type or heavier intensive types) and green roof designs. For example, a filter layer could be included to retain finer substrate particles, drainage layers to allow excess moisture drainage (some designs recommend a water retention design which will facilitate as water source during dry spells), a root barrier for preventing root growth beyond the substrate (depending on the root spreading characteristic of the plant), an insulation layer which is often part of the standard roof design (the location of which is below the roof structure for cold roof and above for warm roof) [10] and water proof or moisture barrier layer to protect insulation and roof from moisture ingression and a structural roof support construction.

The physical features of the green roof, as explained above, are represented in the model as control volumes. For the development of the model, three components are considered which are divided into seven control volumes (CV); plant is control volume 1(CV1); canopy air is CV2; CV3 through CV7 are soil layers, as shown in figure 3.1. Plant layer is treated as a separate control volume, without lumping it with canopy air to account for the specific heat and mass for exchanges such as transpiration. The justification for dividing the soil layer into five control volumes is to provide a division of layers to account for the dynamics of heat and moisture flow along the soil layer. The number of soil layers is fixed for the model as five based on the fact that the majority of green roof substrate depths do not exceed 0.5 m and soil grid spacing reported in SVAT models[58] is around 0.1 m. In the current model's matrix set of equations which is explained in section 3.3 and shown in figure 3-8, as the matrix is not symmetrical about the diagonal, the solution steps have been customized to deal with the specific five rows matrix. While a variable, user specified grid spacing according to the green roof construction is desirable, it is not within the scope of this research and it would involve a two-step development: one to incorporate a solver to accommodate a variable number of equations and two to establish a

guideline for grid spacing according to the dynamics of thermal and moisture fluxes in green roofs. Such an automated process for control volume discretization within the program can be achieved by following the concept of dwell time[46]. Dwell time is a function of thermal capacity, thermal conductivity and layer height. However the steps involved are complex and moreover the dwell time for the moisture transport is different from that of the thermal exchange. The issue of synchronization between the thermal and moisture exchanges also needs to be addressed if automatic discretisation is to be employed. Due to the above reasons the current model is limited to have five soil layers as fixed and the inclusion of variable number of soil layers is reserved for the next stage of model development as outlined in the suggestions for future work in section 6.5.

The method employed to model green roof in this research is the control volume principle in line with the definition of the control volume method as applied in the building simulation program ESP-r with which this model will be integrated. A comprehensive explanation of control volume method as applied to building energy simulation is provided in Clarke 2001 [46] along with its comparison with other numerical methods such as finite difference method. In the numerical method literature [63] three classic methods are identified for solving the physical models represented by partial differential equations: the finite difference method (FDM); the finite element method (FEM); and the control volume method (CVM). Of these the FDM is a differential method whereas CVM and FEM are integral methods. In FDM, the model's governing differential equation is approximated by a truncated Taylor series expansion representing the physical processes in a fixed number of nodes within the domain. In CVM, the physical domain is represented by an ensemble of elements in which the governing differential equation is integrated and the resultant equation is discretized. The mass and energy balances are important in CVM, where the conservation principles are applied by quantifying the incoming and outgoing quantities of mass/energy across the boundaries and their accumulation within the control volume. For the proposed green roof model control volume formulation in this thesis, no mathematical integration is performed on the governing equation. However, all component fluxes (mass and energy) are instead represented in discretized forms across top and bottom layers, the effect of which is the same as integrating the fluxes within these bounds[64]. For the one dimensional green roof model with equally sized

layers, the FDM and CVM method produce a similar set of algebraic equations to be solved. However, the term control volume is used for this model to be in par with the host building simulation program, the ESP-r.
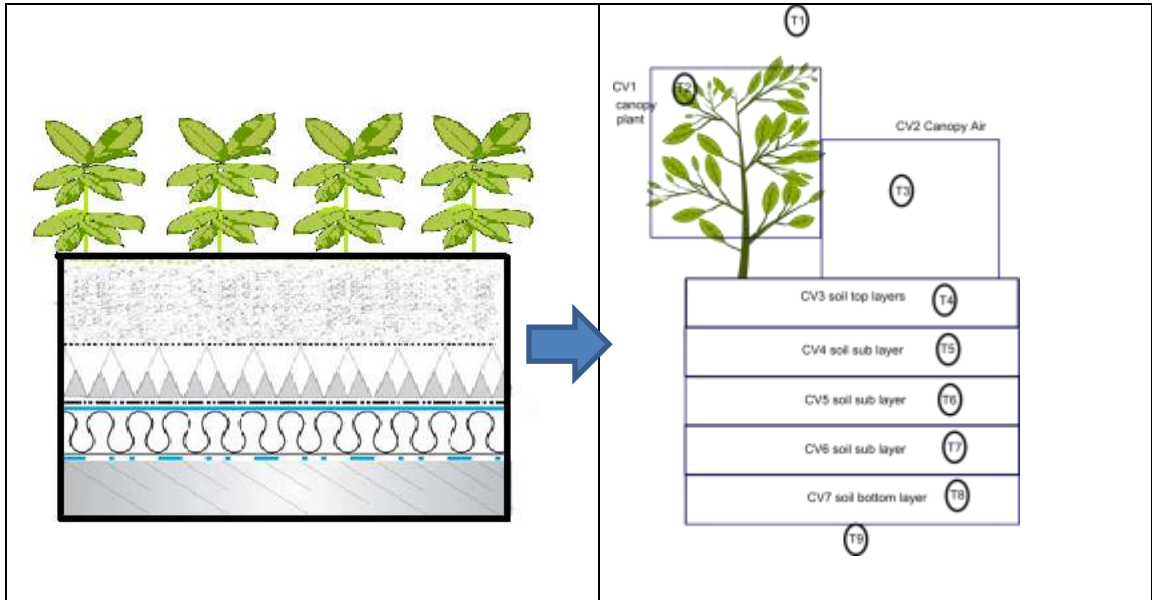
Figure 3-1 Control volume formation of new green roof model

In the following sections thermal and moisture balance equations for each control volume are explained. A detailed listing of the equations, the matrix coefficients obtained after discretisation, and references are given in appendix 3.1

3.2.1 Thermal balance

3.2.1.1 Control volume CV1 - plant

Thermal balance for plant and the constituent fluxes [9] are shown in figure 3.2. The energy balance is expressed as:

$$\rho_p C_p dLAI \frac{dT_p}{dt} = \phi_{rad,sol} + \phi_{rad,long} + \phi_{conv,\alpha-p} - \phi_{conv,p-ca} - \phi_{trans,p-ca}$$

(3-1)

where ρ_p is the leaf density [kg/m^3], C_p is leaf specific heat [J/kgK], d is leaf thickness [m], LAI is leaf area index [m^2/m^2], T_p is plant temperature and t is time [s]. The sign convention used in this and subsequent equations are based on an arbitrary heat flow form CV1 through CV7, treating heat gains as positive and heat losses as negative for the CV under consideration. Obviously the evolution of the state variables will justify

40

the final direction of flux. The thermal exchanges [W/m^2] that are considered for the plant, as shown in equation 3.1 and as numbered in figure 3.1 are: short wave solar radiation received by plant leaves $\phi_{rad,sol}$ ① , convective heat exchange with ambient air $\phi_{conv,\alpha-p}$②, long wave heat exchanges $\phi_{rad,long}$ with sky ③ and with soil surface ④, heat loss due to transpiration heat $\phi_{trans,p-ca}$ ⑤, and convective heat exchange with canopy air $\phi_{conv,p-ca}$ ⑥
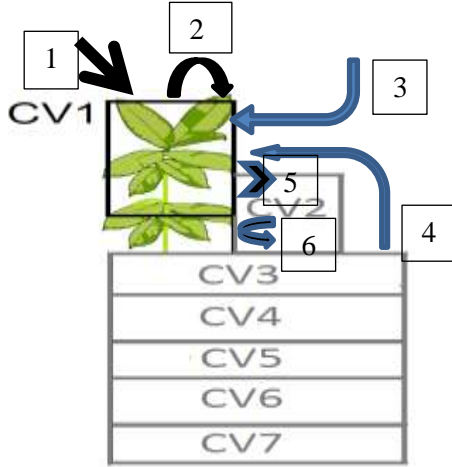
Figure 3-2: Thermal exchanges in control volume 1 –plant

The short wave solar radiation absorbed by the plant is given by [9]:

$$\phi_{rad,sol} = \left[1 - \tau_s - (1 - \tau_s)\rho r_\alpha\right]\left(1 + \tau_s \rho r_g\right)\phi_s \tag{3-2}$$

where ϕ_s is the global horizontal solar radiation, τ_s is the transmittance of canopy, ρr_α is the bulk canopy reflectance and ρr_g is the ground reflectance.

Short wave transmittance τ_s is calculated from LAI and coefficient of extinction for shortwave radiation k_s as:

$$\tau_s = e^{(LAI\ k_s)} \tag{3-3}$$

Long wave radiation exchange with sky and soil surface is given by

$$\phi_{rad,long} = h_{r,sky}\left(T_{sky} - T_p\right) + h_{r,s1}\left(T_{s1} - T_p\right) \tag{3-4}$$

where T_{sky} is sky temperature [K], T_{s1} is soil top layer temperature and $h_{r,s1}$ and $h_{r,sky}$ are linearized radiation transfer coefficients [W/m^{2}K]. Soil to plant radiation transfer coefficient is given by:

$$h_{r,s1} = 4(1 - \tau_l)\varepsilon_{p-s1}\sigma\left(\frac{T_{S1} + T_p}{2}\right)^3 \tag{3-5}$$

where τ_l is the canopy transmittance for long wave radiation, ε_{p-s1} is the effective emissivity between plant and soil surfaces [29], σ is the Stefan Boltzmann constant [W/m²K⁴].

Long wave transmittance τ_l is calculated from LAI and coefficient of extinction for longwave radiation k_l as:

$$\tau_l = e^{(LAI\ k_l)} \tag{3-6}$$

The effective emissivity between plant and soil is given by:

$$\varepsilon_{p-s1} = \frac{1}{\left(\dfrac{1}{\varepsilon_p} + \dfrac{1}{\varepsilon_{s1}} - 1\right)} \tag{3-7}$$

where ε_p is the emissivity of leaves and ε_{s1} is the emissivity of the soil [29], assuming the view factors between plant canopy and soil is similar to that between two parallel plates of infinite lengths. Tabares-Velasco and Srebric [29] conducted experiments to evaluate the difference between various assumptions for evaluating the radiation exchanges between soil and plant of green roof. The authors found that the more detailed assumptions such as parallel plates where the areas between plants and soil were different did not produce results that were significantly different from the default "equal areas" case [29]. Tabares-Velasco and Srebric therefore concluded that it was not necessary to use additional inputs such as view factors and plant heights for explicitly modelling complex radiation heat exchange between soil and plants. The close match in results for various assumptions, was also attributed to the fact that the emissivity values of soil surface and leaves are identical and are close to one (0.95 and 0.96 respectively as explained in section 4.5 in chapter 4).

Linearized radiation transfer coefficient between plant and sky is given by:

$$h_{r,sky} = 4(1 - \tau_l)\varepsilon_p\sigma\left(\frac{T_{sky} + T_p}{2}\right)^3 \tag{3-8}$$

It should be noted that sky temperature T_{sky} is not a state variable and it is taken from existing routines in ESP-r [65].

Convection heat exchange between plant and ambient air is given by

$$\phi_{conv,\alpha-p} = \sigma_f \frac{\rho_\alpha Cp}{r_{e\alpha}} \left(T_\alpha - T_p\right)$$

(3-9)

where σ_f is fractional vegetation coverage [-], ρ_α is the air density [kg/m^3], C_p is air specific heat [J/kg K], $r_{e\alpha}$ is the aerodynamic resistance to heat transfer [s/m] and T_α is ambient air temperature [K].

Convection with canopy air is given by:

$$\phi_{conv,p-ca} = 2LAI \frac{\rho_{ca} Cp}{r_e} \left(T_p - T_{ca}\right)$$

(3-10)

where r_e is the canopy air resistance to heat transfer, LAI is the leaf area index, ρ_{ca} is the canopy air density. 2 LAI is used to account for the contact areas at front and rear surfaces of leaves.

Transpiration is a one way heat exchange, which occurs only if a vapour pressure deficit exists in canopy air. Transpiration heat loss of plant is given by:

$$\phi_{trans,p-a} = 2LAI \frac{\rho_{ca} Cp}{\gamma(r_e + r_i)} \left(e_p - e_{ca}\right)$$

(3-11)

where γ is the psychometric constant [Pa/K], r_i is the stomatal resistance aggregated at plant level, e_p is the vapour pressure at leaf tissues (taken as equal to saturated vapour pressure at plant temperature) [Pa] and e_{ca} is the canopy air vapour pressure [Pa].

3.2.1.2 Control volume CV2 - canopy air

Heat exchanges in canopy air (CV2) consist of three convective heat exchanges, with plants, with ambient air and with soil surface, as shown in figure 3.3.
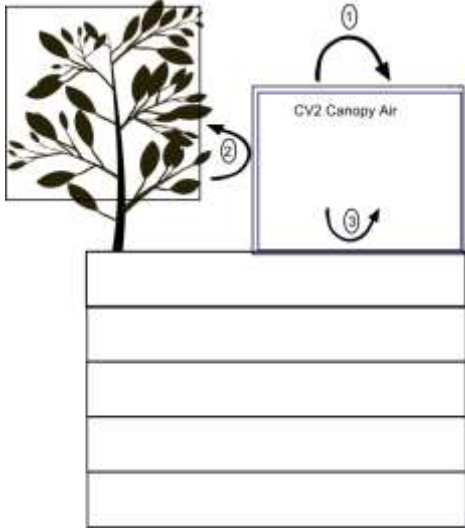
Figure 3-3: canopy air thermal exchanges

$$\rho_{ca} Cpl \frac{dT_{ca}}{dt} = \phi_{conv,p-ca} - \phi_{conv,ca-s1} + \phi_{conv,\alpha-ca} \qquad \text{(3-12)}$$

where l is the canopy height [m], T_{ca} is the canopy air temperature [K], $\phi_{conv,p-ca}$ is the convective heat exchange with plant ②, $\phi_{conv,ca-s1}$ is the convective heat exchange with soil ③ and $\phi_{conv,\alpha-ca}$ is the convective heat exchange with the ambient air ①. These convective exchanges use the following air resistances; r_{ea} plant to canopy air resistance, $r_{e\alpha}$ canopy to ambient air resistance and r_{s1-ca} soil surface to canopy air resistance. An additional moisture dependant surface resistance r_s is used for the soil surface. The air side resistances are as per reference [66] and the surface resistance as per reference [67] and their details are provided in appendix 3.1

Convective heat exchange with soil is given by:

$$\phi_{conv,ca-s1} = \frac{\rho_{ca} Cp}{r_{s1-ca} + r_s} (T_{ca} - T_{s1}) \qquad \text{(3-13)}$$

Convective heat exchange with the ambient air is given by:

$$\phi_{conv,\alpha-ca} = \frac{\rho_\alpha Cp}{r_{e\alpha}} (T_\alpha - T_{ca}) \qquad \text{(3-14)}$$

3.2.1.3 Control volume CV3 - top soil layer

Soil surface layer S1 is the control volume CV3 in the model. Figure 3.4 shows the thermal exchanges in CV3 and are given by:
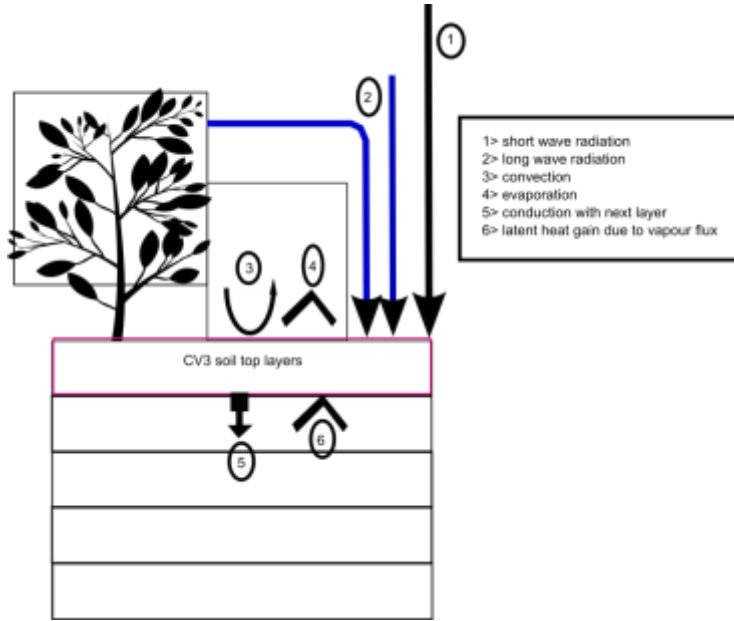
Figure 3-4 : Thermal exchanges in CV3, soil top control volume

$$C_{s1}S1\frac{dT_{s1}}{dt} = \phi_{s,s1} + \phi_{lw,sky-s1} + \phi_{lw,p-s1} + \phi_{conv,ca-s1} - \phi_{evap,s1-ca} - \phi_{cond,s1-s2} + \phi_{vap,s1-s2}$$

(3-15)

where C_{s1} is the volumetric specific heat of soil composition [J/m^{3}K] , S1 is the height of soil top layer [m] and T_{s1} is the temperature of soil top layer[K]. The constituent heat exchanges are as shown in the following relations 3.16 through 3.23.

Solar radiation received at the soil surface $\phi_{s,s1}$ ① is the fraction transmitted through canopy minus the part reflected from soil surface and is given by:

$$\phi_{s,s1} = \left(\tau_s - \tau_s \rho r_g\right)\phi_s$$

(3-16)

where ϕ_s is the total solar radiation incident on the green roof (calculated from ESP-r by using the ESP-r's solar radiation processing routines.)

The longwave heat gains ② from the sky $\phi_{lw,sky-s1}$ and from the plant $\phi_{lw,p-s1}$ are given by (although it is stated here as heat gains, as mentioned in section 3.2.1.1 regarding the sign convention used in this model, it can be a heat exchange in either direction; a positive value indicate a heat gain and a negative value indicate a heat loss):

$$\phi_{lw,sky-s1} = \tau_l h_{r,sky-s1}(T_{sky} - T_{s1})$$

(3-17)

$$\phi_{lw,p-s1} = (1-\tau_l)h_{r,p-s1}(T_p - T_{s1})$$

(3-18)

where the linearized radiation transfer coefficients $h_{r,sky-s1}$ and $h_{r,p-s1}$ are defined in a manner similar to that given in equations 3-5 and 3-8. Detailed listing of all equations and related terms are given in appendix 3.1

$\phi_{conv,\alpha-s1}$ is the convective heat exchange ③, between the soil surface and canopy air and has been defined before in equation 3-13.

$\phi_{evap,s1-\alpha}$ is the heat loss ④ from the soil surface due to evaporation, driven by the vapour pressure deficit of the soil surface ($e_{s1}-e_{ca}$) and across the same resistance ($r_{s1-a}+r_s$) as for the thermal exchange.

$$\phi_{evap,s1-ca} = \frac{\rho_{ca}Cp}{\gamma(r_{s1-ca} + r_s)}(e_{s1} - e_{ca})$$

(3-19)

$\phi_{cond,s1-s2}$ is the conduction heat loss to the lower layer ⑤ as given in equation 3-21, which is the discretized form of equation 3-20, using an average thermal conductivity of the S1 and S2 layer (λ_{S1S2}) and the temperature gradient ($T_{s1}-T_{s2}$) across an interlayer distance of S1S2

$$\phi_{cond} = \lambda\frac{dT}{dz}$$

(3-20)

$$\phi_{cond,s1-s2} = \lambda_{s1s2}\frac{(T_{s1} - T_{s2})}{S1S2}$$

(3-21)

Heat gain due to vapour transport ⑥ $\phi_{vap,s2-s1}$ is given in equation 3-23 which is the discretized form of equation 3-22, using average values of isothermal (pressure driven) vapour conductivity KΨ and thermal vapour conductivity KT, between S1 and S2 layers. L is the latent heat of water and is equal to 2260 kJ/kg

$$\phi_{vap} = LK_{vT\_m}\frac{dT}{dz} + LK_{v\Psi\_m}\frac{d\psi}{dz}$$

(3-22)

$$\phi_{vap,s1-s2} = LKT_{m,s1s2}\frac{T_{s1} - T_{s2}}{S1S2} + LK\Psi_{m,s1s2}\frac{\psi_{s1} - \psi_{s2}}{S1S2}$$

(3-23)

Here it should be noted that the direction of heat flux due to vapour exchange [58] is shown in the upward direction (from S2 to S1), similar to the soil surface evaporation. However, the direction will be adjusted on its own, as the vapour flux $\phi_{vap,s1-s2}$ as consisting of two components, (a temperature difference driven thermal vapour flux

component and a matrix potential difference driven isothermal vapour flux component), is with a plus sign in the net energy balance equation 3.15 and the driving variables (T_{s1}, T_{s2}, ψ_{s1} and ψ_{s2}) are ordered from top to bottom consistently in the subsequent lower layers (equations 3.26 and 3.30). The numerical values of the heat exchanges due to vapour fluxes have been found to be comparatively very small, so that its effect on the overall energy balance is very little. Also the subscript m indicates the respective coefficients are in mass units, in order to obtain the vapour flux in [kg/s], which in turn when multiplied by the latent heat [J/kg] it will be converted to heat flux in [W].

3.2.1.4 Control volume CV4 toCV6 - intermediate soil layers

Thermal exchanges for soil mid layer S2, control volume CV4, are shown in figure 3.5, which is also representative of all the intermediate soil layers.
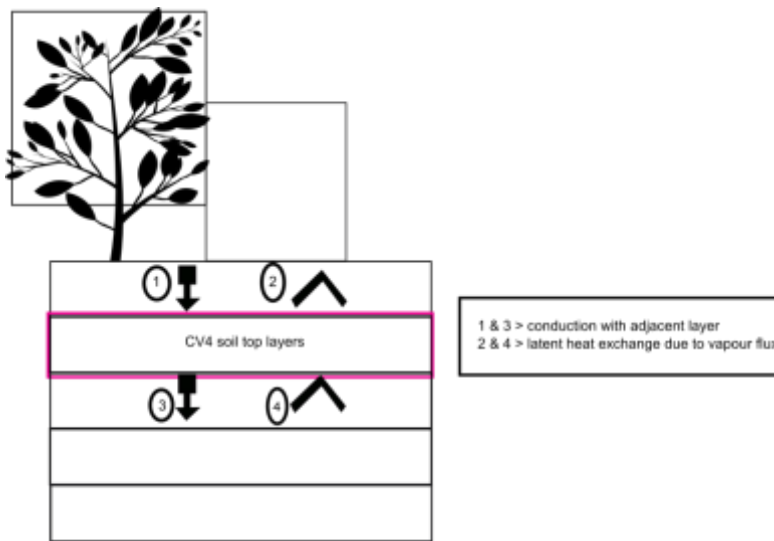
Figure 3-5: Thermal exchanges in CV4; also representative of other intermediate layers (CV5 and CV6)

The energy balance for this control volume is given by:

$$C_{s2}S2\frac{dT_{s2}}{dt} = \phi_{cond,s1-s2} - \phi_{cond,s2-s3} - \phi_{vap,s1-s2} + \phi_{vap,s2-s3}$$

(3-24)

Conduction heat exchanges are $\phi_{cond,s1\text{-}s2}$ ① and $\phi_{cond,s2\text{-}s3}$ ③ and vapour thermal exchanges are $\phi_{vap,s1\text{-}s2}$ ② and $\phi_{vap,s2\text{-}s3}$ ④. In a similar way as in equation 3.21 and 3.23, the exchanges of heat between soil layers S2 and S3 are defined by:

$$\phi_{cond,s2-s3} = \lambda_{s2s3} \frac{\left(T_{s2} - T_{s3}\right)}{S2S3}$$

(3-25)

$$\phi_{vap,s3-s2} = LKT_{m,s2s3} \frac{T_{s2} - T_{s3}}{S2S3} + LK\Psi_{m,s2s3} \frac{\Psi_{s2} - \Psi_{s3}}{S2S3}$$

(3-26)

The average properties for the thermal vapour conductivity (KT) and the isothermal vapour conductivity (KΨ) are similar to that for thermal conductivity (λ) across the soil layers and interlayer distance S2S3 is similar to S1S2

3.2.1.5 Control volume CV7 - soil bottom layer

Thermal exchanges at the lowest soil layer S5, control volume CV7, is as shown in figure 3.6.
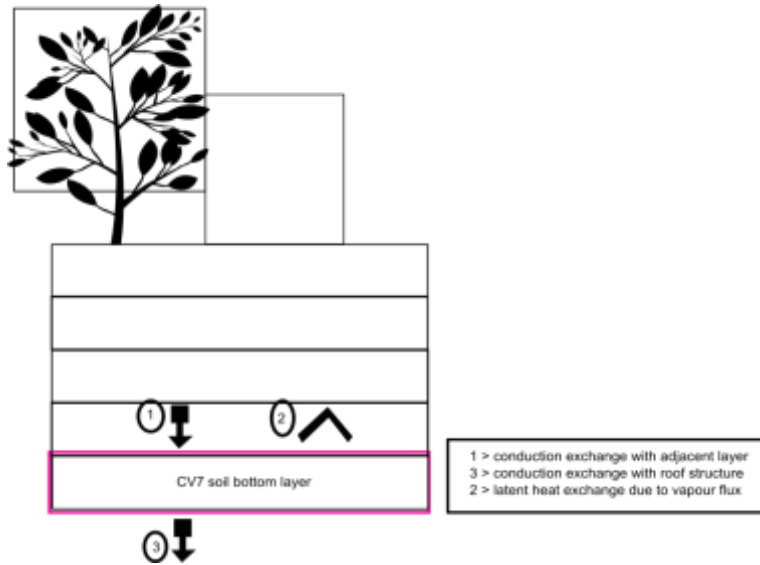
Figure 3-6: Thermal exchanges in CV7 lowest layer

$$C_{s5}S5\frac{dT_{s5}}{dt} = \phi_{cond,s4-s5} - \phi_{cond,s5-x} - \phi_{vap,s4-s5}$$

(3-27)

$\phi_{cond,s4\text{-}s5}$ ① and $\phi_{cond,s5\text{-}x}$ ③ are conduction heat exchanges and $\phi_{vap,s4\text{-}s5}$ is the vapour thermal exchange② with the previous layer. Here T_x represents the bottom boundary temperature of the green roof, which is the variable of exchange at every

time step with the ESP-r's building thermal domain. S5X is taken as half of the layer's thickness.

Definition of conduction vapour fluxes and vapour thermal fluxes are similar to those of the previous layers and are given by equations 3.28 to 3.30:

$$\phi_{cond,s4-s5} = \lambda_{s4s5} \frac{(T_{s4} - T_{s5})}{S4S5}$$
(3-28)

$$\phi_{cond,s5-x} = \lambda_{s5x} \frac{(T_{s5} - T_x)}{S5X}$$
(3-29)

$$\phi_{vap,s4-s5} = LKT_{m,s4s5} \frac{T_{s4} - T_{s5}}{S4S5} + LK\Psi_{m,s4s5} \frac{\psi_{s4} - \psi_{s5}}{S4S5}$$
(3-30)

3.2.2 Moisture balances

The moisture balances in the model are of two parts, a modified Richard's equation based water infiltration into soil [60] for the soil control volumes and a mass balance equation based vapour exchange[32] at canopy air. In iterations, the model solves both of these parts in sequence seeking an overall mass balance. The lower boundary condition for the moisture part is the drainage. Thus unlike the thermal domain of the green roof, the moisture domain is not directly coupled to the building simulation by way of exchanging moisture state variables. However the effect of moisture is on the thermal side state variable (temperature) which is coupled to the building side by way of temperature of the lowest control volume. The building side temperature serves as green roof model's lower boundary condition and the green roof's lowest temperature serves as the boundary temperature for the building's simulation.

The mass balance equation for soil is given by:

$$C_\theta \frac{d\psi}{dt} = \frac{\partial}{\partial z}\left[\left(K_{L,\psi} + K_{v,\psi}\right)\left[\frac{\partial \psi}{\partial z} + 1\right] + \left(K_{L,T} + K_{v,T}\right)\frac{\partial T}{\partial z}\right] - S$$
(3-31)

where ψ is the soil matric potential [m](state variable for moisture domain), C_θ is the specific water content, also known as capillary capacity or differential water capacity [1/m]; $K_{L,\psi}/K_{v,\psi}$ – isothermal liquid and vapour conductivity respectively [m/s] ; $K_{L,T}/K_{v,T}$ – thermal liquid and vapour conductivity respectively [m^2/s K]; S-root

uptake [$m^3/m^3 s=1/s$] of water. For the top soil layer, moisture balance also includes the boundary fluxes of, intercepted precipitation and irrigation (P0) and soil top evaporation (Ev), as shown in equation 3.32.

$$C_\theta \frac{d\psi}{dt} = \frac{\partial}{\partial z}\left[\left(K_{L,\psi}+K_{v,\psi}\right)\left[\frac{\partial \psi}{\partial z}+1\right]+\left(K_{L,T}+K_{v,T}\right)\frac{\partial T}{\partial z}+P0-Ev\right]-S \tag{3-32}$$

Here the units of precipitation and evaporation fluxes are [$m^3/m^2 s=m/s$].

The exact equations for each control volume (and their time/space discretised forms) are given in Appendix 3.2

A separate equation (equation 3.33) is used for the moisture balance at canopy air to account for transpiration from plants $\phi_{vap,p\text{-}ca}$ [kg/m^2 s], evaporation from soil top $\phi_{vap,s1\text{-}ca}$ and vapour exchange with the outside air $\phi_{vap,\alpha\text{-}ca}$ (the subscript 'α' refers to ambient air and 'ca' refers to canopy air)

$$\phi_{vap,ca-\alpha} = \phi_{vap,p-ca} + \phi_{vap,s1-ca} \tag{3-33}$$

The transpiration $\phi_{vap,p\text{-}a}$ is driven by the vapour pressure deficit of the canopy air, as:

$$\phi_{vap,p-ca} = 2LAI\frac{\rho_a Cp}{\gamma L(r_e+r_i)}\left(e_p-e_{ca}\right) \tag{3-34}$$

The soil top evaporation $\phi_{vap,s1\text{-}a}$ is driven by the difference between the soil top vapour pressure and canopy vapour pressure, as:

$$\phi_{vap,s1-ca} = \frac{\rho_a Cp}{\gamma L(r_{s1-ca}+r_s)}\left(e_{s1}-e_{ca}\right) \tag{3-35}$$

Canopy -ambient vapour exchange $\phi_{vap,\alpha\text{-}ca}$ is caused by the respective vapour pressure difference.

$$\phi_{vap\alpha-ca} = \frac{\rho_\alpha Cp}{\gamma L r_{e\alpha}}\left(e_\alpha-e_{ca}\right) \tag{3-36}$$

Canopy vapour pressure e_{ca} is solved from these equations (3.33 to 3.36), which is a boundary condition for the soil side Richard's equation and thus acts as a point of coupling between the two different mass balance equations (3.32 and 3.33). Also, the soil vapour pressure e_{s1}, is a function of soil matric potential ψ_{s1}. The plant moisture

state is determined by the vapour pressure e_p, which is the saturated vapour pressure at the plant temperature.

Although it may seem logical to solve these two domains of equations (3.32 and 3.33) simultaneously, there are some stability issues involved, as it was found during the development stages of this research. One of the reasons for the instability is the fact the mass balance equations for soil evaporation and plant transpiration are irreversible. Mathematically possible conditions of ($e_{ca}>e_p$) and ($e_{ca}>e_{s1}$) have no physical significance. That is to say that moisture does not go back into the plant leaves and soils in a reverse flow. When solving separately, in the canopy vapour pressure equations (3.33 to 3.36), it is possible to incorporate such limiting conditions ($e_{ca}>e_p$, etc.).

The state variable for the moisture balances is matric potential (ψ) which is defined as the energy required extracting unit mass of water from soil [J/kg or Pa or m]. Matric potential is related to moisture content θ [m^3/m^3] in the model by using van Genuchten moisture retention curve [37], which is given by equation 3.37.

$$\theta(\psi) = \theta_r + \frac{\theta_s - \theta_r}{[1 + (\alpha 1 |\psi|)^n]^{1-\frac{1}{n}}} \qquad (3\text{-}37)$$

where θ_s is the saturated moisture content [$m^3 m^{-3}$], θ_r is the residual moisture content [$m^3 m^{-3}$], $\alpha 1$ is a parameter related to the inverse of the air entry suction ($\alpha 1>0$) [m^{-1}], and n is a measure of the pore-size distribution,(n>1 and dimensionless). Methods to determine these parameters are described in chapter 5. For saturated soil and supersaturated soil ($\Psi \geq 0$), $\theta(\Psi)= \theta_s$. These van Genuchten soil parameters are determined from the twelve soil texture classes. Figure 3.7 shows an example of the ψ/θ relation for loam textured soil.
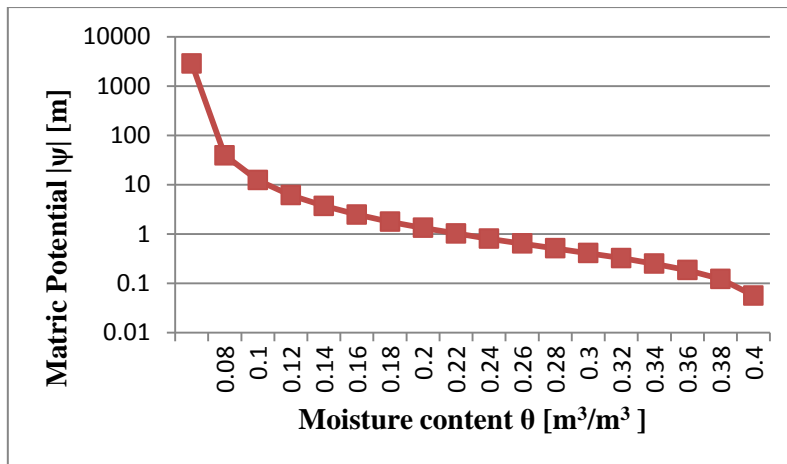
Figure 3-7: van Genuchten moisture curve for loam type of soil

3.3 Numerical implementation

The thermal and mass balance equations described in the previous section are solved separately in succession, by using a semi implicit Crank-Nicolson control volume scheme. The steps involved in obtaining the coefficients of the set of linear equations are:

1. The equations for control volumes, which are differential equations of time derivatives, are discretized in time steps, i.e., the differential terms of the energy and moisture balance equations are replaced by a forward difference expression of explicit nature. '*Explicit*' because they are expressed in terms of present time step values;

2. An '*implicit*' form of the same equation for each energy/moisture balance is created. In implicit form of the equation, the right hand side terms use future time step values;

3. The implicit expression is multiplied by weighing factor α ($0 < \alpha < 1$), the explicit expression by $(1 - \alpha)$ and the two added together to give one equation. When using the Crank-Nicolson scheme, the weighing factor α, is given a value of 0.5, which makes the solution of the differential equation unconditionally stable.

4. The equation is rearranged in a specific manner (all future time row terms on the left hand side of the equation and all present time row terms and flux injections on the right hand side of the equation) to obtain three types of coefficients: self-coupling coefficients are those associated with nodal temperature (or matric potential) of the

52

control volume in consideration, cross coupling coefficients are those associated with the nodal temperatures (or matric potential) of the neighbouring control volumes and right-hand side coefficients are those remaining of known values.

5. All the equations for mass and energy balance for all seven control volumes can be arranged in a matrix form of linear equations as shown in figures 3.8 (thermal domain matrix) and 3.9 (moisture domain matrix).

The thermal domain matrix set of equations consist of a 7x9 matrix [A] of future time coefficients, a 9x1 matrix [T^f] of future values of state variables, a 7x9 matrix [B] of present time coefficients, a 9x1 matrix [T^p] of present values of state variables and a 7x1 matrix [C] of thermal fluxes. The matrix form of equation can be summarized as:

$$[A][T^f] = [B][T^p] + [C] = [Z]$$ (3-38)

where [Z] is a 7x1 matrix obtained by the matric calculation of right hand side known matrices.

For the moisture domain, the matrix equation consist of a 5x5 matrix [M] of future coefficients, a 5x1 matrix [ψ^f] of future values of state variables a 5x5 matrix [N] of present time coefficients, a 5x1 matrix [ψ^p] of present values of state variables and a 5x1 matrix [Q] of moisture fluxes. The matrix form of equation can be summarized as:

$$[M][\psi^f] = [N][\psi^p] + [Q]$$ (3-39)

6. The solution procedure is with Gaussian elimination steps as given in Clarke [46] . For the thermal domain (equation 3.38) , the boundary conditions (Namely ambient air temperature above green roof and building side roof temperature obtained from ESP-r) are moved to the right side leaving a set of seven equations and seven unknowns. For the moisture side, (equation 3.38) the flux boundary conditions (evaporation, precipitation and irrigation at the top of green roof and potential drainage at the bottom) are included in the matrix elements [Q] or calculated in successive iterations. In the Gaussian elimination procedure, matrix elementary row operations are performed to get zeroes below the diagonal of [A] and [M]. Then, in a set of backward substitution steps, all state variables are determined starting from the last and continuing up to the first.

7. After solving for the state variables a new set of coefficients are calculated, and the process of solving for the state variables is repeated. This is continued until the evolution of the state variables converge within an acceptable limit of variation within the state variable. Currently the convergence criteria for the thermal loop are taken as a variation of 0.01 K in the temperatures of all control volumes and that of the moisture loop is 0.01 m in matric potential variation. These convergence criteria were selected after testing the program for its ability to converge for various ranges of values and thus can be described as the most optimum convergence limit of the newly developed program with its current configurations. These values are much smaller than the measurement resolutions of typical sensors; for example the temperature sensors of PTC type used for the validation part of this research are of resolution of 0.1 K. In successive iterations the present value of state variable is taken as the future value of the last time step and is fixed throughout the iteration cycles. Moreover, the equations are highly non-linear in nature and attempts to introduce the Newton Raphson method [68] for root finding algorithm were not successful due to stability issues in both thermal and moisture loops. For each of the state variables that are being solved in the program, a check is done to identify if the variable is changing value towards the opposite direction as compared to the previous time step. An increase followed by a decrease or a decrease then an increase is tested by statements such as *'if incr*incrm1 <0'*, where *incr* is the current step increment and *incrm1* is the previous step increment. The current increment is then compared against the convergence limit to ensure positive convergence. Given the possibility that the above two methods may miss to find the root in certain cases, an additional convergence check is performed by confirming that the cumulative value of the increments over ten successive steps of the iterations is less than a test value (such as 0.1K in thermal loops). Once a state variable is confirmed as converged, its value remains fixed for the remaining iterations. Also, a variable is available for debugging purposes to confirm that all state variables are converged within a maximum limit of the loop count of the iterations cycle.

As an example, the above steps are illustrated for the thermal balance equation of plant CV1, in table 3.1 and table 3.2, where equation 3.1 has been expanded and converted to a form for integration with ESP-r. All thermal and moisture equations for each control volume, their coefficient forms and the derivation of each term are listed in appendices 3.1 (thermal domain) and 3.2 (moisture domain)

Table 3-1: Example of steps illustrated for the derivation of coefficient form of the thermal balance equation for the plant (CV1)

Step 1. Explicit form of discretized equation in terms of present time row
$$\rho_p C_p dLAI\left(\frac{T_p^{t+\Delta t} - T_p^{t}}{\Delta t}\right) = ([1-\tau_s - (1-\tau_s)\rho r_\alpha](1+\tau_s\rho r_g))\phi_s^t + h_{r,sky}^t(T_{sky}^t - T_p^t)$$ $$+ h_{r,s1}^t(T_{s1}^t - T_p^t) + \sigma_f \frac{\rho_\alpha Cp}{r_{ea}^t}(T_\alpha^t - T_p^t)$$ $$- 2LAI\frac{\rho_{ca}Cp}{r_{ea}^t}(T_p^t - T_{ca}^t) - 2LAI\frac{\rho_{ca}Cp}{\gamma(r_{ea}+r_i)^t}(e_p^t - e_{ca}^t)$$
Step 2. Implicit form of discretized equation in terms of future time row
$$\rho_p C_p dLAI\left(\frac{T_p^{t+\Delta t} - T_p^{t}}{\Delta t}\right) = ([1-\tau_s - (1-\tau_s)\rho r_\alpha](1+\tau_s\rho r_g))\phi_s^{t+\Delta t} + h_{r,sky}^{t+\Delta t}(T_{sky}^{t+\Delta t} - T_p^{t+\Delta t})$$ $$+ h_{r,s1}^{t+\Delta t}(T_{s1}^{t+\Delta t} - T_p^{t+\Delta t}) + \sigma_f \frac{\rho_\alpha Cp}{r_{ea}^{t+\Delta t}}(T_\alpha^{t+\Delta t} - T_p^{t+\Delta t})$$ $$- 2LAI\frac{\rho_{ca}Cp}{r_{ea}^{t+\Delta t}}(T_p^{t+\Delta t} - T_{ca}^{t+\Delta t}) - 2LAI\frac{\rho_{ca}Cp}{\gamma(r_{ea}+r_i)^{t+\Delta t}}(e_p^{t+\Delta t} - e_{ca}^{t+\Delta t})$$
Step 3. Explicit equation multiplied by (1-α)
$$(1-\alpha)\rho_p C_p dLAI\left(\frac{T_p^{t+\Delta t} - T_p^{t}}{\Delta t}\right) = (1-\alpha)([1-\tau_s - (1-\tau_s)\rho r_\alpha](1+\tau_s\rho r_g))\phi_s^{t}$$ $$+ (1-\alpha)h_{r,sky}^t(T_{sky}^t - T_p^t) + (1-\alpha)h_{r,s1}^t(T_{s1}^t - T_p^t)$$ $$+ (1-\alpha)\sigma_f \frac{\rho_\alpha Cp}{r_{ea}^t}(T_\alpha^t - T_p^t)$$ $$- (1-\alpha)2LAI\frac{\rho_{ca}Cp}{r_{ea}^t}(T_p^t - T_{ca}^t) - (1-\alpha)2LAI\frac{\rho_{ca}Cp}{\gamma(r_{ea}+r_i)^t}(e_p^t - e_{ca}^t)$$
Step 3. Implicit equation multiplied by α
$$\alpha\rho_p C_p dLAI\left(\frac{T_p^{t+\Delta t} - T_p^{t}}{\Delta t}\right) = \alpha([1-\tau_s - (1-\tau_s)\rho r_\alpha](1+\tau_s\rho r_g))\phi_s^{t+\Delta t}$$ $$+ \alpha h_{r,sky}^{t+\Delta t}(T_{sky}^{t+\Delta t} - T_p^{t+\Delta t}) + \alpha h_{r,s1}^{t+\Delta t}(T_{s1}^{t+\Delta t} - T_p^{t+\Delta t})$$ $$+ \alpha\sigma_f \frac{\rho_\alpha Cp}{r_{ea}^{t+\Delta t}}(T_\alpha^{t+\Delta t} - T_p^{t+\Delta t})$$ $$- \alpha 2LAI\frac{\rho_{ca}Cp}{r_{ea}^{t+\Delta t}}(T_p^{t+\Delta t} - T_{ca}^{t+\Delta t}) - \alpha 2LAI\frac{\rho_{ca}Cp}{\gamma(r_{ea}+r_i)^{t+\Delta t}}(e_p^{t+\Delta t} - e_{ca}^{t+}$$

Table 3-2: Continuation of example of steps illustrated for the derivation of coefficient form of equation for plant

Step 4. Final equation in the coefficient form by adding previous two equations

$$-[\alpha\sigma_f\frac{\rho_\alpha Cp}{r_{e\alpha}^{t+\Delta t}}]T_\alpha^{t+\Delta t}$$

$$+[\frac{\rho_p C_p dLAI}{\Delta t} + \alpha h_{r,sky}^{t+\Delta t} + \alpha h_{r,s1}^{t+\Delta t} + \alpha\sigma_f\frac{\rho_\alpha Cp}{r_{e\alpha}^{t+\Delta t}} + \alpha\frac{2LAI\rho_{ca}Cp}{r_{e\alpha}^{t+\Delta t}}]T_p^{t+\Delta t}$$

$$-[\alpha\frac{2LAI\rho_{ca}Cp}{r_{e\alpha}^{t+\Delta t}}]T_{ca}^{t+\Delta t}$$

$$-[\alpha h_{r,s1}^{t+\Delta t}]T_{s1}^{t+\Delta t}$$

$$=$$

$$[(1-\alpha)\sigma_f\frac{\rho_\alpha Cp}{r_{e\alpha}^t}]T_\alpha^t$$

$$+[\frac{\rho_p C_p dLAI}{\Delta t} - (1-\alpha)h_{r,sky}^t - (1-\alpha)h_{r,s1}^t - (1-\alpha)\sigma_f\frac{\rho_\alpha Cp}{r_{e\alpha}^t} - (1-\alpha)\frac{2LAI\rho_{ca}Cp}{r_{e\alpha}^t}]T_p^t$$

$$+[(1-\alpha)\frac{2LAI\rho_{ca}Cp}{r_{e\alpha}^t}]T_\alpha^t$$

$$+[(1-\alpha)h_{r,s1}^t]T_{s1}^t$$

$$+[(1-\alpha)([1-\tau_s-(1-\tau_s)\rho r_\alpha](1+\tau_s\rho r_g))\phi_s^t + \alpha([1-\tau_s-(1-\tau_s)\rho r_\alpha](1+\tau_s\rho r_g))\phi_s^{t+\Delta t}]$$

$$+[(1-\alpha)h_{r,sky}^t T_{sky}^t + \alpha h_{r,sky}^{t+\Delta t}T_{sky}^{t+\Delta t}]$$

$$-[(1-\alpha)\frac{2LAI\rho_a Cp}{\gamma(r_{ea}+r_i)^t}e_p^t] - [\alpha\frac{2LAI\rho_a Cp}{\gamma(r_{ea}+r_i)^{t+\Delta t}}e_p^{t+\Delta t}]$$

$$+[(1-\alpha)\frac{2LAI\rho_a Cp}{\gamma(r_{ea}+r_i)^t}e_\alpha^t] + [\alpha\frac{2LAI\rho_a Cp}{\gamma(r_{ea}+r_i)^{t+\Delta t}}e_\alpha^{t+\Delta t}]$$

Step 5. Equivalent coefficient form by using matrix coefficients for the non-temperature parameters

$$a_{11} T_\alpha^{t+\Delta t} + a_{12} T_p^{t+\Delta t} + a_{13} T_{ca}^{t+\Delta t} + a_{14} T_{s1}^{t+\Delta t}$$
$$= b_{11} T_\alpha^t + b_{12} T_p^t + b_{13} T_{ca}^t + b_{14} T_{s1}^t + c_1$$

The same procedure is followed for the other six control volumes for the thermal exchanges in the green roof. The resulting seven equations expressed in the format as given in the last line of the table 3.2 is used to develop the matrix form of equation as in equation 3.38 and also shown in figure 3.8. This is subsequently used for solving for the set of state variables, namely the temperatures of the seven control volumes.

A similar set of procedure is done for the moisture balance in the five soil control volumes, resulting in a set of five equations. This is expressed in matrix form as in equation 3.39 and shown in figure 3.9. This is subsequently used to solve for the soil moisture state variables, namely the matric potentials of the five soil layers.

Figure 3.8 shows the matrix structure for thermal domain. The details of definition of the matrix elements (the coefficients: a11, a12 …; b11, b12…; c1, c2 …) are given in appendix 3.1. All of the coefficients are calculated after successive iterations, although

it is sufficient to calculate the future time row coefficients a11, a12 …which are dependent on the future values of state variables. In the current model of green roof, there are certain coefficients (such as a34 in appendix 3.1 that include soil specific heat) included among the future time row coefficients, present time row coefficients and right hand side coefficients which are dependent on the averages of present and future state variable values.

$$
\begin{pmatrix}
a11 & a12 & a13 & a14 & & & & \\
    & a22 & a23 & a24 & & & & \\
    & a32 & a33 & a34 & a35 & & & \\
    & & & a44 & a45 & a46 & & \\
    & & & & a55 & a56 & a57 & \\
    & & & & & a66 & a67 & a68 \\
    & & & & & & a77 & a78 & a79
\end{pmatrix}
\times
\begin{pmatrix}
T\alpha^{t+\Delta t} \\
Tp^{t+\Delta t} \\
Ta^{t+\Delta t} \\
Ts1^{t+\Delta t} \\
Ts2^{t+\Delta t} \\
Ts3^{t+\Delta t} \\
Ts4^{t+\Delta t} \\
Ts5^{t+\Delta t} \\
Tx^{t+\Delta t}
\end{pmatrix}
=
$$

$$
\begin{pmatrix}
b11 & b12 & b13 & b14 & & & & \\
    & b22 & b23 & b24 & & & & \\
    & b32 & b33 & b34 & b35 & & & \\
    & & & b44 & b45 & b46 & & \\
    & & & & b55 & b56 & b57 & \\
    & & & & & b66 & b67 & b68 \\
    & & & & & & b77 & b78 & b79
\end{pmatrix}
\times
\begin{pmatrix}
T\alpha^{t} \\
Tp^{t} \\
Ta^{t} \\
Ts1^{t} \\
Ts2^{t} \\
Ts3^{t} \\
Ts4^{t} \\
Ts5^{t} \\
Tx^{t}
\end{pmatrix}
+
\begin{pmatrix}
c1 \\
c2 \\
c3 \\
c4 \\
c5 \\
c6 \\
c7
\end{pmatrix}
=
\begin{pmatrix}
z1 \\
z2 \\
z3 \\
z4 \\
z5 \\
z6 \\
z7
\end{pmatrix}
$$

Figure 3-8: Coefficient matrix format of thermal domain

The moisture side matrix is as shown in figure 3.9, the details of the matrix elements (the coefficients: m11, m12 …; n11, n12…; q1, q2 …) are given in appendix 3.2

$$
\begin{pmatrix}
m11 & m12 & & & \\
m21 & m22 & m23 & & \\
& m32 & m33 & m34 & \\
& & m43 & m44 & m45 \\
& & & m54 & m55
\end{pmatrix}
\mathbf{X}
\begin{pmatrix}
\psi s1^{t+\Delta t} \\
\psi s2^{t+\Delta t} \\
\psi s3^{t+\Delta} \\
\psi s4^{t+\Delta t} \\
\psi s5^{t+\Delta t}
\end{pmatrix}
=
$$

$$
\begin{pmatrix}
n11 & n12 & & & \\
n21 & n22 & n23 & & \\
& n32 & n33 & n34 & \\
& & n43 & n44 & n45 \\
& & & n54 & n55
\end{pmatrix}
\mathbf{X}
\begin{pmatrix}
\psi s1^{t} \\
\psi s2^{t} \\
\psi s3^{t} \\
\psi s4^{t} \\
\psi s5^{t}
\end{pmatrix}
+
\begin{pmatrix}
q1 \\
q2 \\
q3 \\
q4 \\
q5
\end{pmatrix}
=
\begin{pmatrix}
y1 \\
y2 \\
y3 \\
y4 \\
y5
\end{pmatrix}
$$

Figure 3-9: Coefficient matrix format of moisture domain

The overall solution process consists of solving in sequence the thermal balance equation matrix (equation 3.38), canopy vapour pressure equations (equation 3.33 to 3.36) and the soil moisture balance equation matrix (equation 3.39) as illustrated in the process flow diagram in figure 3.10. The converging state variables of thermal and moisture states of the control volumes are rendering the thermal-moisture interactions. This is because the moisture and thermal coefficients of the successive solutions (and their constituent thermal and moisture characteristics), in turn, are calculated based on the successively evolving thermal and moisture state variables.
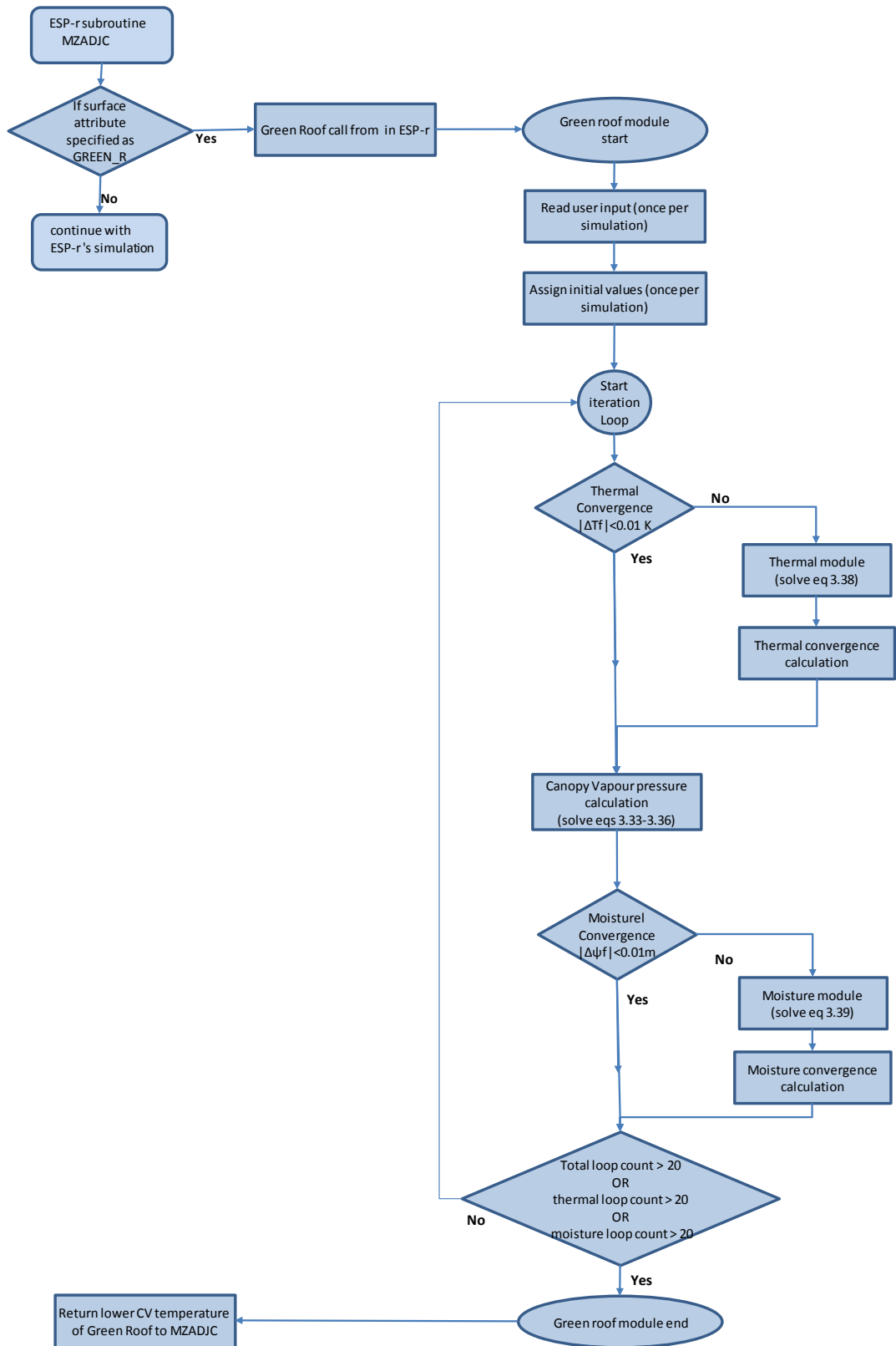
Figure 3-10: Green roof-module flow chart

3.4 Integration with ESP-r

The logic of code implementation in ESP-r is shown in figure 3.10. For thermal loops, the outside temperature as read from climatic file and the solar radiation flux are the top boundary conditions. The bottom boundary condition is the point of coupling with ESP-r, where ESP-r's outdoor surface layer temperature from the previous time-step is used in the green roof module as bottom boundary temperature (temperature T_x in figure 3.8). The model has a built in solver, solving the matrix set of equations (independent of ESP-r's matrix solver), so it can also be used with other building energy simulation programs, with minor adaptations. The choice of external coupling of the green roof module in ESP-r as compared to that incorporated into ESP-r global matrix scheme is based on the following factors:

1. Thermal-moisture coupling in green roof module involves evapotranspiration in addition to the inter-related thermal and moisture characteristics. For example canopy vapour pressure and plant temperature, soil surface resistance and soil moisture content, and stomatal resistance and plant temperature are interdependent thermal-moisture characteristics in the model. For effective thermal moisture coupling, the model needs to be iterated in successive thermal moisture loops, so that the thermal and moisture state variables converge in an interrelated manner.

2. In the green roof module the moisture movement is from outside to the point of interface (drainage layer in green roof), and at this position it adds to drainage rate. An independent moisture loop of the green roof module, as described in section 3.3, is needed to solve this.

3. The bottom boundary temperature of the green roof is a state variable within ESP-r and thus not easy to be modified. So an alternative is to use a new boundary condition for the ESP-r from the green roof module and to use the ESP-r's outdoor surface layer roof temperature as green roof module's boundary temperature.

4. It was observed during test runs, the manner of linkage between the green roof module and ESP-r, which can be described as integrated as boundary condition, is not computationally intensive.

Referring to figure 3.10, integration of the new green roof module with ESP-r involves interfacing with the MZADJC subroutine (in the source code file esrubld/adjb.F) which computes the adjacent temperatures and incident radiation fluxes for all surfaces defined for the building according to their types of surface associations. Examples of the surface boundary conditions are 'EXTERIOR', 'SIMILAR', 'ADIABATIC' etc. and a new type 'GREEN_R' for green roof has been included for the green roof modelling. Once this association is found the ESP-r calls the green roof module and provide the outside face roof surface temperature (of previous time step) which serves as bottom boundary condition for the green roof (T9 in figure 3.1). The radiation fluxes which are otherwise associated with an external surface are set to zero for GREEN_R boundary condition in a surface attribute. Similarly the convection heat exchange at this surface attribute is set to maximum, so that the green roof's lowest layer temperature become the boundary condition for ESP-r's external roof element. These are done by forcing radiation injection zero in MZADJC (where the user sets the usual roof's solar absorptance and transmittance to zero) and setting very high convective heat transfer coefficient (constant at 1000 W/m^{2}K) at the subroutine 'MZCONV' which is a controlling routing to calculate surface convection coefficients and this should be currently done manually by the user. After the green roof module calculates the bottom boundary temperature (T8 in figure 3.1) with the method described in this chapter, the control comes back to MZADJC with the newly found adjacent temperature that corresponds to the bottom layer of the green roof soil (T8 in figure 3.1).

The set of alterations that are done in ESP-r is provided in detail in appendix 4.

3.5 Summary

The structure of the newly developed green model is explained in this chapter starting with the specificities of individual control volumes and detailing the solution process. Within the new model, coupling has been achieved between thermal and moisture exchanges and between control volumes. The integration of the model to ESP-r at each time step has also been achieved. Although the model is a self-contained module by itself, the principles of ESP-r's solution process, such as the control volume approach

and the flexibility of choice of degree of implicit/explicit treatment of the solution process, are used within the model. From the test runs, the model is not a substantial computing burden to the rest of the ESP-r simulation, although it is called in tandem with the ESP-r main routines. Although the model is rigid in terms of the number of control volumes it contains, it is flexible in the sense that alternative equations defining a constituent parameter (such as, choice of equation for aerodynamic resistance or stomatal resistance) can be incorporated by changing the coefficient part of the model and maintaining the rest of the model as it is. Thus the new green roof model is able to simulate the green roof's thermal effect on a building in accordance with the ESP-r's principal characteristics (discretising the system in representative control volumes, simultaneous solution, etc.). To use the new model the user is required to prepare a set of input data, which are related to plants and soils and are generally unfamiliar to the engineering community. Next chapter deals with the input data base for the model, briefly explaining their nature and the methods to acquire to acquire them.

CHAPTER 4

DATABASES AND INPUT AVAILABILITY

4. Databases and input availability

4.0 Introduction

This chapter discusses the requirements for the user specified input for the green roof model. Details of experimental methods and sources of literature which can be used to generate new data are included. Many of the input data for the green roof model are related to plants and soil, which could be often unknown to the building simulation practitioners. Hence it is important to provide data collection guidelines together with the model so that it can be used in a variety of situations. However this is not an exhaustive data collection but a simple data model, which can be used for simulation of common green roof designs by users and which can be further built upon by future model developers.

A listing of input parameters is provided in Table 4.1 together with the current model's default values, which could match a real green roof situation. Brief explanations of the input parameters according to their classification are given in sections 4.1 through 4.5. The inputs are currently made available with a data file in the model. An example of an ASCII file that is used as an input file for green roof model is provided in Appendix 2.

A summary of data collected from a case study green roof (CSET building, University of Nottingham, Ningbo, China) and test cell is given in section 4.6 .It should be noted that the green roof module, with some minor adaptations, is capable of simulating the dynamic nature of the input variables. For example, if a plant parameter such as the leaf area index (LAI) or the plant height can be produced as a schedule, the program is capable of predicting the outcome of such variations. Examples of variable LAI for some annual plant crops are provided in section 4.7.

A sensitivity analysis is also conducted to estimate the comparative degree of influence of each of the input items on the model output; the output considered critical in this case being the temperature of the lowest layer of soil in green roof. Although it is not a full scale uncertainty analysis, a ranking of input variables according to their sensitivity is expected to help the user to look for the desired level of precision in each

of the input variables. Method employed to get this sensitivity analysis and the
obtained results are explained in section 4.8.

Table 4-1: Listing of user input data required for the green roof model

Classification	Input parameter	Variable name in code	Default value used in code
Plant morphology	plant height	plantHt	0.4 m
	leaf area index (LAI)	plantLAI	4
	leaf characteristic dimension	leafChDim	0.015 m
	leaf thickness	leafThk	0.0005m
Plant thermal properties	leaf density	rhoLeaf	700 kg/m^3
	leaf specific heat	cpLeaf	3500 J/kg
Plant moisture exchange	minimum stomatal resistance	stomatResMin	120 s/m
	plant wilting point	plantWiltPt	-80 m
Soil texture class (also in Table 4.5)and related thermal moisture properties	saturated moisture content	MoistCont_sat	0.45 m^3/m^3
	residual moisture content	MoistCont_res	0.067 m^3/m^3
	saturated hydraulic (moisture) conductivity	hydCond_sat	2.89e-06 m/s
	moisture retention curve factors (n,α)	soilnIndex, soilAlphaIndex	1.4, 0.02 cm^{-1}
	soil organic fraction	soilOrgFr	0.1 m^3/m^3
	soil mineral fraction	soilMinFr	0.45 m^3/m^3
	soil clay fraction	Clay_fr	0.2 m^3/m^3
Radiation related	reflectivity of canopy	reflCan	0.25
	reflectivity of ground	reflGround	0.15
	reflectivity and transmissivity at leaf tissue level	reflLeafTis, transmLeafTis	0.3 0.2
	emissivity of leaves	emissLeaves	0.96
	emissivity of ground	emissSoil	0.95
	Coefficient of extinction for long wave radiation	extinLong	0.829
weather : precipitation data	hourly precipitation data for the location	precip_mm	Hangzhou TRMM data mm/h
General/site related	location altitude	siteAlt	100 m
	fraction of vegetation coverage	fracVeg	0.95
	substrate(soil) height	soilHt	0.3 m
	irrigation schedule	TimesPerDay_time(12) TimesPerDay_day(12)	0, 0

4.1 Plant morphology parameters

4.1.1 Leaf Area Index

Leaf area index is a parameter that specifies how dense is a canopy in blocking solar radiation from reaching the ground. By definition it is the ratio of the total of leaf top surface areas to the ground area below; unit is $[m^2/m^2]$. A zero value represents bare ground; a value 3-5 is common for shrub covers normally found in green roofs, 5 being fairly dense with almost no radiation going through. It can thought of as a number that represents how many times a vertical beam of light will be intercepted by the canopy leaves if it were to travel from the top of canopy to the ground, penetrating every leaf as it hits.

The main factors affecting leaf area index are plant type and its phase of development. For deciduous plants with seasonal variation in leaf density, leaf area index will change over season. Agricultural corps with short life span of 3 to 4 months is also reported to be used in the green roofs. They show distinctive variation of LAI over the life span which is reported in FAO's crop evapotranspiration guide [45]

For evergreen types of shrubs usually found in intensive green roofs, pruning and maintenance have more influence than seasons and stage of development.

LAI measurements were conducted in field test using Delta-T Devices Sun Scan Canopy Analysing System type SS1[69]. A 'beam fraction sensor' is used to measure total PAR radiation (photo synthetically active radiation; 400 nm to 700 nm range; contains 48% of solar radiation energy) above canopy. Below canopy, a 1 m long 'Sun scan probe' with 64 LED sensors, is used to measure the PAR. A built in software within the system calculates LAI by comparing these two readings. Manufacturers' accuracy limit is 10% which can be compromised at poor sun light strength and for plant morphology with vertical leaves. Representative values of LAI measurements for plants at CSET green roof is given in table 4.3 in section 4.6

4.1.2 Canopy physical dimensions

Canopy height is used in the calculation of aerodynamic resistance at canopy top and to determine the canopy air volume. Canopy height is, in general, dependant on the plant species. However, in a green roof environment as the plants are maintained on an artificial environment, with limited soil height as growth medium and occasional trimming of plants to maintain aesthetics, it could be generally considered as site specific. From the site measurements (at CSET green roof), it was found that for intensive green roofs with shrub type of plants, 0.4 m to 0.7 m is a common height. Also from the case study site observation, for extensive types of green roofs with grass, the common height is around 0.06 m, for a well maintained lawn.

Leaf characteristic dimension, used in the model in aerodynamic resistance calculation within canopy, is in fact the leaf width[55]. This is dependent on the plant species. Leaf widths of 10 mm to 30 mm were found for the plants in the site measurement at CSET building.

Leaf thickness is again plant species dependent. It is used (together with LAI, density and specific heat) in the calculation of thermal storage in canopy. Values of 0.3 mm to 0.6 mm were observed in the plants in the site measurement. If unknown a value 0.5 mm is a good estimation [70], which is the value found to be representative for shrub type of plants commonly found in extensive type of green roofs.

4.2 Plant thermal characteristics

Specific heat and density of plant leaves can be sourced from the literature. For example Stahghellini, 1987 [71] gives a value of 3500 J/kg K for specific heat and 700 kg/m^3 for density. These values are theoretical estimate based on the fact that plant tissues consist of 70-80% water. Jayalakshmi, 2010 [72] reports experimental studies and gives specific heat values in the vicinity of 1260 J/kg K and leaf density around 860 kg/m^3 for shrub type of plant.

4.3 Minimum stomatal resistance

Stomatal are the small openings on leaf surface through which exchange of oxygen carbon dioxide and water vapour occurs in leaf tissues. The size of the stomata opening and the resistance to vapour flow across it are sensitive to light, water availability, ambient carbon dioxide concentration, air pollution and healthy state of plant. The measurement of actual stomatal resistance is done in field tests under the most ideal conditions (at bright day light, sometime after irrigation, when it is windy and when plants looked healthy). A cycling porometer from Delta-T devices calibrated on site conditions is used for the measurements. To get the minimum stomatal resistance, measurements were taken under favourable conditions for plants, as mentioned above. In the instrument, the method of getting stomatal resistance is by measuring time taken by plant leaf to release water vapour to a chamber in head so that the relative humidity inside changes by a fixed step. Prior to the leaf measurement, the instrument is calibrated with a calibration plate containing pores of known resistances. The calibration was done on site to have similar conditions for calibration plate and leaf. The field measurement data is given in section 4.6 at table 4.3.

4.4 Soil Characteristics

The model uses Richard's equation, as shown below and as has been described in section 3.2.2, to determine the soil moisture state (as specified by its moisture content or matric potential) and the moisture state in turn is used in the thermal domain calculations.

$$C_\theta \frac{\partial \psi}{\partial t} = \frac{\partial}{\partial z}\left[K\Psi\left[\frac{\partial \psi}{\partial z} + 1 \right] + KT \frac{\partial T}{\partial z} + P0 - Ev \right] - S \tag{4-1}$$

which is equivalent to equation 3.31 as in section 3.3.2 and of same symbolic notations.

As discussed in chapter 3, for moisture related calculations, the state variable used is matric potential (Ψ) which is a negative pressure that holds water in a vertical column of soil against gravity. It is the result of capillary and adsorptive forces present in the soil matrix. These forces bind water in the soil and lower its potential energy below

that of bulk water. The matric potential is also defined as the energy required for extracting unit mass of water from soil. Sometimes it is referred to as suction head in length units. The units for matric potentials are [J/kg], [m], [Pa] and [pF] (pF = logarithm to base ten of suction head in cm). Matric potential for saturated soil is zero. Another state variable which is exchangeable with matric potential is soil moisture content (θ) which is the volumetric ratio of water to bulk soil [m^3/m^3]. In soil the moisture content can range from a smallest possible value, the residual moisture content (θr) to a maximum value, the saturated moisture content (θs). The relation between θ and Ψ is called the water retention characteristic and is specific to a soil of certain texture. A well accepted relation is given by van Genuchten [37] and has been described in chapter 3 by equation 3.37.

The soil texture characteristics used in the model and in equation 3.37, can be determined with an experimental method which is briefed in section 4.6.2

4.5 Other input parameters

Emissivity is defined as the ratio of energy radiated by a particular material to the energy radiated by a black body at the same temperature. In this model, emissivity is used in the calculation of long wave radiation exchange between plant and soil, sky radiation exchange with plant and sky radiation exchange with soil. Emissivity of most natural materials is between 0.95 and 1. The default values used in the model are 0.95 for soil and 0.96 for plant [55]

The coefficient of extinction together with LAI is used to calculate the radiation interception by canopy as per Beer's law [55] which states:

$$I/Io = e^{-(k\ LAI)} \tag{4-2}$$

where Io is in the incident radiation, I is the transmitted radiation and k is the coefficient of extinction. The extinction coefficient for short wave radiation(ks) can be calculated from the extinction coefficient for long wave radiation (kl) [9] as ks=0.74kl. Extinction coefficient for long wave is dependent on the leaf angle [71] as:

Leaf distribution horizontal   kl = 1

Leaf distribution 45 degree   kl = 0.829

Leaf distribution vertical   kl = 0.436

Spherical leaves kl = 0.684

Plant wilting is a measure of the ability of the plant to survive in low moisture soil by reducing its metabolic activities and it depends on the type of the plant. It is sourced from literature [73] as -80 m which is applicable for most plants used in green roofs.

4.6 Input data collection

4.6.1 Plant data

A set of data has been collected, by experimental means, in a real green roof environment at the Centre for Sustainable Energy Technologies in the University of Nottingham Ningbo China, to facilitate, as an example, the use of green roof model in building energy simulation and demonstrate the model input data collection procedure. The plants are mainly of evergreen shrub type. Their layout is given in Figure 4.1, which is a photo of CSET green roof taken from above. The plants' names and brief descriptions are given in Table 4.2, according to the location number as given in figure 4.1.
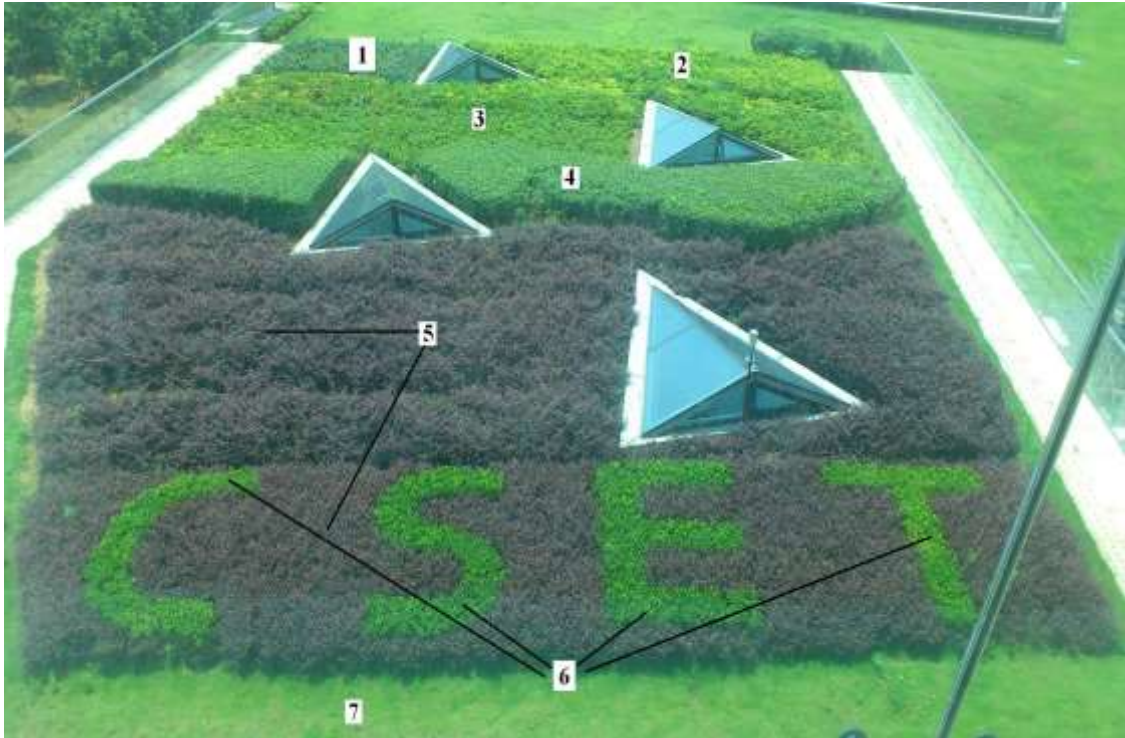
Figure 4-1 Layout of plants at CSET green roof

The morphological properties of the plants as has been described in section 4.1 and the stomatal resistance, as has been described in section 4.3, are measured periodically throughout the validation period and their representative values are given in table 4.3.

Table 4-2: Plants species at CSET green roof

Location	Name	Picture	Description
1	Camellia Sasanqua		Evergreen shrub found in China and Japan; leaf size 3–7 cm long, 1.2–3 cm width;
2	Rhododendron		Rhododendron is a broad classification and exists in many hybrids of cultivation; the specific plant at CSET green roof is evergreen shrub.
3	Ligustrum Japonicum 'Howardii'		Evergreen shrub found in east Asia; easily maintained and considered invasive at times.
4	Viburnum Dilatatum (Thunb)		Deciduous shrub which can grow up to 5 m
5	Lorpetalum Chinense var.Rubrum		Evergreen shrub (also exist in semi evergreen varieties); leaf size about 5cm long 3.5 cm wide; Plants have good pest and disease resistance.
6	Buxus sinica		Evergreen shrubs found in many parts of the world; plant height is about 50 cm; slow growing, require little or no maintenance; It is also known as Chinese box
7	Lawn		

Table 4-3: Summary of data collected from CSET green roof plants

Location	Name	LAI	Height [m]	Leaf Angle	Leaf width [mm]	Leaf thickness [mm]	Minimum stomatal resistance s/m
1	Camellia Sasanqua	2.18	0.4	45	23.4	0.56	288
2	Rhododendron	1.85	0.5	60	30.0	0.5	161
3	Ligustrum Japonicum 'Howardii'	4.93	0.48	60	20.2	0.46	172
4	Viburnum Dilatatum (Thunb)	6.28	0.7	30	31.2	0.54	212
5	Lorpetalum Chinense var.Rubrum	5.27	0.7	30	21.0	0.32	228
6	Buxus sinica	4.03	0.45	60	11.2	0.42	165
7	Lawn	NA	0.06	60	4	0.6	NA
8	Test Cell- Buxus sinica	4.8	0.4	60	10.8	0.46	165

For lawn, in table 4.3, values of LAI and stomatal resistances are not available, because the height and leaf sizes are too small for the respective instruments. However the reference FAO[45] give an indicative value for lawn's minimum stomatal resistance as 100 s/m and a rule of thumb for LAI as LAI=24h, where h is the plant height in [m]. Row number 8, in table 4.3, refers to the test cell plant details, which is used for validation purposes as detailed in section 5.2 in the next chapter.

4.6.2 Soil moisture characteristic data

The soil moisture retention parameters (θr, θs, α and n) were determined by first measuring the soil test sample particle sizes and fit the results in a USDA soil texture triangle [74] and then using the reference Carsel 1988 [75] which gives the soil

characteristics classified according to the 12 soil texture classifications of USDA(figure 4.3).

Experimental results of a soil sample test were produced with a Bettersize2000 laser particle size analyzer and are given in table 4.4 and figure 4.2. The reference Leij 1996 [74] gives the size range of soil components as: Sand > 50 µm; silt 2-50 µm and clay <2 µm. These size ranges are highlighted in table 4.4 and the composition in the sample is read as: percentage of clay = 22.2%, percentage of sand =100-89.37= 10.63% and percentage of silt =100-(10.63+22.2) = 67.17%

Table 4-4: Soil test result: particle size distribution

D µm	PPC %	CPPC %	D µm	PPC %	CPPC %	D µm	PPC %	CPPC %
0.020-0.024	0	0	0.911-1.161	3.21	10.75	44.04-56.13	2.68	**89.37**
0.024-0.030	0	0	1.161-1.479	3.51	14.25	56.13-71.52	1.86	91.22
0.030-0.039	0	0	1.479-1.885	3.83	18.08	71.52-91.14	1.75	92.98
0.039-0.049	0	0	1.885-2.403	4.12	**22.2**	91.14-116.1	2.22	95.19
0.049-0.063	0	0	2.403-3.062	4.34	26.54	116.1-147.9	2.44	97.63
0.063-0.080	0	0	3.062-3.902	4.47	31.01	147.9-188.5	1.79	99.43
0.080-0.102	0	0	3.902-4.972	4.67	35.68	188.5-240.3	0.54	99.97
0.102-0.131	0	0	4.972-6.336	4.94	40.62	240.3-306.2	0.03	100
0.131-0.167	0	0	6.336-8.074	5.25	45.87	306.2-390.2	0	100
0.167-0.212	0	0	8.074-10.28	5.74	51.61	390.2-497.2	0	100
0.212-0.271	0	0	10.28-13.11	6.33	57.93	497.2-633.6	0	100
0.271-0.345	0.16	0.16	13.11-16.70	6.71	64.64	633.6-807.4	0	100
0.345-0.440	0.73	0.9	16.70-21.28	6.73	71.37	807.4-1028.8	0	100
0.440-0.561	1.55	2.44	21.28-27.12	6.27	77.64	1028.8-1311.0	0	100
0.561-0.715	2.28	4.72	27.12-34.56	5.2	82.83	1311.0-1670.6	0	100
0.715-0.911	2.82	7.54	34.56-44.04	3.85	86.69	1670.6-2000.0	0	100

Key: **D - Diameter µm;**
PPC - Percentage particle count %
CPPC: Cumulative percentage particle count %
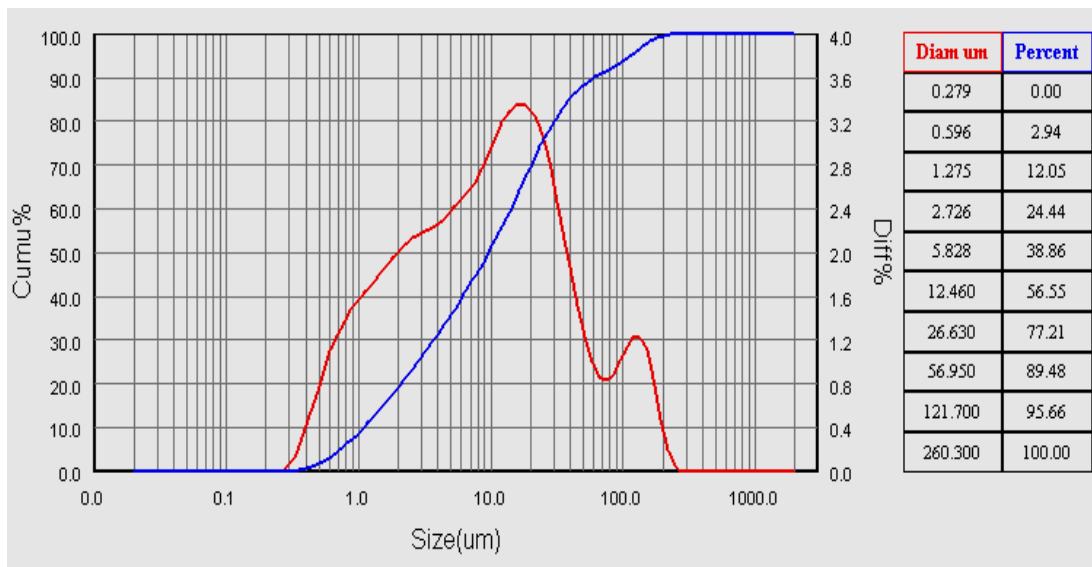
Figure 4-2: Soil particle size distribution

Diam um	Percent
0.279	0.00
0.596	2.94
1.275	12.05
2.726	24.44
5.828	38.86
12.460	56.55
26.630	77.21
56.950	89.48
121.700	95.66
260.300	100.00
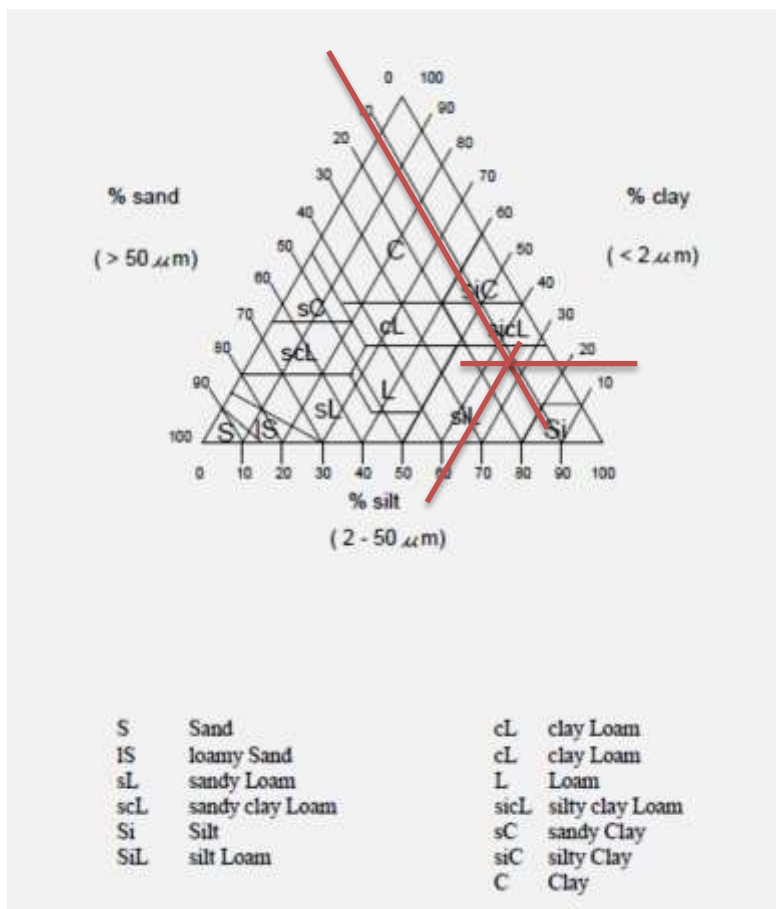
Figure 4-3: USDA soil triangle and textures

S	Sand	cL	clay Loam
lS	loamy Sand	cL	clay Loam
sL	sandy Loam	L	Loam
scL	sandy clay Loam	sicL	silty clay Loam
Si	Silt	sC	sandy Clay
SiL	silt Loam	siC	silty Clay
		C	Clay

Table 4-5: Soil characteristics according to texture class

Texture Class	Residual moisture content θr [m³/m³]	Saturated moisture content θs [m³/m³]	Index α [1/cm]	Index n [-]	Saturated moisture conductivity Ks [m/s]
Sand	0.045	0.43	0.145	2068	8.25E-05
Loamy sand	0.057	0.41	0.125	2.28	4.05E-05
Sandy Loam	0.065	0.41	0.075	1.89	1.23E-05
Loam	0.078	0.43	0.036	1.56	2.89E-06
Silt	0.034	0.46	0.016	1.37	6.94E-07
Silt loam	0.067	0.45	0.020	1.41	1.25E-06
Sandy clay loam	0.100	0.39	0.059	1.48	3.64E-06
Clay loam	0.095	0.41	0.019	1.31	7.22E-07
Silty clay loam	0.089	0.43	0.010	1.23	1.94E-07
Sandy clay	0.100	0.38	0.027	1.23	3.33E-07
Silty clay	0.070	0.36	0.005	1.09	5.56E-08
Clay	0.068	0.38	0.008	1.09	5.56E-07

The texture class obtained is Silt-Loam as determined by entering the percentage composition 22.2% Clay, 67.17% Silt and 10.63% Sand, in figure 4.3. The soil input parameters were determined from Table 4.5 [75]: θr=0.067 m³/m³, θs=0.45 m³/m³, α=0.02 cm^{-1} and n=1.41 [-]

4.6.3 Soil organic mineral fractions

Volume fractions of soil organic fraction and mineral fractions are used in the calculation [55] of soil matrix volumetric specific heat [J/m³].

$$C_{soil} = \rho_{min} Cp_{min} MF + \rho_{org} Cp_{org} OF + \rho_{wat} Cp_{wat} \theta \qquad (4\text{-}3)$$

where ρ_{min} – density of soil minerals (2650 kg/m³), Cp_{min} – specific heat of soil minerals (870 J/kg), MF- volumetric mineral fraction (m³ minerals/m³ soil), ρ_{org} – density of organic matter (1300 kg/m³), Cp_{org} – specific heat of organic matter (1920 J/kg), OF- volumetric organic fraction (m³ organic matter/m³ soil), ρ_{wat} – density of water (1000 kg/m³), Cp_{wat} – specific heat of water (4180 J/kg), θ- soil moisture content

(m^3 water/m^3 soil). As moisture content is varying so does the soil specific heat. The soil specific heats mentioned in section 3.2.1 are thus dynamic values, calculated in successive iterations as per evolving values of moisture contents. The solid components of soil are divided into minerals and organic matters. Organic matter constitutes the part that is formed by breakdown of plant and animal matter and mainly consists of carbon. The method used to determine the organic fraction is the method of Loss on ignition [76] which is a simple procedure of subjecting soil sample to high temperatures allowing carbon materials to oxidize. However the temperature should not go too high to cause the carbonate (CO_3) components of the minerals to disintegrate. At optimum temperature of 400 °C is recommended in literature [76]. The procedure consist of subjecting soil sample to 110 °C for eight hours in a drying oven and subsequently subjecting it to a 400°C for four hours in a furnace. Weights of sample before and after each procedure are taken to determine moisture fraction and organic matter fraction by weight. Soil bulk density is used to convert weight fraction to volume fraction as shown below. The bulk density of soil is determined by taking the weight s and water displacements by soil sample on a measuring jar. The results from the test cell's soil sample are summarized below:

Organic fraction by weight = 0.024633 kg org/kg soil

Mineral fraction by weight = 0.777432 kg min/kg soil

Moisture fraction by weight = 0.197935 kg org/kg soil

Bulk density of soil = 1777.188 kg/m^3

Volumetric organic fraction = $\dfrac{0.024633\frac{kg\ org}{kg\ soil} \ X\ 1777.188\frac{kg\ soil}{m^3 soil}}{1300\frac{kg\ org}{m^3 org}} = 0.033675\ \dfrac{m^3\ org}{m^3\ soil}$

Volumetric mineral fraction = $\dfrac{0.777432\frac{kg\ min}{kg\ soil} \ X\ 1777.188\frac{kg\ soil}{m^3 soil}}{2650\frac{kg\ min}{m^3 min}} = 0.521375\ \dfrac{m^3\ min}{m^3\ soil}$

Volumetric moisture content = $\dfrac{0.197935\frac{kg\ wat}{kg\ soil} \ X\ 1777.188\frac{kg\ soil}{m^3 soil}}{1000\frac{kg\ wat}{m^3 wat}} = 0.351768\ \dfrac{m^3\ wat}{m^3\ soil}$

A check on the above procedure shows:

air fraction = 1-(0.033675+0.521375+0.351768)=0.093182 ;

and the total of moisture content and air fraction =(1-(0.033675+0.521375)= 0.444950

which is close to the expected saturated moisture content (0.45 m^3/m^3) obtained in soil particle analysis test (section 4.6.2)

4.7 Schedules for inputs

One of the key benefits of a control volume simulation is that it can accommodate the true dynamic nature of the model's variables. The living mediums of plants in a green roof, in some cases, respond to climatic variations and go through changes along their development stages. For example, this is the case for perennials and crops which typically have life spans of three to four months. For evergreen shrubs, the plant morphology variables can be treated as constant, provided management and trimming are carried out regularly.

Agricultural crops, although not common, are reported to be in use in green roofs. As an illustration for scheduled input, plant LAI can be provided as a schedule if chosen to be so by the user. However, currently the model does not accept such inputs. Minor modifications are required to be introduced in the model, such as preparing an array of the input variable that is time-changing (such as LAI and plant height), introducing additional steps in the program coding to call such an array and to synchronize it with the simulation period and the simulation time-step. This revision is proposed as the next stage development in section 6.3. The availability of such time-varying input data data will be demonstrated in the next section.

4.7.1 Variable LAI

AquaCrop [77] is an open-source crop-growth simulation program developed by the Land and Water Division, Food and Agricultural Organization of the United Nations (FAO). The AquaCrop model predicts the biomass and yield response to various conditions of water availability, soil conditions, weather etc. This program is generally used in the agriculture sector to predict irrigation requirements and other needs for crops in different locations of the world. Among others it can be used to predict potential crop development through the stages of sowing, germination, vegetative

development, flowering, yield formation and ripening. Various crops' growths were simulated with AquaCrop to predict the potential canopy cover (CC) evolution as a demonstration of the changes in plant morphology throughout the crops' life cycle. It should be noted that the canopy cover is a crop variable defined according to its morphology and it is not the fraction of vegetation coverage as mentioned in table 4.1. Fraction of vegetation coverage is a variable that specifies the fraction of green roof area planted. The simulations with AquaCrop were performed without any limitations from water stress and crop management practices in order to show the crops' natural development potential. However the user can also prepare crop data for a variety of conditions, including unfavourable ones, if the building simulation task requires such an analysis.

The canopy cover is the percentage of light intercepted by canopy thus not getting to the ground below. It is known to be related to plant LAI by the relation [78]:

$$CC = 100.5\big[1 - e^{(-0.6\,LAI)}\big]^{1.2} \qquad\qquad (4\text{-}4\ )$$

Strictly speaking this relation (equation 4.4) is established for one crop, maize and is provided here only for demonstration. There also a few variations of the relation between CC and LAI for other crops in the literature [79] [80]. Since the variations are small, the above equation (4.4) is exclusively used here for converting the CC into LAI. Figures 4.4 through 4.11 below show the crop developments predictions, obtained from AquaCrop simulations, in terms of CC and LAI for various crops under ideal conditions. This is done for demonstrating the variations of these variables for specific crops within their natural life cycle and for showing the variations between crops. A tabular listing of the LAI for all these crops is given in table 4.6
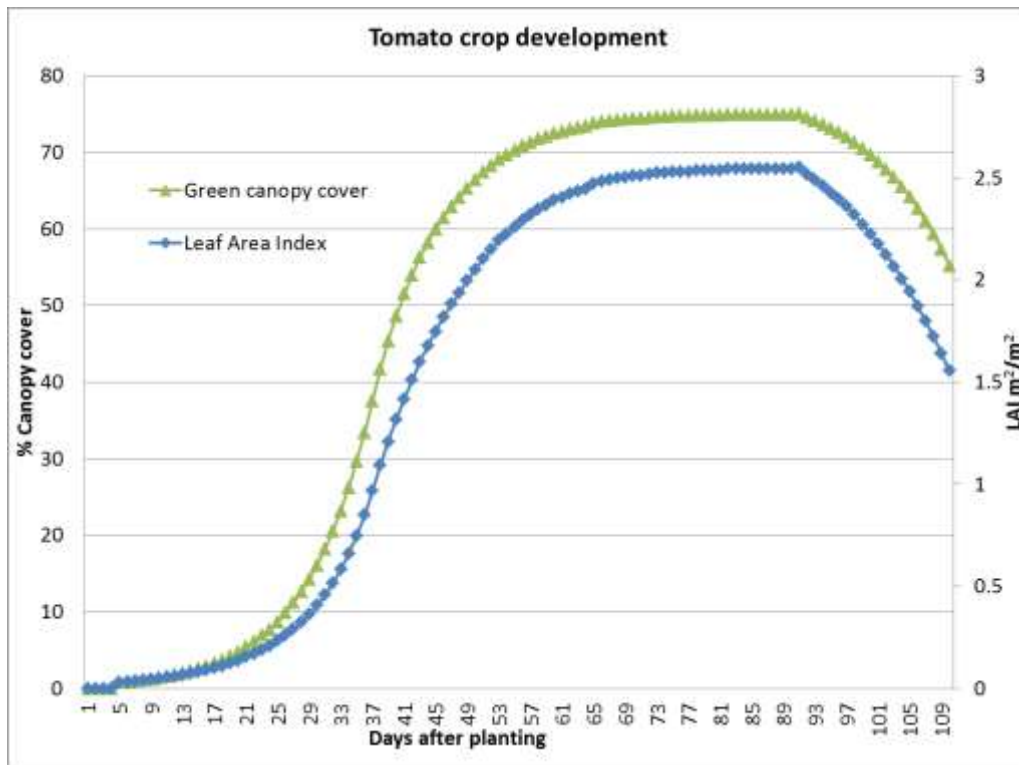
Figure 4-4: Potential canopy cover and LAI evolution for tomato life cycle
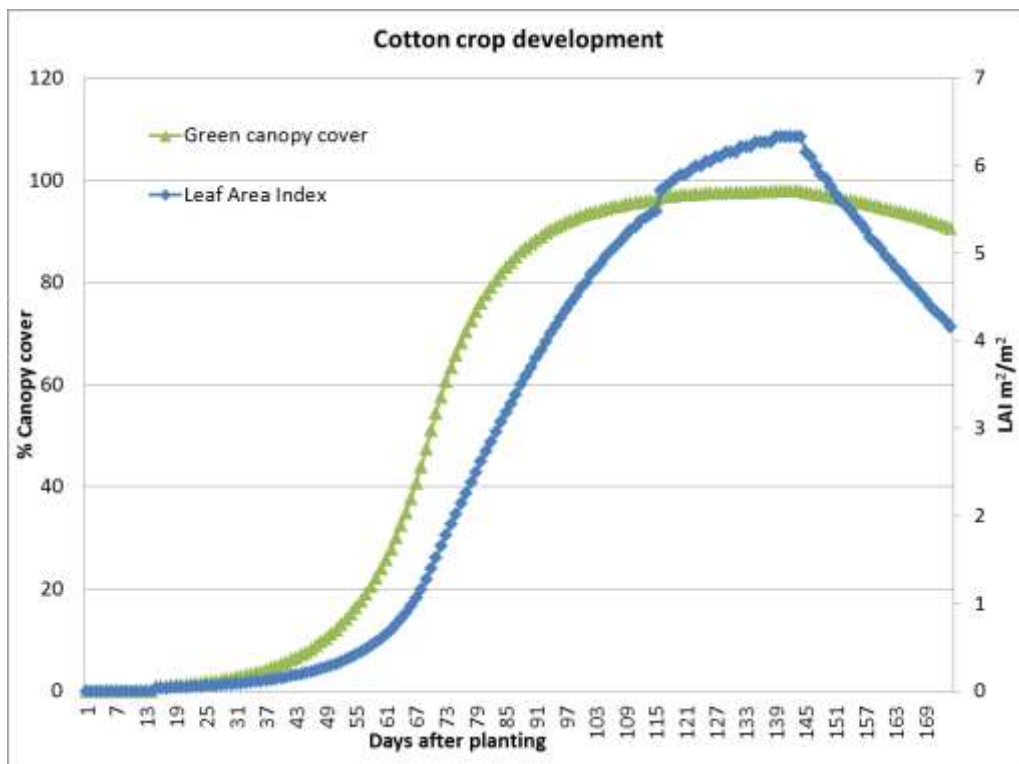
Figure 4-5: Potential canopy cover and LAI evolution for cotton life cycle
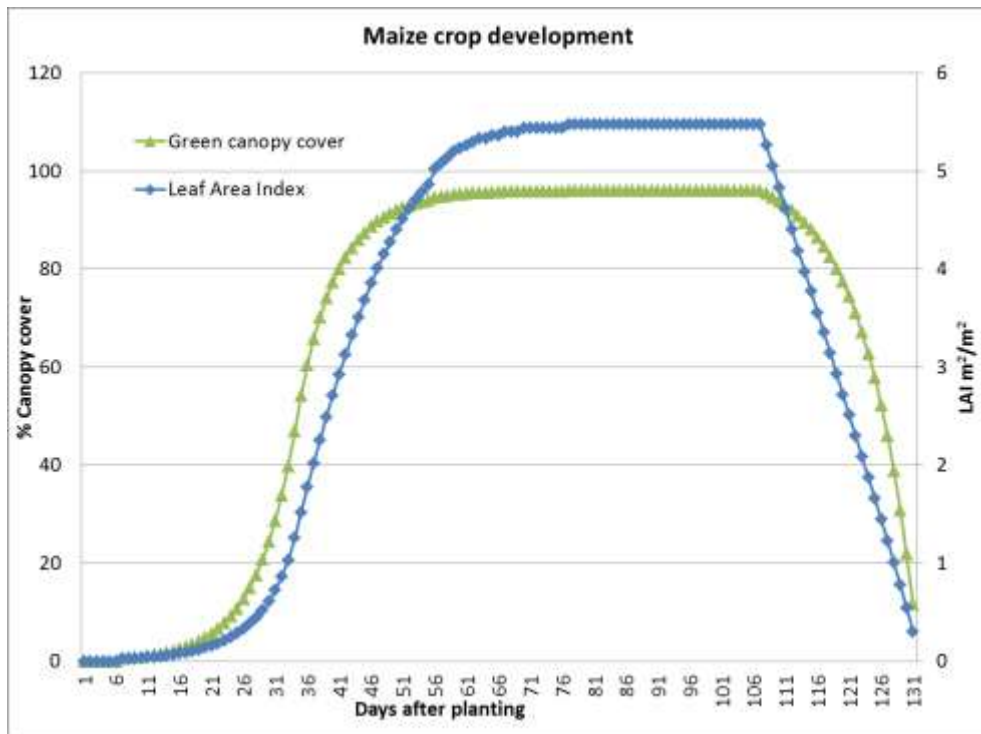
Figure 4-6: Potential canopy cover and LAI evolution for maize life cycle
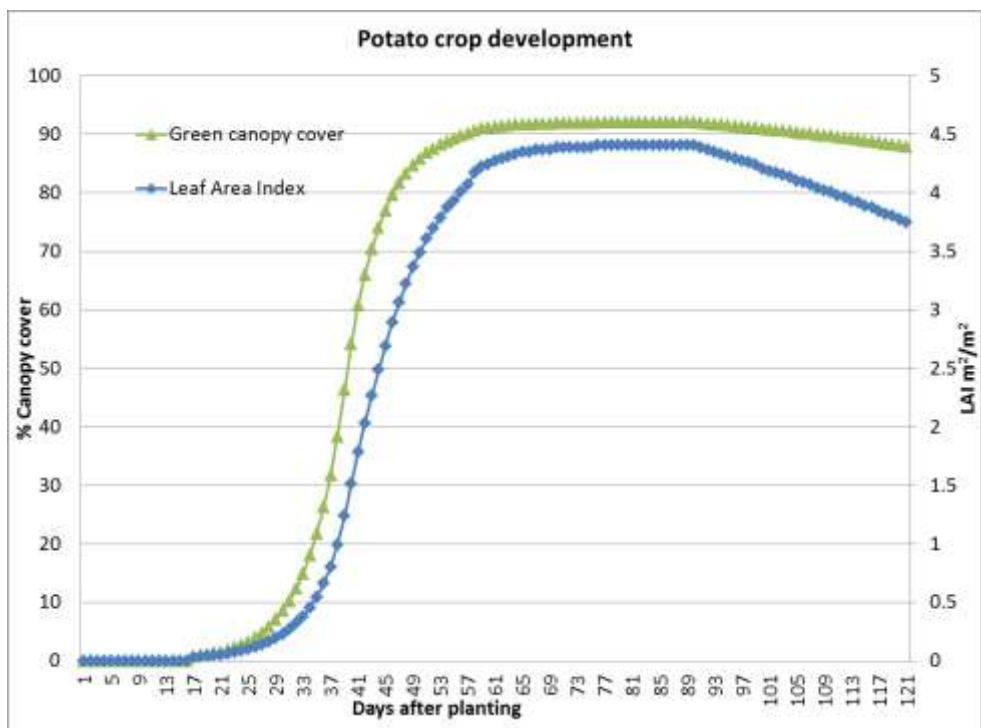
Figure 4-7: Potential canopy cover and LAI evolution for potato life cycle
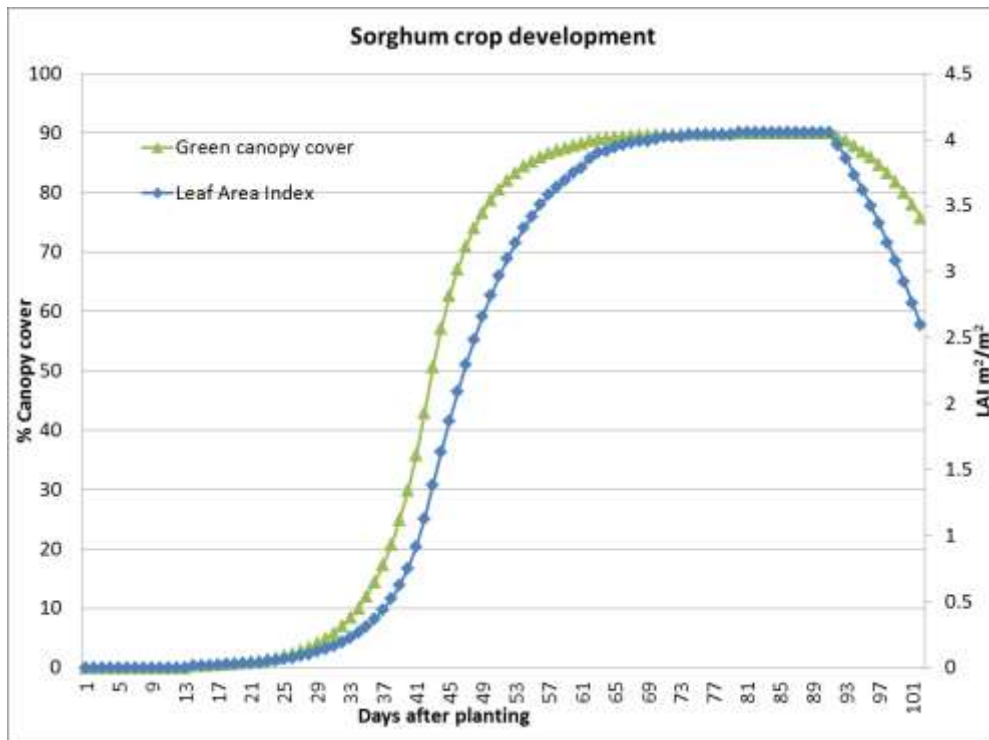
Figure 4-8: Potential canopy cover and LAI evolution for sorghum life cycle
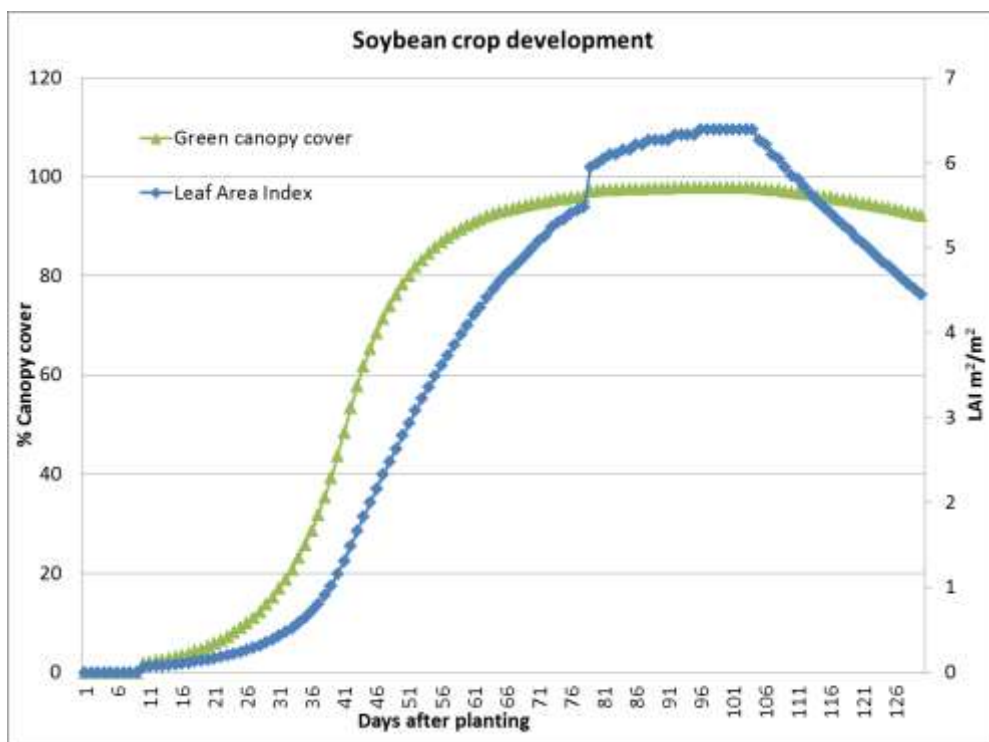
Figure 4-9: Potential canopy cover and LAI evolution for soybean life cycle
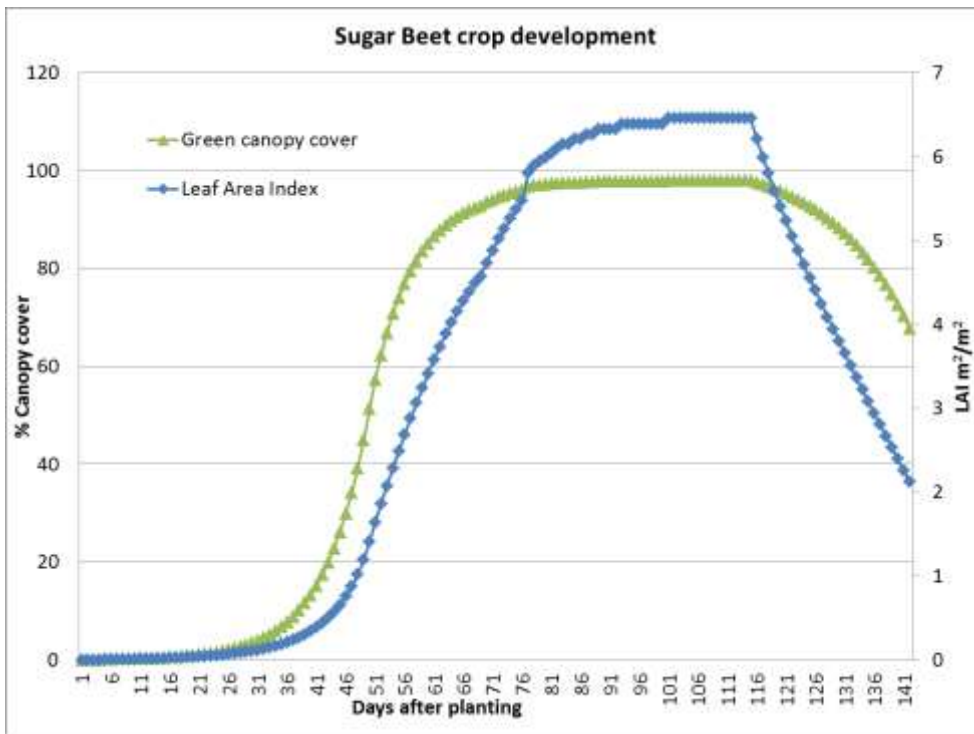
Figure 4-10: Potential canopy cover and LAI evolution for sugar beet life cycle
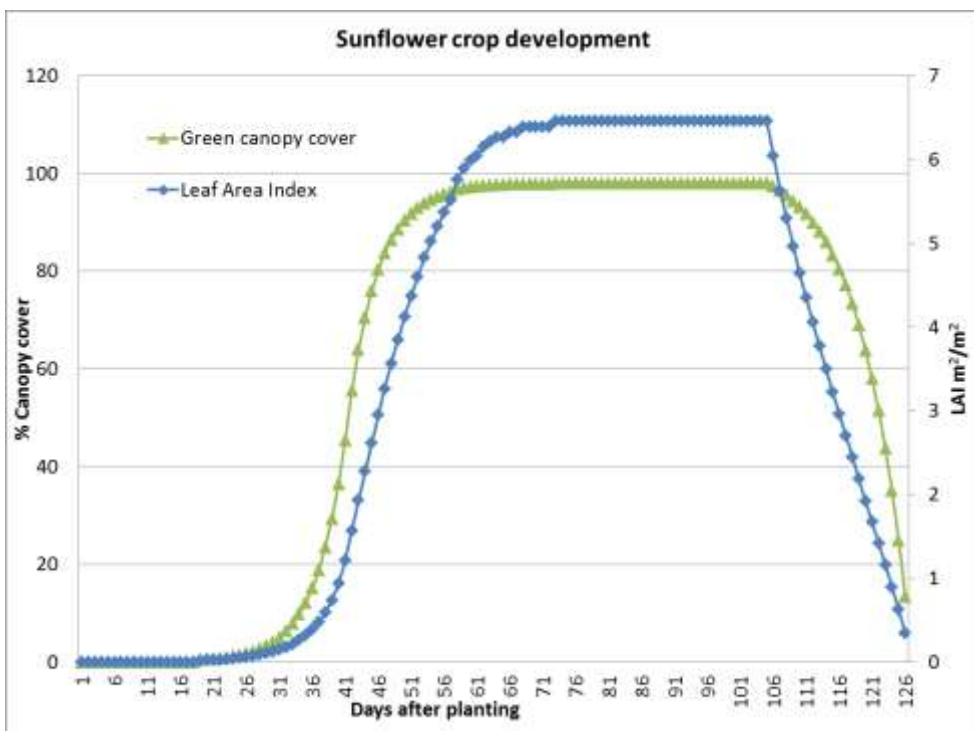
Figure 4-11: Potential canopy cover and LAI evolution for sunflower life cycle

83

Table 4-6: LAI evolution through life-span of some agricultural crops

Days after planting	Leaf Area Index m^2/m^2							
	Tomato	Cotton	Maize	Potato	Sorghum	Soybean	Sugar beet	Sunflower
1	0.000	0.000	0.000	0.000	0.000	0.000	0.000	0.000
5	0.030	0.000	0.000	0.000	0.000	0.000	0.005	0.000
10	0.048	0.000	0.033	0.000	0.000	0.059	0.009	0.000
15	0.081	0.030	0.068	0.000	0.013	0.094	0.017	0.000
20	0.135	0.039	0.138	0.045	0.030	0.150	0.033	0.020
25	0.232	0.057	0.282	0.100	0.065	0.240	0.057	0.045
30	0.409	0.076	0.612	0.228	0.140	0.387	0.102	0.118
35	0.747	0.107	1.518	0.545	0.311	0.648	0.184	0.313
40	1.315	0.148	2.712	1.514	0.752	1.154	0.339	0.934
45	1.748	0.206	3.681	2.690	1.868	1.996	0.655	2.612
50	2.051	0.292	4.409	3.486	2.818	2.787	1.410	4.119
55	2.261	0.413	4.859	3.930	3.419	3.486	2.485	5.200
60	2.391	0.600	5.232	4.240	3.746	4.086	3.408	5.993
65	2.472	0.891	5.366	4.350	3.945	4.596	4.152	6.268
70	2.511	1.400	5.438	4.389	4.006	4.993	4.734	6.391
75	2.531	2.021	5.438	4.389	4.037	5.332	5.366	6.457
80	2.537	2.619	5.474	4.409	4.053	5.993	5.993	6.457
85	2.544	3.182	5.474	4.409	4.053	6.152	6.209	6.457
90	2.544	3.694	5.474	4.409	4.053	6.268	6.328	6.457
95	2.428	4.169	5.474	4.313	3.618	6.328	6.391	6.457
100	2.227	4.596	5.474	4.204	2.923	6.391	6.391	6.457
105	1.943	4.965	5.474	4.102		6.268	6.457	6.457
110	1.556	5.265	4.833	4.006		5.848	6.457	4.641
115		5.474	3.773	3.886		5.474	6.457	3.221
120		5.895	2.720	3.773		5.108	5.402	1.924
125		6.044	1.660			4.783	4.553	0.625
130		6.152	0.547			4.449	3.801	
135		6.268					3.079	
140		6.328					2.397	
145		6.152						
150		5.757						
155		5.402						
160		5.050						
165		4.711						
170		4.389						

Another alternative for the prediction of LAI is by using WOFOST (World Food Studies) model [59] from Wageningen University. This is a simulation model for the prediction of the growth and production of annual field crops. LAI is available as an output in this program, so no need of conversions as in the case with AquaCrop. Currently the available crops and the supporting weather data are limited. However the tool could still be useful in some cases of crops and locations. The use of the above tools could therefore facilitate the generation of inputs for the green roof model.

4.8 Sensitivity analysis for model inputs

A simplified sensitivity analysis is conducted on the model by varying the input variables individually and observing the variations in the output. This is done to provide the user a sense of relative importance among the input variables, given the high number of input variables. A one-parameter-at-a-time (OAT) approach [81] is adapted whereby each input variable is independently changed within the range of interest for the simulation and the change in output is recorded. The interrelation between input variables which may exist across some variables (such as LAI and plant height; soil saturated moisture content and residual moisture content) are not considered here and may be required in an elaborate parametric study such as in an uncertainty analysis. The scope of the current study is limited to ranking the list of input variables for green roof in their order of their sensitivity to the output. The output of interest in this context is the lowest control volume temperature of the green roof, which links to the roof as a boundary condition for the building side simulation in ESP-r. A single value of this temperature, arbitrarily chosen as at time step 85 (correspond to 2 PM of the simulation day) was chosen for comparison for all the cases of sensitivity analysis.

A java based program Genopt [82] is used and it is coupled with ESP-r to run the multiple simulation runs. Genopt is mainly an optimization program which runs with other simulation programs to determine the optimum value of a selected input variable as per the user defined criteria. The user defined criteria are often called *cost function*. Genopt can also automate parametric runs of simulations. Information concerning which variable to change, in what manner to change it, how to run the simulation program (in this case ESP-r with the green roof module integrated) from a set of script

commands and how to retract the output are set up in Genopt with a set of files called initiation file, configuration file and command file. A published work on coupling between ESP-r and Genopt [83], gives details of setting up of these files for an optimization problem, which were then adapted for a parametric run and used in this research. An illustration of the data flow between ESP-r and Genopt, adapted from Peeters 2010 [83] is shown in figure 4.12. Each of the input variables are changed in 50 linear continuous steps within the ranges as specified in table 4.7. A single value of the temperature of the lowest layer of soil is used as output consistently for all the simulation runs. For this purpose a separate text file was generated in the green roof program reporting the sequential time step and the temperature of CV7, and the Genopt was directed to retrieve one value from this file, i.e., the value at time step 85. The results of the sensitivity analysis exercise are presented in the following subsections, according to three groups of inputs, namely the plant related, the soil related and the radiation related. The results are shown as graphs with temperature of the lowest layer of green roof (T8) in y-axis and the input variable in the x-axis. The y-axes have been scaled equally within each group to illustrate their comparative effects. The original results without any scaling are given for reference in appendix 5.
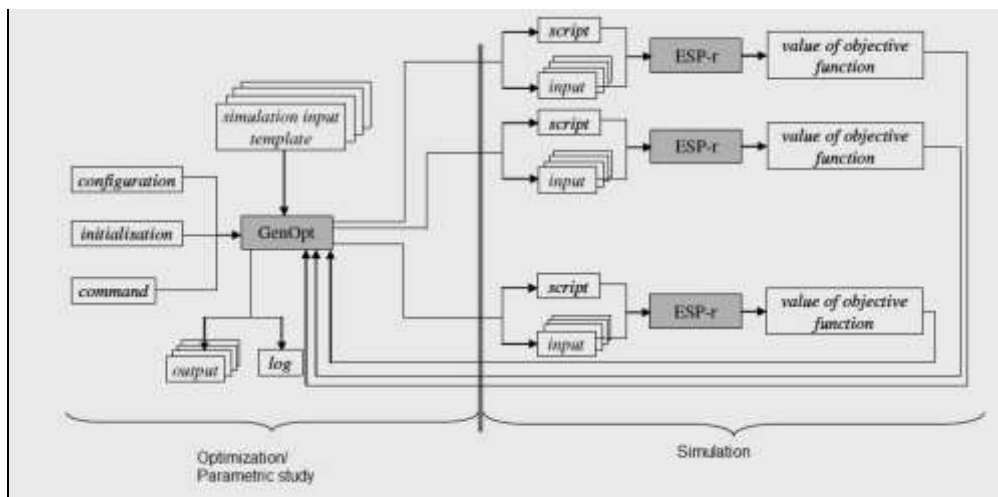
Figure 4-12: Illustration of data flow between ESP-r and Genopt [83]

4.8.1 Sensitivity analysis for plant variables

Figures 4.13 to 4.15 show the sensitivity analysis results for eight plant related inputs; the inputs are varied in 50 equal steps between the minimum and maximum values as shown in their respective x axes.
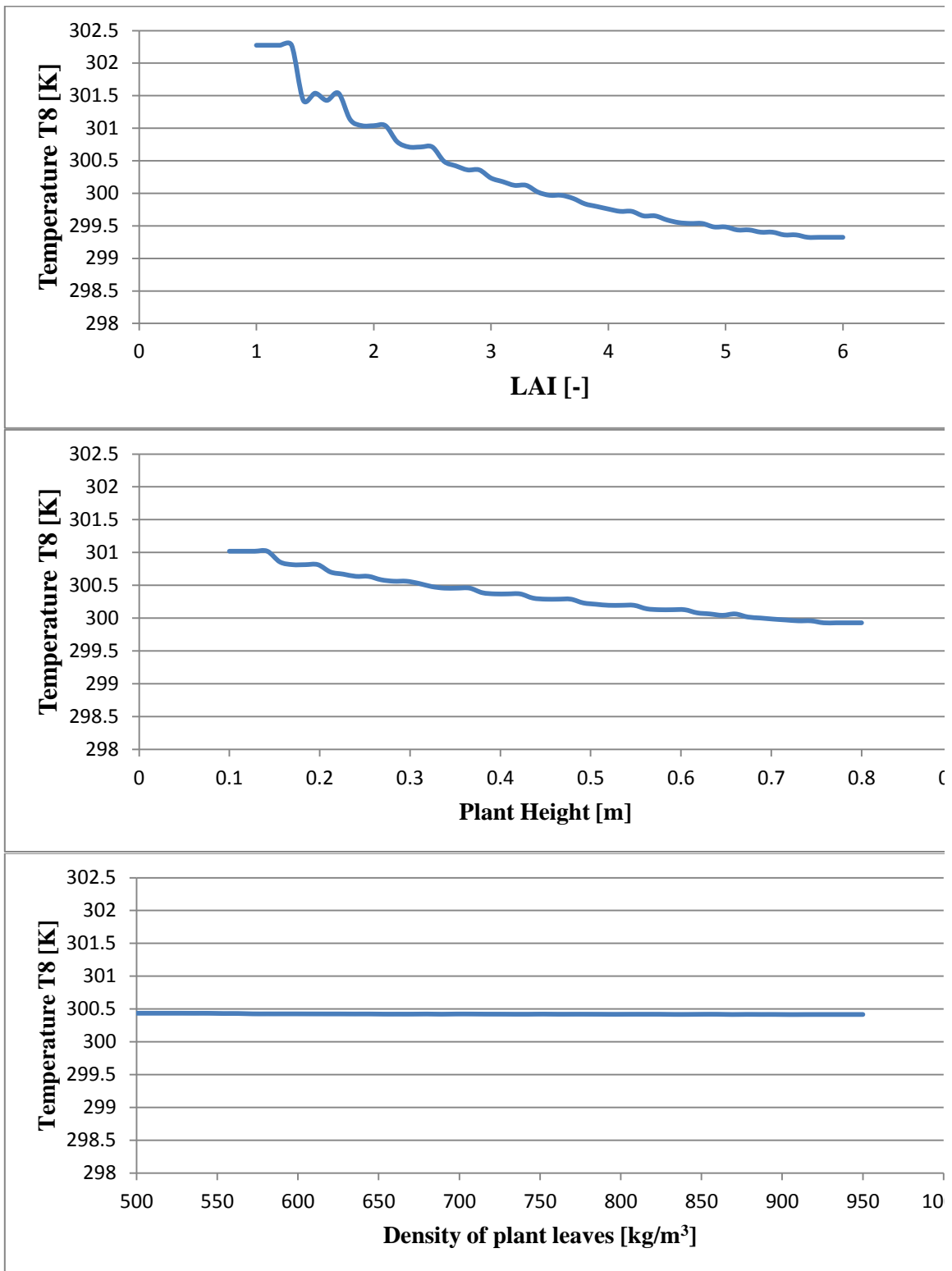
Figure 4-13: Sensitivity analysis results for LAI, plant height and leaf density (showing variations of temperature T8 at time step 85)
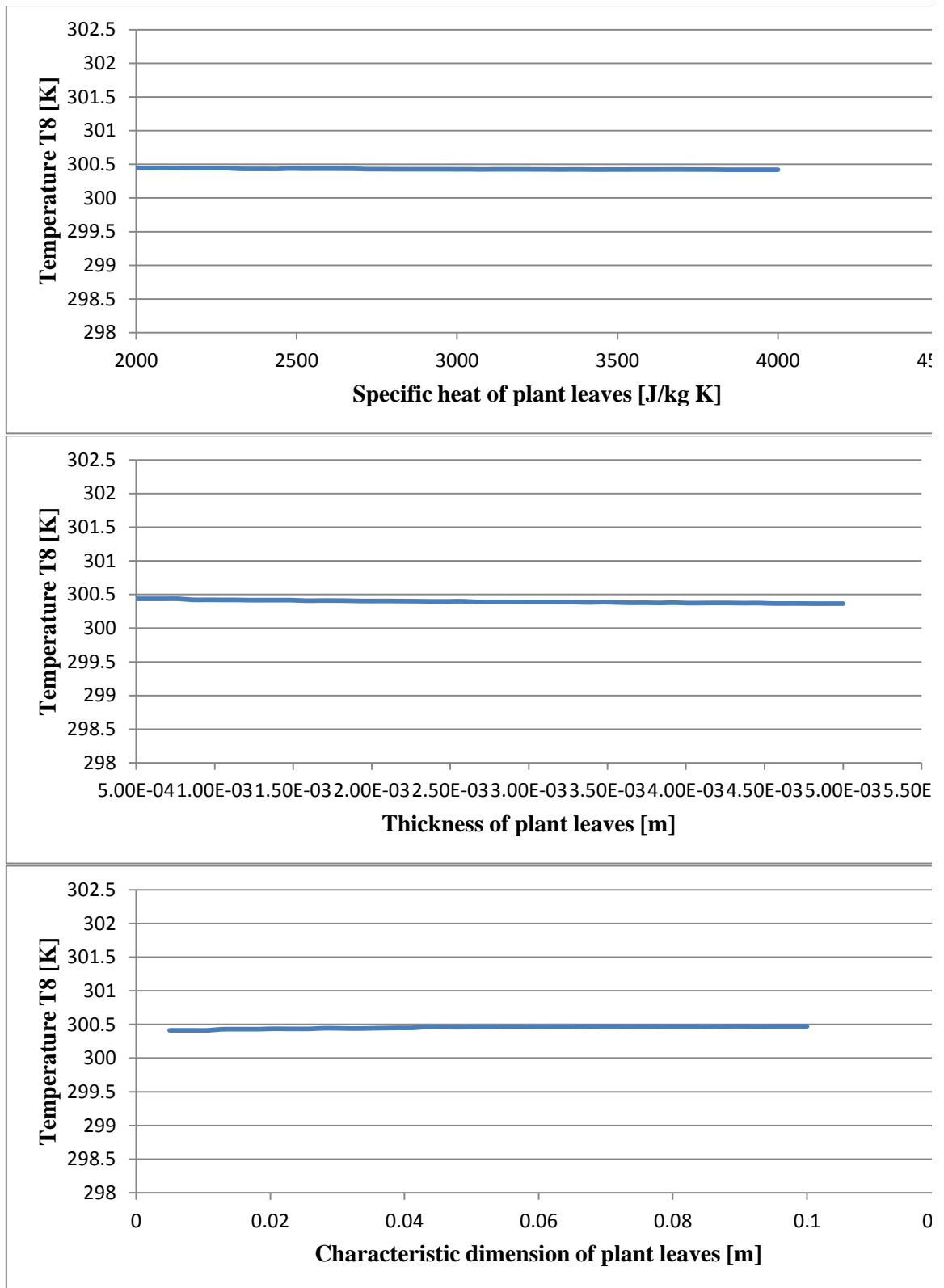
Figure 4-14: Sensitivity analysis results for specific heat, thickness and size of plant leaves (showing variations of temperature T8 at time step 85)
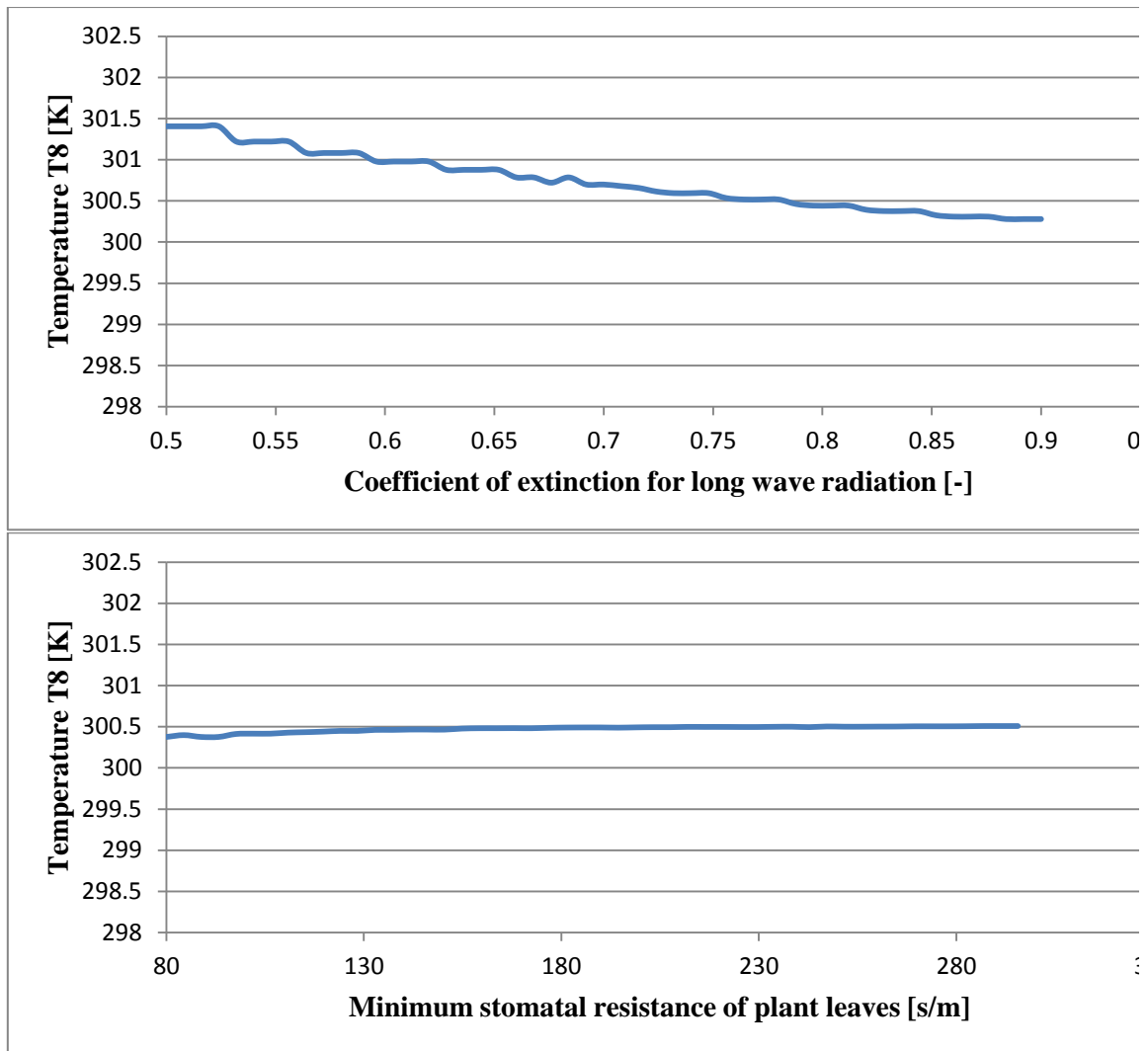
Figure 4-15: Sensitivity analysis results for plant's extinction coefficient and stomatal resistance (showing variations of temperature T8 at time step 85)

As expected, it can be inferred, from figures 4.13, 4.14 and 4.15, that all of the inputs for the plant characteristics, except the leaf size and the stomatal resistance, have an influence on decreasing the green roof temperature.

4.8.2 Sensitivity analysis for soil variables

Figures 4.16 to 4.18 show the sensitivity analysis results for eight soil related inputs.
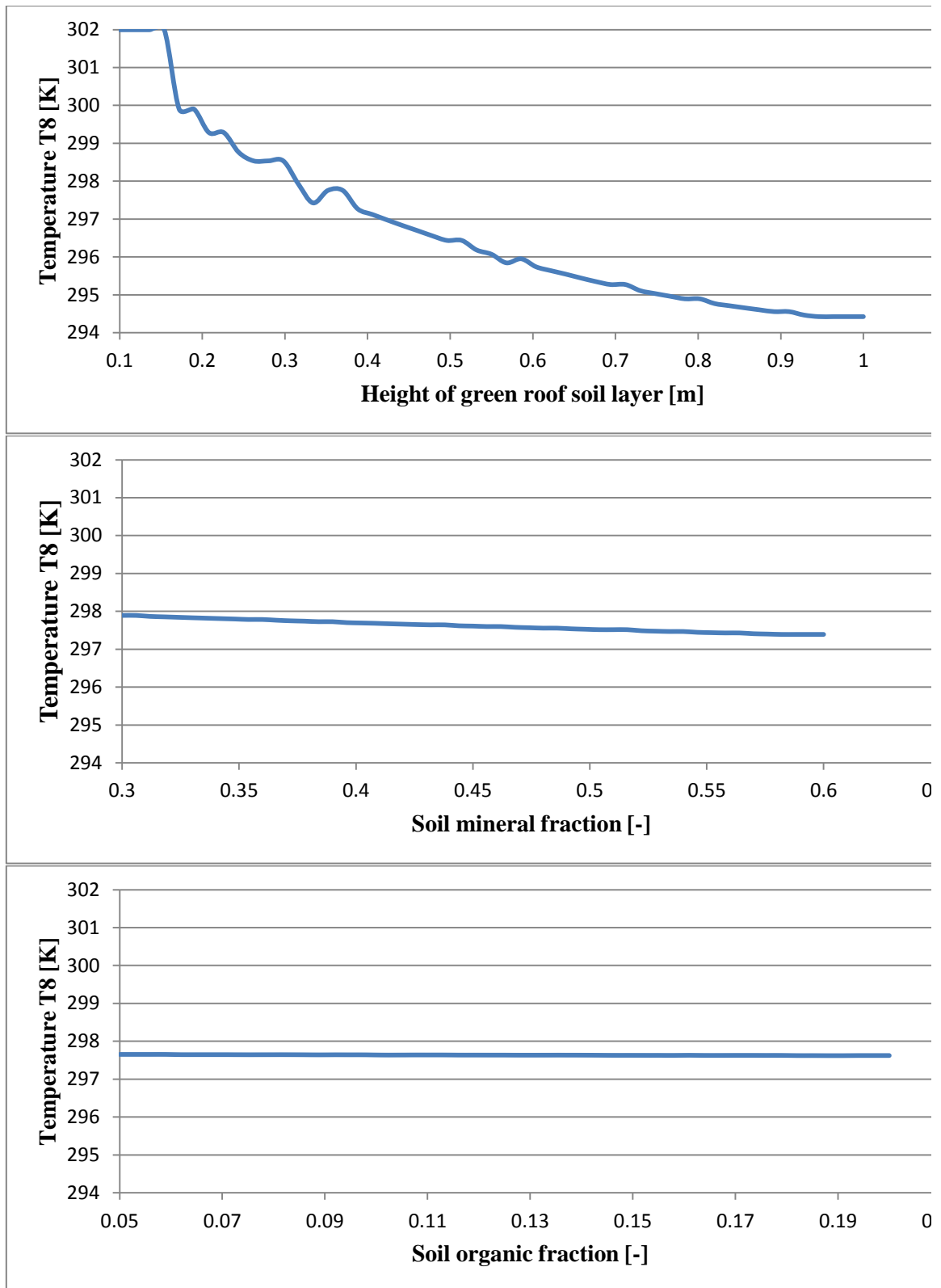
Figure 4-16: Sensitivity analysis results for soil height, mineral fraction and organic fraction (showing variations of temperature T8 at time step 85)
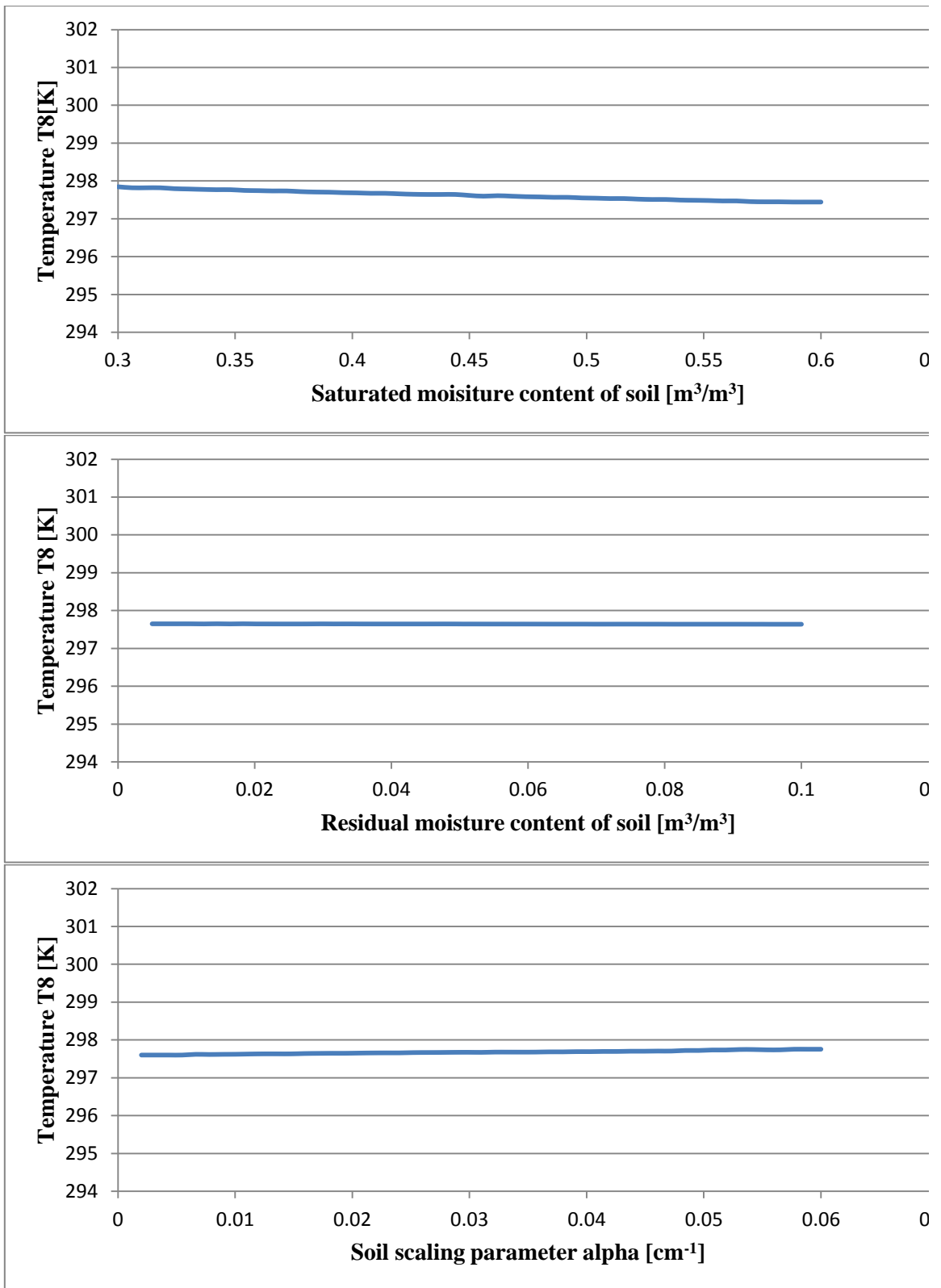
Figure 4-17: Sensitivity analysis results for soil's saturated moisture content, residual moisture content and alpha index (showing variations of temperature T8 at time step 85)
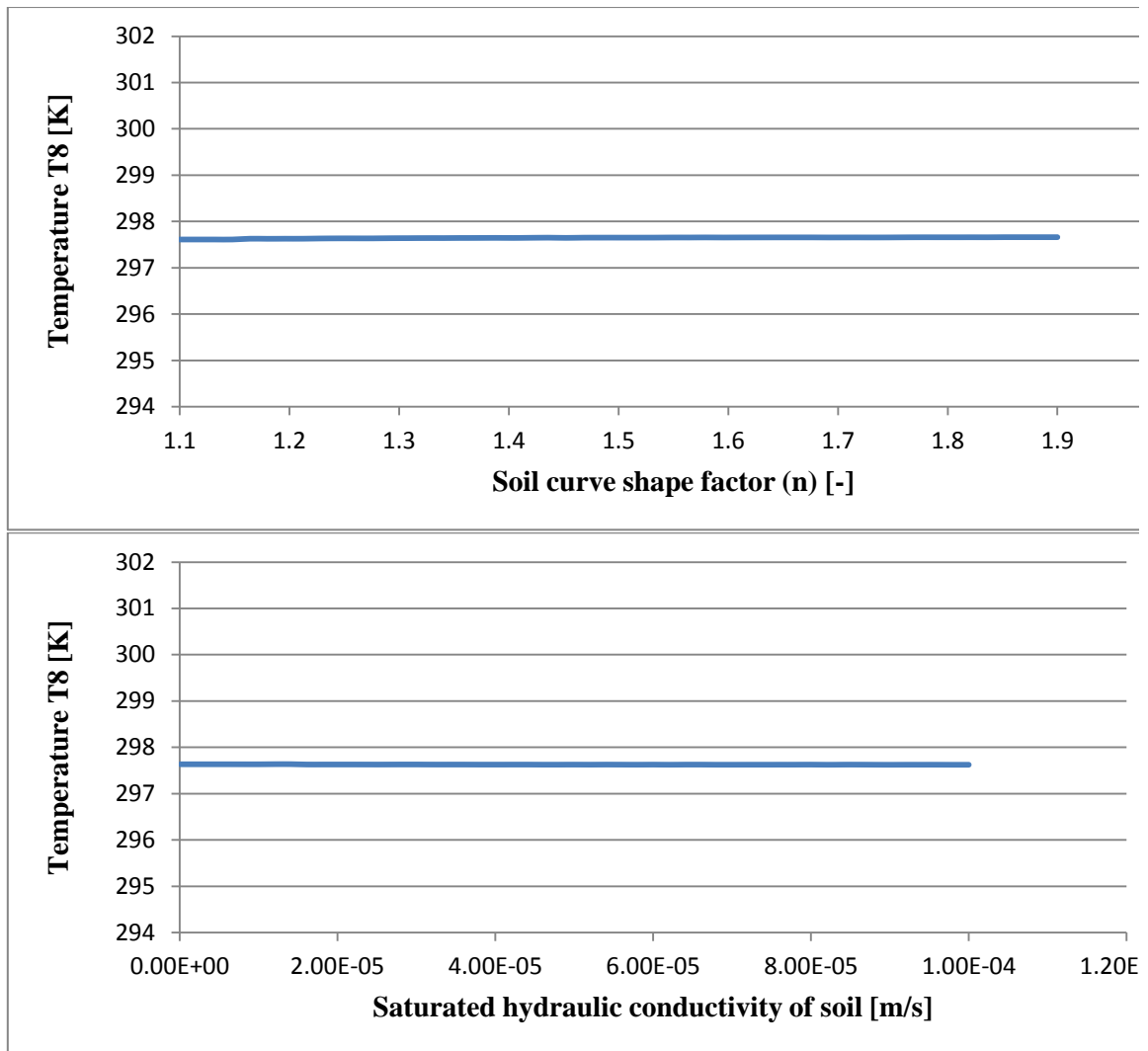
Figure 4-18: Sensitivity analysis results for soil's curve shape factor index n and saturated hydraulic conductivity (showing variations of temperature T8 at time step 85)

From figures 4.16, 4.17 and 4.18, it can be inferred that all characteristics of soil, except soil's 'alpha' index, have an influence of decreasing the green roof temperature under the specific conditions that the simulations were done.

4.8.3 Sensitivity analysis for radiation variables

Figures 4.19 and 4.20 show the sensitivity analysis results for radiation related inputs.
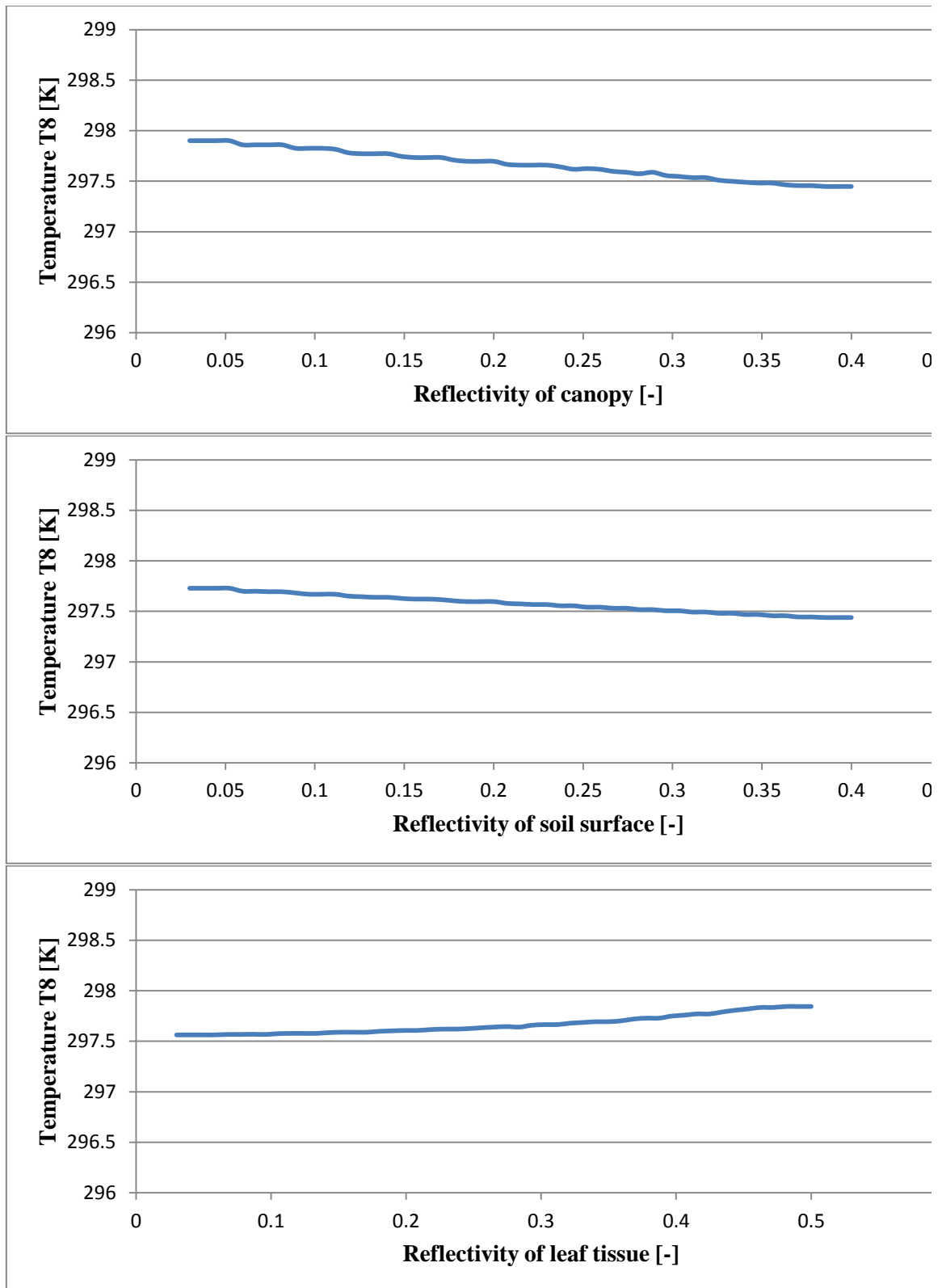
Figure 4-19: Sensitivity analysis results for reflectivity of canopy bulk, soil surface and leaf at tissue level (showing variations of temperature T8 at time step 85)
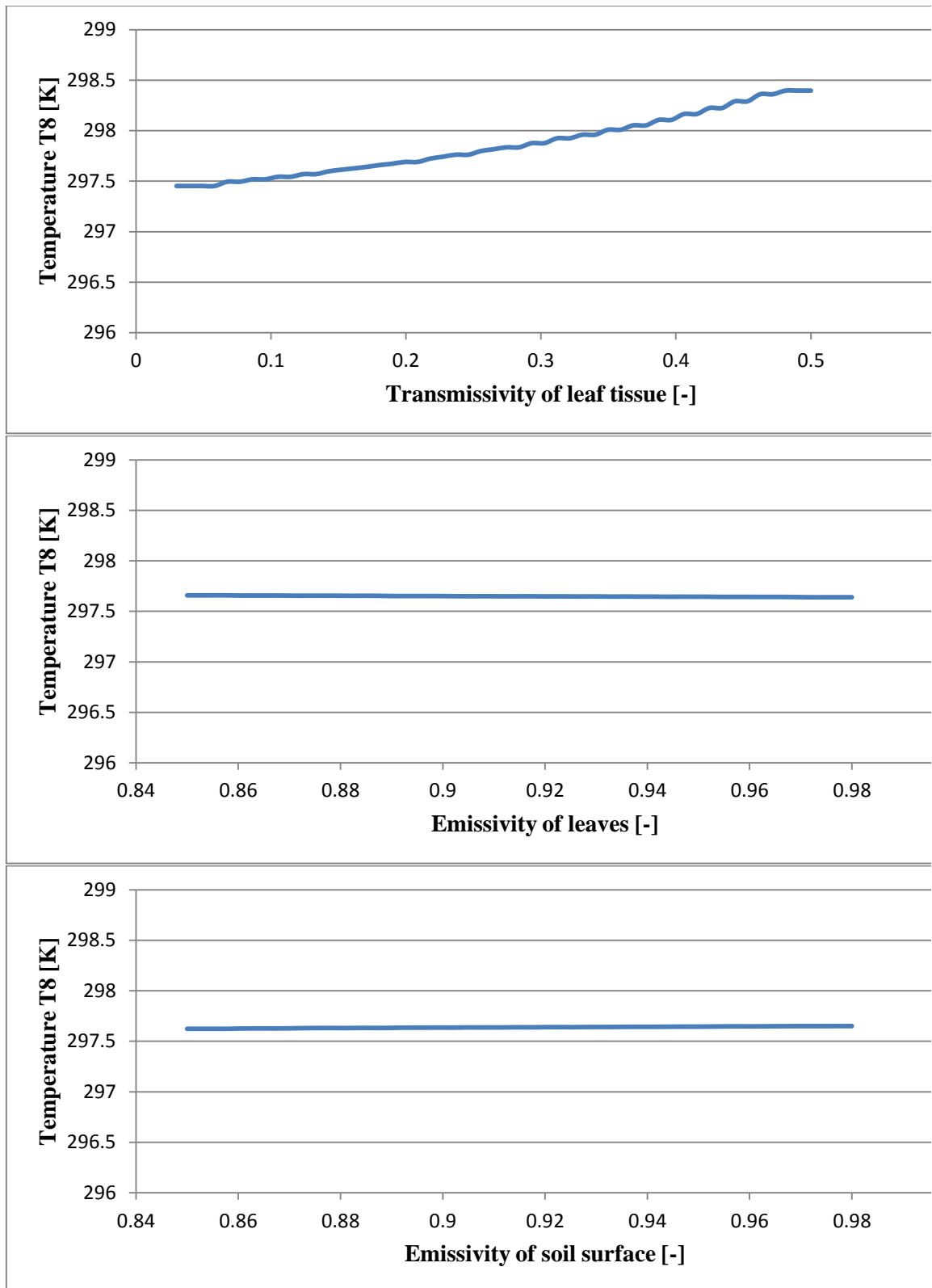
Figure 4-20 Sensitivity analysis results for leaf transmissivity, and radiation emissivity for leaves and soil surface (showing variations of temperature T8 at time step 85)

From figures 4.19 and 4.20, it can be inferred that, except for leaf's tissue level reflectivity and transmissivity, all properties have an influence of decreasing the green roof temperature. The increase of green roof temperature with the increase in the reflectivity of leaf tissue is not rational. Inspecting the equation involving this variable (as given in appendix 3.1 and repeated here);

$$k_s = [(1 - \tau_t)^2 - \rho r_t^2]^{1/2} k_l \tag{4-5}$$

it is evident that an increase in leaf tissue reflectivity ρr_t will cause a decrease in coefficient of extinction for short wave radiation (k_s) for a given transmissivity of leaf tissues (τ_t) and coefficient of extinction for long wave radiation (k_l) and thus letting more radiation energy to reach the soil and increasing the green roof temperature. However in reality, an increase in ρr_t occurs together with a decrease in τ_t and the net effect will be an increase in the coefficient of extinction and further shielding on onward radiation. However, within the context of the sensitivity analysis, only one variable is changed at a time, which explains the irrational results.

4.8.4 Sensitivity analysis summary

All of the above results are compared to show their relative influence and reproduced in table 4.7. The ranges of values selected for each of the input variables are as per the usual minimum and maximum values of green roof construction, plant properties and soil characteristics. The main limitation of this analysis is that it did not consider the inter-relation between the input variables, such as the transmissivity and reflectivity of leaf tissues. Also within the Genopt program, one value of the result is required as an *objective function* to compare and therefore one arbitrary temperature is chosen to compare. Although the single value of the temperature chosen served as a point of comparison for the parametric runs, a more realistic comparison for a set of output values would be a measure such as the root mean square deviation. However, implementation of such comparisons in Genopt would require some advanced customizations.

Table 4-7 Sensitivity analysis order for input variables

Significance rank	Input	Range of input change	Output change (absolute) [K]
1	Height of green roof soil layer [m]	0.1 to 1	7.57141
2	Plant LAI	1 to 6	2.95118
3	Coefficient of extinction for long wave radiation [-]	0.5 to 0.9	1.1264
4	Plant Height [m]	0.1 to 0.8	1.0906
5	Transmissivity of leaf tissue [-]	0.03 to 0.5	0.94406
6	Soil mineral fraction [-]	0.3 to 0.6	0.50104
7	Reflectivity of canopy [-]	0.03 to 0.4	0.45343
8	Saturated moisture content of soil [-]	0.3 to 0.6	0.40271
9	Reflectivity of soil surface [-]	0.03 to 0.4	0.29016
10	Reflectivity of leaf tissue [-]	0.03 to 0.5	0.28113
11	Soil scaling parameter alpha [cm^{-1}]	0.002 to 0.06	0.15366
12	Minimum stomatal resistance of plant leaves [s/m]	80 to 300	0.13208
13	Thickness of plant leaves [m]	0.0005 to 0.005	0.07178
14	Characteristic dimension of plant leaves [m]	0.005 to 0.1	0.0607
15	Soil curve shape factor (n) [-]	1.1 to 1.9	0.04993
16	Soil organic fraction [-]	0.05 to 0.2	0.03158
17	Emissivity of soil surface [-]	0.85 to 0.98	0.02713
18	Specific heat of plant leaves [J/kg K]	2000 to 4000	0.02527
19	Density of plant leaves [kg/m^3]	500 to 950	0.02044
20	Emissivity of leaves [-]	0.85 to 0.98	0.01874
21	Saturated hydraulic conductivity of soil [m/s]	1e-4 to 1e-7	0.01285
22	Residual moisture content of soil [-]	0.005 to 0.1	0.01217

4.9 Conclusion

A general review of the input data required for the newly developed green roof model has been presented in this chapter, which include information gathered from literature and measurements carried out in a typical green roof site. The measurement methods explained in this chapter is expected to help the users of the simulation model to plan the required data collection as applied to the modeling situation. Furthermore the sensitivity analysis is conducted to give an indication to the user regarding the significance of each of the input variables and the degree of accuracy required in the input data.

CHAPTER 5

VALIDATION

5. Validation

5.0 Introduction

The objective of this chapter is to present the results of an experimental validation study that was conducted for comparing the results from the newly developed green roof model with those measured in a proposed experimental setup. The chapter starts with an explanation of the procedure for validation experiments, then moves on to give the details of test cell facilities and instrumentation and concludes with the presentation of the results.

5.1 Experimental procedure

Validation is done by comparing the measurements on a green roof test cell and the simulated values from the model. As the model consist of seven control volumes (plant, canopy air and five soil layers) and calculates the temperatures evolving within them in every defined time-step (as explained in section 3.3 in the model development chapter), temperatures of similar locations are recorded with a data logger for an experimental test cell in order to compare them with the model data. For the soil moisture data (also as explained in section 3.3), although the model calculates matric potentials [m] at five control volumes, only three CV's moisture data was recorded in the test cell, due to the comparatively large size of the moisture sensor probe. The moisture data collected was moisture content [m^3/m^3] which is also calculated in the model from the matric potential using the equation 3.37. The physical details of the test cell were entered in a model input file. The local climatic details were collected from weather stations and entered into model weather file. A separate text file is created for precipitation input. A portable temperature logger with nine temperature sensors is used in the test cell to gather temperatures of the control volumes considered in the model. The temperature at the bottom of the soil layer is recorded in a text file and used as the bottom boundary condition for the model (which otherwise comes from the building side of ESP-r interface). For the moisture data, three moisture content sensors and one matric potential sensor are used together with a data logger on

the test cell as is explained later in this chapter in section 5.3. The measured state variables (temperatures and moisture contents) were compared against the simulated values. Among all the state variables, the bottom soil layer temperature, is of particular significance, as it is passed on to the building side of ESP-r's every time step for the whole building simulation. The data for the loggers has been collected periodically from August to December 2014. A selection of data as explained in section 5.7 is used for the validation study of the model.

5.2 Test Cell construction

An artificial green roof is constructed on a test box in which the temperature and moisture variations will be studied. The test box is made from an open top stainless steel frame (2070mm length x 1050mm width x 300 mm height) reinforced on all edges with angle iron bars. All sides of the box are then attached with 50mm extruded polystyrene (XPS) insulation in order to reduce multi-dimensional conduction heat losses/gains from these surfaces. The box under construction is shown in figure 5.1.

Figure 5-1: Test cell under construction-XPS boards are being attached to the stainless steel box

Care was also taken to insulate the metal part well so that there will be no effects of thermal bridges by metal parts. The insulated metal box was covered with damp proof membrane (DPM) to prevent moisture entering the XPS boards and thereby reducing its thermal insulation strength. A drainage pipe was attached at the centre of the box, for collecting drain water for measurement. The completed box was placed on hollow concrete bricks with intermediate wood supports. Inside the box a 50 mm layer of gravel and over it a 200mm height soil bed were laid. The soil used is the local garden soil and its texture class has been identified as silt loam according to the procedure as mentioned in section 4.6.2 where by its composition has been determined as 22.2% clay, 67.17% silt and 10.63% sand. A selection of plant was planted on the test cell on 26 August 2013. The plant selected is an evergreen shrub type of garden plant of scientific name 'Buxus sinica', as has been described in table 4.2 and its properties as given in table 4.3. The completed test cell installation is shown in figure 5.2.

Figure 5-2: Completed test cell installation at CSET rooftop.

Figure 5-3: Thermal and moisture data logging facility installed at green roof test cell

5.3 Temperature logging

Temperatures at the selected points in the green roof test cell have been recorded using a nine channel thermometer with data logging facility. The temperature sensors of PTC type, were calibrated against a low temperature (melting ice) and a high temperature before they are placed in the test cell. The battery powered instrument was placed in an instrument panel attached to the test cell (figure 5.3) and readings were occasionally transferred to a PC. The thermometer data logger is shown in figure 5.4. These sensors record the following nine temperatures: ambient air, plant leaf surface, canopy air, five soil depths representing five control volumes and soil bottom. The salient features of the thermometer are summarized in table 5.1

Figure 5-4: WT0T1-9-02 Temperature data logger

Table 5-1: Features of temperature data logger and sensors

Manufacturer	Wangyunshan Fuzhou Information Technology Co Ltd
Model number	WT0T1-9-02
Measuring range	Temperature: -30 ºC ~ 84 ºC
Accuracy	Temperature: standard room temperature $\pm$ 0.5 ºC at 25 ºC
Resolution	Temperature: 0.1 ºC
Sensor type	Resistance type (PTC)
Record interval	6 seconds or above
Number of channels	20 max /custom made to order
System clock error	1 s/day
Sensor cable	2 wire/ 2 m long

Prior to using the sensors they were calibrated with laboratory tests. The sensors were first placed on hot water and temperatures read on all sensors as the water was let to cool by itself. 1 minute interval readings were logged for about one and half hour. The results are shown in figure 5.5. The maximum standard deviation between the readings from all 9 sensors was found to be 0.417 ^{0}C. This gives a tolerance estimate[84] of 0.834 ^{0}C which is higher than the published value of accuracy 0.5^{0}C. This is due to some spikes in readings, which when removed resulted in a maximum standard deviation of 0.115 ^{0}C and corresponding tolerance limit 0.230 ^{0}C, which is in agreement with the manufacturer's value of accuracy
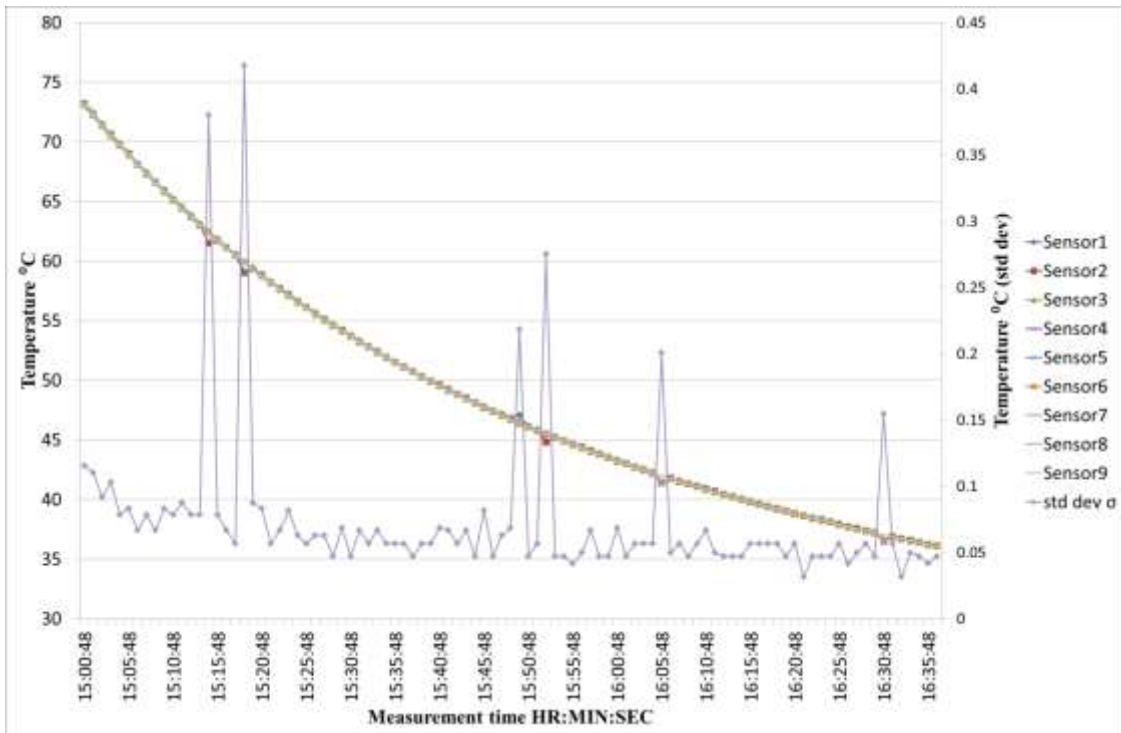
Figure 5-5: Results of calibration test for 9 temperature readings at high temperature

The experiment was repeated for low temperatures by immersing all sensors in ice cubes and recording the individual values as the ice melts. The calibration results are shown in figure 5.6.
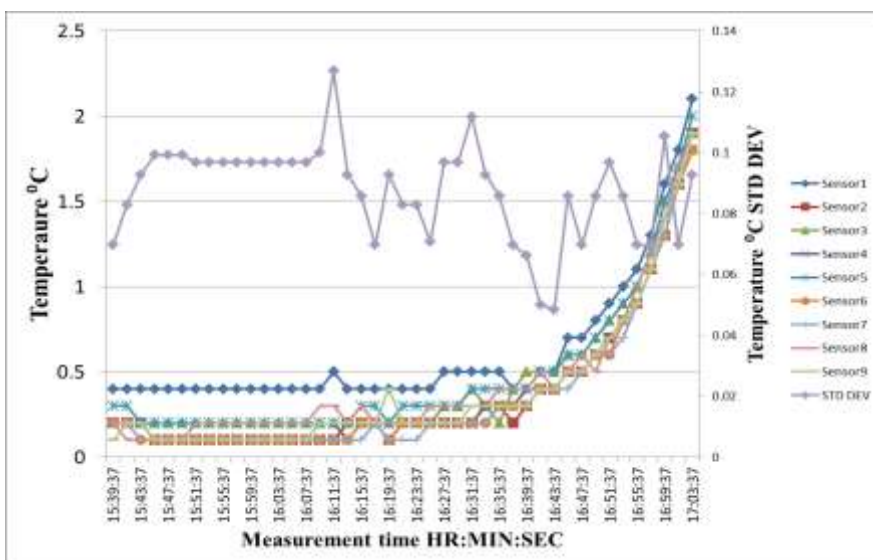
Figure 5-6: Results of calibration test for 9 temperature readings at low temperature

It was noted that while ice is still at solid phase there are some differences among individual sensor readings probably due to the local temperature differences. As the ice melted and liquid was well mixed this temperature difference disappeared. The standard deviation maximum value was 0.127 ^{0}C which corresponds to a tolerance of 0.254 ^{0}C.

5.4 Moisture logging

Soil moisture contents and matric potentials at test cell were measured and logged using a set of Delta-T Devices'; ML2 Theta-probes, an EQ2 Equi-tensiometer and a DL6 Data-logger. The sensor sizes of both ML2 and EQ2 are large (6 cm), thus making it impossible to install at representative depths of control volumes in the test cell soil (height 20 cm). The 20 cm soil bed is divided into five control volumes of 4cm heights, with CV1 covering (0-4cm), CV2(4-8cm), CV3 (8-12cm), CV4 (12-16cm) and CV5 (16-20cm). Three theta-probes were installed at representative depths of CV2, CV3 and CV4, at 6 cm, 10 cm and 14 cm respectively and a tensiometer at 10 cm depth for CV3. Readings were logged at a 10 minute interval from July to December 2014 and subsequently selected for validation evaluations.

The Theta-Probe soil moisture sensors work on a principle of dependency of di-electric constant of soil on its moisture content. An array of four steel rods in the sensor is used to measure the dielectric constant of soil after injecting a signal of 100 MHz into the soil. A linear relation is assumed between the square root of dielectric constant (ε) and moisture content (θ) as:

$$\sqrt{\epsilon} = a_0 + a_1\,\theta \qquad\qquad\qquad (5\text{-}1\ )$$

where a_0 and a_1 are coefficients which are either determined by laboratory calibration procedure for specific soil or used as supplied by manufacturer for generalized soil classes. Two sets of general coefficients are provided by the manufacturer, namely a_0=1.6 and a_1=8.4 for mineral soils and a_0=1.3 and a_1=7.7 for organic soils. The set for the mineral soils are used for the data collection at the test cell. The accuracy of using the generalized coefficients were found to be sufficient enough for the soil

moisture content measurement in validation studies. Table 5.12 gives a summary of instrument specifications.

Table 5-2: Specification for Theta-Probe ML2 for measuring soil moisture content

Manufacturer	Delta T
Model type	ML2
Range	0.05-0.6 m^3/m^3
Accuracy (calibrated for specific soil)	$\pm$ 0.01 m^3/m^3 at 0-40 ºC $\pm$ 0.02 m^3/m^3 at 40-70 ºC
Accuracy (using generalised coefficients)	$\pm$ 0.05 m^3/m^3 at 0-70 ºC
Response time	Less than 0.5 s

The principle of measuring matric potential with a tensiometer is by measuring moisture content and then converting it to matric potential. The EQ2 probe consists of a theta probe that is embedded in a porous medium of known matric potential/ moisture content characteristics. In the soil, the water content in the porous medium and that of surrounding soil come to an equilibrium. The soil moisture content is converted to matric potential readings. The specification summary is given in table 5.3.

Table 5-3: Specification for tensiometer EQ2 for measuring soil matric potential

Manufacturer	Delta T
Model type	EQ2
Range	0 to -1000 kPa
Accuracy	$\pm$ 10 kPa at range 0 to -100 kPa $\pm$ 5 % at range -100 to -1000 kPa
Soil types	non-saline soils
Output	150 to 550 mV non linear (as per calibration graph)

A calibration graph is provided by the manufacturer which is specific to the sensor's serial number and it is shown in figure 5.7.

The chart shows a plot with "EQ2 output (mV)" on the x-axis (0 to 600.0) and "Matric Potential (kPa)" on the y-axis (0 to -400). Data points are labelled "Matric Potential (kPa)" with a "polynomial curve fit" line. The equation displayed is:

$$y = 3.83628E\text{-}12x^6 - 78.47338E\text{-}10x^5 + 6.37949E\text{-}6x^4 - 25.82104E\text{-}4x^3 + 52.29821E\text{-}2x^2 - 42.98971E\text{+}0x + 62.26373E\text{+}0$$
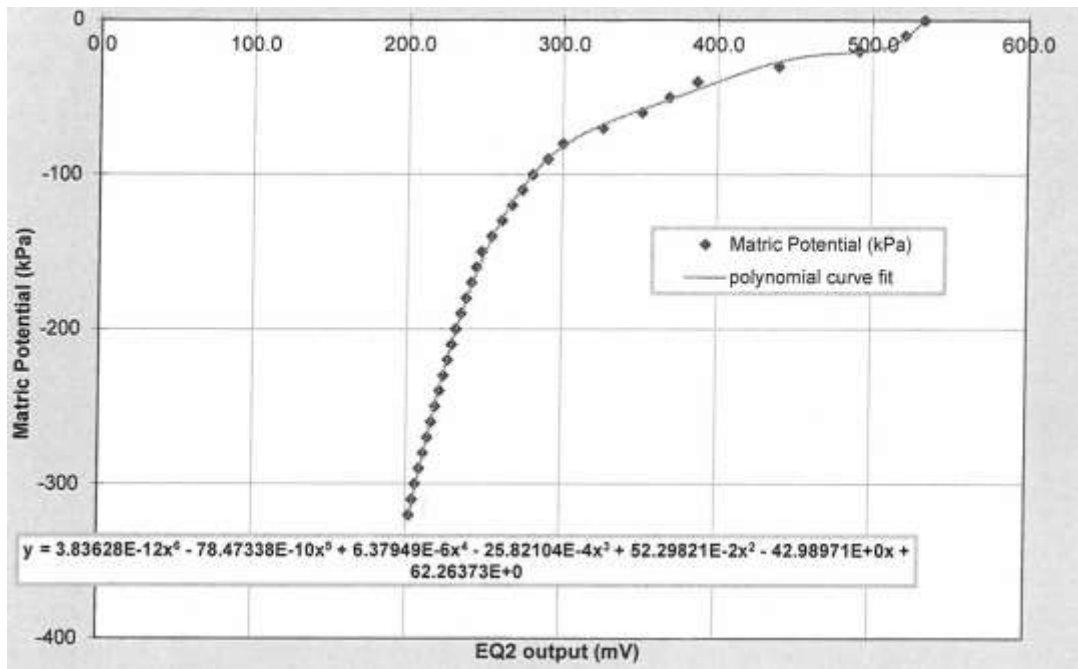
Figure 5-7: Extract from the calibration data for EQ2 tensiometer provided by manufacturer

The DL6 data logger is a battery powered nine channel logger which can accommodate up to six analogue channels suitable for soil moisture sensors, one resistance channel suitable for temperature sensor, one event counter channel suitable for a rain gauge, and one multipurpose relay channel. Figure 5.8 shows a screen shot of the menu of DL6 setup screen with the green roof test cell data settings entered.

As all the data loggers are battery powered, they are kept on an electrical panel box close to the test cell. Thus the errors caused by sensors cable lengths and resistances are kept to a minimum in the validation experiments.
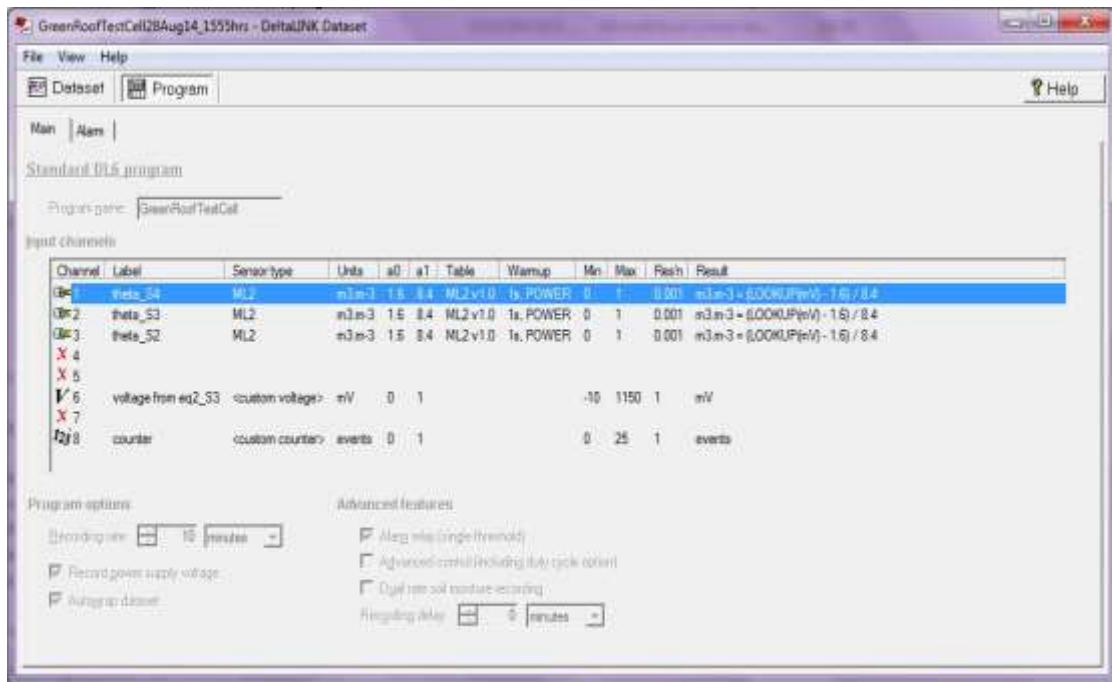
Figure 5-8: DL6 data logger program settings as used for the validation data collection

5.5 Weather file

Weather files for the model's validation studies have been prepared by compiling logged data collected from an on-site weather station and a pyranometer that were located next to the test cell. ESP-r standard weather files consist of hourly data of six weather variables, namely, diffuse horizontal solar radiation, dry bulb temperature, direct normal or global horizontal solar radiation, wind speed, wind direction and relative humidity. To work with shorter time steps ESP-r has a facility to create weather files of sub-hourly resolution in temporal files. This feature was used in this validation study to create a 10 minutes' resolution weather data. Figure 5.9 shows an extract of the temporal weather file for a few time steps on the day number 229 (17 August).

In addition to the standard ESP-r climatic data, the green roof module requires precipitation data, which is provided by a separate ASCII file of hourly single column data of precipitation in mm.

Figure 5-9: Extract from temporal weather file used for validation

5.5.1 Weather station

A fixed-mount 'Orion' weather station facility installed at CSET (placed next to the test cell) is used to gather weather file data of temperature, wind speed, wind direction and relative humidity and precipitation.

In the weather station, wind speed and wind direction are measured by using ultrasonic sensors. Three equally spaced ultrasonic sensors are used to measure the time taken by ultrasound to traverse the distance between them. Wind speed is calculated by measuring forward and reverse transmit times along the three paths and computing the net speed. As cancellations of forward and reverse paths are involved in the calculation, the influences of physical parameters such as temperature and humidity on the measured value of wind speed are mutually cancelled. Wind direction is not calculated when wind velocity falls below 0.05 m/s, and the previously calculated record is maintained.

Temperature is measured with a capacitive ceramic sensor whereas relative humidity measurement is based on a capacitive thin film polymer sensor.

Rainfall is measured by using a piezo-electric impact sensor, which measures the size and impact of individual rain drops. The impact is proportional to the volume of the drops. Accumulated precipitation is computed and reported in the instrument from the sum of the measurements taken from the beginning of every day.

Figure 5.10 shows the general arrangement of weather station installation and Table 5.4 shows the sensors' accuracy for each of the weather parameters.

Table 5-4: Sensor specification for Orion weather station

Sensor	Range	Accuracy	Resolution
Temperature	-60 to 140°F (-52 to +60°C)	±0.5°F (±0.3°C) at 68°F (+20°C)	0.1°F (0.1°C)
Wind Speed	0 - 135 mph (0 - 60 m/s)	±3% at 10 m/s	1 mph (1 m/s)
Wind Direction	Azimuth:0 - 360°	±2°	1°
Relative Humidity	0 - 100%RH	±3%RH (0-90%), ±5% (90-100%)	1%RH
Rainfall	Range: cumulative Collection Area: 60 cm2	±5% (spatial variations may exist)	0.01 in. (0.254mm)
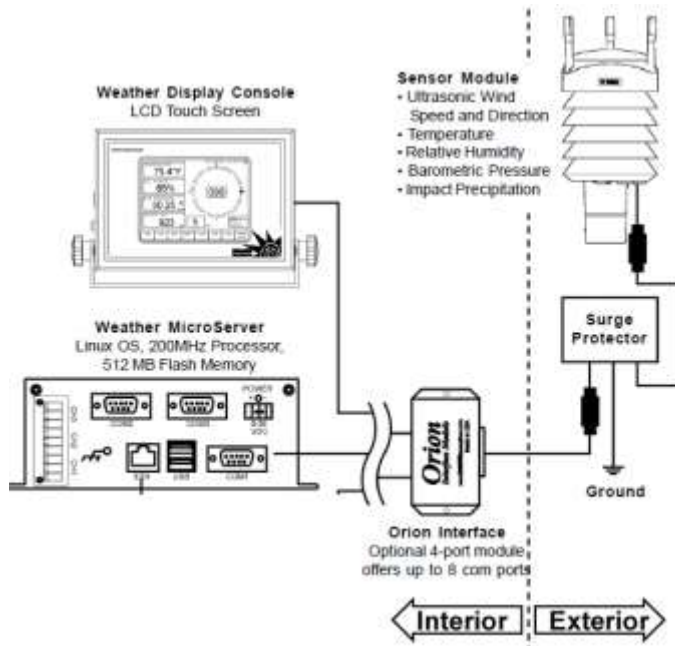
Figure 5-10: Orion weather station components schematic

5.5.2 Solar Radiation Measurements

A Pyranometer facility that has been installed next to the test cell is used to gather solar radiation data for the validation study. The unit used is SPN1 Sunshine Pyranometer. The instrument measures the global horizontal radiation, the diffused radiation and the sun shine's presence. SPN1 uses seven thermopile sensors placed on a hexagonal grid and covered by a special perforated hemispherical shadow mask dome. The unique shape of the shadow mask ensures that at least one sensor is always exposed to solar light, at least one is always masked and all sensors receive diffused light equally, as shown in figure 5.11.

Figure 5-11: SPN1 Sunshine Pyranometer

The pyranometer covers a spectrum of solar light of range 400 nm ~ 2700 nm, which are all the visible and infra-red ranges of thermal significance. Cosine response of a pyranometer [85] is the sensitivity of a flat surfaced sensor as against an ideal spherically shaped sensor and it varies as the cosine of angle between the incident radiation and sensor surface. Cosine response is worse when the sun is close to horizon. The ESP-r weather file and the temporal file can be set to use the direct solar radiation as either a global horizontal value or a direct normal value by setting a flag among the header lines as 123 or zero (line 15 of the tdfa file shown in figure 5.9). Direct normal radiation is the radiation intensity on a plane perpendicular to the direction of radiation. The instrument readings from the pyranometer can be converted from global to direct normal values by:

$$DN = \frac{GH - Diff}{cos\theta} \tag{5-2}$$

where DN is the direct normal radiation [W/m^2], GH is the global horizontal radiation [W/m^2] and θ is the solar zenith angle [rad] (angle between sun rays and vertical). A spreadsheet supplied by the manufacturer facilitates this conversion which involves calculating solar angles based on local coordinates and time. But as this feature is available in ESP-r global horizontal values are used in the compiled weather file. Table 5.2 shows summary of specifications

Table 5-5: Pyranometer SPN1 specifications summary

Manufacturer	Delta T
Model type	SPN1
General range	0 - 2000 W/m^2
Overall accuracy for global and diffuse radiations	±5% Daily integrals ±5% at 10 W/m^2 Hourly averages ±8% at 10 W/m^2 Individual readings
Spectral response	± 10% from 400nm to 2700nm
Sunshine status threshold	120 W/m^2 in the direct beam
Sunshine accuracy	± 10%
Cosine response	± 2% over 0-90° zenith angle
Temperature range	-40°C - +70°C

5.5.3 Compilation of weather data measurement

A 10 minute resolution data from 15 August 2014 to 21 December 2014 is used to create a validation weather file. Further, the temperatures on validation test days are replaced with ambient temperature reading measured at test cell by the sensors described in section 5.3. This was done as it was observed that the temperatures measured at the weather station and the temperatures measured at the test cell's ambient sensor are slightly different (Pearson coefficient of correlation =0.84), although of similar profile as shown in figure 5.12. It is noted that some of these variations are due to occasional spikes observed in test cell temperature sensors which could be originated in the instruments electronic circuitry. Similar spikes were noted during the instrument calibration procedure as described in section 5.3.
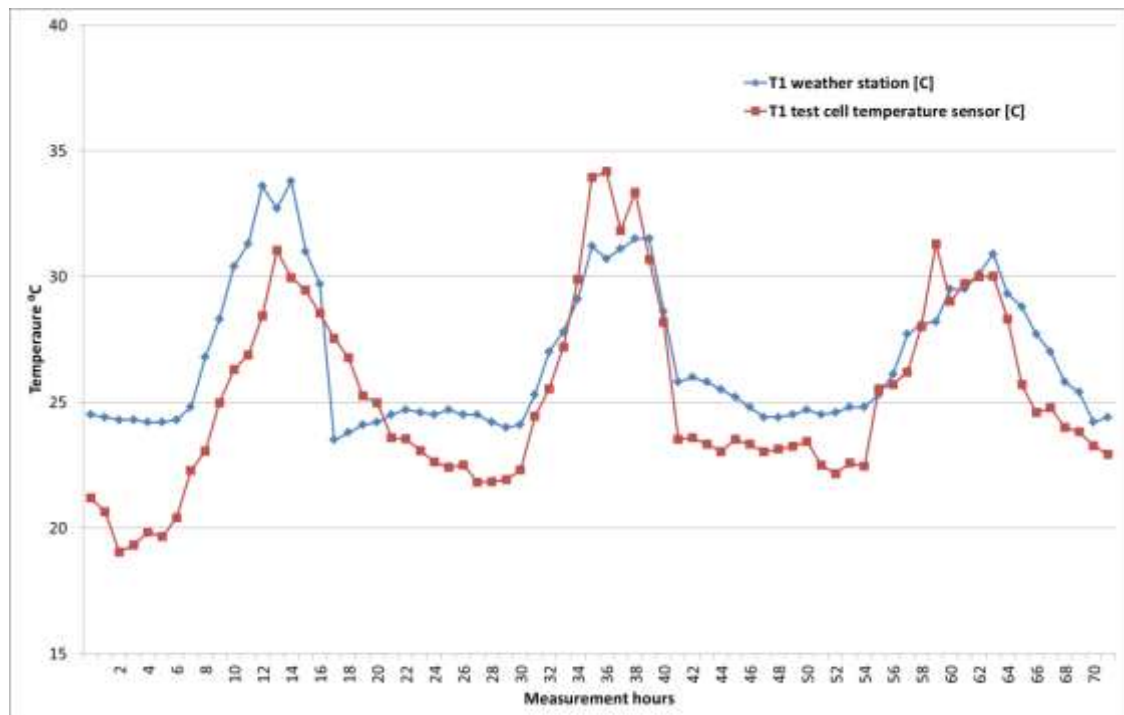
Figure 5-12: Comparison of ambient temperatures obtained from Orion weather station and test cell ambient sensor

5.6 Drain Measurement

Drain measurement is done by directing the drain pipe from the test cell to a graduated white plastic 'jerrican' container (Figure 5.13) and taking timed photos with a compact Raspbery-pi/camera setup (figure 5.14). The sequenced photo and its time record are

used to calculate the dynamic flow rate data. Figure 5.14 shows a selection of photos from the Raspberry board.

Figure 5-13: Drain measurement setup- graduated semi clear container

Figure 5-14: Drain measurement setup- Raspberry-pi/camera assembly placed facing the container
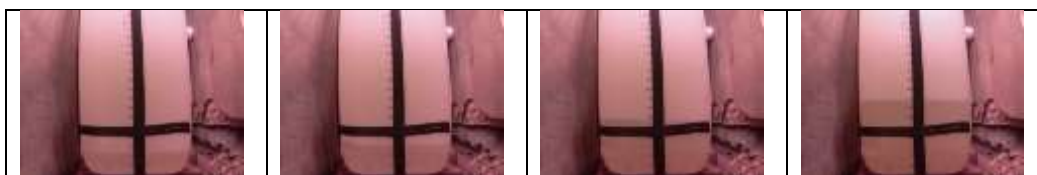
Figure 5-15: An extract from the sequence of photos taken with the programmed Raspberry-pi board

113

5.7 Validation Results and Discussion

Six validation periods were used from August 2014 to December 2014 to analyse the thermal and moisture predictions of the model. The validation dates were selected to represent a wide variety of weather conditions. This has been done after evaluating the whole data collection from the test cell instrumentation from 15 August 2014 to 21 December 2014. Typical weather patterns of Ningbo with long summer and winter, short autumn, all seasons rains and occasional thunderstorms, played a role in selecting these test days. Table 5.6 shows the selection criteria for the validation test dates. Separately a drainage test was conducted to test the models ability to predict run-off characteristics of green roof.

Table 5-6: Validation test dates and weather conditions

No	Test dates	Number of days (including start-up days)	Prevailing weather conditions
1	August 17- 18	2	Summer, moderate rain
2	August 28-30	3	Summer, heavy rain
3	September 26-27	2	Autumn, dry hot
4	October 17-18	2	Autumn, medium temperature, dry
5	October 30	1	Winter onset, strong winds, dry
6	December 5-6	2	Winter low temperature, dry

The following steps of procedure are done for the validation tests.

Step 1: A weather file is created with a 10 minutes resolution, in the ESP-r's temporal file format, using the data collected from weather station and pyranometer which has been imported to the ESP-r file. The ambient temperature (as it was found to be slightly different from the weather file data, as shown in figure 5.12) is replaced with the ambient temperature collected at the test cell (indicated as 'Ambient temperature T1' with a sign ⟹ in figure 5.16). A coma separated value (CSV) file is created and converted to the ESP-r temporal file format using the facility within ESP-r's project manager.

Step 2: A separate column file for precipitation is created for precipitation with one hour resolution. This file is read within the green roof module. The common sources

of precipitation data are of three hour resolution thus one hour resolution for validation is comparatively acceptable option.

Step 3: A column text file is created specifically for validation tests to feed in the lower boundary condition of the test cell to the green roof module (indicated as 'Bottom boundary temperature T9' with a sign ⟹ in figure 5.16). In the normal running of the program this value is read from the building side of ESP-r.

Step 4: Specific green roof input files are created for each test date, using the LAI and plant heights as measured for the test months (as explained in section 4.6.1 which deals with the plant data collection).

Step 5: Within the green roof module for the purposes of validation, CSV files that include variables being monitored are exported (written out in file); variables saved are the temperatures of all control volumes, the moisture contents and the matric potentials of soil control volumes and the drain rate.

Step 6: Test cell data from thermometer logger and moisture data loggers are compiled to do the comparison between simulated results and measured values. A moving average method [86] is used to remove instrument spikes from the thermometer logged data. All nine temperature pairs are compared (including the sets; the measured T1 against the simulated T1 and the measured T9 against the simulated T9, which are the same values for the validation as shown in figure 5.16) to ensure the data sets coming from different sources are aligned correctly (thus T1-T1 and T9-T9 pairs match perfectly). The scheme of the validation comparison is shown figure 5.16. Root mean square error (RMSE) and Pearson's Correlation coefficients are used as measures of deviations between the measured and simulated sets of variables. These two measures of deviations have been widely used in validation studies such as Sailor[40].
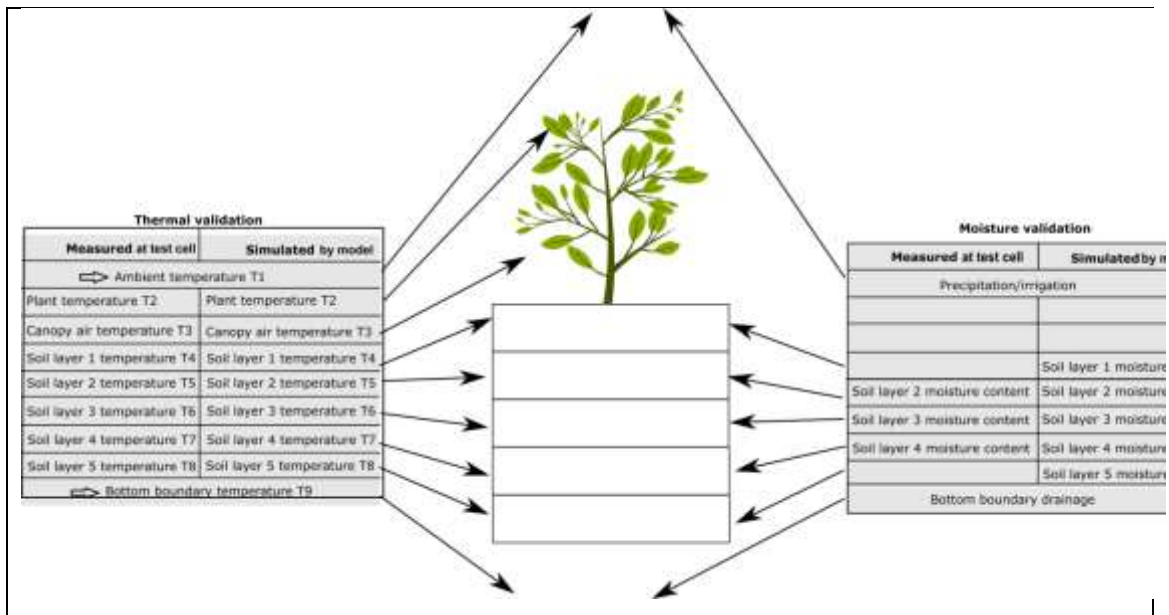
Figure 5-16: Measured and simulated parameters in thermal and moisture validation tests

5.7.1 Thermal validation results

All test dates are analysed in the following subsections for thermal validation. For comparing measured and simulated values two non-dimensional, statistical indices are used, the root mean square deviation (RMSD) and Pearson correlation coefficient (γ).

$$RMSD = \sqrt{\frac{\sum(I_s - I_m)^2}{N}}$$

(5-3)

$$\gamma = \frac{N\sum I_m I_s - \sum I_m \sum I_s}{\sqrt{[N\sum I_m{}^2 - (\sum I_m)^2]}\sqrt{[N\sum I_s{}^2 - (\sum I_s)^2]}}$$

(5-4)

where I_m is each measured value, I_s is each simulated value and N is the number of measured/simulated items in the set. RMSD indicate how close the values are, zero being a perfect match. Pearson coefficient indicates linear consistency between the compared pairs, one indicating a perfectly linear relation and zero indicating no relation at all.

116

5.7.1.1 Results for test days August 17-18 - summer days with moderate rain

The temperatures of the seven control volumes evolved during the test days are shown in figure 5.18. Detailed pair by pair comparison for all temperature sets are given in appendix 6. Statistical indices obtained for the validation test 1 is given in table 5.7 below, which is also presented in chart for comparative illustration in figure 5.17.

Table 5-7: Comparative measures for validation test 1

Temperatures	CV1 Plant	CV2 Canopy air	CV3 Soil top layer	CV4 Soil layer 2	CV5 Soil layer 3	CV6 Soil layer 4	CV7 Soil bottom layer
RMSD [K]	2.415	2.854	1.047	1.209	1.488	0.813	0.764
Pearson correlation coefficient	0.9503	0.9056	0.9028	0.8130	0.6502	0.7357	0.5371
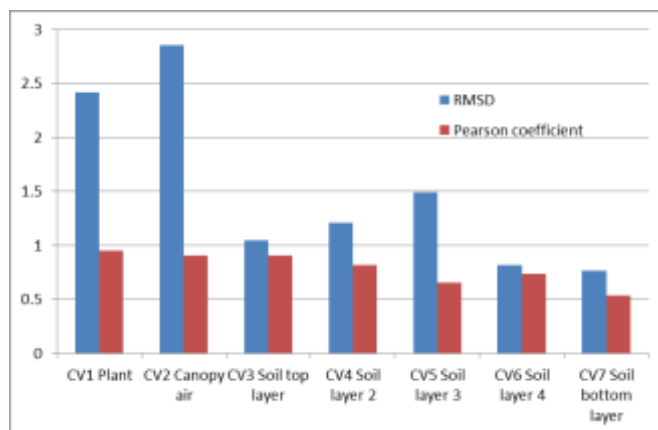
Figure 5-17: Validation test 1- statistical indices for all control volumes

From the results it can be observed that there is an increase in agreement between the simulated and measured temperatures, from CV1 to CV7 as the RMSDs between measured and simulated results decrease from 2.4[K] to 0.76 [K] and there is an increase in non-linearity in the deviations from CV1 to CV7, with a decrease in Pearson correlation coefficients, from 0.95 to 0.54. It can be generally concluded that at CV1 the agreement is poor but with a predictable difference and at CV7 end the result is good, with small but unpredictable deviations. This is further elaborated in section 5.7.1.7.
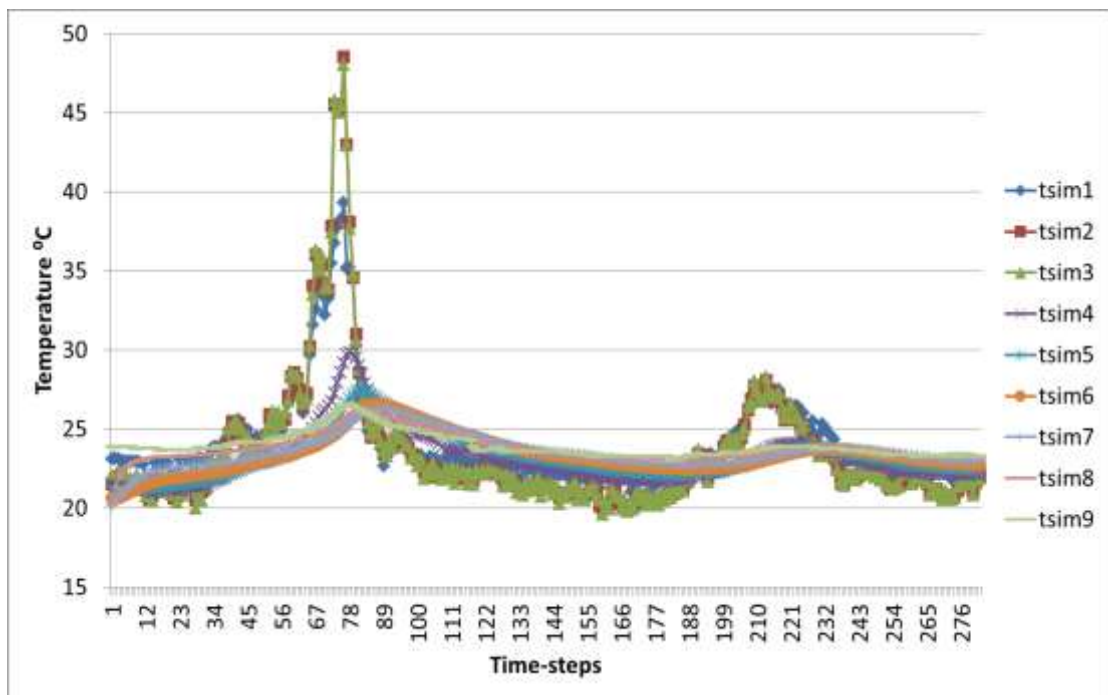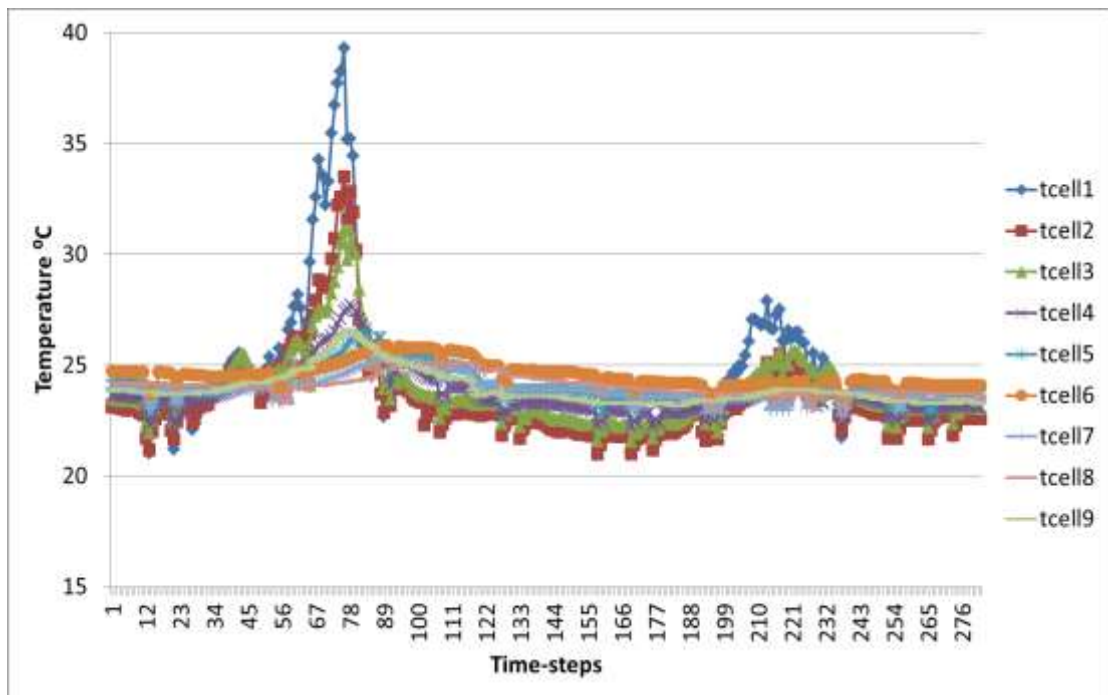
Figure 5-18: Illustration of temperatures measured (above) and simulated (below) against time step (10 minutes) number for the green roof test cell for validation test 1

5.7.1.2 Results for test days August 28-30- summer days with heavy rain

The temperatures evolved during the test days are shown in figure 5.19 and the comparative indices in table 5.8.
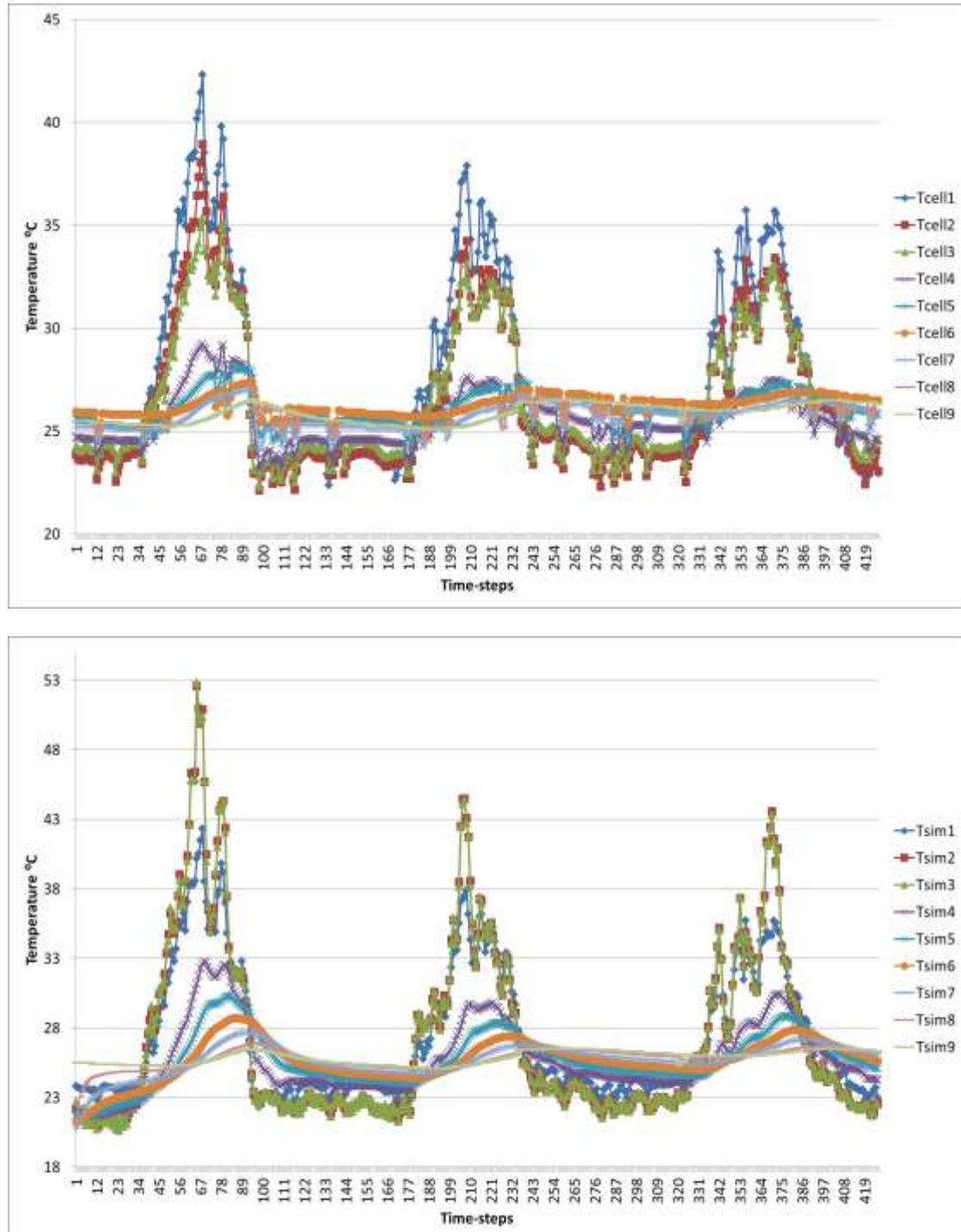
Figure 5-19: Illustration of temperatures measured (above) and simulated (below) against time step (10 minutes) number for the green roof test cell for validation test 2

Table 5-8: Comparative measures for validation test 2

Temperatures	CV1 Plant	CV2 Canopy air	CV3 Soil top layer	CV4 Soil layer 2	CV5 Soil layer 3	CV6 Soil layer 4	CV7 Soil bottom layer
RMSD [K]	3.196	3.670	1.494	1.387	1.355	0.874	0.457
Pearson correlation coefficient	0.9603	0.9389	0.9134	0.8243	0.6458	0.6642	0.8570

The trend of results is similar to the validation test 1 with RMSD decreasing from 3.2 [K] at CV1 to 0.46 [K] at CV7 and Pearson coefficient decreasing from 0.96 at CV1 to 0.66 at CV6. Compared to the test 1, it can be inferred that the results are slightly better both in terms of closeness of simulation to measurements and the linearity of deviations between them. The poor results in the Pearson correlation at CV5 and CV6 are due to the quality of measurement reading from test cell with spikes in instrument readings.

5.7.1.3 Results for test days September 26-27-autumn, dry hot days

The temperatures' comparative indices for the third test days are as shown in table 5.9 and the temperature evolution as in figure 5.20. The trend of results again is observed to be similar to the previous test, with an increasing trend of closeness between simulation and measurements from CV1 to CV7 and increasing trend of non-linearity in the same direction.

Table 5-9: Comparative measures for validation test 3

Temperatures	CV1 Plant	CV2 Canopy air	CV3 Soil top layer	CV4 Soil layer 2	CV5 Soil layer 3	CV6 Soil layer 4	CV7 Soil bottom layer
RMSD [K]	5.010	5.372	2.380	2.195	1.985	1.281	0.719
Pearson correlation coefficient	0.9270	0.9044	0.9409	0.8351	0.6244	0.7619	0.7185
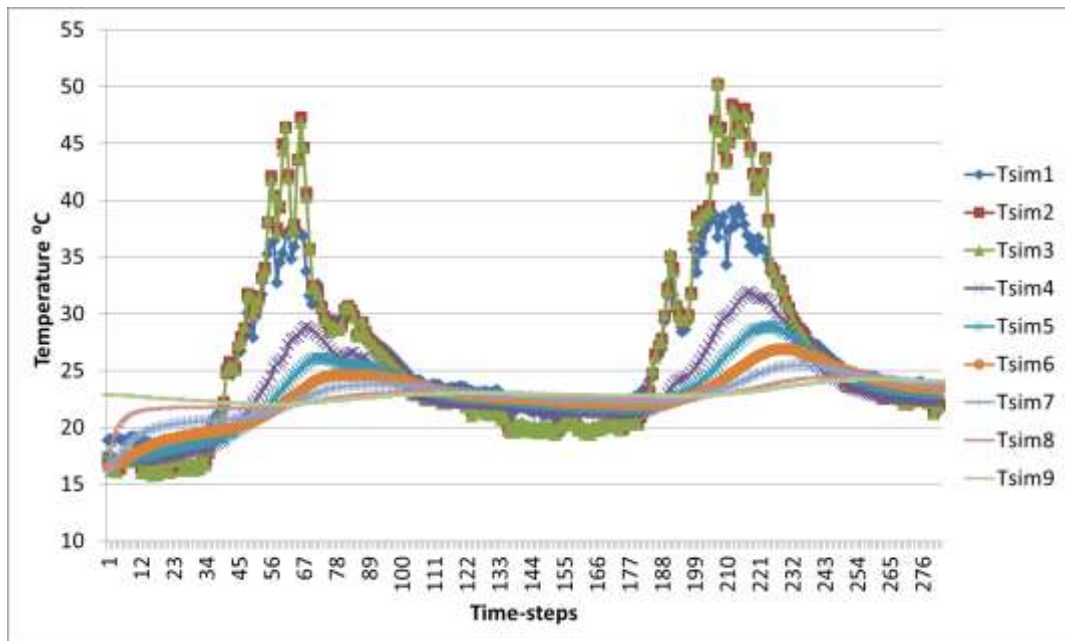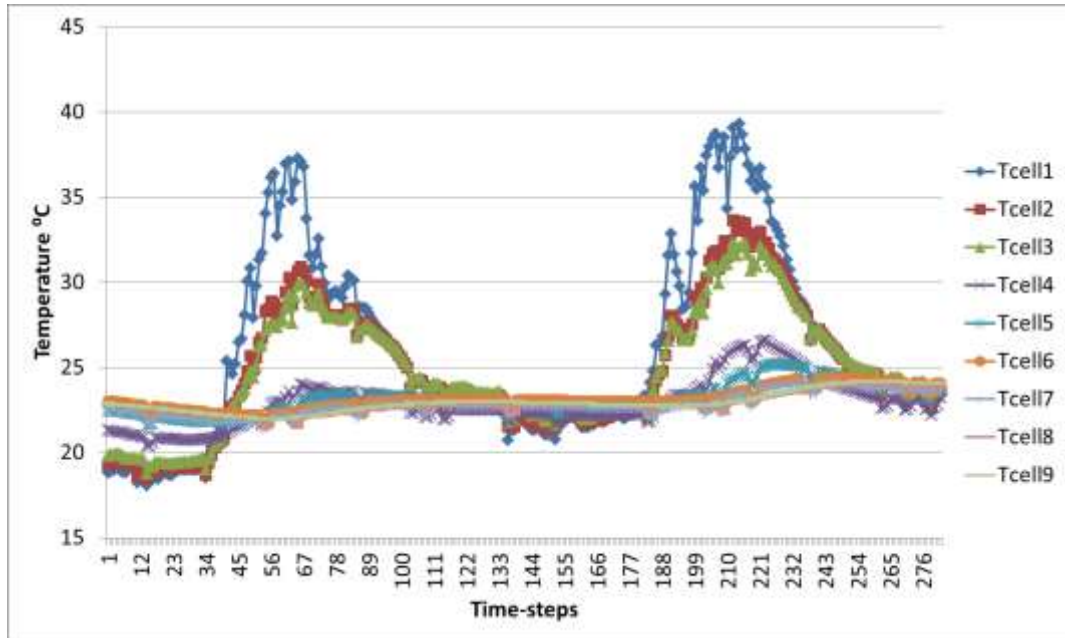
Figure 5-20: Illustration of temperatures measured (above) and simulated (below) against time step (10 minutes) number for validation test 3

121

5.7.1.4 Results for test days October 17-18 - autumn dry days with medium temperature

The temperatures evolution for the fourth test days are shown in figure 5.21 and the temperature comparative indices in table 5.10.
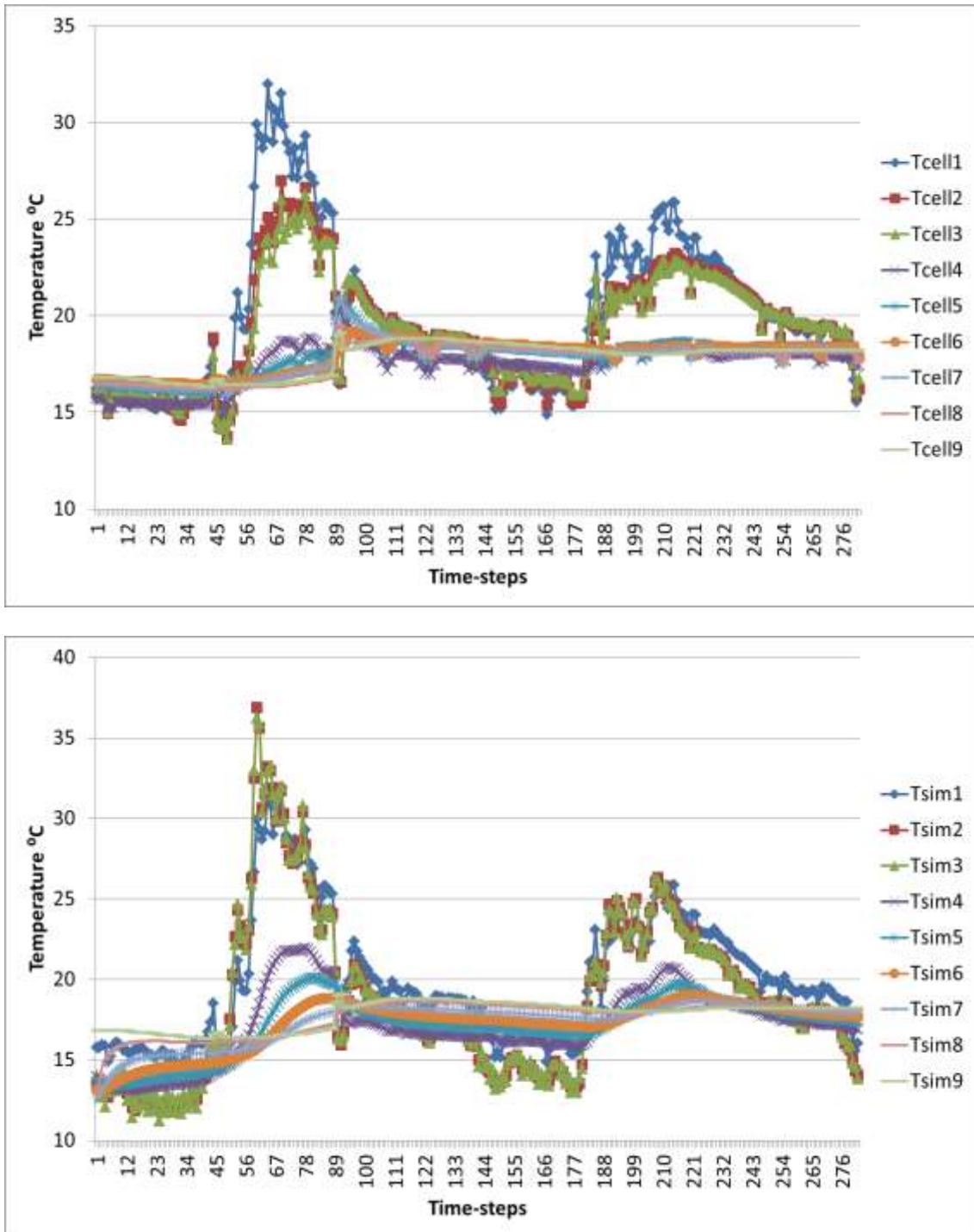
Figure 5-21: Illustration of temperatures measured (above) and simulated (below) against time step (10 minutes) number for validation test 4

Table 5-10: Comparative measures for validation test 4

Temperatures	CV1 Plant	CV2 Canopy air	CV3 Soil top layer	CV4 Soil layer 2	CV5 Soil layer 3	CV6 Soil layer 4	CV7 Soil bottom layer
RMSD [K]	2.871	3.155	1.520	1.473	1.228	0.839	0.397
Pearson correlation coefficient	0.8833	0.8404	0.8429	0.7556	0.7917	0.8379	0.9265

Here the trend of RMSD results is similar to the previous cases, but the Pearson coefficient values are now of the opposite trend towards CV7. The inconsistent nature of variations in the Pearson correlation coefficient again strengthen the assertion, as previously stated, that the sources of non-linearity are the instrument spikes at the test cell.

5.7.1.5 Results for test day October 30, winter onset, dry and strong winds

The statistical comparative indices for the fifth test day are shown in table 5.11 and the temperatures of control volumes in figure 5.22. This set of results confirms the general trend of results obtained in the previous studies of this chapter. From CV1 to CV7 RMSD improves and Pearson correlation deteriorates.

Table 5-11: Validation test 5 comparative measures

Temperatures	CV1 Plant	CV2 Canopy air	CV3 Soil top layer	CV4 Soil layer 2	CV5 Soil layer 3	CV6 Soil layer 4	CV7 Soil bottom layer
RMSD [K]	2.117	2.133	1.098	1.223	1.106	0.747	0.475
Pearson correlation coefficient	0.9368	0.9270	0.9489	0.8861	0.7819	0.8043	0.6897
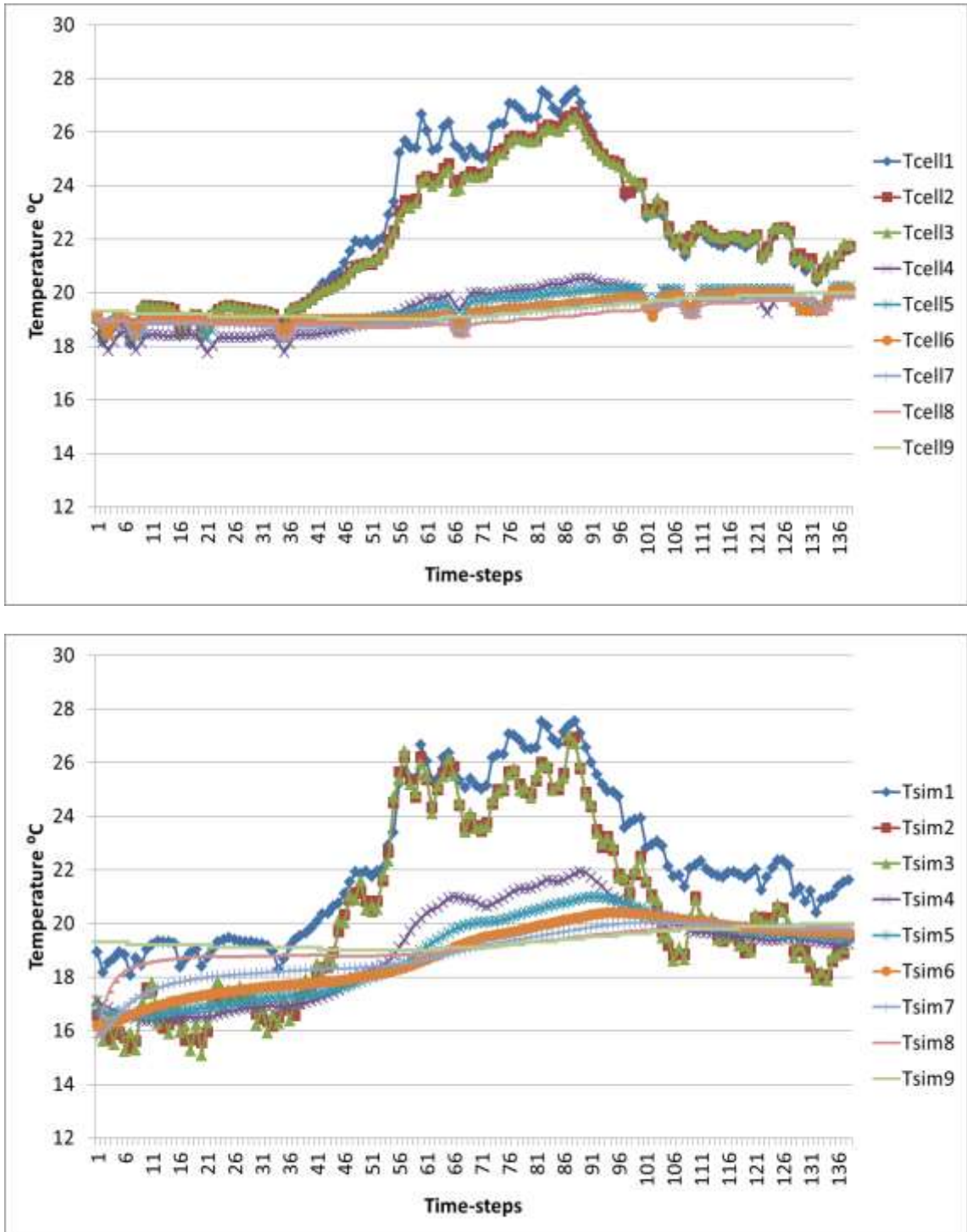
Figure 5-22: Illustration of temperatures measured (above) and simulated (below) against time step (10 minutes) number for validation test 5

5.7.1.6 Results for test days December 5-6, winter dry days

The statistical comparative indices for the fifth test days are shown in table 5.12and the temperatures of control volumes in figure 5.23
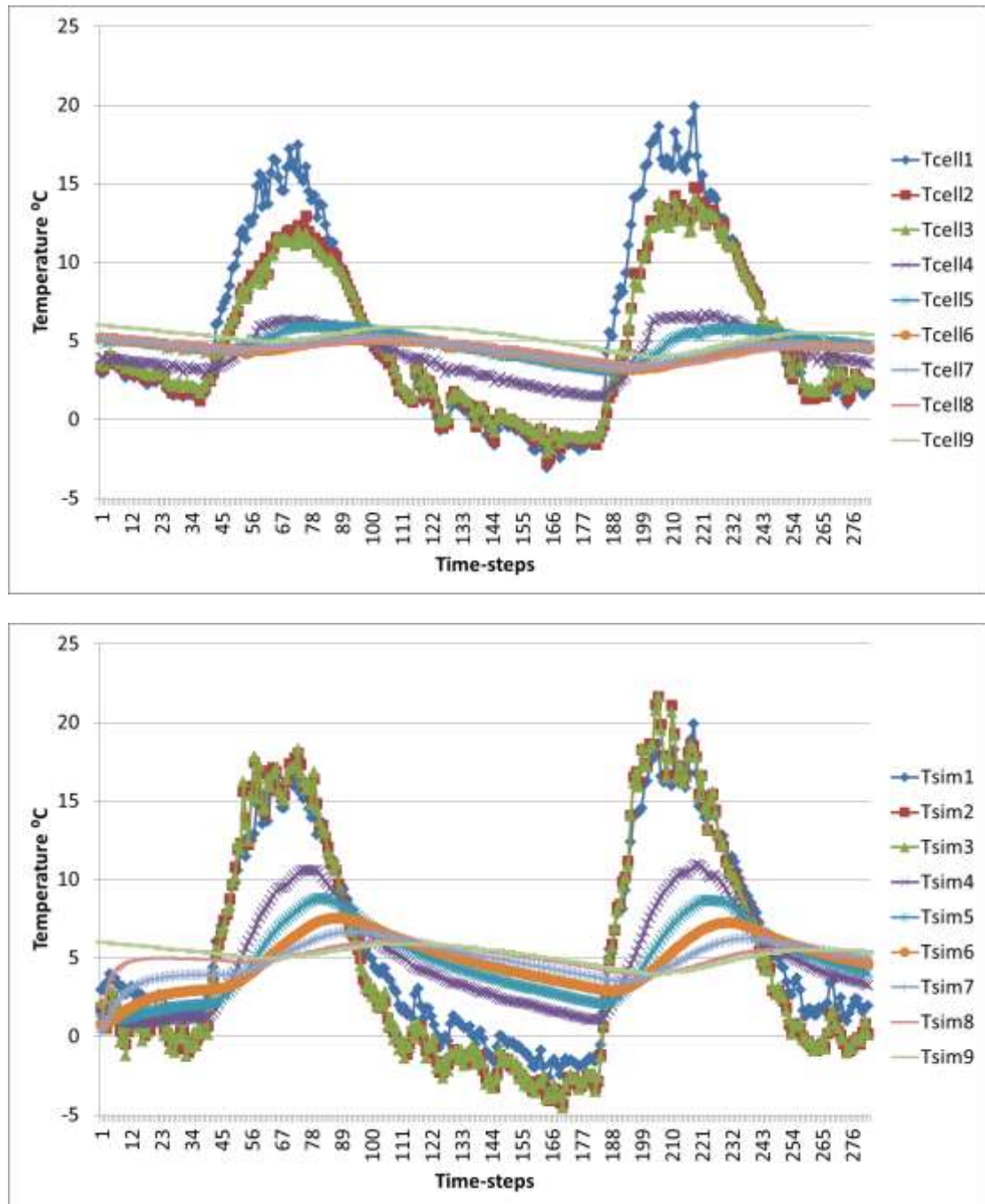
Figure 5-23: Illustration of temperatures measured (above) and simulated (below) against time step (10 minutes) number for validation test 6

Table 5-12: Validation test 6 comparative measures

Temperatures	CV1 Plant	CV2 Canopy air	CV3 Soil top layer	CV4 Soil layer 2	CV5 Soil layer 3	CV6 Soil layer 4	CV7 Soil bottom layer
RMSD [K]	3.212	3.359	2.016	1.809	1.669	1.132	0.827
Pearson correlation coefficient	0.9494	0.9448	0.9156	0.7536	0.29475	0.4257	0.50642

It can be seen from the above table that there is a marked deterioration in the quality of results for both RMSD and Pearson correlation. Possible justifications are provided in the next section.

5.7.1.7 Conclusion for thermal validations

In general, thermal validation results show that model is able to predict the lowest control volume, CV7, temperature fairly accurately, showing RMSD in the vicinity of 0.5 [K] except for the case of winter test where RMSD is approximately 0.8 [K]. This is due to the reversal of direction of heat flow that happens in the test cell in the winter case, due to the very small temperature difference between the top and bottom boundary temperatures of the test cell. Moreover in future revisions, the model has to be tested for its ability to overcome such problems by using smaller time-steps together with the coordinated validation time -steps. The problem is however unlikely to happen in a building simulation case with considerable difference between indoor and outdoor temperatures. However this shows an insignificant drawback of the model in case of simulating for weather conditions when little or no difference in temperature exists between indoors and outdoors.

It is to be noted that the plant temperature and canopy air temperatures are over predicted in all cases during day times. The model assumes a fixed specific heat for the plant and calculates its temperature as a function of the thermal energy absorbed by the canopy. However plant is a living organism with several mechanisms for regulating its body temperature. The model does take into account the stomata opening dynamics following some of the environmental stimuli. However such phenomena are

complex and the model is only the first version of what could be further developed in terms of plant biophysics. However this issue is not of concern for the model's progress towards meeting its final objective, which is to accurately predict the lowest soil temperature. Also, from the Pearson correlation comparison, it can be seen that there is a high linearity in the way the prediction changes from the real value for the plant and canopy air temperatures. It would therefore be possible to introduce a factor hardcoded into the model to account for the difference between the measured and simulated values of temperature.

In all test results, that include the complete test results of start-up days (pre-run of the simulation prior to the actual test period, to make the program stable) and test days, it takes less than ten time steps for the simulation to stabilize. This means that the green roof model by itself does not require many start-up days.

As the model calibration has been carried out across seasonal variations (from summer to winter) it can be presumed to be valid for building simulations with green roof for heating and cooling seasons.

5.7.2 Moisture validation results

Moisture validation was done in two stages. Firstly moisture content values of the test cells' soil layer was compared against the simulated values. For this purpose, four of the test dates as with the thermal simulations were used (all the six test dates as given in table 5.6 could not be used for moisture validation due to some unrecorded irrigation events for which the boundary conditions could not be properly estimated). Secondly for the comparisons, a separate drainage test was conducted by irrigating the test cells and measuring the resulting drainages and comparing it with simulated drain values. This was conducted on a separate test date chosen to avoid influences of rain and moist soils and conducted with a finer resolution of testing of 5 minutes.

5.7.2.1 Soil moisture content validations

The test days employed for this test validation are (1) August 17-18, (2) September 26-27, (3) October 17-18 and (4) December 5-6. The criteria for the selection of dates are

to include hot and cold days and to include dry and rainy days (as listed in table 5.6). Moisture contents of mid soil layers 2, 3 and 4 were measured and compared with the respective simulated values. The results are as briefed in the following sub-sections.

- **Test day 17-18 August (summer, moderate rain):**

The test days include occasional rains. The results are shown in figure 5.24
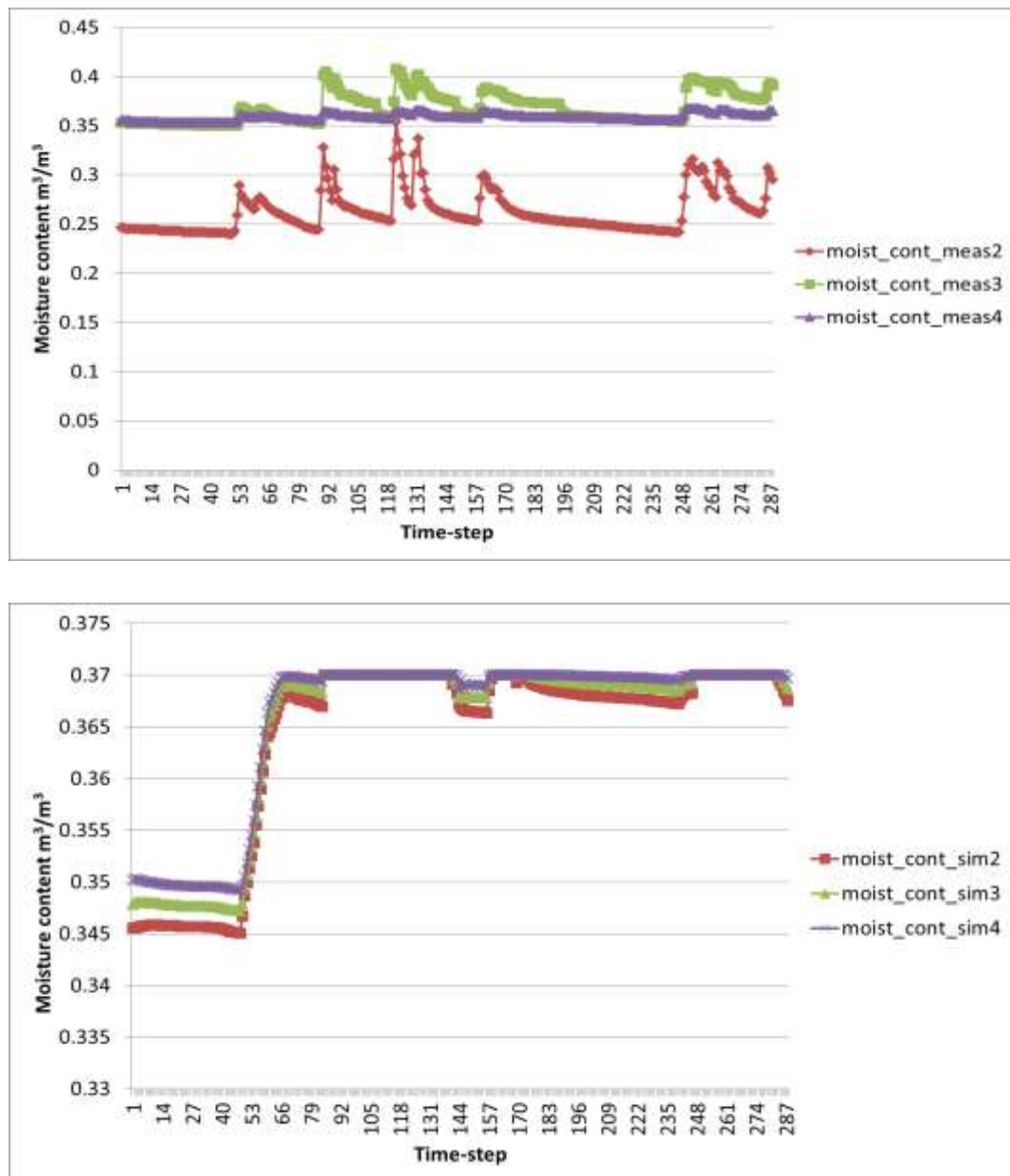
Figure 5-24: Measured (above) and simulated (below) values of soil moisture contents for validation test days 17-18 August

Although the pattern looks different for the two plots, the simulation results are fairly satisfactory as per the following reasons:

1. The simulation is able to track the events such as rain, moisture infiltration and drying.

2. The measured readings' comparative values are of some uncertainty as all three of them did not reach the same saturated value as expected in a soil bed. This may be due to air pockets present in soil around the sensor probes. This is prevailing in all of the moisture validation tests. The uncertainty is also obvious from the fact three sensors did not produce readings in the order expected. At the drying stage, moisture content is expected to increase in the order of depth, as evaporation is happening at the top surface. But it is not the case with the readings obtained, for example at time step 170 in figure 5.24 measured data set, the order is: moist_cont_meas2< moist_cont_meas4< moist_cont_meas3. The comparatively bigger size of soil moisture probes as against the test cell's soil layer height is a contributing factor and concern for the quality of reading.

3. The initial guess values in simulation model are not aligned with the sensor readings, and it is unlikely to happen in a real simulation situation, unless the simulation is started with some events such as rain, at which time the moisture content reaches a definite value such as saturation. This is because the moisture state of the soil is strongly dependent on irregular events such as rain and irrigation in addition to the regular predictable day/night cycles and seasonal variations. The thermal state however is dependent on the predictable events and during simulation the starting thermal state can be determined by a timed pre-run of the simulation program. However this is a common problem to all green roof moisture simulations and a work around need to be incorporated in future revisions.

4. Moisture content in soil varies only within a small range, as from 0.05 to 0.5. The lower limit is the residual moisture content and higher limit is the saturated moisture content. The RMSD obtained for soil layer 3 and 4, as shown in table 5.13 are within the range, usually obtained in environmental soil models (for example [8])

The statistical indices of comparison are as shown in table 5.13

Table 5-13: Moisture Validation indices for test date August 17-18

Moisture	Soil layer 2	Soil layer 3	Soil Layer 4
RMSD [m^3/m^3]	0.104	0.013	0.009
Pearson correlation coefficient	0.461	0.568	0.660

Higher root mean square difference and lower Pearson correlation coefficients for the top sensor location show that there are uncertainties concerning the match between measured and simulated values. This appears to be the case also for all the four validation periods for the moisture domain.

- **Test day 26-27 September (autumn, dry hot):**

These are dry days with gradual drying of soils. The results are shown in figure 5.25

It is to be noted that the order of the initial guess values for the simulation set which is opposite of that of the measured value, is maintained throughout the test period. The comparison figures are as given in table 5.14

Table 5-14: Moisture Validation indices for test date September 26-27

Moisture	Soil layer 2	Soil layer 3	Soil Layer 4
RMSD [m^3/m^3]	0.146	0.007	0.005
Pearson correlation coefficient	0.993	0.966	0.984

Here it can be seen that the model is strong in the unsaturated range as the linear correlation is close to 1 in all the three readings.
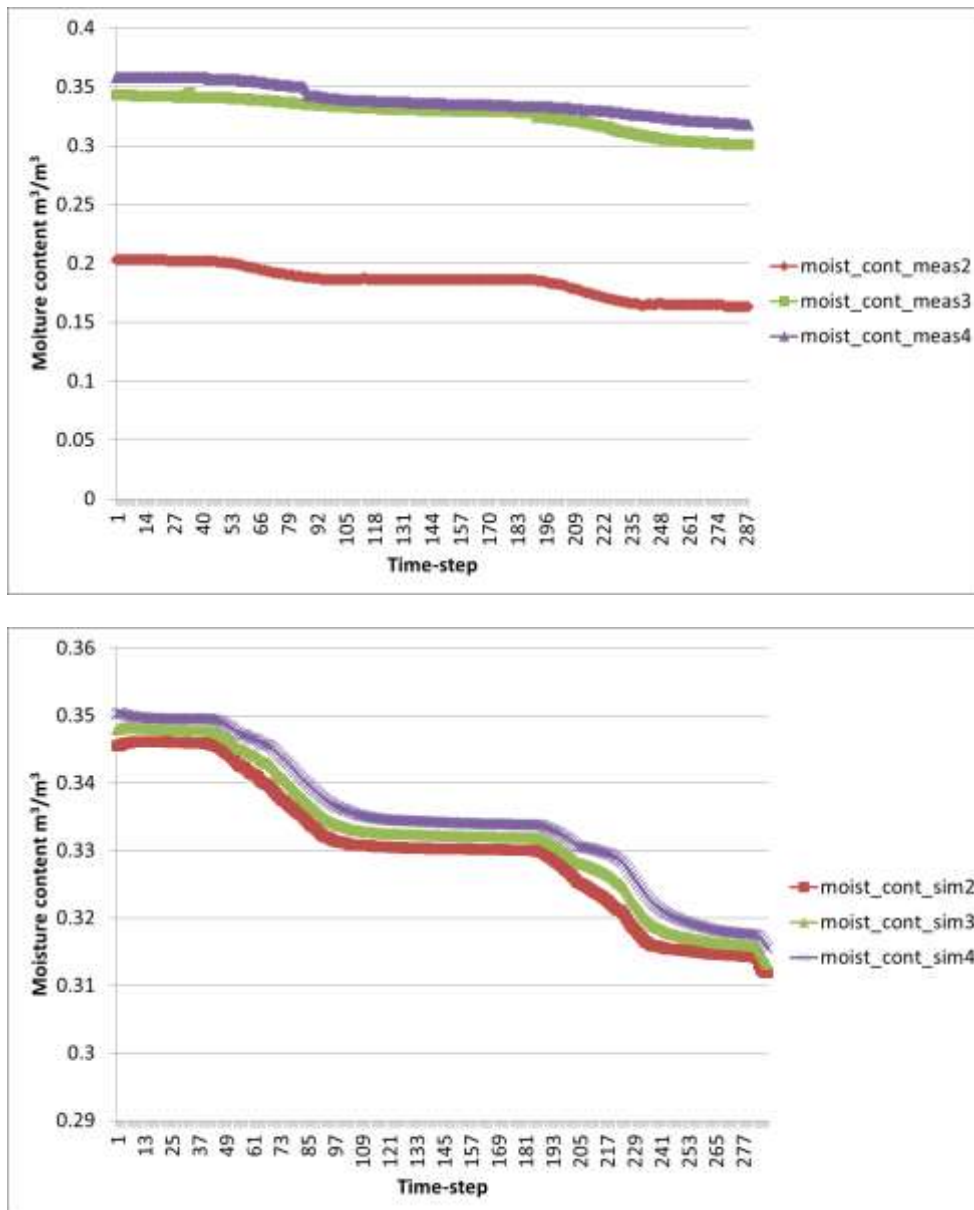
Figure 5-25: Measured (above) and simulated (below) values of soil moisture contents for validation test days 26-27 August

- **Test day 17-18 October (autumn, medium temperature, dry):**

These are medium temperature days with gradual drying of soils. The results are shown in figure 5.26. There are two events of drizzling which is shown as sharp increments in measurements but reflected as a gradual bend in simulation
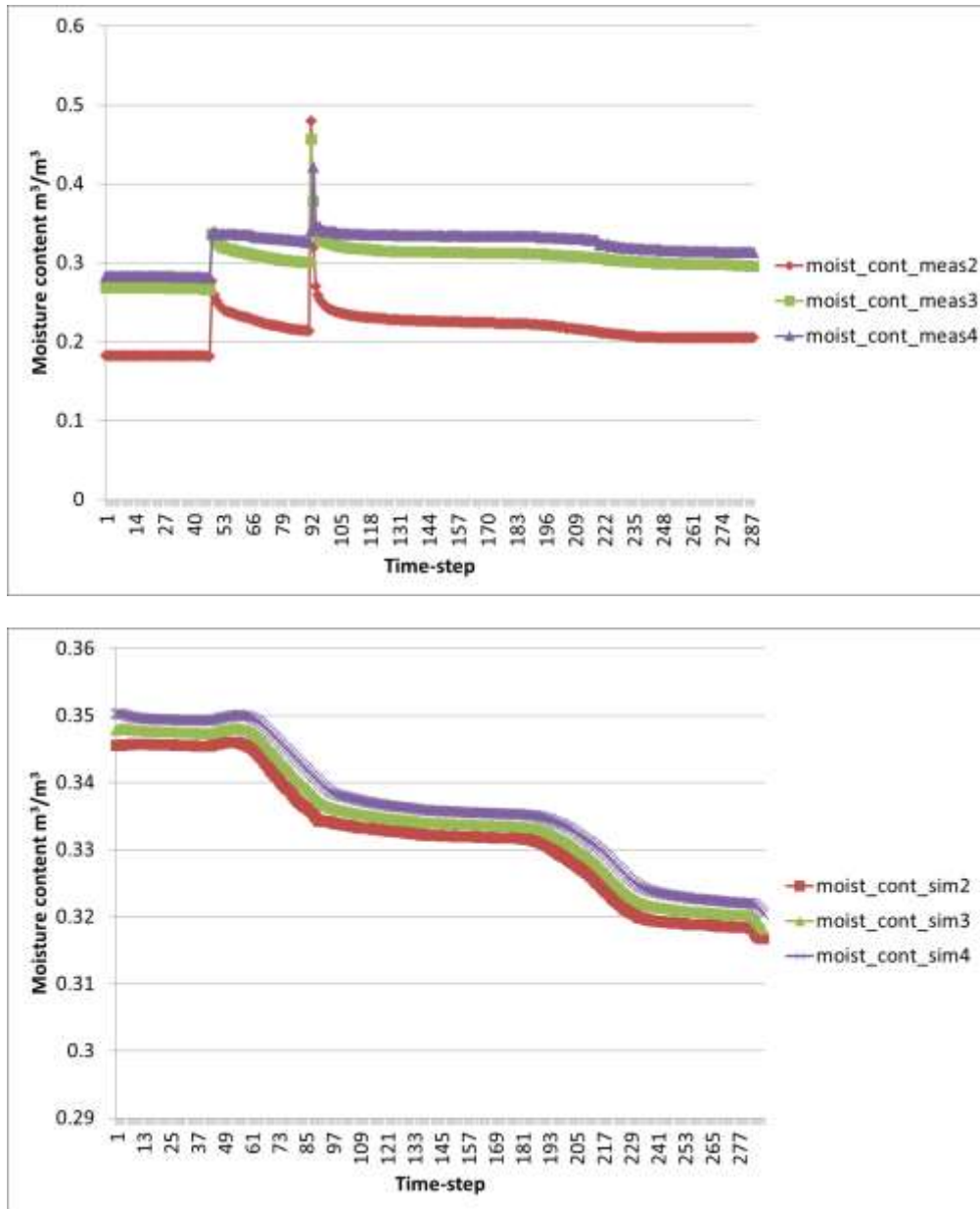
Figure 5-26: Measured (above) and simulated (below) values of soil moisture contents for validation test days 17-18 October

The comparison figures are in table 5.15

Table 5-15: Moisture Validation indices for test date October 17-18

Moisture	Soil layer 2	Soil layer 3	Soil Layer 4
RMSD [m^3/m^3]	0.119	0.038	0.027
Pearson correlation coefficient	-0.063	-0.260	-0.261

As with the previous cases soil layer 4 show better root mean square errors. In this period poor correlations are observed for all layers due to the fact that the two sensor spikes are not captured in the simulation and perhaps unrecorded irrigations occurring.

- **Test day 5-6 December(winter low temperature, dry):**

These are dry cold days. The results are shown in figure 5.27 and table 5.16

The comparison figures are in table 5.16

Table 5-16: Moisture Validation indices for test date December 5-6

Moisture	Soil layer 2	Soil layer 3	Soil Layer 4
RMSD [m^3/m^3]	0.116	0.004	0.021
Pearson correlation coefficient	0.980	0.971	0.974

In this case again except for the top reading, the model is performing well which is reflected from the low root mean square error and high coefficient of correlation.
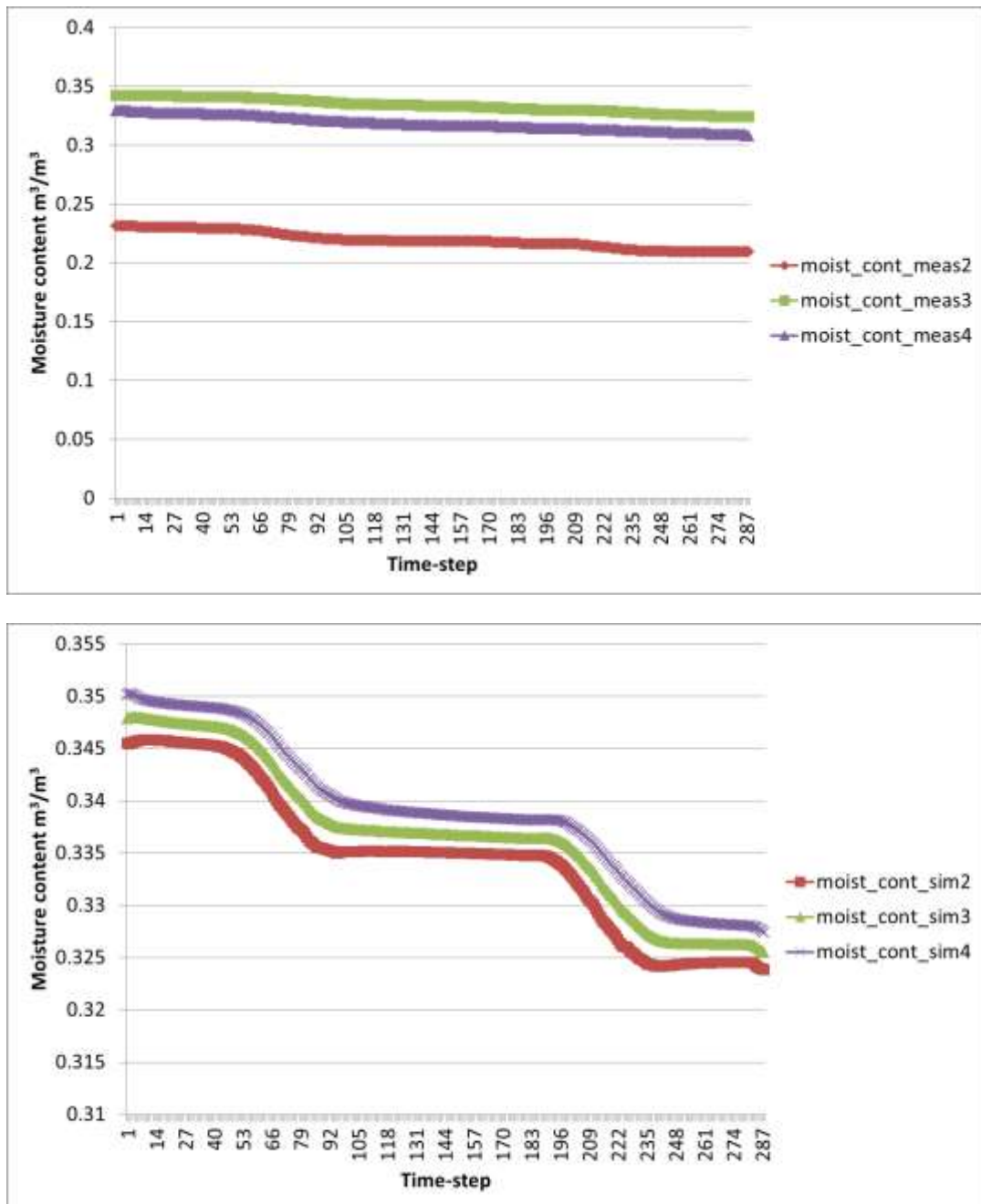
Figure 5-27: Measured (above) and simulated (below) values of soil moisture contents for validation test days 5-6 December

5.7.2.2 Drainage rate validations

The drainage test was conducted on 25 September. To test the test cell drain rate, manually controlled irrigation was supplied to the test cell. Five buckets (6.8L size) of water emptied over the test cell uniformly in 7.7 minutes. Timed measurement of drain is done by an arrangement of Raspberry-Pi camera and graduated container. Irrigation figures and the test conditions were set as input to the model.

134

Simulation was carried out with three sets of soil properties as represented by the Van Genuchten moisture retention curve indices; one corresponding to the silt-loam texture class; second one corresponding to a 'best fit' procedure conducted on the measured readings (as explained in the section 5.7.2.3) and third simply a trial and error test result conducted from a range of values of soil texture class as given in the reference, Carsel [75].

The test results are shown in figure 5.34 and also listed in table 5.13 to allow individual side by side comparison. The input data set is provided in table 5.17

From the validation data set it can be seen that all three sets of soil properties are able to predict the drainage rate and delay in different ways. The silt loam set of input predicts maximum drainage value closely but lags behind in predicting the delay of drainage run off. The best fit set is able to predict the delay in drainage, but poor in matching the maximum value. The selected set is able to predict the maximum value closely but again it does not accurately predict the delay. As expected, in all cases the total drainage is less than the irrigation value.
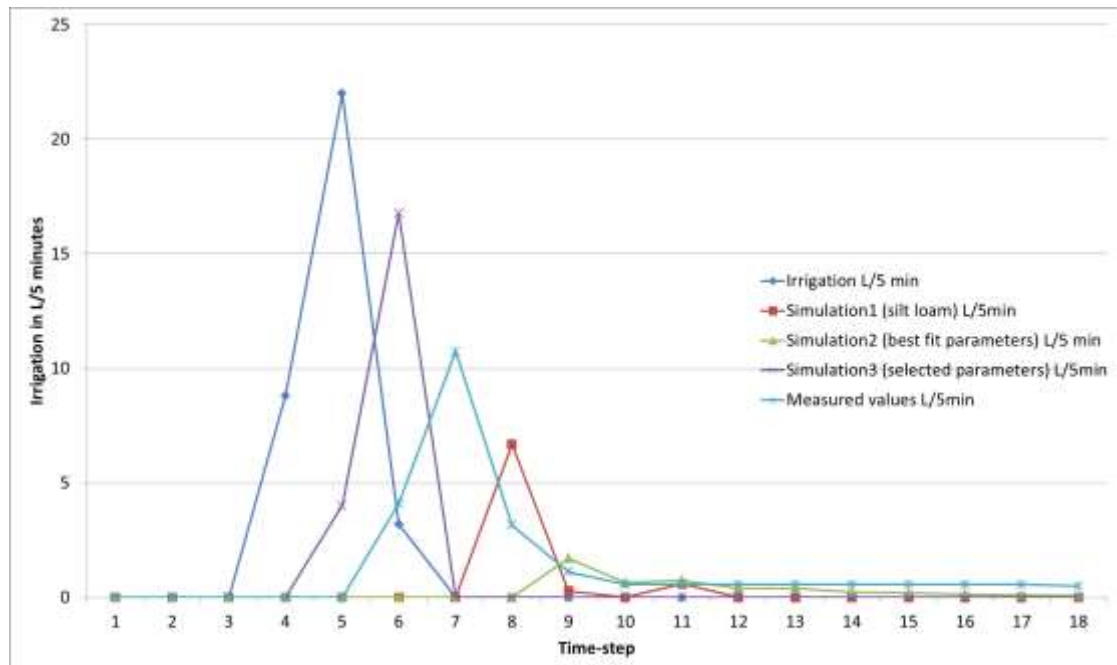
Figure 5-28: Drainage validation results - comparing irrigation, drainage measured and drainage simulated

Table 5-17: Drainage validation data set

Time step number	Irrigation [L/5min]	Drain simulation 1 silt loam [L/5min]	Drain simulation 2 best fit [L/5min]	Drain simulation 3 select [L/5min]	Drain measured [L/5min]
1					
2	0	0	0	0	0
3	0	0	0	0	0
4	8.798413	0	0	0	0
5	21.99603	0	0	4.0186734	0
6	3.205555	0	0	16.7763	4.095
7	0	0	0	0	10.7375
8	0	6.6893778	0	0	3.168963
9	0	0.28660181	1.7177128	0	1.126088
10	0	0	0.64788	0	0.566327
11	0	0.59423995	0.7546362	0	0.566327
12	0	0	0.4077536	0	0.566327
13	0	0	0.3894387	0	0.566327
14	0	0	0.2336269	0	0.566327
15	0	0	0.2025692	0	0.566327
16	0	0	0.1364605	0	0.566327
17	0	0	0.1047373	0	0.566327
18	0	0	7.00E-02	0	0.493851
19	0	0	5.02E-02	0	0.269319
20	0	0	3.14E-02	0	0.14
21	0	0	1.95E-02	0	0.14
22	0	0	9.04E-03	0	0.14
23	0	0	2.68E-03	0	0.133786
24	0	0	0	0	0.114536
25	0	0	0	0	0.103448
26	0	0	0	0	0.103448
27	0	0	0	0	0.103448
28	0	0	0	0	0.103448
29	0	0	0	0	0.097347
30	0	0	0	0	0.081256
31	0	0	0	0	0.076923
32	0	0	0	0	0.076923
33	0	0	0	0	0.076923
34	0	0	0	0	0.053846
35	0	0	0	0	0
	34	**7.57**	**4.78**	**20.79**	**25.97**

5.7.2.3 Procedure for determining best fit soil properties

The relation between soil moisture content and matric potential is determined using van-Genuchten (VG) equation in the model, as described in section 4.4. The parameters of the VG equation (i.e., residual moisture content (m^3/m^3), saturated moisture content (m^3/m^3), water retention parameter 'α' (cm^{-1}), water retention model parameter 'n' index), are determined based on the soil texture class. The soil in test cell is determined as of silt-loam texture class.

From the test cell moisture data, an observed moisture content-matric potential curve is plotted in figures 5.29 through 5.34. This is compared against theoretical curves (also plotted in these charts, side by side) obtained by VG relation using various soil texture properties. The comparison for four of the texture class set plots are shown in figures 5.29 to 5.32. Among them, figure 5.31 represents the silt loam texture class, which has been determined as the texture class of the experimental test cell and the data of which was used throughout the validation exercises. In addition, a mix-and-match selection of the parameters was chosen among all the 12 texture classes to get a close match between the measured and calculated curves and its comparison is shown in figure 5.33. Further, a best fit was determined using a statistical procedure namely generalized reduced gradient Frank–Wolfe algorithm [87] [88] and the obtained result is shown in figure 5.34.

From these illustrations (figures 5.29 to 5.34) the following observations are made:

- The model is very sensitive to the choice of VG indices of the soil.

- In addition to the method of determining them from the soil texture class, they can also be determined by a statically best fit procedure if some soil moisture data (moisture content and matric potential) are available. The modelling results are closer to the measured ones by the statistical method.

- The soil texture class used in this validation study is relatively better choice among the texture classes, producing closer match between the calculated and measured moisture retention curves.
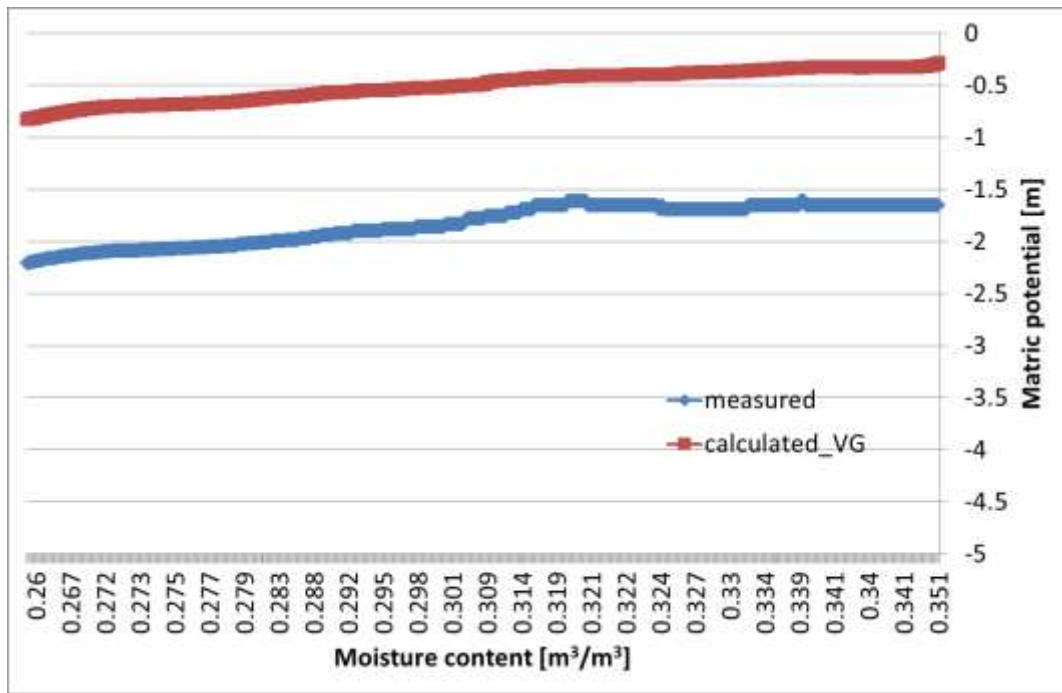
Figure 5-29: Soil texture Loam- moisture retention curve compared to measured data
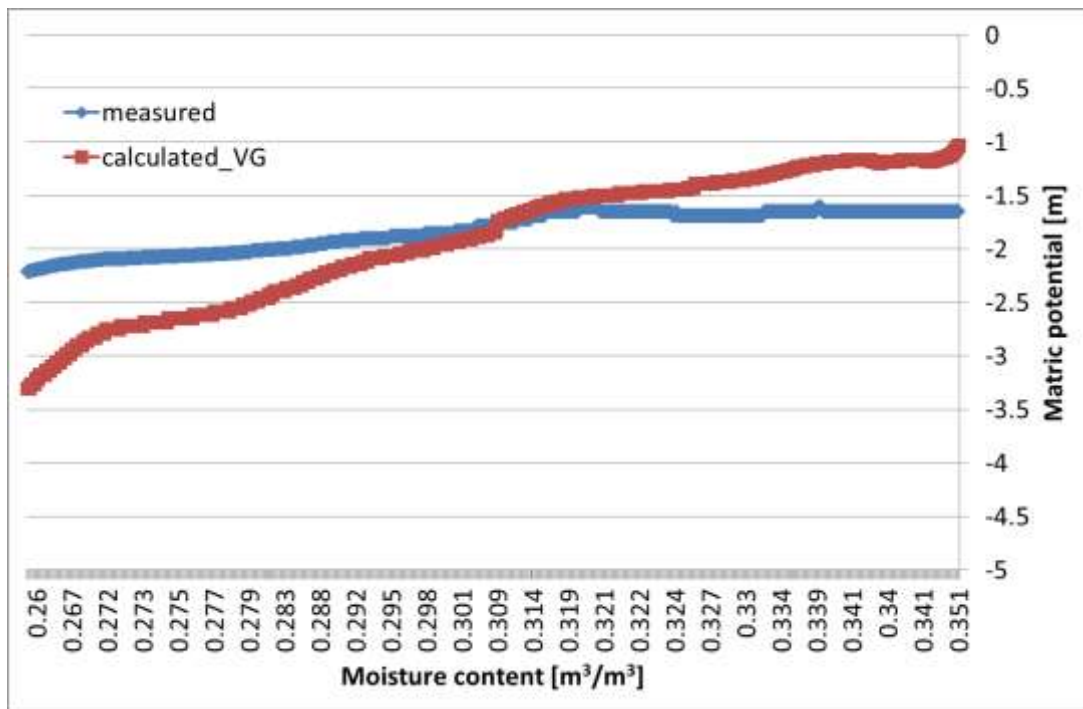
Figure 5-30: Silt - moisture retention curve compared to measured data
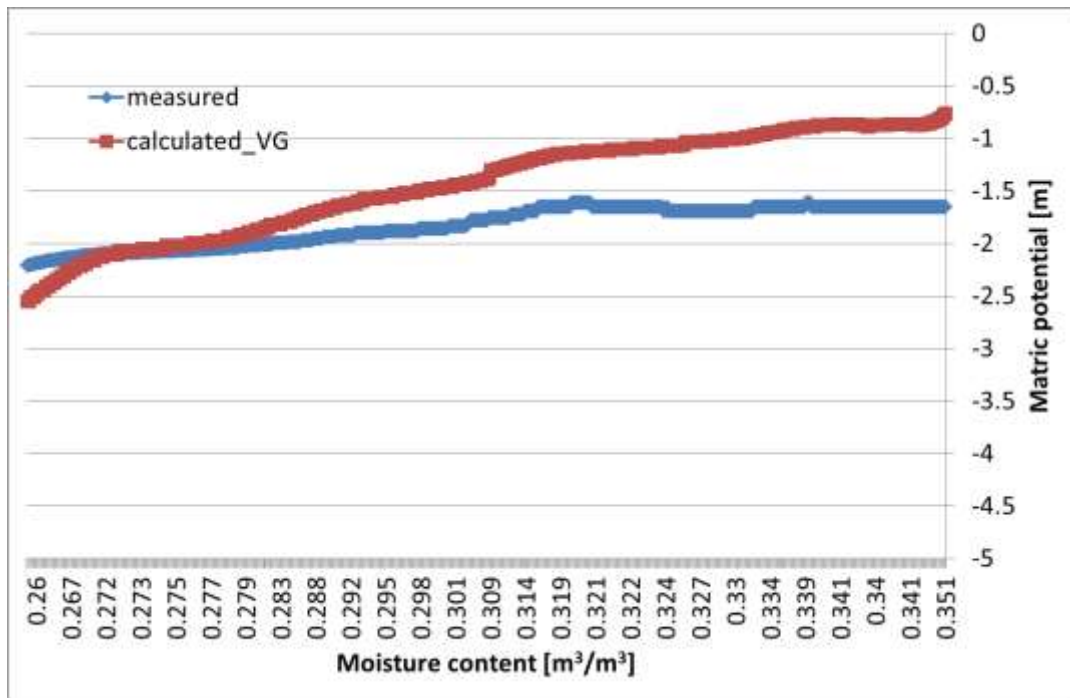
Figure 5-31: Silt Loam- moisture retention curve compared to measured data (type of soil used in the model validation)
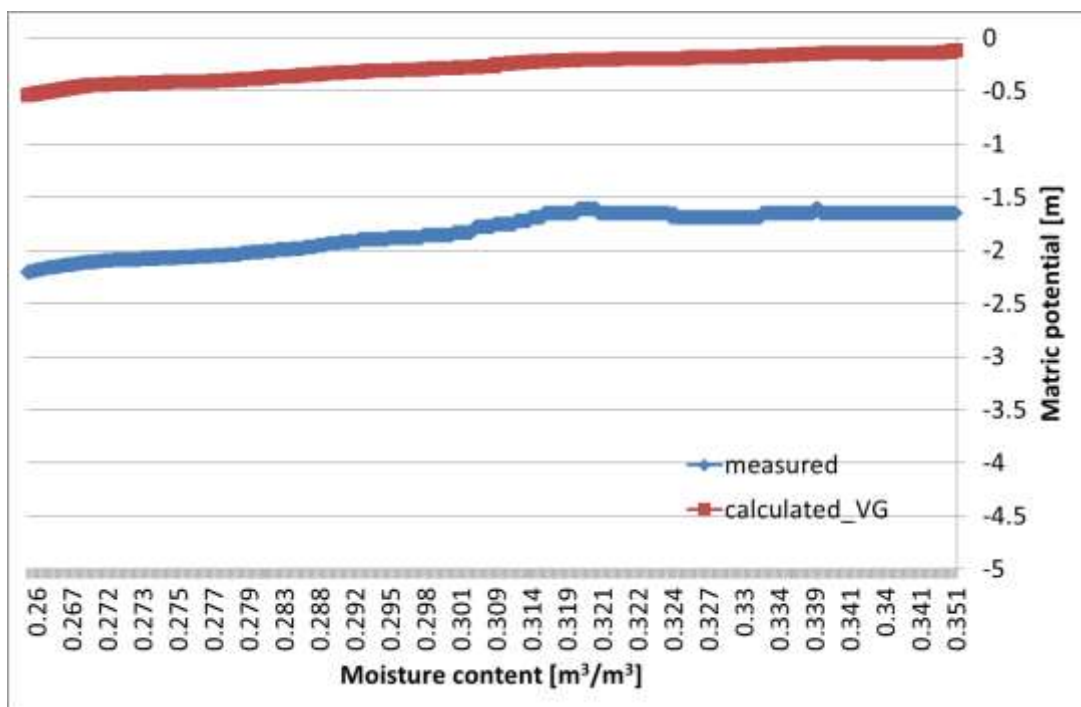
Figure 5-32: Sandy Clay Loam- moisture retention curve compared to measured data
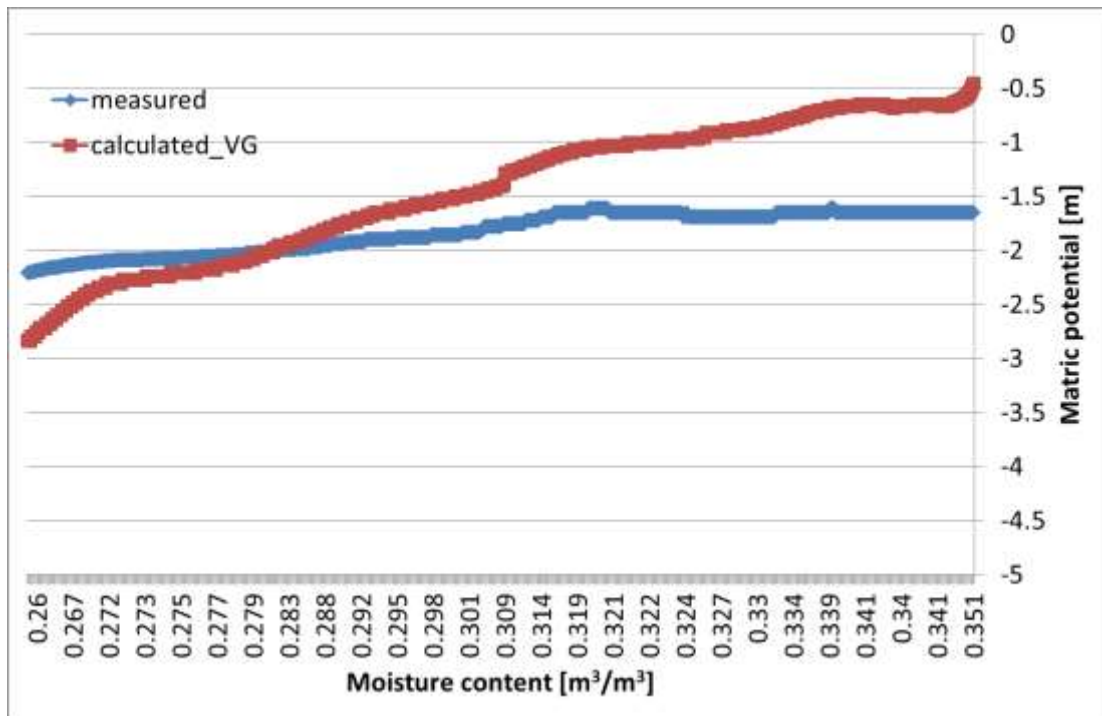
Figure 5-33: Selection set (not of any particular class, mix-and-match combination) - moisture retention curve compared to measured data
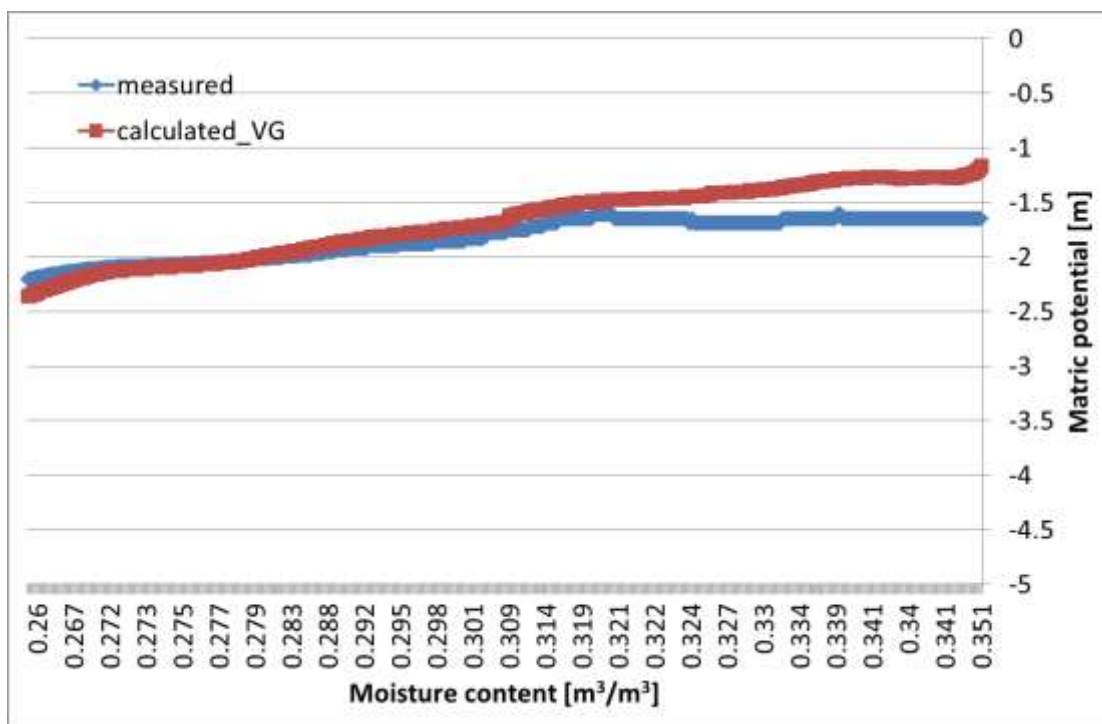
Figure 5-34: Best fit set (by statistical procedure) - moisture retention curve compared to measured data

Table 5.18 shows the VG indices used for the illustration of comparison with the measured data

Table 5-18: Drainage validation soil properties

VG (Van Genutchen indices)	Loam	Silt	Silt loam	Sandy clay loam	Selected set (mix and match)	Best fit set(statistical procedure)
Residual moisture content θ_r (m^3/m^3)	0.078	0.034	0.067	0.1	0.076	0.067
Saturated Moisture Content θ_s (m^3/m^3)	0.43	0.46	0.45	0.39	0.37	0.45
Water retention parameter 'α' (cm^{-1})	0.036	0.016	0.02	0.059	0.008	0.008
Water retention model parameter 'n' index	1.56	1.37	1.41	1.48	1.482	1.9

5.7.2.4 Conclusions for moisture domain validations

The moisture validation studies tested the model ability to track the moisture variations within soil and predict green roof influence on run-off rate. As is evident from the above results, the model is able to simulate the moisture conditions of unsaturated soil fairly well whereas there are some issues with the prediction when the soil attains saturation. This is due to the nature of the relation between the state variables in the soil, namely the matric potential and moisture content. The model solves matric potential in successive iterations (as explained in section 3.3) by seeking optimum match and trying values above and below. In the context of soil, the matric potentials are negative values reaching to a maximum of zero at saturated condition. The moisture contents range from a minimum residual value (θ_r) to a maximum saturated value (θ_s). The conversion function between matric potential and moisture content uses these limiting values (θ_r and θ_s) and determine the moisture content at successive iterations from the evolving state variable of the moisture balance equations, the matric potential. A particular problem arises as the soil moves towards a state of saturation. Moisture contents for matric potentials zero and above are always one single value, the saturated moisture content of soil. This limiting behaviour of soil

moisture relation limits the numerical solvers root seeking capability. As a solution, a stabilizing factor was introduced to the bottom boundary flow to keep the model in stable loop of moisture iterations.

5.8 Conclusion for validation tests

Validation tests involving experimental test cell measurements were conducted in a variety of environmental conditions to determine how close the state variables are to the measured values. The thermal results are satisfactory except for the plant and canopy regions, but this did not influence the final result for the temperature of the bottom layer which is used as a boundary condition in the whole building simulation in ESP-r. Further, the analysis showed that the nature of variations between the simulated and measured values at the plant and canopy level is linearly predictable (with relatively high Pearson correlation coefficient).

For the moisture domain, the results are fairly close for non-saturated soils and some deviations between the measurements and simulations are evident for the case of saturated soils. Comparatively poorer agreement of soil moisture measurements with the simulation results at the soil surface is attributed to the sensitivity of the sensor probes for air gaps and is recognized as a common problem in soil moisture measurements near the surface [89]. The validation exercise also revealed the conditions for variations of the model which helped in model improvement. In general, it can be said that the model achieves its objective of representing a green roof element in a whole building energy simulation.

CHAPTER 6
CONCLUSIONS

6. Conclusions

6.0 Introduction

The objective of this chapter is to summarize the research conducted and presented in this thesis and to summarize the achievements of the research project with regard to the development of a green roof simulation model for whole building energy simulations. The chapter ends with some suggestions for future developments on the topic of the research and for including additional features in the model.

6.1 Summary of research report

In chapter 1, the aim and objectives of the research were explicitly stated and the research justifications were presented. A very brief outline of the research methodology was also given in chapter 1.

A literature review covering various aspects of existing green roof models was presented in chapter 2, along with a brief description of ESP-r's model structure that is relevant to this research. Key features of some soil-vegetation models with energy and moisture exchanges similar to that of a green roof are also outlined in chapter 2. After reviewing the existing green roof model literature, research gaps were identified. ESP-r's methodologies were reviewed and available model resources in environmental models were identified. Subsequently a new green roof model was developed based on the control volume principles.

Theoretical formulation of the new green roof model and its implied assumptions were described in chapter 3 where the numerical solution process of the governing thermal and moisture equations were detailed. A comprehensive listing of the definitions of the thermal and moisture domain equations is given in appendix 3.1 and 3.2. A method of integrating the model with the building simulation program ESP-r was also given in chapter 3. The new model which assimilated thermal and moisture interactions was integrated with ESP-r as a modification of its external surface boundary condition. The model's integration was found not to be much computing burden, although the model was running in tandem with ESP-r, at every time-step, taking ESP-r's external temperature as its boundary condition, solving and supplying the results as ESP-r's

new boundary condition. The model required some input data related to plants and soil, which are unfamiliar to building simulation practitioners.

Details of model's inputs and methods for obtaining them were briefed in chapter 4 where it is demonstrated as a guideline for deriving unfamiliar inputs of soil and plant. A sensitivity analysis conducted to identify the degree of influence of the various input variables on the model's results was also described in chapter 4. By ranking the various model inputs according to their influence on model results is expected to provide guidelines concerning which one needed more careful consideration than others. Plant data collections described as part of the validation studies in chapter 5 can be construed as supplementary to the data collection methods for the model.

Experimental validation studies conducted, on a test cell, for verifying thermal and moisture domain results of the model and to compare the models' results with experimental data, were described in chapter 5, where the detailed results were also presented. The results of thermal validation studies demonstrated that close match exist for temperatures of CV7 temperature (RMSD range from 0.39 K to 0.82 K, for six validation studies) which will be eventually used as the ESP-r boundary condition. Plant and canopy CVs results showed some variations (relatively high RMSD) but also indicated predictable natures of these deviations (high value of Pearson's correlation coefficient). For the six thermal validation studies, RMSD of CV1 plant temperature deviations ranged from 2.1 K to 5 K whereas RMSD of CV2 canopy air temperature varied from 2.1 K to 5.3 K. Values of Pearson's correlation coefficients for the CV1 temperatures varied from 0.88 to 0.96 and that for CV2 temperatures varied from 0.84 to 0.94. For the four moisture domain validation studies conducted to compare the moisture contents measured and simulated in CV2, CV3 and CV4, the results were better for inner soil layers (average RMSD 0.016 m^3/m^3 for both CV3 and CV4) compared to the near top layer CV2 (average RMSD for CV2, 0.121 m^3/m^3). The reason for the poorer result of CV2 is attributed to the possible influence of air space at the moisture sensor probe. A drainage validation study conducted for the new model was also described in chapter 5. Comparisons were done by running simulations with different sets of soil input data and it was found that a set derived from a statistical best fit procedure rendered the best results for drainage simulation.

6.2 Meeting objectives of research

The following three research objectives were outlined at the onset of this thesis, which are all achieved in this research. The objectives achieved are:

- A new green roof model has been developed based on the control volume approach, which is capable of simulating the dynamic thermal and moisture flows and the interactions between them.

- The model has been successfully integrated with the parent whole building energy simulation program ESP-r and tested to be working with it.

- The newly developed green roof model has been validated with several experiments conducted at different intervals over a half year period.

A methodology for collecting model's inputs has been demonstrated which could guide the practitioners in using the program. In addition to the usual weather file data, the use of precipitation and irrigation data within the model has also been specified.

In addition to meeting the objectives, two additional achievements of the research work are:

- The green roof module is self-contained with its matrix solver steps included, thus with some tailored adaptations the model can be integrated with other building energy simulation programs.

- The model also predicts drain rate of the green roof and could become a valuable tool for modern landscapes requiring assessments of run-off characteristics of buildings. However the model's drainage function has limitations as is evident from the validation results and it needs additional refinement in terms of the empirical moisture functions as explained in section 5.7.2.

6.3 Features of the new green roof model

The method used for the development of green roof model involves dividing the green roof elements into control volumes and identifying the governing thermal and moisture exchange equations. These equations were further made into a set of time-discretised

equations which were then solved for successive time steps. The control volume equations were combined and a matrix of linear equations was formed for facilitating simultaneous solving for state variables. The coefficients of these matrix equations were defined in terms of thermal and moisture related properties of the various elements of green roof. These coefficients were themselves time varying, so they were determined at each time step by procedures defined for all the coefficients in the model and by making use of the time-evolving parameters (as described in section 3.3). The equations were solved by successive iterations. Within a successive iteration, thermal and moisture equations were processed in succession ensuring the thermal-moisture coupling.

The following are the key benefits of the model:

- The control volume model is capable of capturing inter-layer interactions and thermal/moisture domain interactions. In particular the thermal moisture coupling is rendered effective by the use of properties that are dependent on the thermal and moisture state variables in the calculation of moisture and thermal state variables respectively as demonstrated in the model's equations in chapter 3, appendix 3.1 and appendix 3.2. For example, the thermal conductivity of thermal equations is dependent on moisture content and the stomatal resistance of moisture exchange is dependent on temperature and soil moisture content. In addition, some properties which are used in both thermal and moisture exchange calculations are dependent on either one or both of thermal moisture state variables. For example, the aerodynamic resistance (used in moisture and thermal domain calculations) is a function of temperatures and the vapour conductivities (used in moisture and thermal domain calculations) are functions of temperatures, moisture contents and matric potentials.

- Integrated in whole building energy simulation the model serves as a valuable assessment tool for the building sector's decision makers.

- The model is capable of predicting drainage rate and the delay in the run-off, as has been demonstrated in section 5.7.2 and in figure 5.28. This feature of the

green roof is much sought after now with the fast changing weather patterns and is required to be simulated in urban landscape models.

- The model is self-contained, making it adaptable for a variety of host building simulation programs. When integrated with a whole building energy program, the model calculates the boundary condition required by the host program for its green-roof carrying structure and the model in turn takes the building structure temperature for its boundary condition for the following time step. Currently the model uses only temperatures as boundary condition. However, it would be possible to have both thermal flux and temperatures as boundary conditions with some minor modifications within the control volume formulated model.

- The model incorporates features of SVAT (soil-vegetation-atmosphere) environmental models which are confidently established in the hydrology field. Examples of such features are: the moisture infiltration model into the soil defined by Richard equation[58], the moisture retention characteristics of the model defined by van Genuchten [37] function and the plant- root's moisture uptake model.

The results of the validation tests confirm that the model is able to predict the thermal moisture exchanges in the green roof fairly accurately. From the six thermal validation studies conducted during the period August to December 2014, the results indicate average RMSD on temperatures simulated as varying from 3.4 K at canopy air to 0.6 K at the soil bottom layer. The closeness of prediction at the soil bottom later is significant as it is being used as a boundary condition linking the newly developed model with ESP-r simulation program. Similarly for the four moisture validation, also conducted during the same period, the results indicate average RMSD of simulated moisture contents for the inner soil layer as 0.01 m^3/m^3 whereas that of the top layer is 0.12 m^3/m^3. Soil moisture sensors' limitations on the surface measurements (as stated in section 5.8) is considered to be the reason for inferior results at the surface. In general results were better for unsaturated soil as compared to that for saturated soil.

6.4 Model's scope limitations

The following are some of the features for which improvements could be made:

- Currently the model employs fixed five layers of soil as control volumes which are suitable for common intensive green roof dimensions. It is preferable to include features of adaptive gridding in the model which will give the user, flexibility to model any size of green roof with additional accuracy and also to adopt the required balance between the computational burden and the model's precision.

- The model incorporates only one model for the soil moisture retention characteristics (van Genuchten model[37]), which in turn requires its specific and often hard to obtain input parameters such as the saturated moisture content [$m^3 m^{-3}$], the residual moisture content [$m^3 m^{-3}$], α1 air entry parameter and n the pore-size distribution index.

6.5 Suggestions for future developments

Based on the limitations listed in the section 6.3 the following areas of further development are proposed.

- To make the control volume numbers more versatile by including include adaptive gridding and a choice of separate grid structure for thermal and moisture domains. As the green roof sizes vary and continue to evolve the model should adapt to the wide range of green roof characteristics such as having mixed types of plants, constructed as green roof gardens and having different types of substrates and drainage layers.

- To develop an interface for the model that can be used to link the model to building energy simulation programs with open data models, other than ESP-r.

- To further develop the input data model to a database; this would be a beneficial feature of the models since the green roof types are continuously evolving and the users are often unaware of how to obtain inputs for green roof simulations.

- To expand the data model in order to enable schedule of input for plant variables to be entered, such as time varying plant height and LAI. This could be implemented by modifying the program to have a choice of selecting either a single value of the variable or a time array of the variable.

- To expand the moisture domain calculations of the model by including other choices of moisture retention models such as Campbell [8] in addition to the existing van Genuchten model [37], so that the user can choose the type of model according to the availability of input data.

- To further improve the drainage model [90] by incorporating adaptive boundary conditions, i.e., to include a feature in the model to automatically choose zero flux boundary conditions for non-saturated soil conditions (no drainage) and zero potential boundary condition for saturated conditions (drainage occurring). It is also preferable to include varying head for drainage calculations which may be required for simulating the exponential type of slowdown of drainage observed (section 5.7.2) in the drainage validation study.

References

1.	Weiler, S.K. and K. Scholz-Barth, *Green roof systems : a guide to the planning, design and construction of building over structure*. 2009: J. Wiley & Sons.
2.	Snodgrass, E.C. and L.L. Snodgrass, *Green roof plants : a resource and planting guide*. 2006: Timber Press.
3.	Council, U.S.G.B., *LEED reference guide for building design and construction*. 2013.
4.	Barlow, S. and E. Building Research, *Guide to breeam*. 2011, Lobdon: RIBA Publishing.
5.	Santamouris, M., *Cooling the cities – A review of reflective and green roof mitigation technologies to fight heat island and improve comfort in urban environments.* Solar Energy, 2014. **103**(0): p. 682-703.
6.	Sailor, D.J., *A green roof model for building energy simulation programs.* Energy and Buildings, 2008. **40**(8): p. 1466-1478.
7.	Djedjig, R., E. Bozonnet, and R. Belarbi, *Analysis of thermal effects of vegetated envelopes: Integration of a validated model in a building energy simulation program.* Energy and Buildings, 2015. **86**(0): p. 93-103.
8.	Bittelli, M., et al., *Coupling of heat, water vapor, and liquid water fluxes to compute evaporation in bare soils.* Journal of Hydrology, 2008. **362**(3–4): p. 191-205.
9.	Barrio, E.P.D., *Analysis of the green roofs cooling potential in buildings.* Energy and Buildings, 1998. **27**(2): p. 179-193.
10.	Newton, J., et al., *BUILDING GREENer: Guidance on the use of green roofs, green walls and complementary features on buildings*. 2007, London: CIRIA.
11.	GRO, *GRO 2011 The GRO Green Roof Code - Green Roof Code of Best Practice for the UK*. 2011, Green Roof Organisation: Sheffield.
12.	FLL, *FLL 2008 Guidelines for the Planning, Construction and Maintenance of Green Roofing*. 2008, Forschungsgesellschaft Landschaftsentwicklung Landschaftsbau e.V. (FLL): Bonn.
13.	Darkwa, J., G. Kokogiannakis, and G. Suba, *Effectiveness of an intensive green roof in a sub-tropical region.* Building Services Engineering Research and Technology, 2013. **34**(4): p. 417-432.
14.	Kokogiannakis, G., A. Tietje, and J. Darkwa, *The role of Green Roofs on Reducing Heating and Cooling Loads: A Database across Chinese Climates.* Procedia Environmental Sciences, 2011. **11, Part B**(0): p. 604-610.
15.	Hui, S.C.M., *Development of technical guidelines for green roof systems in Hong Kong*, in *Proceedings of the Joint Symposium 2010 on Low Carbon High Performance Buildings*. 2010, Conference organisers. p. 1.
16.	Saadatian, O., et al., *A review of energy aspects of green roofs.* Renewable and Sustainable Energy Reviews, 2013. **23**: p. 155-168.
17.	Alexandri, E. and P. Jones, *Developing a one-dimensional heat and mass transfer algorithm for describing the effect of green roofs on the built environment: Comparison with experimental results.* Building and Environment, 2007. **42**(8): p. 2835-2849.
18.	Pielke, R.A., *Mesoscale Meteorological Modeling*. Second Edition ed. INTERNATIONAL GEOPHYSICS SERIES. Vol. VOL 78. 2002, Great Britain: ACADEMIC PRESS LTD. 676.
19.	Sellers, P.J., et al., *A Revised Land Surface Parameterization (SiB2) for Atmospheric GCMS. Part I: Model Formulation.* Journal of Climate, 1996. **9**(4): p. 676-705.
20.	Takebayashi, H. and M. Moriyama, *Surface heat budget on green roof and high reflection roof for mitigation of urban heat island.* Building and Environment, 2007. **42**(8): p. 2971-2979.

21.   Santamouris, M., et al., *Investigating and analysing the energy and environmental performance of an experimental green roof system installed in a nursery school building in Athens, Greece.* Energy, 2007. **32**(9): p. 1781-1788.

22.   Niachou, A., et al., *Analysis of the green roof thermal properties and investigation of its energy performance.* Energy and Buildings, 2001. **33**(7): p. 719-729.

23.   Martens, R., B. Bass, and S. Alcazar, *Roof–envelope ratio impact on green roof energy performance.* Urban Ecosystems, 2008. **11**(4): p. 399-408.

24.   Yu, C., *The Intervention of Plants in the Conflicts between Buildings and Climate —a Case Study in Singapore*, in *Department of Building*. 2006, National University of Singapore. p. 315.

25.   Santamouris, M., ed. *Energy and climate in the urban built environment*. 2001, James and James Science Publishers: London.

26.   Wong, N.H., et al., *Investigation of thermal benefits of rooftop garden in the tropical environment.* Building and Environment, 2003. **38**(2): p. 261-270.

27.   Wong, N.H., et al., *The effects of rooftop garden on energy consumption of a commercial building in Singapore.* Energy and Buildings, 2003. **35**(4): p. 353-364.

28.   Buhl, W.F., et al., *DOE-2 REFERENCE MANUAL, VERSION 2.1A*. Vol. Rev. 2. 1981: Los Alamos National Laboratory.

29.   Tabares-Velasco, P.C. and J. Srebric, *A heat transfer model for assessment of plant based roofing systems in summer conditions.* Building and Environment, 2012. **49**(0): p. 310-323.

30.   Tabares-Velasco, P.C., *Predictive Heat and Mass Transfer Model of Plant-based Roofing Material for Assessment of Energy Savings*, in *Department of Architectural Engineering*. 2009, The Pennsylvania State University. p. 179.

31.   Ayata, T., P.C. Tabares-Velasco, and J. Srebric, *An investigation of sensible heat fluxes at a green roof in a laboratory setup.* Building and Environment, 2011. **46**(9): p. 1851-1861.

32.   de Munck, C.S., et al., *The GREENROOF module (v7.3) for modelling green roof hydrological and energetic performances within TEB.* Geosci. Model Dev., 2013. **6**(6): p. 1941-1960.

33.   Boone, A., et al., *The Influence of the Inclusion of Soil Freezing on Simulations by a Soil–Vegetation–Atmosphere Transfer Scheme.* Journal of Applied Meteorology, 2000. **39**(9): p. 1544-1569.

34.   Masson, V., *A Physically-Based Scheme For The Urban Energy Budget In Atmospheric Models.* Boundary-Layer Meteorology, 2000. **94**(3): p. 357-397.

35.   Masson, V., et al., *The SURFEXv7.2 land and ocean surface platform for coupled or offline simulation of earth surface variables and fluxes.* Geosci. Model Dev., 2013. **6**(4): p. 929-960.

36.   Clapp, R.B. and G.M. Hornberger, *Empirical equations for some soil hydraulic properties.* Water Resources Research, 1978. **14**(4): p. 601-604.

37.   van Genuchten, M.T., *A Closed-form Equation for Predicting the Hydraulic Conductivity of Unsaturated Soils1.* Soil Sci. Soc. Am. J., 1980. **44**(5): p. 892-898.

38.   Moody, S.S. and D.J. Sailor, *Development and application of a building energy performance metric for green roof systems.* Energy and Buildings, 2013. **60**(0): p. 262-269.

39.   Luo, C., B. Moghtaderi, and A. Page, *Modelling of wall heat transfer using modified conduction transfer function, finite volume and complex Fourier analysis methods.* Energy and Buildings, 2010. **42**(5): p. 605-617.

40.   Sailor, D.J. and B. Bass, *Development and features of the Green Roof Energy Calculator.* Journal of Living Architecture, 2014. **1**(3): p. 36-58.

41.   Djedjig, R., et al., *Development and validation of a coupled heat and mass transfer model for green roofs.* International Communications in Heat and Mass Transfer, 2012. **39**(6): p. 752-761.

42.   Jaffal, I., S.-E. Ouldboukhitine, and R. Belarbi, *A comprehensive study of the impact of green roofs on building energy performance.* Renewable Energy, 2012. **43**(0): p. 157-164.

43.   Ouldboukhitine, S.E., et al., *Assessment of green roof thermal behavior: A coupled heat and mass transfer model.* Building and Environment, 2011. **46**(12): p. 2624-2631.

44.   Celia, M.A., E.T. Bouloutas, and R.L. Zarba, *A general mass-conservative numerical solution for the unsaturated flow equation.* Water Resources Research, 1990. **26**(7): p. 1483-1496.

45.   Allen, R.G., et al., *Crop evapotranspiration - Guidelines for computing crop water requirements - FAO Irrigation and drainage paper 56*. 1998, FAO - Food and Agriculture Organization of the United Nations: Rome. p. 326.

46.   Clarke, J.A., *Energy simulation in building design [Electronic book]*. 2nd ed. 2001, Oxford: Butterworth-Heinemann.

47.   Clarke, J., N. Kelly, and D. Tang, *A review of ESP-r's flexible solution approach and its application to prospective technical domain developments.* Advances in building energy research, 2007. **1**(1): p. 227-247.

48.   Beausoleil-Morrison, I., *The Adaptive Coupling of Heat and Air Flow Modelling Within Dynamic Whole-Building Simulation*, in *ESRU*. 2000, University of Strathclyde: Glasgow. p. 241.

49.   Kelly, N.J., *Towards a design environment for building-integrated energy systems: the integration of electrical power flow modelling with building simulation*, in *ESRU*. 1996, University of Strathclyde: Glasgow. p. 285.

50.   Macdonald, I.A., *Quantifying the effects of uncertainty in building simulation*, in *ESRU*. 2002, University of Strathclyde: Glasgow. p. 267.

51.   Arora, V., *MODELING VEGETATION AS A DYNAMIC COMPONENT IN SOIL-VEGETATION-ATMOSPHERE TRANSFER SCHEMES AND HYDROLOGICAL MODELS.* Reviews of Geophysics, 2002. **40**(2): p. 3-1-3-26.

52.   Feddes, R.A., G.H. de Rooij, and J.C. van Dam, *Unsaturated-zone Modeling: Progress, Challenges and Applications*. 2004: Springer.

53.   Kirkham, M.B., *Principles of Soil and Plant Water Relations*. 2014: Elsevier Science.

54.   Hunter, A.M., et al., *Quantifying the thermal performance of green façades: A critical review.* Ecological Engineering, 2014. **63**: p. 102-113.

55.   Campbell, G.S. and J.M. Norman, *An introduction to environmental biophysics / Gaylon S. Campbell, and John M. Norman*. Environmental biophysics. 1998: Springer-Verlag.

56.   Qin, Z., P. Berliner, and A. Karnieli, *Numerical solution of a complete surface energy balance model for simulation of heat fluxes and surface temperature under bare soil environment.* Applied Mathematics and Computation, 2002. **130**(1): p. 171-200.

57.   Noilhan, J. and S. Planton, *A Simple Parameterization of Land Surface Processes for Meteorological Models.* Monthly Weather Review, 1989. **117**(3): p. 536-549.

58.   van Dam, J.C., et al., *Advances of Modeling Water Flow in Variably Saturated Soils with SWAP* Vadose Zone J., 2008. **7**(2): p. 640-653.

59.   van Diepen, C.A., et al., *WOFOST: a simulation model of crop production.* Soil Use and Management, 1989. **5**(1): p. 16-24.

60.   Saito, H., J. Šimůnek, and B.P. Mohanty, *Numerical Analysis of Coupled Water, Vapor, and Heat Transport in the Vadose Zone.* Vadose Zone J., 2006. **5**(2): p. 784-800.

61.   Clarke, J., *Moisture flow modelling within the ESP-r integrated building performance simulation system.* Journal of Building Performance Simulation, 2013. **6**(5): p. 385-399.

62.   Šimůnek, J., M.T. van Genuchten, and M. Šejna, *Development and Applications of the HYDRUS and STANMOD Software Packages and Related Codes.* Vadose Zone Journal, 2008. **7**(2): p. 587-600.

63.   Peiró, J. and S. Sherwin, *Finite difference, finite element and finite volume methods for partial differential equations*, in *Handbook of materials modeling*. 2005, Springer. p. 2415-2446.

64.   Chakraborty, S., *Fundamentals of Discretization: Finite Volume Method*, in *NPTEL (National Programme on Technology Enhanced Learning)*. 2012, Indian Institute of Technology, Kharagpur.

65.   Martin, M. and P. Berdahl, *Characteristics of infrared sky radiation in the United States.* Solar Energy, 1984. **33**(3): p. 321-336.

66.   Choudhury, B.J. and J.L. Monteith, *A four-layer model for the heat budget of homogeneous land surfaces.* Quarterly Journal of the Royal Meteorological Society, 1988. **114**(480): p. 373-398.

67.   van de Griend, A.A. and M. Owe, *Bare soil surface resistance to evaporation by vapor diffusion under semiarid conditions.* Water Resources Research, 1994. **30**(2): p. 181-188.

68.   Acton, F.S., *Numerical Methods that Work*. 1990: Mathematical Association of America.

69.   Webb, N., et al., *User Manual for the SunScan Canopy Analysis System type SS1*. Vol. Version 3.0. 2013, Derbyshire, U.K.: Delta-T Devices Ltd.

70.   Gausman, H.W. and W.A. Allen, *Optical Parameters of Leaves of 30 Plant Species.* Plant Physiology, 1973. **52**(1): p. 57-62.

71.   Stahghellini, C., *Transpiration of greenhouse crops*. 1987, Ph. D. Dissertation, Agricultural University, Wageningen, 1987 in (Palomo Del Barrio E., Analysis of the green roofs cooling potential in buildings, Energy and Buildings 27 (1998) 179–193).

72.   Jayalakshmy, M.S. and J. Philip, *Thermophysical Properties of Plant Leaves and Their Influence on the Environment Temperature.* International Journal of Thermophysics, 2010. **31**(11-12): p. 2295-2304.

73.   Simunek, J., M.T. Van Genuchten, and M. Sejna, *The HYDRUS-1D software package for simulating the one-dimensional movement of water, heat, and multiple solutes in variably-saturated media*. 2005, University of California-Riverside. p. 240.

74.   Leij, F.J. and N.R.M.R. Laboratory, *The UNSODA unsaturated soil hydraulic database: user's manual*. 1996: National Risk Management Research Laboratory, Office of Research and Development, U.S. Environmental Protection Agency.

75.   Carsel, R.F. and R.S. Parrish, *Developing joint probability distributions of soil water retention characteristics.* Water Resources Research, 1988. **24**(5): p. 755-769.

76.   Sutherland, R., *Loss-on-ignition estimates of organic matter and relationships to organic carbon in fluvial bed sediments.* Hydrobiologia, 1998. **389**(1-3): p. 153-167.

77.   Steduto, P., et al., *AquaCrop—The FAO Crop Model to Simulate Yield Response to Water: I. Concepts and Underlying Principles All rights reserved. No part of this periodical may be reproduced or transmitted in any form or by any means, electronic or mechanical, including photocopying, recording, or any information storage and retrieval system, without permission in writing from the publisher.* Agron. J., 2009. **101**(3): p. 426-437.

78.   Hsiao, T.C., et al., *AquaCrop—The FAO Crop Model to Simulate Yield Response to Water: III. Parameterization and Testing for Maize All rights reserved. No part of this periodical may be reproduced or transmitted in any form or by any means, electronic*

or mechanical, including photocopying, recording, or any information storage and retrieval system, without permission in writing from the publisher. Agron. J., 2009. **101**(3): p. 448-459.

79. Nielsen, D.C., J.J. Miceli-Garcia, and D.J. Lyon, *Canopy Cover and Leaf Area Index Relationships for Wheat, Triticale, and Corn.* Agron. J., 2012. **104**(6): p. 1569-1573.

80. Farahani, H.J., G. Izzi, and T.Y. Oweis, *Parameterization and Evaluation of the AquaCrop Model for Full and Deficit Irrigated Cotton All rights reserved. No part of this periodical may be reproduced or transmitted in any form or by any means, electronic or mechanical, including photocopying, recording, or any information storage and retrieval system, without permission in writing from the publisher.* Agron. J., 2009. **101**(3): p. 469-476.

81. Nguyen, A.-T. and S. Reiter, *A performance comparison of sensitivity analysis methods for building energy models.* Building Simulation, 2015. **8**(6): p. 651-664.

82. Wetter, M., *GenOpt Generic Optimization Program User Manual Version 3.1.0*. 2011, Berkeley, CA Lawrence Berkeley National Laboratory.

83. Peeters, L., *The coupling of esp-r and genopt: a simple case study.* Lawrence Berkeley National Laboratory, 2010.

84. Ryan, T.P., *Modern Engineering Statistics*. 2007: Wiley-Interscience.

85. Collins, B.G., *Determination of the cosine response of pyranometers.* Journal of Scientific Instruments, 1966. **43**(11): p. 837.

86. Seborg, D.E., et al., *Process Dynamics and Control*. 2010: John Wiley & Sons.

87. Frank, M. and P. Wolfe, *An algorithm for quadratic programming.* Naval Research Logistics Quarterly, 1956. **3**(1-2): p. 95-110.

88. Bazaraa, S., H.D. Sherali, and C.M. Shetty, *Nonlinear programming: theory and algorithms*. 1993: Wiley.

89. Evett, S., et al., *Field estimation of soil water content: A practical guide to methods, instrumentation, and sensor technology.* IAEA: Vienna, 2008.

90. Simunek, J., et al., *The HYDRUS-1D software package for simulating the one-dimensional movement of water, heat, and multiple solutes in variably-saturated media- version 4.08*. 2009, University of California-Riverside. p. 240.

91. Nayak, J.K., et al., *The relative performance of different approaches to the passive cooling of roofs.* Building and Environment, 1982. **17**(2): p. 145-161.

92. Eumorfopoulou, E. and D. Aravantinos, *The contribution of a planted roof to the thermal protection of buildings in Greece.* Energy and Buildings, 1998. **27**(1): p. 29-36.

93. Takakura, T., S. Kitade, and E. Goto, *Cooling effect of greenery cover over a building.* Energy and Buildings, 2000. **31**(1): p. 1-6.

94. Onmura, S., M. Matsumoto, and S. Hokoi, *Study on evaporative cooling effect of roof lawn gardens.* Energy and Buildings, 2001. **33**(7): p. 653-666.

95. Bass, B., K.K.Y. Liu, and B.A. Baskaran, *Evaluating Rooftop and Vertical Gardens as an Adaptation Strategy for Urban Areas*. 2003.

96. Theodosiou, T.G., *Summer period analysis of the performance of a planted roof as a passive cooling technique.* Energy and Buildings, 2003. **35**(9): p. 909-917.

97. Lazzarin, R.A., F. Castellotti, and F. Busato, *Experimental measurements and numerical modelling of a green roof.* Energy and Buildings, 2005. **37**(12): p. 1260-1267.

98. Gaffin, S., et al. *Energy balance modeling applied to a comparison of white and green roof cooling efficiency*. in *Third Annual Greening Rooftops for Sustainable Communities Conference*. 2005. Washington, D.C.

99. Feng, C., Q. Meng, and Y. Zhang, *Theoretical and experimental analysis of the energy balance of extensive green roofs.* Energy and Buildings, 2010. **42**(6): p. 959-965.

100. D'Orazio, M., C. Di Perna, and E. Di Giuseppe, *Green roof yearly performance: A case study in a highly insulated building under temperate climate.* Energy and Buildings, 2012. **55**(0): p. 439-451.

101. Hodo-Abalo, S., M. Banna, and B. Zeghmati, *Performance analysis of a planted roof as a passive cooling technique in hot-humid tropics.* Renewable Energy, 2012. **39**(1): p. 140-148.

102. Permpituck, S. and P. Namprakai, *The energy consumption performance of roof lawn gardens in Thailand.* Renewable Energy, 2012. **40**(1): p. 98-103.

103. Kokogiannakis, G., J. Darkwa, and K. Yuan, *A combined experimental and simulation method for appraising the energy performance of green roofs in Ningbo's Chinese climate.* Building Simulation, 2014. **7**(1): p. 13-20.

104. Shuttleworth, W.J. and J. Wallace, *Evaporation from sparse crops-an energy combination theory.* Quarterly Journal of the Royal Meteorological Society, 1985. **111**(469): p. 839-855.

105. Flerchinger, G.N., *The Simultaneous Heat and Water (SHAW) Model: Technical Documentation*. 2000, USDA Agricultural Research Service: Idaho. p. 40.

106. Teh, C.B.S., *Introduction to Mathematical Modeling of Crop Growth: How the Equations are Derived and Assembled Into a Computer Model*. 2006: Brown Walker Press.

107. Flerchinger, G.N. and F.B. Pierson, *Modeling plant canopy effects on variability of soil temperature and water.* Agricultural and Forest Meteorology, 1991. **56**(3–4): p. 227-246.

108. Dawson, T. *Integrative Biology - Plant Ecophysiology*. 2005 [cited 2012 3 Sept]; Available from: http://ib.berkeley.edu/courses/ib151/.

109. Choudhury, B.J. and S.B. Idso, *Evaluating plant and canopy resistances of field-grown wheat from concurrent diurnal observations of leaf water potential, stomatal resistance, canopy temperature, and evapotranspiration flux.* Agricultural and Forest Meteorology, 1985. **34**(1): p. 67-76.

110. Roy, J., et al., *PA—Precision Agriculture: convective and ventilation transfers in greenhouses, Part 1: the greenhouse considered as a perfectly stirred tank.* Biosystems Engineering, 2002. **83**(1): p. 1-20.

111. Parkhurst, D.F., et al., *Wind-tunnel modelling of convection of heat between air and broad leaves of plants.* Agricultural Meteorology, 1968. **5**(1): p. 33-47.

112. Frankenstein, S. and G.G. Koenig, *FASST Vegetation Models*. 2004, US Army Corps of Engineers, Engineer Research and Development Center, Cold Regions Research and Engineering Laboratory.

113. Atarassi, R.T., M.V. Folegatti, and R.P.C.d. Brasil, *Convection regime between canopy and air in a greenhouse.* Scientia Agricola, 2006. **63**(1): p. 77-81.

114. Pitman, A.J., et al., *Description of BareEssentials of Surface Transfer for the Bureau of Meteorology Research Centre AGCM*. 1991, BMRC. p. 127.

115. Campbell, G.S., *Soil physics with BASIC : transport models for soil-plant systems / Gaylon S. Campbell*. Developments in soil science ; 14. 1985, Amsterdam ; New York :: Elsevier.

116. Burman, R.D., M. Jensen, and R.G. Allen. *Thermodynamic Factors in Evapotranspiration*. in *Irrigation Systems for the 21st Century*. 1987: American Society of Civil Engineers.

117. Mualem, Y., *A new model for predicting the hydraulic conductivity of unsaturated porous media.* Water Resources Research, 1976. **12**(3): p. 513-522.

118. Mermoud, A., *Cours de physique du sol*. 2006, Ecole Polytechnique Federale de Lausanne.

119. Stull, R., *Wet-Bulb Temperature from Relative Humidity and Air Temperature.* Journal of Applied Meteorology and Climatology, 2011. **50**(11): p. 2267-2269.
120. Feddes, R.A., P.J. Kowalik, and H. Zaradny, *Simulation of Field Water Use and Crop Yield*. 1978: John Wiley & Sons Australia, Limited.
121. Kovarik, K., *Numerical Models in Groundwater Pollution*. 2000: Springer.
122. Mulqueen, J., *The flow of water through gravels.* Irish Journal of Agricultural and Food Research 2005. **44**(1): p. 83-94.

Appendix 1: Chronological list of green roof simulation models

Several research studies have been conducted concerning green roof performance. A review of selected green roof models is presented in chapter 2. This appendix presents an extended list of what has been briefed in chapter 2.

Table A.1 Green-roof simulation models

Year	Researchers	Model brief
1982 [91]	Nayak, J. K., Srivastava, A., Singh, U., Sodha, M. S.	Hourly heat flux calculated of a 'roof garden' which is treated as an evaporative cooling system. Using an early days' 'ECIL-78' computer
1998 [9]	Elena Palomo Del Barrio	Finite volume method to solve set of partial differential equations depicting thermal and moisture exchanges in roof, soil and canopy sub models in Matlab simulation. Equations for soil thermal conductivity and non-isothermal vapour diffusivity serve as thermal-moisture coupling
1998 [92]	Eumorfopoulou, E., Aravantinos, D.	Considered green roof as an added insulation to the roof affecting its U value
2000 [93]	Takakura, T., Kitade, S., Goto, E.	Numerical model with14 nodes and 14 differential equations solved in CSMP built-in function (CSMP - Continuous System Modelling Program). Experimental validation done in test cell. Evapotranspiration measurements done by periodic weighing of a buried pot in the test cell.
2001 [22]	Niachou, A., Papakonstantinou, K., Santamouris, M., Tsangrassoulis, A., Mihalakakou, G.	Considered green roof as an added insulation to the roof affecting its U value in TRNSYS simulation. Experimental measurements were conducted in summer of 2000 in a hotel situated in the extended Athens basin
2001 [94]	Onmura, S., Matsumoto, M., Hokoi, S.	Numerical finite difference model calculating simultaneous transport of heat and moisture in a combination of experiment and simulation. Thermal moisture coupling implemented in transport equations. Field measurement on a lawn garden set up in a three storey building and wind-tunnel experiment to analyse heat and moisture transport were done.

2003 [95]	Bass, B., Liu, K. K. Y., Baskaran, B. A.	Thermal effect of green roof and green walls modelled as additional insulation and shading in Visual DOE. Field monitoring done on an experimental field site, the Field Roofing Facility (FRF), at the National Research Council (NRC) campus in Ottawa
2003 [96]	Theodosiou, T. G.	Numerical finite elements model of 21 nodes dine in Suncode PC. Planted roof simulation within a complete building analysis performed. Coupling is effected by variation of some thermo-physical properties according to time and water content. Validation done by the use of real data taken from a building in the Mediterranean area
2003 [26]	Wong Nyuk Hien, Chen Yu, Ong Chui Leng, Sia Angelia	Change in roof U value with and without green roof measured. Thermal effects of rooftop garden under tropical climate were investigated through the field measurement
2005 [97]	Lazzarin, R., Castellotti, F., Busato, F.	Numerical finite difference model, with 3 nodes for soil, 1 for drain and 1 for water-proof membrane and 1 for concrete implemented in TRNSYS. A dedicated module to simulate the green roof was developed. On site measurements done covering two summer periods and one winter period.
2006 [24]	Chen Yu	A new 'Green Sol Air Temperature' to calculate ETTV was introduced and extensive field tests were conducted in Singapore.
2006 [98]	Gaffin, S., Rosenzweig, C., Parshall, L., Beattie, D., Berghage, R., Keefe, G., Braman, D.	It is a quasi-steady state energy balance model neglecting heat storage term. Bowen ratio was used for latent heat estimation. Experiment measurements conducted from six separate buildings, three with green roofs and three with dark roofs
2007 [17]	Alexandri, E., Jones, P.	It is a finite difference model of 17 nodes distributed across layers of air, canopy, soil and concrete in which hourly calculations were performed. Thermal and air moisture exchanges are modelled as parallel networks with interactions. Experimental measurements conducted on two test cells, one plain concrete and another green roof, installed on a building roof

Table A1 Contd.

2007 [21]	Santamouris, M., Pavlou, C., Doukas, P., Mihalakakou, G., Synnefa, A., Hatzibiros, A., Patargias, P.	This model considered green roof as an added insulation to the roof affecting its U value and implemented in TRNSYS 15.1. Experimental investigation conducted on a green roof system in a nursery school building in Athens
2008 [23]	Martens, R., Bass, B., Alcazar, S.	A rooftop energy balance model for a green roof is integrated into a building energy simulation tool in order to determine its performance. It was implemented in ESP-r, as a modified convective coefficient, modified using Bowen ratio to include evaporative heat loss. Simulation based parametric studies conducted for analysis.`
2008 [6]	Sailor, D.	It is implemented as 'ecoroof' module in EnergyPlus, which is using conduction transfer function scheme by solving two equations, one for foliage energy balance and another for soil energy balance. Coupling done by updating soil thermal conductivity as a function of moisture content. Parametric and field tests conducted on office buildings in Chicago and Houston.
2010 [99]	Feng, Chi, Meng, Qinglin, Zhang, Yufeng	Energy balance equation consisting of elements of plants net photosynthetic energy, among others solved with a combination of experimental measurements. Summer measurements conducted on a research building in Guangzhou China
2011 [31]	Ayata, T., Tabares-Velasco, P. C., Srebric, J.	A new equation for convective heat transfer between plant and air was developed. Convective coefficient was expressed as a function of volumetric water content. Experimental measurements conducted on test cell to validate newly developed formula.
2011 [43]	Ouldboukhitine, S. E., Belarbi, R., Jaffal, I., Trabelsi, A.	Model was implemented in MATLAB by solving two equations, one for foliage energy balance and another for soil energy balance. Thermal moisture coupling introduced by relating moisture content with thermal conductivity. Experimental verification conducted at a 1:10 platform
2012 [100]	D'Orazio, M., Di Perna, C., Di Giuseppe, E.	Experimental measurements were used to assess thermal transmittance U values. Summer and winter measurements conducted on a real scale experimental building in Ancona Italy

Year / Ref	Authors	Description
2012 [41]	Djedjig, R., Ouldboukhitine, S. E., Belarbi, R., Bozonnet, E.	This model involves solving three equations, 1st for foliage energy balance, 2nd for soil energy balance and 3rd for soil moisture balance. (1 and 2 include thermal capacitance terms). Coupling introduced by moisture transfer equation. Experimental verification conducted at a 1:10 platform
2012 [101]	Hodo-Abalo, S., Banna, M., Zeghmati, B.	In this model numerical simulation and parametric analysis were done to establish a relation for Solar Heat gain Factor (ratio of incident to transmitted solar radiation) in terms of LAI and Biot number
2012 [42]	Jaffal, I., Ouldboukhitine, S. E., Belarbi, R.	It is a model solving two equations, one for foliage energy balance and another for soil energy balance and implemented as a new module in TRNSYS building simulation
2012 [102]	Permpituck, S., Namprakai, P.	In this study overall heat transfer coefficient (U-Value) of the roof lawn garden was estimated by using data from site measurements and simulated in VISUAL DOE 4.0 to determine annual benefits. Field test conducted on a model situated at Phitsanulok Province, Thailand.
2012 [29]	Tabares-Velasco, P. C., Srebric, J.	Quasi-steady state equations modelling energy balance implemented where moisture thermal inter-related functions were included. Extensive experimental verification conducted of all related equations
2013 [32]	de Munck, C. S., Lemonsu A., Bouzouidja, R., Masson, V., Claverie R.	Green roof model implemented as part of a town energy balance model interfacing with atmospheric model. Experimental verifications done in Nancy, France
2014 [103]	Kokogiannakis, G., Darkwa, J., Yuan, K.	A combined experimental and simulation study at Ningbo China in which measured green roof temperatures were used as modified boundary conditions in ESP-r to simulate the carbon emission benefits in summer and winter.
2014 [7]	Djedjig, R., Bozonneta, E, Belarbia, R.	TRNSYS implemented vegetated building envelope model which include green walls and green roofs. A thermal moisture coupled model with experimental verifications on a test system consisting of green roof and green walls at La Rochelle France.

Appendix 2: Code listing of ASCII file used for data input

An example of the input text file, which can be used with the new green model is given in this appendix.

```
#GR_input
# ***Plant
# VARIABLE        DESCRIPTION [UNIT]
# plantLAI        Leaf area index [-]
# plantHt         Plant height[m]
# rhoLeaf         Density of leaf[Kg/m3]
# cpLeaf          Specific heat of leaf[J/kg K]
# leafThk         Leaf thickness[m]
# leafChDim       Leaf dimensions (L,W)[m]
# extinLong       Long wave extinction coefficient[-]
# stomatResMin    Minimum Stomata resistance[s/m]
# plantWiltPt     Plant wilting point matric potential[m]
3.0 0.4 700.0 3500.0 0.001 0.015 0.829 120.0 -80.0
# ***Soil
# VARIABLE        DESCRIPTION [UNIT]
# soilHt          Soil depth[m]
# soilMinFr       Soil mineral fraction[m3/m3]
# soilOrgFr     Soil organic fraction[m3/m3]
# MoistCont_sat Saturated moisture content[m3/m3]
# Clay_fr         Soil clay fraction[kg/kg]
# MoistCont_res   Residual moisture content[m3/m3]
# soilnIndex    Soil 'n' index       (van-Genutchen function)
#                     -curve shape factor related to soil pore-size
distribution
# soilAlphaIndex Soil 'alpha' index (van-Genutchen function)
#                     -scaling parameter related to the inverse of
#                     -the air entry pressure[cm-1]
# hydCond_sat     Saturated hydraulic conductivity[m/s]
0.4 0.45 0.1 0.45 0.2 0.067 1.4 0.02 1.25e-6 0.13 4.7
# ***Roof
# VARIABLE        DESCRIPTION [UNIT]
# ***Radiation
# VARIABLE        DESCRIPTION [UNIT]
# reflCan         Canopy reflectivity[-]
# reflGround    Ground reflectivity[-]
# reflLeafTis   Leaf tissue reflectivity[-]
# transmLeafTis Leaf tissue transmissivity[-]
# emissLeaves   Emissivity of leaves[-]
# emissSoil       Emissivity of ground[-]
0.25 0.15 0.3 0.2 0.96 0.95
# ***Site
# VARIABLE        DESCRIPTION [UNIT]
# siteAlt         Site  Site altitude[m]
# fracVeg         Fraction of vegetation[-]
100.0 0.95
# ***Simulation
# VARIABLE        DESCRIPTION [UNIT]
# alphaGR         weighing factor for Crank Nicolson
#                   (m1alphaGR = 1 - alphaGAM)
0.9
# ***Maintenance
```

```
# VARIABLE          DESCRIPTION [UNIT]
# TimesPerDay_time(1)    Jan        |these two together tells
# TimesPerDay_day(1)                |how many times per day
# TimesPerDay_time(2)    Feb        |range      TimesPerDay_time 0 to
4
# TimesPerDay_day(2)                |          TimesPerDay_day 0 to
4
# TimesPerDay_time(3)    Mar        |if TimesPerDay_time=0
# TimesPerDay_day(3)                |then TimesPerDay_day=0 (no irrig)
# TimesPerDay_time(4)    Apr        |if TimesPerDay_time=1
# TimesPerDay_day(4)                |then TimesPerDay_day=1 to 4
# TimesPerDay_time(5)    May        |if TimesPerDay_time=2 to 4
# TimesPerDay_day(5)                |then TimesPerDay_day=1
# TimesPerDay_time(6)    Jun        |(more than once daily)
# TimesPerDay_day(6)
# TimesPerDay_time(7)    Jul
# TimesPerDay_day(7)
# TimesPerDay_time(8)    Aug
# TimesPerDay_day(8)
# TimesPerDay_time(9)    Sep
# TimesPerDay_day(9)
# TimesPerDay_time(10)   Oct
# TimesPerDay_day(10)
# TimesPerDay_time(11)   Nov
# TimesPerDay_day(11)
# TimesPerDay_time(12)   Dec
# TimesPerDay_day(12)
# IrrQty          Amount of irrigation each time [mm]
0 0 0 0 0 0 1 2 1 1 1 4 2 1 0 0 0 0 0 0 0 0 0 0
5.0
#***** Weather data    Solar radiation[W/m2]
#          Wind velocity[m/s]
#          Hourly Precipitation[mm]
#          Sky temperature[K]


#
```

Appendix 3.1 Thermal model equations and coefficient tables

This appendix provides an organized documentation for all the coefficients, their derivations and in some cases a few alternative choices, for the thermal domain equations. Also the format of the equations for the thermal balances in each control volumes is given.

Thermal Balance Equations

Thermal exchange matrix for eight control volumes:

$$
\begin{pmatrix}
a11 & a12 & a13 & a14 & & & & \\
a21 & a22 & a23 & a24 & & & & \\
 & a32 & a33 & a34 & a35 & & & \\
 & & & a44 & a45 & a46 & & \\
 & & & & a55 & a56 & a57 & \\
 & & & & & a66 & a67 & a68 \\
 & & & & & & a77 & a78 & a79
\end{pmatrix}
\times
\begin{pmatrix}
T\alpha^{t+\Delta t} \\
Tp^{t+\Delta t} \\
Ta^{t+\Delta t} \\
Ts1^{t+\Delta t} \\
Ts2^{t+\Delta t} \\
Ts3^{t+\Delta t} \\
Ts4^{t+\Delta t} \\
Ts5^{t+\Delta t} \\
Tx^{t+\Delta t}
\end{pmatrix}
=
\begin{pmatrix}
b11 & b12 & b13 & b14 & & & & \\
b21 & b22 & b23 & b24 & & & & \\
 & b32 & b33 & b34 & b35 & & & \\
 & & & b44 & b45 & b46 & & \\
 & & & & b55 & b56 & b57 & \\
 & & & & & b66 & b67 & b68 \\
 & & & & & & b77 & b78 & b79
\end{pmatrix}
\times
\begin{pmatrix}
T\alpha^{t} \\
Tp^{t} \\
Ta^{t} \\
Ts1^{t} \\
Ts2^{t} \\
Ts3^{t} \\
Ts4^{t} \\
Ts5^{t} \\
Tx^{t}
\end{pmatrix}
+
\begin{pmatrix}
c1 \\
c2 \\
c3 \\
c4 \\
c5 \\
c6 \\
c7
\end{pmatrix}
=
\begin{pmatrix}
z1 \\
z2 \\
z3 \\
z4 \\
z5 \\
z6 \\
z7
\end{pmatrix}
$$

1. Canopy plant

Energy Balance

$$\rho_p C_p dLAI \frac{dT_p}{dt} = \phi_{rad,sol} + \phi_{rad,long} + \phi_{conv,\alpha-p} - \phi_{conv,p-ca} - \phi_{trans,p-ca}$$

$$\phi_{rad,sol} = \left[1 - \tau_s - (1-\tau_s)\rho r_\alpha\right]\left(1 + \tau_s \rho r_g\right)\phi_s$$

$$\phi_{rad,long} = h_{r,sky}\left(T_{sky} - T_p\right) + h_{r,s1}\left(T_{s1} - T_p\right)$$

$$\phi_{conv,\alpha-p} = \sigma_f \frac{\rho_\alpha Cp}{r_{e\alpha}}\left(T_\alpha - T_p\right)$$

$$\phi_{conv,p-ca} = 2LAI \frac{\rho_{ca} Cp}{r_e}\left(T_p - T_{ca}\right)$$

$$\phi_{trans,p-ca} = 2LAI \frac{\rho_{ca} Cp}{\gamma(r_e + r_i)}\left(e_p - e_{ca}\right)$$

Energy Balance CV1 Plant leaves
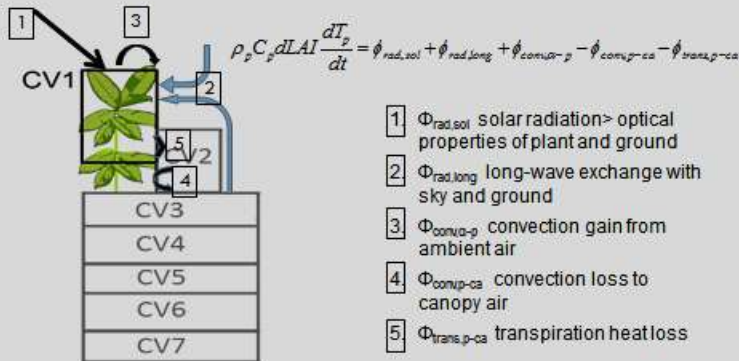
$$\rho_p C_p dLAI \frac{dT_p}{dt} = \phi_{rad,sol} + \phi_{rad,long} + \phi_{conv,a-p} - \phi_{conv,p-ca} - \phi_{trans,p-ca}$$

CV1

CV2

CV3
CV4
CV5
CV6
CV7

1. $\Phi_{rad,sol}$ solar radiation> optical properties of plant and ground
2. $\Phi_{rad,long}$ long-wave exchange with sky and ground
3. $\Phi_{conv,a-p}$ convection gain from ambient air
4. $\Phi_{conv,p-ca}$ convection loss to canopy air
5. $\Phi_{trans,p-ca}$ transpiration heat loss

Coefficient form

$$-\left[\alpha \sigma_f \frac{\rho_a C p}{r_{ea}^{t+\Delta t}}\right] T_\alpha^{t+\Delta t}$$

$$+\left[\frac{\rho_p C p dLAI}{\Delta t} + \alpha h_{r,sky}^{t+\Delta t} + \alpha h_{r,s1}^{t+\Delta t} + \alpha \sigma_f \frac{\rho_a C p}{r_{ea}^{t+\Delta t}} + \alpha \frac{2LAI \rho_a C_{pa}}{r_e^{t+\Delta t}}\right] T_p^{t+\Delta t}$$

$$-\left[\alpha \frac{2LAI \rho_a C_{pa}}{r_e^{t+\Delta t}}\right] T_{ca}^{t+\Delta t}$$

$$-\left[\alpha h_{r,s1}^{t+\Delta t}\right] T_{s1}^{t+\Delta t}$$

$$=$$

$$\left[(1-\alpha)\sigma_f \frac{\rho_a C p}{r_{ea}^t}\right] T_\alpha^t$$

$$+\left[\frac{\rho_p C_p dLAI}{\Delta t} - (1-\alpha)h_{r,sky}^t - (1-\alpha)h_{r,s1}^t - (1-\alpha)\sigma_f \frac{\rho_a C p}{r_{ea}^t} - (1-\alpha)\frac{2LAI \rho_a C_{pa}}{r_e^t}\right] T_p^t$$

$$+\left[(1-\alpha)\frac{2LAI \rho_a C_{pa}}{r_e^t}\right] T_{ca}^t$$

$$+\left[(1-\alpha)h_{r,s1}^t\right] T_{s1}^t$$

$$+\left[(1-\alpha)\left([1-\tau_s - (1-\tau_s)\rho_a](1+\tau_s \rho_g)\right)\phi_s^t + \alpha\left([1-\tau_s - (1-\tau_s)\rho_a](1+\tau_s \rho_g)\right)\phi_s^{t+\Delta t}\right]$$

$$+\left[(1-\alpha)h_{r,sky}^t T_{sky}^t + \alpha h_{r,sky}^{t+\Delta t} T_{sky}^{t+\Delta t}\right]$$

$$-\left[(1-\alpha)\frac{2LAI \rho_a C_{pa}}{\gamma(r_e+r_i)^t}e_p^t\right] - \left[\alpha \frac{2LAI \rho_a C_{pa}}{\gamma(r_e+r_i)^{t+\Delta t}}e_p^{t+\Delta t}\right]$$

$$+\left[(1-\alpha)\frac{2LAI \rho_a C_{pa}}{\gamma(r_e+r_i)^t}e_{ca}^t\right] + \left[\alpha \frac{2LAI \rho_a C_{pa}}{\gamma(r_e+r_i)^{t+\Delta t}}e_{ca}^{t+\Delta t}\right]$$

165

(a11)	$-\alpha\,\sigma_f\,\dfrac{\rho_\alpha Cp}{r_{e\alpha}^{t+\Delta t}}$							

Time invariant data	Defining Equations and Remarks	Initial Value	Unit	Required data			Couple Info
				Input	Parameters	Calculated Variables	
σ_f fractional vegetation coverage		0.98	-	σ_f			
Cp air specific heat		1005	J/kg K		Cp_α		

Time variant data	Defining Equations and Remarks	Initial Value	Unit	Required data			Couple Info
				Input	Parameters	Calculated Variables	
ρ_α air density (Note 6)	$\rho = \dfrac{p}{101.325}\dfrac{273.16}{T}\,1.293$	1.16	kg/m^3			ρ_α	
$r_{e\alpha}^{t+\Delta t}$ aerodynamic heat transfer coefficient	Reference [104] $$r_{e\alpha} = \frac{\ln\frac{(z-d)}{z_o}}{k^2\,uz}\left[\ln\left(\frac{(z-d)}{(h-d)}\right) + \frac{h}{\alpha(h-d)}\left[\exp\left(\alpha\left\{1 - \frac{(d+z_o)}{h}\right\}\right) - 1\right]\right]$$ k = von Karman's constant = 0.41 z= reference height of measurement of wind velocity uz (2m) h=plant height d = zero plane displacement = 0.64 h z$_o$ = roughness length =0.13 h α = canopy diffusion coefficient 2.5 for agricultural crops	13.7	s/m	h uz			
(Alternative) $r_{e\alpha}^{t+\Delta t}$ aerodynamic heat transfer coefficient	Reference [105] [55] $$r_{e\alpha} = \frac{\left[ln\left(\frac{z-d+z_H}{z_H}\right) + \psi_H\right]\left[ln\left(\frac{z-d+z_m}{z_m}\right) + \psi_m\right]}{k^2\,u}$$ k = von Karman's constant = 0.41 z= reference height of measurement of wind velocity u d = zero plane displacement = 0.65 L; L is the plant height	58.5	W/m2 K	L z u	CPα ρα	Tα Ta	

166

z_m = surface roughness parameters for momentum = 0.1 L
z_H = surface roughness parameters for temperature = 0.2 z_m

ψ_H = atmospheric stability correction factors for heat
ψ_m = atmospheric stability correction factors for momentum

Values for this correction factors are to be determined according to the value of a stability parameter: (Note 1)

$$s = -\frac{k\,z\,g\,H}{\rho_\alpha Cp_\alpha\,T_\alpha u_*^3}$$

H = sensible heat = $\frac{\rho_\alpha Cp_\alpha}{r_{e\alpha}}\left(T_\alpha - T_p\right)$ between canopy plant Tp and ambient air Tα

u_* = friction velocity = $\frac{uk}{\left[ln\left(\frac{z-d+z_m}{z_m}\right)+\psi_m\right]}$

For stable conditions (s positive)
$$\psi_H = \psi_m = 6\,ln(1+s)$$
For unstable conditions (s negative)
$$\psi_H = -2\,ln\left[\frac{1+(1-16s)^{1/2}}{2}\right]; \quad \psi_m = 0.6\,\psi_H$$

a12	$\frac{\rho_p C_p d\,LAI}{\Delta t} + \alpha h_{r,sky}^{t+\Delta t} + \alpha h_{r,s1}^{t+\Delta t} + \alpha\,\sigma_f\,\frac{\rho_\alpha Cp_\alpha}{r_{e\alpha}^{t+\Delta t}} + \alpha\,\frac{2\,LAI\,\rho_a\,C_{pa}}{r_e^{t+\Delta t}}$							
Time invariant data	**Defining Equations and Remarks**	**Initial Value**	**Unit**	**Required data**			**Couple Info**
				Input	**Parameters**	**Calculated Variables**	
LAI Leaf Area Index	Input by user by selecting plant type. The plant database – also include seasonal schedule	3	m^2/m^2	LAI			
ρ_p plant leaf density	Plant DB; seasonal schedule	400	kg/m^3	ρ_p			
Cp plant leaf specific heat	Plant DB; seasonal schedule	2000	J/kg K	C_p			
Cp_a canopy air specific heat		1005	J/kg K		C_{pa}		
Cp_α ambient air specific heat		1005	J/kg K		$C_{p\alpha}$		
d average leaf thickness	Plant DB; seasonal schedule	0.001	m	d			
σ_f fractional vegetation coverage		0.98	-	σ_f			

Time variant data	Defining Equations and Remarks	Initial Value	Unit	Required data			Couple Info
				Input	Parameters	Calculated Variables	
ρ_{ca} canopy air density	$\rho = \dfrac{p}{101.325}\dfrac{273.16}{T}\,1.293$	1.18	kg/m3			ρ_{ca}	
ρ_{α} ambient air density	$\rho = \dfrac{p}{101.325}\dfrac{273.16}{T}\,1.293$	1.16	kg/m3			ρ_{α}	
$h_{r,sky}$ radiation transfer coefficient sky -plant	Sub – based on previous time values of plant temperature and sky temperature $h_{r,sky} = 4\,(1-\tau_l)\,\sigma\left(\dfrac{T_{sky}+T_p}{2}\right)^3$ σ Stefan Boltzmann constant = 5.6704×10^{-8} W/m^2 K^4 τ_l longwave transmittance $\tau_l = e^{-(k_l\,LAI)}$ k_l Coefficient of extinction-long wave given by Leaf distribution horizontal kl = 1 Leaf distribution 45 degree kl = 0.829 Leaf distribution vertical kl = 0.436 spherical leaves kl = 0.684 Emissivity to be included-Note 7	5.6	W/m^{2}K	LAI k_l	σ	Tsky Tp	
$h_{r,s1}$ radiation transfer coefficient soil surface - plant	Sub – based on current values of plant temperature and soil surface temperature $h_{r,s1} = 4\,(1-\tau_l)\,\sigma\left(\dfrac{T_{S1}+T_p}{2}\right)^3$ Emissivity to be included-Note 7	5.4	W/m^{2}K	LAI k_l	σ	T_{S1} T_p	
$r_{e\alpha}^{t+\Delta t}$ aerodynamic heat transfer coefficient	As defined above	58.5	W/m2K	L z u	CPα ρα	Tα Ta	
r_e aerodynamic heat transfer coefficient between plant and canopy air	Reference : [106] $r_e = \dfrac{\alpha}{0.012\,LAI\left[1 - exp\left(\dfrac{-\alpha}{2}\right)\right]\sqrt{\dfrac{uh}{w}}}$ α =wind attenuation coefficient for canopy = 2.5 for agricultural crops LAI = leaf area index uh = wind velocity at plant height, given by	10.4	s/m	LAI w h			

	$uh = uz \, \dfrac{\ln\left(\dfrac{h-d}{z_o}\right)}{\ln\left(\dfrac{z-d}{z_o}\right)}$ z= reference height of measurement of wind velocity uz (2m) h=plant height d = zero plane displacement = 0.64 h z_o = roughness length =0.13 h w= leaf width					
(Alternative) r_e aerodynamic heat transfer coefficient between plant and canopy air	Sub - For r_e:[107] [55] (note 3) $r_e = 7.392 \, \hat{\rho} \left(\dfrac{d_c}{u}\right)^{1/2}$ where dc is the characteristic dimension (m) of the leaves (leaf width as in [108] Note 5) u is wind speed (m s^{-1}) within the canopy layer, and 7.4 is a coefficient (m^{2}s$^{0.5}$ mol^{-1}) specific for thermal diffusivity and viscosity of air and $\hat{\rho}$ is the molar density at canopy air temperature $\hat{\rho} = 44.6 \, \dfrac{p}{101.3} \, \dfrac{273.15}{T_a}$ Wind velocity within canopy is determined as follows: Wind velocity at the canopy top: $u(L) = \dfrac{u(z)}{ln\left(\dfrac{z-d}{z_m}\right)} \, ln\left(\dfrac{L-d}{z_m}\right)$ L is the canopy height u(z) is the wind velocity at instrument height z d is the zero plane displacement given by 0.65L z_m is the momentum roughness parameter given by 0.1L (Assumed for a PAI of 3; small difference for other values of PAI exist, details in fig 5.5 p70 in [55] Wind velocity within canopy is determined as: $u(z_c) = u(L)exp\left[a\left(\dfrac{z_c}{L}-1\right)\right]$ z_c is the height within canopy drag coefficient a is given by: $a = \left(\dfrac{0.2 \, LAI \, L}{I_m}\right)^{1/2}$	116.7	s/m	d_c L u(z) z LAI	p	T_a

	mean distance between leaves I_m is given by : $I_m = \left(\frac{6\,d_c^2\,L}{\pi\,LAI}\right)^{1/3}$ For a start canopy wind velocity at 0.8L is taken as a representative value (note 4); z_c= 0.8L u = u(z_c) in the first equation in this section					
	Alternative arrangement: to consider 50% time as forced laminar (as above) and 50% time as free convection. Forced convection: $r_{e,forced} = 7.392\,\hat{\rho}\left(\frac{d_c}{u}\right)^{1/2}$ Free convection [55]: $r_{e,free\,low} = 20.639\,\hat{\rho}\left(\frac{d_c}{T_p-T_a}\right)^{1/4}$ for top surface (assuming Tp>Ta) $r_{e,free\,high} = 42.866\,\hat{\rho}\left(\frac{d_c}{T_p-T_a}\right)^{1/4}$ for bottom surface (assuming Tp>Ta higher resistance for heat flowing downward) If Tp<Ta, equations are just exchanged between top and bottom surface. So in the general formulation of the coefficient 1 LAI is to be assigned lower resistance and 1 LAI is to be assigned higher resistance (total area 2 LAI) The coefficient element (5th) of **(a12),** in this case need to be modified from $\alpha\,\dfrac{2\,LAI\,\rho_a\,C_{pa}}{r_e^{t+\Delta t}}$ to $0.5\,\alpha\,\dfrac{2\,LAI\,\rho_a\,C_{pa}}{r_{e,forced}^{t+\Delta t}} + 0.5\left[\alpha\,\dfrac{LAI\,\rho_a\,C_{pa}}{r_{e,free\,low}^{t+\Delta t}} + \alpha\,\dfrac{LAI\,\rho_a\,C_{pa}}{r_{e,free\,high}^{t+\Delta t}}\right]$					
	Alternative equation [109] (note 2) $r_e = \dfrac{\ln^2\left[\dfrac{z-di}{z_o}\right]}{k^2\,u\left[1+\dfrac{4.7\,(z-di)g\left(T_p-T_a\right)}{u^2\,T_a}\right]^2}$ u wind velocity (m/s) from weather file z instrument height for u (m) usually 2m k von Karmen constant (0.41) g acceleration due to gravity 9.81 m/s[2] di zero displacement di = 0.56 x CH m	s/m				

	z_o roughness height $z_o = 0.3(CH-di)$ m CH = crop height m (input by user by selecting plant type and CH will be included in plant database)					
	Alternate equation for re [45] (http://www.fao.org/docrep/X0490E/x0490e06.htm#aerodynamic%20resistance%20%28ra%29) $$r_a = \frac{ln\left[\frac{z_m - d}{z_{om}}\right]\ ln\left[\frac{z_h - d}{z_{oh}}\right]}{k^2\,u_z}$$ where r_a aerodynamic resistance [s m^{-1}], z_m height of wind measurements [m], z_h height of humidity measurements [m], d zero plane displacement height [m], z_{om} roughness length governing momentum transfer [m], z_{oh} roughness length governing transfer of heat and vapour [m], k von Karman's constant, 0.41 [-], u_z wind speed at height z [m s^{-1}].					
	Alternate equation for r_e [9] [71] $$r_e = \frac{al^m}{\left(l\left|T_p - T_a\right| + bu^2\right)^n}$$ l - leaves characteristic length u - wind speed. a, b, m and n are empirical coefficients (a = 1174, b=207,m=0.5,n=0.25fortomato crops).					
	Alternative equation for r_e in terms of h_c $\left(h_c = \frac{\rho\ C_p}{r_e}\right)$ [110] and [111] - For free convection from vertical leaves: Nu = 0.480 Gr$^{1/4}$ - For free convection from the upper surface of a horizontal leaf warmer than the air, or to the lower surface of such a leaf cooler than the air: Nu = 0.497 Gr$^{1/4}$ - For free convection from the lower surface of a warmer-than-air horizontal leaf, or to the upper surface of a cooler-than-air horizontal leaf: Nu = 0.249 Gr$^{1/4}$ - For forced convection to or from a leaf having a uniform heat flux from its surface and with the fluid flowing parallel to its surface: Nu = 0.812 Re$^{1/2}$					

	- For forced convection to or from a leaf having a uniform-temperature surface in parallel flow: Nu = 0.595 Re$^{1/2}$ - For a horizontal flat leaf in forced convection in parallel flow: Nu = 0.032 Re$^{0.8}$ Gr/Re2<0.1 Forced flow; laminar if Re<5e4; turbulent if Re> 5e4 Gr/Re2>16 Free flow; laminar if Gr<1e8; turbulent if Gr> 1e8 Parkhurst 1968 provide list of definition of characteristic lengths for various leaf shapes $Nu = \frac{h\,L}{k}$; $Re = \frac{u\rho L}{\mu}$; $Gr = \frac{\beta g \rho^2 L^3 (t_l - t_a)}{\mu^2}$ L = effective dimension in the direction of air flow; u wind velocity; g acceleration due to gravity, The physical properties of air are to be taken at the mean of the air and leaf temperatures: k = thermal conductivity, β temperature coefficient of volume expansion, μ absolute viscosity and ρ density						
	Alternative formulation as in FASST model [112] (eq 7 pg6, original equation for sensible heat transfer need to be changed in the format of FASST; eq 7,10,11 and 12 are required to complete the model.)						

(a13)	$\alpha \dfrac{2\,LAI\,\rho_a\,Cp_a}{r_e^{t+\Delta t}}$						
Time invariant data	**Defining Equations and Remarks**	**Initial Value**	**Unit**	**Required data**			**Couple Info**
				Input	**Parameters**	**Calculated Variables**	
LAI Leaf Area Index	Input by user by selecting plant type. The plant database – also include seasonal schedule	3	m^2/m^2	LAI			
Cpa air specific heat		1005	J/kg K		Cpa		
Time variant data	**Defining Equations and Remarks**	**Initial Value**	**Unit**	**Required data**			**Couple Info**
				Input	**Parameters**	**Calculated Variables**	
ρ_{ca} canopy air density	$\rho = \dfrac{p}{101.325} \dfrac{273.16}{T} 1.293$	1.18	kg/m3			ρ_{ca}	
r_e aerodynamic heat transfer coefficient	(Defined above) $r_e = 7.4\,\hat{\rho}\left(\dfrac{d_c}{u}\right)^{1/2}$	re=116.7	s/m				

172

(a14)	$-\alpha h_{r,s1}^{t+\Delta t}$ (as defined above)									
Time invariant data	**Defining Equations and Remarks**		**Initial Value**	**Unit**	**Required data**			**Couple Info**		
					Input	**Param eters**	**Calcul ated Variab les**			
Time variant data	**Defining Equations and Remarks**		**Initial Value**	**Unit**	**Required data**			**Couple Info**		
					Input	**Param eters**	**Calcul ated Variab les**			

'b' coefficients use time varying parameters one time step prior to that in 'a' coefficients

In addition, wherever present, multipliers α change to 1-α.

$$b11 = (1 - \alpha)h_{r,sky}^{t} \ (1 - \alpha)\,\sigma_f\,\frac{\rho_a Cp_a}{r_{e\alpha}^{t}}$$

$$b12 = \frac{\rho_p C_p d\,LAI}{\Delta t} - (1 - \alpha)h_{r,sky}^{t} - (1 - \alpha)h_{r,s1}^{t} - (1 - \alpha)\sigma_f\,\frac{\rho_a Cp_a}{r_{e\alpha}^{t}} - (1 - \alpha)\frac{2\,LAI\,\rho_a\,C_{pa}}{r_e^{t}}$$

$$b13 = (1 - \alpha)\frac{2\,LAI\,\rho_a\,C_{pa}}{r_e^{t}}$$

$$b14 = (1 - \alpha)h_{r,s1}^{t}$$

| (c11) | $\left[\begin{array}{l}\left[(1-\alpha)\left([1-\tau_s-(1-\tau_l)\rho r_a](1+\tau_s\rho r_g)\right)\phi_s^t+\alpha\left([1-\tau_s-(1-\tau_l)\rho r_a](1+\tau_s\rho r_g)\right)\phi_s^{t+\Delta t}\right] \\ +\left[(1-\alpha)h_{r,sky}^t T_{sky}^t+\alpha\, h_{r,sky}^{t+\Delta t}\, T_{sky}^{t+\Delta t}\right] \\ -\left[(1-\alpha)\dfrac{2\,LAI\,\rho_a Cp_a}{\gamma\,(r_e\,+\,r_i)^t}e_p^t\right]-\left[\alpha\dfrac{2\,LAI\,\rho_a Cp_a}{\gamma\,(r_e\,+\,r_i)^{t+\Delta t}}e_p^{t+\Delta t}\right] \\ +\left[(1-\alpha)\dfrac{2\,LAI\,\rho_a Cp_a}{\gamma\,(r_e\,+\,r_i)^t}e_a^t\right]+\left[\alpha\dfrac{2\,LAI\,\rho_a Cp_a}{\gamma\,(r_e\,+\,r_i)^{t+\Delta t}}e_a^{t+\Delta t}\right]\end{array}\right]$ |

(c11)

$$\left[\begin{array}{l}\left[(1-\alpha)\left([1-\tau_s-(1-\tau_l)\rho r_a](1+\tau_s\rho r_g)\right)\phi_s^t+\alpha\left([1-\tau_s-(1-\tau_l)\rho r_a](1+\tau_s\rho r_g)\right)\phi_s^{t+\Delta t}\right] \\ +\left[(1-\alpha)h_{r,sky}^t T_{sky}^t+\alpha\, h_{r,sky}^{t+\Delta t}\, T_{sky}^{t+\Delta t}\right] \\ -\left[(1-\alpha)\dfrac{2\,LAI\,\rho_a Cp_a}{\gamma\,(r_e\,+\,r_i)^t}e_p^t\right]-\left[\alpha\dfrac{2\,LAI\,\rho_a Cp_a}{\gamma\,(r_e\,+\,r_i)^{t+\Delta t}}e_p^{t+\Delta t}\right] \\ +\left[(1-\alpha)\dfrac{2\,LAI\,\rho_a Cp_a}{\gamma\,(r_e\,+\,r_i)^t}e_a^t\right]+\left[\alpha\dfrac{2\,LAI\,\rho_a Cp_a}{\gamma\,(r_e\,+\,r_i)^{t+\Delta t}}e_a^{t+\Delta t}\right]\end{array}\right]$$

Time invariant data	Defining Equations and Remarks	Initial Value	Unit	Required data			Couple Info
				Input	Parameters	Calculated Variables	
Canopy radiation absorption	$[1-\tau_s-(1-\tau_l)\rho r_a](1+\tau_s\rho r_g)$ Function of LAI, coefficient of short wave extinction, coefficient of long wave extinction, canopy reflectivity and ground reflectivity Short wave transmittance: $\tau_s=e^{-(k_s LAI)}$ Coefficient of extinction-short wave $k_s=[(1-\tau_t)^2-\rho r_t{}^2]^{1/2}k_l$ k_l Coefficient of extinction-long wave; τ_t, ρr_t transmittance and reflectance of leaf tissue (Plant DB) k_l Coefficient of extinction-long wave (leaf distribution horizontal-kl = 1, leaf distribution 45 degree-kl = 0.829; leaf distribution vertical-kl = 0.436; spherical leaves-kl = 0.684) Approximately: $k_s=0.74k_l$ Further approximation: for horizontal leaves $k_s=1.10$; for vertical leaves $k_s=0.29$ short wave reflectance $\rho r_s=(1-\tau_l)\rho r_a$ ρr_a Canopy reflectance Plant DB ρr_g Ground reflectance Soil DB	0.77	-	k_l τ_t ρr_t ρr_a ρr_g			
γ psychometric constant	$\gamma=0.000665\,P$; P- atmospheric pressure (Pa)	67.4	Pa/K		P		
Cpa canopy air specific heat		1005	J/KgK		Cpa		

Time variant data	Defining Equations and Remarks	Initial Value	Unit	Required data			Couple Info
				Input	Parameters	Calculated Variables	
ρ_{ca} canopy air density	$\rho=\dfrac{p}{101.325}\dfrac{273.16}{T}1.293$	1.18	kg/m3			ρ_{ca}	
ϕ_s^t solar radiation	Data from weather file; values to be used are those of immediate past and previous-to-that	250,24	W/m²	ϕ_s			

	time steps	0 (of two time steps)					
$h_{r,su}^t T_{su}^t$	Data of previous two time steps Sub – based on current values of plant temperature and soil surface temperature $h_{r,s1} = 4\,(1 - \tau_l)\,\sigma \left(\dfrac{T_{S1} + T_p}{2}\right)^3$ τ_l longwave transmittance $\tau_l = e^{-(k_l\,LAI)}$	1610, 1615 (of two time steps)	W/m^2	LAI k$_l$	σ	T$_{s1}$ T$_p$	
$(r_e + r_i)^t$ air resistance + stomatal resistance	Air resistance as previously defined: $r_e = 7.4\,\hat{\rho}\left(\dfrac{d_c}{u}\right)^{1/2}$ Stomatal resistance:[9] [29]-Table 5 ri= $r_{min}\left(\dfrac{\dfrac{\emptyset_s}{2\,LAI} + C_1}{\dfrac{\emptyset_s}{2\,LAI} + C_2}\right)\left(1 + C_3\left[T_p - T_a\right]^2\right)\left(1 + C_4\left[CO_2 - 200\right]^2\right)\left(1 + C_5\left[e_p - e_a\right]^2\right)$ r_{min} minimum possible value depending on plant physiology Other plant dependent variables: LAI, C_1, C_2, C_3, C_4, C_5 Environmental variables $\emptyset_s$ (solar radiation), Tp (plant temperature), Ta (medium temperature), CO_2 (PPM concentration of CO_2), e$_p$(vapour pressure at plant temperature), e$_{ca}$ (vapour pressure at canopy air temperature)	re 40.48 40.21 ri 113.7 112.3	s/m	r$_{min}$ φ$_s$ LAI C$_1$ C$_2$ C$_3$ C$_4$ C$_5$ CO$_2$		T$_p$ T$_a$ e$_p$ e$_{ca}$	
e_p^t vapour pressure at plant temperature	$e_p = \dfrac{RH}{100}\,610.8\,exp\left[\dfrac{17.27\,t_p}{t_p + 237.3}\right]$ RH relative humidity (%) from weather data t$_p$ plant temperature °C	1050, 1120 (of two time steps)	Pa			t$_p$ RH	
e_a^t vapour pressure at canopy air temperature	$e_a = \dfrac{RH}{100}\,610.8\,exp\left[\dfrac{17.27\,t_a}{t_a + 237.3}\right]$ RH relative humidity (%) from weather data t$_a$ canopy air temperature °C	1155, 1230 (of two time steps)	Pa			t$_a$ RH	

Notes on unresolved matters canopy plant

1. Convection transfer with outside air not in the equation.

Possibility to replace Tsky with To to be checked later.

Problem: What is the area to be used in the upper part of plant?

2. Equation for external aerodynamic resistance re for plant using zero displacement and roughness height related to whole canopy; it should be at the leaf level.
3. Inconsistency noted between Flerchinger formula (307) and Campbel formula (7.4) Unit conversion between m^2s/mol to s/m is $7.4*44.6(mol/m^3$ molar density of air)=330.04 (not 307)

Resolved now

Molar density need to be calculated at current temperature and pressure as

$$\hat{\rho} = 44.6 \, \frac{p}{101.3} \, \frac{273.15}{T}$$

p pressure in kPa and T temperature in K

Alternately, formula in terms of properties (properties of air to be taken at the current temperature of air; e.g. table A1, Campbell)

$$gH = \frac{0.664 \, D_H Re^{1/2} Pr^{1/3}}{d} = 0.664 \, D_H \left(\frac{1}{\nu}\right)^{1/2} \left(\frac{\nu}{D_H}\right)^{1/3} \sqrt{\frac{u}{d}}$$

$$r_H = \frac{1}{0.664 \, D_H \left(\frac{1}{\nu}\right)^{1/2} \left(\frac{\nu}{D_H}\right)^{1/3}} \sqrt{\frac{d}{u}}$$

4. A representative height within canopy is to be determined to use a single value of canopy wind velocity

$$u(z_c) = u(h)exp\left[a\left(\frac{z_c}{h} - 1\right)\right]$$

5. leaf characteristic length is stated as(length + width)/2 in SiB
6. It is to be decided whether air density need to be taken as time invariant or as a function of temperature (as in Campbell book and in Bittelli paper) or even as a psychometric function depending on temperature and humidity or vapour pressure (CIBSE)
7. Appropriate emissivity to be included in long wave radiation exchanges (eq 14,15,17 Tabares-Velasco 2012)

2. Canopy air

Energy Balance

$$\rho_a Cpl \frac{dT_{ca}}{dt} = \phi_{conv,p-ca} - \phi_{conv,ca-s1} + \phi_{conv,\alpha-ca}$$

$$\phi_{conv,p-ca} = 2LAI \frac{\rho_{ca} Cp}{r_e}\left(T_p - T_{ca}\right)$$

$$\phi_{conv,ca-s1} = \frac{\rho_{ca} Cp}{r_{s1-ca} + r_s}\left(T_{ca} - T_{s1}\right)$$

$$\phi_{conv,\alpha-ca} = \frac{\rho_\alpha Cp}{r_{e\alpha}}\left(T_\alpha - T_{ca}\right)$$

Coefficient form

$$-\left[\alpha \frac{\rho_\alpha^{t+\Delta t} Cp_\alpha}{r_{e\alpha}^{t+\Delta t}}\right] T_\alpha^{t+\Delta t}$$

$$-\left[\alpha 2LAI \frac{\rho_a Cp}{r_e^{t+\Delta t}}\right] T_p^{t+\Delta t}$$

$$+\left[\frac{\rho_a Cpl}{\Delta t} + \alpha \frac{\rho_\alpha^{t+\Delta t} Cp}{r_{e\alpha}^{t+\Delta t}} + \alpha 2LAI \frac{\rho_a Cp}{r_e^{t+\Delta t}} + \alpha \frac{\rho_a Cp}{\left(r_{s1-a}^{t+\Delta t} + r_s^{t+\Delta t}\right)}\right] T_{ca}^{t+\Delta t}$$

$$-\left[\alpha \frac{\rho_a Cp}{\left(r_{s1-a}^{t+\Delta t} + r_s^{t+\Delta t}\right)}\right] T_{s1}^{t+\Delta t}$$

$$=$$

$$\left[(1-\alpha)\frac{\rho_\alpha^t Cp}{r_{e\alpha}^t}\right] T_\alpha^t$$

$$+\left[(1-\alpha)2LAI \frac{\rho_a Cp}{r_e^t}\right] T_p^t$$

$$+\left[\frac{\rho_a Cpl}{\Delta t} - (1-\alpha)\frac{\rho_\alpha^t Cp}{r_{e\alpha}^t} - (1-\alpha)2LAI \frac{\rho_a Cp}{r_e^t} - (1-\alpha)\frac{\rho_a Cp}{\left(r_{s1-a}^t + r_s^t\right)}\right] T_{ca}^t$$

$$+\left[(1-\alpha)\frac{\rho_a Cp}{\left(r_{s1-a}^t + r_s^t\right)}\right] T_{s1}^t$$

Energy Balance CV2 Canopy air

□ Thermal exchanges

$$\rho_a Cp\, l \frac{dT_{ca}}{dt} = \phi_{conv,p-ca} - \phi_{conv,ca-s1} + \phi_{conv,\alpha-\alpha}$$

CV1

1. $\Phi_{conv,p-ca}$ convection gain from plant
2. $\Phi_{conv,ca-s1}$ convection loss to ground
3. $\Phi_{conv,\alpha-ca}$ convection gain from outside air

CV3
CV4
CV5
CV6
CV7

(a21)	$-\alpha \frac{\rho_\infty Cp}{r_{e\alpha}^{t+\Delta t}}$ (all variables as defined previously)							
Time invariant data	**Defining Equations and Remarks**	**Initial Value**	**Unit**	**Required data**			**Couple Info**	
				Input	**Param eters**	**Calcul ated Variab les**		
Time variant data	**Defining Equations and Remarks**	**Initial Value**	**Unit**	**Required data**			**Couple Info**	
				Input	**Param eters**	**Calcul ated Variab les**		

(a22)	$-\alpha \frac{2\,LAI\,\rho_a Cp}{r_e^{t+\Delta t}}$ (all variables as defined previously)							
Time invariant data	**Defining Equations and Remarks**	**Initial Value**	**Unit**	**Required data**			**Couple Info**	
				Input	**Param eters**	**Calcul ated Variab les**		
Time variant data	**Defining Equations and Remarks**	**Initial Value**	**Unit**	**Required data**			**Couple Info**	
				Input	**Param eters**	**Calcul ated Variab les**		

(a23)	$\frac{\rho_a Cp}{\Delta t}\frac{l}{} + \alpha \frac{\rho_\infty Cp}{r_a^{t+\Delta t}} + \alpha \frac{2\,LAI\,\rho_a Cp}{r_a^{t+\Delta t}} + \alpha \frac{\rho_a Cp}{r_{s1-a}^{t+\Delta t}+r_s^{t+\Delta t}}$							
Time invariant data	**Defining Equations and Remarks**	**Initial Value**	**Unit**	**Required data**			**Couple Info**	
				Input	**Param eters**	**Calcul ated Variab**		

178

					les	
l plant height	Input by user – to be in plant database	0.4	m	L		
Δt simulation time step	Input by user	1800	s	Δt		
Cpa canopy air specific heat		1005	J/kgK		Cpa	

Time variant data	Defining Equations and Remarks	Initial Value	Unit	Required data			Couple Info
				Input	Parameters	Calculated Variables	
ρ_{ca} canopy air density	$$\rho = \frac{p}{101.325}\frac{273.16}{T}1.293$$	1.18	kg/m3			ρca	
r_{s1-a} soil to canopy air resistance	Choudhury and Monteith [66] $$r_{s1-a} = \frac{ln\left(\frac{z-d}{zo}\right)h\,exp(\alpha)}{\alpha\,k^2 u_z(h-d)}\left[exp\left(\frac{-\alpha\,zo1}{h}\right) - exp\left(\frac{-\alpha(d+zo)}{h}\right)\right]$$ u_z = wind velocity[m/s] at measurement height z [m] h= lant height [m] d= zero plane displacement =0.64 h [m] zo=roughness length at canopy top = 0.13 h[m] zo1= roughness length at soil surface = 0.01 [m] k= von Karmen constant = 0.41 α=diffusion coefficient =2.5		s/m				
r_s soil surface resistance	van de Griend [67] $$r_s = r_{s1}e^{\alpha(\theta_{min}-\theta)}$$ r_{s1} = minimum surface resistance = 10 s/m α=diffusion coefficient 35.63 θ=soil moisture content [m^3/m^3] θ_{min}=minimum soil moisture content [m^3/m^3] =0.15		s/m				
h_{s1} convective heat transfer coefficient (alternative for resistance definition above) $(h = \frac{\rho_a Cp}{r_{s1-a}+r_s})$	Ref FASST model [112] $$h = \left(e_0 + \rho_a C_{pa}\,C_h^g u\right)$$ e_0 = windless exchange coefficient for sensible heat (2.0 W/m^2) $\rho_a = \frac{p}{R\,T_a}$; p= 101.3 x 10^3 Pa (default); R = 286.9 J/kgK u = wind velocity at canopy; given by: $u = 0.83\,\sigma_f W'\sqrt{C_{hn}^f} + (1-\sigma_f)W'$ σf= fractional vegetation coverage	2.83	W/m2 K	u(z) z σf L	p R Cpa	Ta Tsu	

W' = u(z) or 2 m/s if u(z) is less than 2

C_{hn}^{f} bulk transfer coefficient at the top of the foliage; given by:

$$C_{hn}^{f} = \left[\frac{k}{\ln\left(\frac{z - Z_d}{z_0^{f}}\right)} \right]^2$$

k= von Karmen constant = 0.41

z = height of measurement of air temperature (and wind speed)

z_0^{f} = foliage roughness height given by : $0.131 \, L^{0.997}$, L height of foliage

Z_d = foliage zero displacement height given by : $0.701 \, L^{0.975}$

The bulk transfer coefficient for sensible heat is given by:

$$C_{h}^{g} = \Gamma_h \left[(1 - \sigma_f) C_{hn}^{g} + \sigma_f \, C_{hn}^{f} \right]$$

Γ_h stability correction factor for non-neutral conditions, which depend on bulk Richardson number:

$$R_{ib} = \frac{2 \, g \, z \, (T_a - T_{su})}{(T_a + T_{su}) \, u^2}$$

$\Gamma_h = 1$ if R_{ib}=0; $\Gamma_h = \frac{1}{(1 - 16 \, R_{ib})^{0.5}}$ if R_{ib}< 0; $\Gamma_h = \frac{1}{(1 - 5 \, R_{ib})}$ if 0<R_{ib}< 0.2

$$C_{hn}^{g} = \frac{\left[\frac{k}{\ln\left(\frac{z}{z_0^{g}}\right)} \right]^2}{r_{ch}}$$

r_{ch}= Schmidt number = 0.63 (assumed for all soil types)

z_0^{g} = ground roughness height is assumed as 0.001 m for all soil types

Alternative 1: In terms of r_d ($h_{s1} = \frac{\rho \, C_p}{r_d}$) ; r_d is the ground to canopy air resistance Ref SiB2 [19]

$$r_d = \frac{C_2}{u_2} = \int_{zs}^{ha} \frac{1}{K_m} dz$$

It is to be calculated in an offline program together with other two resistances; r_b plant to canopy air and r_a canopy air to outside air

Input: Plant properties (l_w, l_L, X_L, LAI) heights (z_s, z_1, z_c, z_2, z_t, z_m) and empirical constant G_1

	and G_4 Output: Only once calculation to populate a table for N types of plants x 17 LAI values (0 to 8 in steps of 0.5) and x 5 aerodynamic parameters (C1, C2, C3, z_0 and d) The main program to access this matrix to obtain current value of aerodynamic parameters and to calculate the respective resistances $r_b = \frac{C_1}{u_2^{1/2}}$ and $r_a = \frac{C_3}{u_m}$ (Ref Sellers et al 1995)							
	Alternative formulae for hsu and hα from [113] $$\frac{Gr}{Re^2} = \frac{g\beta l |T_p - T_a|}{u^2}$$ g=9.81 m/s^2 β=coefficient of thermal expansion (3.42 x 10^{-3} K^{-1} for air) l=characteristic length ($\sqrt{leaf\ area}$ u = wind velocity m/s Free convection if Gr/Re^2 >16 Forced convection if Gr/Re^2 <0.1							
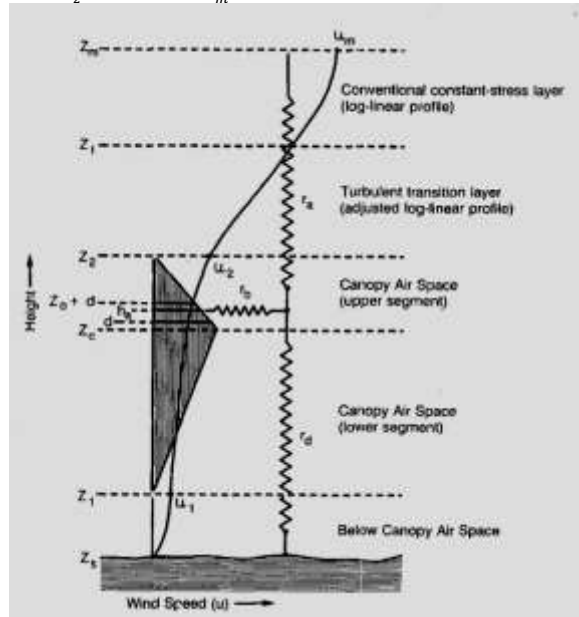
	Other cases leads to mixed convection For mixed convection: $$h = \frac{1174\ l^{0.5}}{(l\ |T_l - T_a| + 207\ u^2)^{0.25}}$$ For forced convection $$h = \frac{\left[\frac{1}{\alpha u}\right]^{1/2} Pr^{1/6}}{1.328\ LAI}$$ α thermal diffusion coefficient (m^2/s) Values hs1=296 h$_\alpha$ =2.94								
	Alternative detailed equation set in [114] eq 7.19,7.12, etc								

(a24)	$-\alpha\ \frac{\rho_a Cp}{r_{s1-a}^{t+\Delta t} + r_s^{t+\Delta t}}$ (as defined previously)								
Time invariant data	**Defining Equations and Remarks**	**Initial Value**	**Unit**	**Required data**			**Couple Info**
				Input	**Param eters**	**Calcul ated Variab les**	
Time variant data	**Defining Equations and Remarks**	**Initial Value**	**Unit**	**Required data**			**Couple Info**
				Input	**Param eters**	**Calcul ated Variab les**	

b21 $(1-\alpha)\dfrac{\rho_a Cp}{r_{e\alpha}^t}$

b22 $(1-\alpha)\dfrac{2\,LAI\,\rho_a Cp}{r_e^t}$

b23 $\dfrac{\rho_a Cp_a L}{\Delta t}-(1-\alpha)\dfrac{\rho_\alpha Cp}{r_{e\alpha}^t}-(1-\alpha)\dfrac{2\,LAI\,\rho_a Cp_a}{r_e^t}-(1-\alpha)\dfrac{\rho_a Cp}{r_{s1-a}^t+r_s^t}$

b24 $(1-\alpha)\dfrac{\rho_a Cp}{r_{s1-a}^t+r_s^t}$

(c21)	(No C coefficient for this CV) (Note 2)							
Time invariant data	**Defining Equations and Remarks**	**Initial Value**	**Unit**	**Required data**				**Couple Info**
				Input	**Param eters**	**Calcul ated Variab les**		
Time variant data	**Defining Equations and Remarks**	**Initial Value**	**Unit**	**Required data**				**Couple Info**
				Input	**Param eters**	**Calcul ated Variab les**		

Notes on unresolved matters canopy air

1. Sign of stability parameter determined in Bittelli's program as below.
- r_H determined with ψ_H and ψ_m taken as zero
- s determined using r_H
- according to sign of s, ψ_H and ψ_m are determined
- This loop is repeated 3 times to finalize r_H

2. No C coefficient for this CV, but it does not affect the solution

$$
\begin{bmatrix}
a11 & a12 & a13 & 0 & 0 & 0 & 0 \\
0 & a22 & a23 & a24 & 0 & 0 & 0 \\
0 & 0 & a33 & a34 & a35 & 0 & 0 \\
0 & 0 & 0 & a44 & a45 & a46 & 0 \\
0 & 0 & 0 & 0 & a55 & a56 & a57
\end{bmatrix}
X
\begin{bmatrix}
T_{sky}^{t+\Delta t} \\
T_y^{t+\Delta t} \\
T_a^{t+\Delta t} \\
T_{zn}^{t+\Delta t} \\
T_{zm}^{t+\Delta t} \\
T_{sl}^{t+\Delta t} \\
T_z^{t+\Delta t}
\end{bmatrix}
$$

$$
=
\begin{bmatrix}
b11 & b12 & b13 & 0 & 0 & 0 & 0 \\
0 & b22 & b23 & b24 & 0 & 0 & 0 \\
0 & 0 & b33 & b34 & b35 & 0 & 0 \\
0 & 0 & 0 & b44 & b45 & b46 & 0 \\
0 & 0 & 0 & 0 & b55 & b56 & b57
\end{bmatrix}
X
\begin{bmatrix}
T_{sky}^t \\
T_p^t \\
T_a^t \\
T_{zn}^t \\
T_{zm}^t \\
T_{sl}^t \\
T_z^t
\end{bmatrix}
+
\begin{bmatrix}
c11 \\
c21 \\
c31 \\
c41 \\
c51 \\
c61 \\
c71
\end{bmatrix}
=
\begin{bmatrix}
z11 \\
z21 \\
z31 \\
z41 \\
z51 \\
z61 \\
z71
\end{bmatrix}
$$

3. Soil Upper layer CV3 (S1)

Energy Balance

$$C_{s1} S1 \frac{dT_{s1}}{dt} = \phi_{s,s1} + \phi_{lw,sky-s1} + \phi_{lw,p-s1} + \phi_{conv,a-s1} - \phi_{evap,s1-a} - \phi_{cond,s1-s2} + \phi_{vap,s1-s2}$$

C_{s1} = volumetric specific heat of soil composition

$$\phi_{s,s1} = \left(\tau_s - \tau_s \rho r_g \right) \phi_s$$

$$\phi_{lw,sky} = h_{r,sky-s1} \left(T_{sky} - T_{s1} \right)$$

$$\phi_{lw,sky-s1} = \tau_l h_{r,sky-s1} \left(T_{sky} - T_{s1} \right)$$

$$\phi_{lw,p-s1} = \left(1 - \tau_l \right) h_{r,p-s1} \left(T_p - T_{s1} \right)$$

$$\phi_{conv,a-s1} = \frac{\rho_a C p_a}{\left(r_{av} + r_s \right)} \left(T_a - T_{s1} \right)$$

$$\phi_{evap,s1-a} = \frac{\rho_a C p_a}{\gamma \left(r_{av} + r_s \right)} \left(e_{s1} - e_a \right)$$

$$\phi_{cond} = \lambda \frac{dT}{dz} \ ; \qquad \phi_{cond,s1-s2} = \lambda_{s1s2} \frac{\left(T_{s1} - T_{s2} \right)}{S1S2}$$

$$\phi_{vap} = LK_{vT\_m} \frac{dT}{dz} + LK_{v\psi\_m} \frac{d\psi}{dz} \ ;$$

$$\phi_{vap,s1-s2} = LK_{vT\_m-s1s2} \frac{T_{s1} - T_{s2}}{S1S2} + LK_{v\psi\_m-s1s2} \frac{\psi_{s1} - \psi_{s2}}{S1S2}$$

Properties with subscript s1s2 are averages of properties at soil s1 layer and soil s2 layer

Length S1S2 = (S1+S2)/2

Coefficient form

$$
\begin{aligned}
&- \left[\alpha\,(1-\eta)\,h_{r,p-s1}^{t+\Delta t}\right] T_p^{t+\Delta t} \\
&- \left[\alpha\,\frac{\rho_a Cp}{r_{s1-a}^{t+\Delta t} + r_s^{t+\Delta t}}\right] T_{ca}^{t+\Delta t} \\
&+ \left[\frac{C_{s1}S1}{\Delta t} + \alpha\eta h_{r,sky-s1}^{t+\Delta t} + \alpha(1-\eta) h_{r,p-s1}^{t+\Delta t}\right] + \\
&\left[+\alpha\,\frac{\rho_a C_{pa}}{(r_{s1-a}^{t+\Delta t} + r_s^{t+\Delta t})} + \alpha\frac{\lambda_{s1s2}^{t+\Delta t}}{S1S2} - \alpha\frac{LK_{vT\_m-s1s2}^{t+\Delta t}}{S1S2}\right] T_{s1}^{t+\Delta t} \\
&+ \left[-\alpha\frac{\lambda_{s1s2}^{t+\Delta t}}{S1S2} + \alpha\frac{LK_{vT\_m-s1s2}^{t+\Delta t}}{S1S2}\right] T_{s2}^{t+\Delta t} \\[2mm]
&= \\
&\left[(1-\alpha)(1-\eta)\,h_{r,p-s1}^{t}\right] T_p^{t} \\
&+ \left[(1-\alpha)\frac{\rho_a C_{pa}}{r_{s1-a}^{t} + r_s^{t}}\right] T_{ca}^{t} \\
&+ \left[\frac{C_{s1}S1}{\Delta t} - (1-\alpha)\eta h_{r,sky-s1}^{t} - (1-\alpha)(1-\eta) h_{r,p-s1}^{t}\right] + \\
&\left[-(1-\alpha)\frac{\rho_a Cp}{(r_{av}^{t} + r_s^{t})} - (1-\alpha)\frac{\lambda_{s1s2}^{t}}{S1S2} + (1-\alpha)\frac{LK_{vT\_m-s1s2}^{t}}{S1S2}\right] T_{s1}^{t} \\
&+ \left[(1-\alpha)\frac{\lambda_{s1s2}^{t}}{S1S2} - (1-\alpha)\frac{LK_{vT\_m-s1s2}^{t}}{S1S2}\right] T_{s2}^{t} \\[2mm]
&+ \left[(1-\alpha)(\tau_s - \tau_s\rho r_g)\phi_s^{t} + \alpha(\tau_s - \tau_s\rho r_g)\phi_s^{t+\Delta t}\right] + \left[(1-\alpha)\eta h_{r,sky-s1}^{t} T_{sky}^{t} + \alpha\eta h_{r,sky-s1}^{t+\Delta t} T_{sky}^{t+\Delta t}\right] \\[2mm]
&- \left[(1-\alpha)\frac{\rho_a C_{pa}}{\gamma(r_{s1-a}^{t} + r_s^{t})}\left(e_{s1}^{t} - e_{ca}^{t}\right)\right] - \left[\alpha\frac{\rho_a C_{pa}}{\gamma(r_{av}^{t+\Delta t} + r_s^{t+\Delta t})}\left(e_{s1}^{t+\Delta t} - e_{ca}^{t+\Delta t}\right)\right] \\[2mm]
&+ \left[(1-\alpha)\frac{LK_{v\psi\_m-s1s2}^{t}}{S1S2}\left(\psi_{s1}^{t} - \psi_{s2}^{t}\right) + \alpha\frac{LK_{v\psi\_m-s1s2}^{t+\Delta t}}{S1S2}\left(\psi_{s1}^{t+\Delta t} - \psi_{s2}^{t+\Delta t}\right)\right]
\end{aligned}
$$

Energy Balance CV3 Soil upper layer

□ Thermal exchanges

$$C_{s1}S1\frac{dT_{s1}}{dt} = \phi_{s,s1} + \phi_{lw,sky-s1} + \phi_{lw,p-s1} + \phi_{conv,ca-s1} - \phi_{evap,s1-ca} - \phi_{cond,s1-s2} + \phi_{vap,s2-s1}$$

CV1

CV3
CV4
CV5
CV6
CV7

1. $\Phi_{s,s1}$ solar radiation at uncovered surface
2. Φ_{lw} long-wave exchange with sky and plant
3. $\Phi_{conv,ca-s1}$ convection gain from canopy air
4. $\Phi_{evap,s1-ca}$ evaporation loss to canopy air
5. $\Phi_{cond,s1-s2}$ conduction loss downward
6. $\Phi_{vap,s2-s1}$ latent heat gain from vapour exchange

186

(a32)	$-\alpha(1-\tau_l)h_{r,p-s1}^{t+\Delta t}$							
Time invariant data	**Defining Equations and Remarks**	**Initial Value**	**Unit**	**Required data**			**Couple Info**	
				Input	**Param eters**	**Calcul ated Variab les**		
τ_l longwave transmittance	$\tau_l = e^{-(k_l\,LAI)}$ k_l Coefficient of extinction-long wave (leaf distribution horizontal-kl = 1, leaf distribution 45 degree-kl = 0.829; leaf distribution vertical-kl = 0.436; spherical leaves-kl = 0.684)	0.08	-	LAI k_l			
Time variant data	**Defining Equations and Remarks**	**Initial Value**	**Unit**	**Required data**			**Couple Info**	
				Input	**Param eters**	**Calcul ated Variab les**		
$h_{r,p-s1}^{t+\Delta t}$ radiation transfer coefficient	$h_{r,p-s1}^{t+\Delta t} = \dfrac{1}{\dfrac{1}{\epsilon_g}+\dfrac{1}{\epsilon_p}-1}\ 4\ \sigma\left(\dfrac{\mathrm{T_p}+\mathrm{T_{s1}}}{2}\right)^3$ ϵ_p emissivity of canopy surface assumed 0.96 (Campbell 1998 table 11.3)	5.3	W/m2 K			Tp Ts1	

(a33)	$-\alpha\,\dfrac{\rho_a Cp_a}{r_{av}^{t+\Delta t}+r_s^{t+\Delta t}}$							
Time invariant data	**Defining Equations and Remarks**	**Initial Value**	**Unit**	**Required data**			**Couple Info**	
				Input	**Param eters**	**Calcul ated Variab les**		
Cp_a canopy air specific heat		1005	J/kgK		Cp_a		
Time variant data	**Defining Equations and Remarks**	**Initial Value**	**Unit**	**Required data**			**Couple Info**	
				Input	**Param eters**	**Calcul ated Variab les**		

ρ_{ca} canopy air density	$\rho = \dfrac{p}{101.325}\dfrac{273.16}{T}1.293$	1.18	kg/m3			ρ_{ca}	
r_{av} aerodynamic resistance on soil surface	FASST model as in (a23)						
	Alternative equation Ref [8] $r_v = \dfrac{1}{u^* k}\left[ln\left(\dfrac{z_{ref} - d - z_H}{z_H}\right) + \phi_H \right]$ k – von Karmen constant (0.41) u* is the friction velocity given by $u^* = uk\left[ln\left(\dfrac{z_{ref} - d - z_M}{z_M}\right) + \phi_M \right]^{-1}$ u is the wind velocity (m/s) at measurement height z_{ref} (m) z_H - surface roughness factor for heat flux (0.1 m) z_M - surface roughness factor for momentum flux (0.1 m) d – zero pane displacement (m) ϕ_H is the atmospheric stability correction factor for the heat flux ϕ_M is the atmospheric stability correction factor for the momentum flux $\phi_H = \phi_M = -\xi f$ $\xi = \dfrac{z - z_M - d}{\Lambda}$ f is a constant (4.7) Λ is the Monin–Obukhov's stability parameter given by $\Lambda = \dfrac{u^{*3} Ch\, T_a}{kgH}$ Ch is volumetric heat of air (1200J/m³K) T_a is air temperature g is the gravitational constant k is the von Karman constant H sensible heat flux at surface (estimate) or simplified equation without considering atmospheric stability: $r_v = \dfrac{ln\left[\dfrac{z_M - d}{z_{0M}}\right] ln\left[\dfrac{z_H - d}{z_{0H}}\right]}{k^2\, U_z}$ z_M - measurement height for wind speed Uz, (m/s) (typically 2m)	40	s/m				

188

	z_H - measurement height for air temperature (also typically 2m) k - von Karmen constant 0.41, z_{0M} - roughness length parameters for momentum (=0.123 h_c crop height) z_{0H} - roughness length parameters for sensible heat transport (=0.1 z_{0M}) d - zero plane displacement height.(=2/3 h_c,)							
r_s – soil surface resistance	Ref: [56] $r_s = 100 \left(0.413\dfrac{\theta_s}{\theta}\right)^{1.5}$ θ volumetric soil water content m3/m3 θ_s volumetric soil water content at saturation m3/m3 (soil property) e.g.0.56 (Bittelli)	44	s/m	θ_s		θ	soil moistu re
	Alternative: 3 formulae listed in [8] p5							

(a34)	$\dfrac{C_{s1}S1}{\Delta t} + \alpha\,\tau_l\,h_{r,sky-s1}^{t+\Delta t} + \alpha\,(1-\tau_l)h_{r,p-s1}^{t+\Delta t} + \alpha\,\dfrac{\rho_a Cp_a}{r_{av}^{t+\Delta t} + r_s^{t+\Delta t}} + \alpha\,\dfrac{\lambda_{s1s2}{}^{t+\Delta t}}{S1\_S2} + \alpha\,\dfrac{L\,K_{vT-m-s1s2}^{t+\Delta t}}{S1\_S2}$						
Time invariant data	**Defining Equations and Remarks**	**Initial Value**	**Unit**	**Required data**			**Couple Info**
				Input	**Param eters**	**Calcul ated Variab les**	
τ_l longwave transmittance	$\tau_l = e^{-(k_l\,LAI)}$ k_l Coefficient of extinction-long wave (leaf distribution horizontal-kl = 1, leaf distribution 45 degree-kl = 0.829; leaf distribution vertical-kl = 0.436; spherical leaves-kl = 0.684)	0.08	-	LAI k_l			
S1 soil upper layer thickness		0.1	m	SU			
S1_S2 distance between soil upper layer and lower layer centres	$S1\_S2 = \left(\dfrac{S1 + S2}{2}\right)$	0.1	m	SU SM			
Δt simulation time step		1800	s	Δt			
Cpa canopy air specific heat		1005	J/kg K		Cpa		
C_{s1} volumetric specific heat	$C_s = \rho_m C_m x_m + \rho_w C_w x_w + \rho_a C_a x_a + \rho_o C_o x_o$ subscripts m, w, a and o indicate mineral, water, air and organic fractions of soil; x is the volumetric fraction (Campbell table 8.2)	1.9 e 6	J/m3 K	x_m x_a x_o	ρ_m, C_m ρ_w, C_w ρ_{ca}, C_a ρ_o, C_o	x_w =θ_{su}	
Time variant data	**Defining Equations and Remarks**	**Initial**	**Unit**	**Required data**			**Couple**

		Value		Input	Parameters	Calculated Variables	Info
$h_{r,sky-s1}^{t+\Delta t}$ radiation transfer coefficient (note 1)	$$h_{r,sky-s1}^{t+\Delta t} = \epsilon_g \, 4 \, \sigma \left(\frac{T_{sky} + T_{s1}}{2}\right)^3$$ ϵ_g emissivity of soil surface assumed 0.95 (Campbell 1998 table 11.3)	5.9	W/m2 K			Tsky Tsu	
$h_{r,p-s1}^{t+\Delta t}$ radiation transfer coefficient	$$h_{r,p-s1}^{t+\Delta t} = \frac{1}{\frac{1}{\epsilon_g} + \frac{1}{\epsilon_p} - 1} \, 4 \, \sigma \left(\frac{T_p + T_{s1}}{2}\right)^3$$ ϵ_p emissivity of canopy surface assumed 0.96 (Campbell 1998 table 11.3)	5.3	W/m2 K			Tp Tsu	
ρ_{ca} canopy air density	$$\rho = \frac{p}{101.325} \frac{273.16}{T} 1.293$$	1.18	kg/m3				
r_{av} aerodynamic resistance on soil surface r_s soil surface heat/mass transfer resistance	As defined above	420 (Note 2) 44	s/m s/m				
λs1s2 – average thermal conductivity of soil of upper and middle layers	Ref: [56] [115] $$\lambda_{s1} = A + 2.8 \, V_s \left(\frac{\theta}{\rho_w}\right)^2 + (A - B) \exp\left(-\left(\frac{C\theta}{\rho_w}\right)^4\right)$$ θ volumetric soil water content in the layer (s1,s2 …s5) ρ_w water density = 1000 kg/m^3 $$A = \frac{0.57 + 1.73 \, V_q + 0.93 \, V_m}{1 - 0.74 \, V_q - 0.49 \, V_m} - 2.8 \, V_s(1 - V_s)$$ $$B = 0.03 + 0.7 \, V_s^2$$ $$C = 1 + \frac{2.6}{(m_c)^{1/2}}$$ V – volumetric fractions subscripts w – water, q- quartz, m-minerals, s – solids (q+m) $V_s = V_q + V_m$ m_c – mass fraction clay (Campbell) Some sample soil data from Bittelli [8] : Name of the soil Imperial Valley Wat Cont [m^3/m^3] Textural Class silty clay loam 0.45 Mass Silt [g/g] 0.1 0.4 Mass Clay [g/g] 0.48 0.35 Bulk Density [g/cm^3] 1.4 0.3 Particle density [g/cm^3] 2.65 0.25	2.62	W/mK	V_q V_m m_c	ρ_w	θ_{su} θ_{sm}	moisture content

	$\lambda_{s1s2} = \left(\dfrac{\lambda_{s1} + \lambda_{s2}}{2}\right)$					
	In terms of composition $\lambda_{s1} = \dfrac{F_w V_w \lambda_w + F_q V_q \lambda_q + F_m V_m \lambda_m + F_o V_o \lambda_o + F_a V_a \lambda_a}{F_w V_w + F_q V_q + F_m V_m + F_o V_o + F_a V_a}$ F – shape factors V – volumetric fractions λ – thermal conductivities subscripts w – water, q- quartz, m-minerals, o – organic matter, a- air, g- gas					
$K_{vT-m-s1s2}^{t+\Delta t}$ thermal vapour conductivity[62]	$K_{v\psi} = D_v \dfrac{\partial \rho_{vs}}{\partial T} h\, \eta_e$ Dv- vapour diffusivity in soil [m^{2}s^{-1}] $D_v = \tau_g a_v D_a$ Da- diffusivity of water vapour in air It is given by: $Da = Do\left(\dfrac{T}{273.15}\right)^2$ Do- reference value of diffusivity = 2.12e-5 m^{2}s-^{1} T – temperature of medium [K] av – air filled porosity [-] porosity can be calculated as: av=θs-θ θs-saturated moisture content [m^{3}m^{-3}] and θ current moisture content [m^{3}m^{-3}] τ$_g$= turtosity factor[-] is given by: $\tau_g = \dfrac{(a_v)^{7/3}}{(\theta_s)^2}$ ρ$_{vs}$- saturated vapour density [kgm^{-3}] at a given temperature T K is given by: $\rho_{vs} = 1e - 3\, \dfrac{e^{\left(31.3716 - \frac{6014.79}{T} - 7.92495e - 3T\right)}}{T}$ M- molar mass of water 0.018015 kg mol^{-1} g- acceleration due to gravity 9.81 ms-^{2} R- universal gas constant 8.314 J moil^{-1} K^{-1} T – soil temperature in K h- relative humidity [-]					

	expressing it in terms of soil matric potential ψ[m] : $h = e^{\left(\frac{\psi M g}{RT}\right)}$ η_e enhancement factor [60] $\eta_e = 9.5 + 3\dfrac{\theta}{\theta_s} - 8.5\, e^{\left(-\left[\left(1+\frac{2.6}{\sqrt{fc}}\right)\frac{\theta}{\theta_s}\right]^4\right)}$ where θ - moisture content [m³/m³], θ$_s$ - saturated moisture content [m³/m³] and fc is soil's clay fraction					
Alternative definition for K$_{vT\_m}$ as: K$_{vT\_m}$=hsDv as per reference [56] ; terms in detail in the next four rows						
h$_{s1s2}$ relative humidity of the gas filled in the soil pore (average value of that of soil upper layer and soil middle layer)	$h = \exp\left(\dfrac{M_w \psi}{RT}\right)$ Mw molecular weight of water 0.018 kg/mol R universal gas constant 8.314 J/mol K ψ – soil water potential at the layer J/kg T soil temperature at the layer K $h_{s1s2} = \left(\dfrac{h_{s1} + h_{s2}}{2}\right)$	0.99992	-			ψ$_{su}$ T$_{su}$ ψ$_{sm}$ T$_{sm}$	
s$_{s1s2}$ slope of saturated vapour pressure with temperature (average value of that of soil upper layer and soil middle layer)	$s = \dfrac{5307\, ev}{T^2}$ ev = saturated vapour pressure $ev = \left[\dfrac{exp\left(26.6904 - \frac{6109.74}{T} - 0.00916189\, T\right)}{10}\right]$ kPa $s_{s1s2} = \left(\dfrac{s_{s1} + s_{s2}}{2}\right)$	0.21	kPa/K			T$_{su}$ T$_{sm}$	
L Latent heat of water	$L = 2.543\ 10^6$ J/kg	2.54 e6	J/kg		L		
$Dv_{s1s2}^{t+\Delta t}$ Apparent vapour diffusivity (average value of that of soil upper layer and soil middle layer)	$D_v = D_a \dfrac{0.622\, \rho_a}{P}\left[\dfrac{V_a - u}{1 - u}\right]^v$ P - total gas pressure (kPa), $D_a = (2.22 + 0.158\, T_c) * 10^{-5}$ (m²/s) vapour diffusivity in the air at temperature Tc u=0.05 v=1.5 $Dv_{s1s2} = \left(\dfrac{Dv_{s1} + Dv_{s2}}{2}\right)$	1.48 e-9	kg/m/s /kPa		P	T$_{su}$ T$_{sm}$	

(a35)	$-\alpha\,\dfrac{\lambda_{s1s2}}{S1\_S2} - \alpha\,\dfrac{L\,K^{t+\Delta t}_{vT-m-s1s2}}{S1}$ (all variables as defined previously)						

Time invariant data	Defining Equations and Remarks	Initial Value	Unit	Required data			Couple Info
				Input	Parameters	Calculated Variables	

Time variant data	Defining Equations and Remarks	Initial Value	Unit	Required data			Couple Info
				Input	Parameters	Calculated Variables	

b32 $(1-\alpha)\,(1-\tau_l)h^t_{r,p-s1}$

b33 $(1-\alpha)\dfrac{\rho_a Cp_a}{r^t_{av}+r^t_s}$

b34 $\dfrac{C_{s1}S1}{\Delta t} - (1-\alpha)\,\tau_l\,h^t_{r,sky-s1} - (1-\alpha)\,(1-\tau_l)h^t_{r,p-s1} - (1-\alpha)\dfrac{\rho_a Cp_a}{r^t_{av}+r^t_s} - (1-\alpha)\dfrac{\lambda_{s1s2}{}^t}{S1\_S2} + (1-\alpha)\dfrac{L\,K^t_{vT-m-s1s2}}{S1\_S2}$

b35 $(1-\alpha)\dfrac{\lambda_{s1s2}{}^t}{S1\_S2} - (1-\alpha)\dfrac{L\,K^t_{vT-m-s1s2}}{S1\_S2}$

(c31)	$\left[(1-\alpha)(\tau_s - \tau_s\,\rho r_g)\phi^t_s + \alpha(\tau_s - \tau_s\,\rho r_g)\phi^{t+\Delta t}_s\right] + \left[(1-\alpha)\,\tau_l\,h^t_{r,sky-su}T^t_{sky} + \alpha\,\tau_l\,h^{t+\Delta t}_{r,sky-su}T^{t+\Delta t}_{sky}\right] - \left[(1-\alpha)\dfrac{\rho_a Cp_a}{\gamma\,(r^t_{av}+r^t_s)}(e^t_{s1} - e^t_a)\right]$ $-\left[\alpha\dfrac{\rho_a Cp_a}{\gamma\,(r^{t+\Delta t}_{av}+r^{t+\Delta t}_s)}(e^{t+\Delta t}_{su} - e^{t+\Delta t}_a)\right] + \left[(1-\alpha)\dfrac{L\,K^t_{v\psi-m-s1s2}}{S1\_S2}(\psi^t_{s1} - \psi^t_{s2})\right] + \left[\alpha\dfrac{L\,K^{t+\Delta t}_{v\psi-m-s1s2}}{S1\_S2}(\psi^{t+\Delta t}_{s1} - \psi^{t+\Delta t}_{s2})\right]$

193

| Time invariant data | Defining Equations and Remarks | Initial Value | Unit | Required data | | | Couple Info |
				Input	Parameters	Calculated Variables	
τ_s Short wave transmittance:	As defined in (c11)						
τ_l Long wave transmittance	As defined in (a12)						
ρr_g ground reflectance	As defined in (c11)						
Cp_a specific heat of air		1005	J/Kg K		Cpa		
γ psychometric constant	$\gamma = 0.000665\, P$; P- atmospheric pressure (Pa)	67.4	Pa/K		P		
L Latent heat of water	$L = 2.543\ 10^6$ J/kg		J/kg		L		
SU soil upper layer thickness		0.1	m	SU			

| Time variant data | Defining Equations and Remarks | Initial Value | Unit | Required data | | | Couple Info |
				Input	Parameters	Calculated Variables	
ϕ_s^t solar radiation	Data from weather file; values to be used are those of immediate past and previous-to-that time steps	250,240 (of two time steps)	W/m^2	ϕ_s			
$h_{r,sky-su}$ radiation transfer coefficient	As defined in (a 34)						
T_{sky}	Note 3				T_{sky}		
ρ_α air density (Note 6)	$\rho = \dfrac{p}{101.325}\dfrac{273.16}{T}\,1.293$	1.16	kg/m^3			ρ_α	
r_{av} aerodynamic resistance on soil surface r_s soil surface heat/mass transfer resistance	As defined above						
e_{su}, e_{ca} vapour pressure at SU and canopy air	working variables at moisture transfer part of the model						e_{su}, e_{ca}
ev – saturation vapour pressure	ev = saturated vapour pressure $ev = \left[\dfrac{exp\left(26.6904-\frac{6109.74}{T}-0.00916189\,T\right)}{10}\right]$ kPa	3.17	kPa			T_{su}	
$K_{v\psi-m-s1s2}^{t}$ - isothermal vapour conductivity[62]	$K_{v\psi\_m} = D_v\,\rho_{vs}\dfrac{Mg}{RT}h$ where all the definitions are as described above for the coefficient (a34)						

Alternative form of vapour pressure dependent vapour flux is by the relation[8] $$Lev_{s1s2}Dv_{s1s2}\frac{h_{s1}-h_{s2}}{S1S2}$$ ev -saturated vapour pressure								
D_v^t Apparent vapour diffusivity	As defined in (a34)						
h_{s2}, h_{s1} relative humidity at S1 and canopy air	$h=\frac{e}{e_v}$ ratio of vapour pressure to saturated vapour pressure As defined in (a34)						

Notes on soil upper layer

1. Emissivity to be included in radiation transfer coefficient, but transmittance functions to be shown separately for clarity; also to be in consistent with CV1 coefficient definitions.
2. rav from FASST model is 420 s/m much higher than boundary layer. It do make sense, but need to check against others (3 models: Deardorff, Sellers and Pitman models)
3. The effective sky temperature is about 10-20 degrees below the ambient temperature at ground level at clear sky conditions and close to and just below (1-2 deg) the ambient temperature during cloudy conditions (ref: http://sel.me.wisc.edu/trnsys/mailinglist/archive2003/msg00095.html) & Infrared Handbook by W. L. Wolfe and G.J. Zissis

4. Soil Middle layers CV4-CV6 (S2-S4)

Energy Balance

$$C_{s2}S2\frac{dT_{s2}}{dt} = \phi_{cond,s1-s2} - \phi_{cond,s2-s3} - \phi_{vap,s1-s2} + \phi_{vap,s2-s3}$$

C_{s2} = volumetric specific heat of soil composition

$$\phi_{cond} = \lambda \frac{dT}{dz} \; ;$$

$$\phi_{cond,s1-s2} = \lambda_{s1s2}\frac{(T_{s1} - T_{s2})}{S1S2}$$

$$\phi_{cond,s2-s3} = \lambda_{s2s3}\frac{(T_{s2} - T_{s3})}{S2S3}$$

$$\phi_{vap} = LhsDv\frac{dT}{dz} + LevDv\frac{dh}{dz} \; ;$$

$$\phi_{vap,s1-s2} = LK_{vT\_m-s1s2}\frac{T_{s1} - T_{s2}}{S1S2} + LK_{v\psi\_m-s1s2}\frac{\psi_{s1} - \psi_{s2}}{S1S2}$$

$$\phi_{vap,s2-s3} = LK_{vT\_m-s2s3}\frac{T_{s2} - T_{s3}}{S2S3} + LK_{v\psi\_m-s2s3}\frac{\psi_{s2} - \psi_{s3}}{S2S3}$$

Properties with subscript s1s2 are averages of properties at soil s1 layer and soil s2 layer

Properties with subscript s2s3 are averages of properties at soil s2 layer and soil s3 layer

Length S1S2 = (S1+S2)/2

Length S2S3 = (S2+S3)/2

Coefficient form CV4 (S2)

$$\left[-\alpha \frac{\lambda_{s1s2}^{t+\Delta t}}{S1S2} + \alpha \frac{LK_{vT\_m-s1s2}^{t+\Delta t}}{S1S2} \right] T_{s1}^{t+\Delta t}$$

$$+ \left[\frac{C_{s2}S2}{\Delta t} + \alpha \frac{\lambda_{s1s2}^{t+\Delta t}}{S1S2} + \alpha \frac{\lambda_{s2s3}^{t+\Delta t}}{S2S3} - \alpha \frac{LK_{vT\_m-s1s2}^{t+\Delta t}}{S1S2} - \alpha \frac{LK_{vT\_m-s2s3}^{t+\Delta t}}{S2S3} \right] T_{s2}^{t+\Delta t}$$

$$+ \left[-\alpha \frac{\lambda_{s2s3}^{t+\Delta t}}{S2S3} + \alpha \frac{LK_{vT\_m-s2s3}^{t+\Delta t}}{S2S3} \right] T_{s3}^{t+\Delta t}$$

$$=$$

$$\left[(1-\alpha) \frac{\lambda_{s1s2}^{t}}{S1S2} - (1-\alpha) \frac{LK_{vT\_m-s1s2}^{t}}{S1S2} \right] T_{s1}^{t}$$

$$+ \left[\frac{C_{s2}S2}{\Delta t} - (1-\alpha) \frac{\lambda_{s1s2}^{t}}{S1S2} - (1-\alpha) \frac{\lambda_{s2s3}^{t}}{S2S3} \right]$$

$$+ \left[(1-\alpha) \frac{LK_{vT\_m-s1s2}^{t}}{S1S2} + (1-\alpha) \frac{LK_{vT\_m-s2s3}^{t}}{S2S3} \right] T_{s2}^{t}$$

$$+ \left[(1-\alpha) \frac{\lambda_{s2s3}^{t}}{S2S3} - (1-\alpha) \frac{LK_{vT\_m-s2s3}^{t}}{S2S3} \right] T_{s3}^{t}$$

$$- (1-\alpha) \frac{LK_{v\psi\_m-s1s2}^{t}}{S1S2} \left(\psi_{s1}^{t} - \psi_{s2}^{t} \right) + (1-\alpha) \frac{LK_{v\psi\_m-s2s3}^{t}}{S2S3} \left(\psi_{s2}^{t} - \psi_{s3}^{t} \right)$$

$$- \alpha \frac{LK_{v\psi\_m-s1s2}^{t+\Delta t}}{S1S2} \left(\psi_{s1}^{t+\Delta t} - \psi_{s2}^{t+\Delta t} \right) + \alpha \frac{LK_{v\psi\_m-s2s3}^{t+\Delta t}}{S2S3} \left(\psi_{s2}^{t+\Delta t} - \psi_{s3}^{t+\Delta t} \right)$$

Coefficient form CV5 (S3):

$$\left[-\alpha \frac{\lambda_{s2s3}^{t+\Delta t}}{S2S3} + \alpha \frac{LK_{vT\_m-s2s3}^{t+\Delta t}}{S2S3} \right] T_{s2}^{t+\Delta t}$$

$$+ \left[\frac{C_{s3}s3}{\Delta t} + \alpha \frac{\lambda_{s2s3}^{t+\Delta t}}{S2S3} + \alpha \frac{\lambda_{s3s4}^{t+\Delta t}}{S3S4} - \alpha \frac{LK_{vT\_m-s2s3}^{t+\Delta t}}{S2S3} - \alpha \frac{LK_{vT\_m-s3s4}^{t+\Delta t}}{S3S4} \right] T_{s3}^{t+\Delta t}$$

$$+ \left[-\alpha \frac{\lambda_{s3s4}^{t+\Delta t}}{S3S4} + \alpha \frac{LK_{vT\_m-s3s4}^{t+\Delta t}}{S3S4} \right] T_{s4}^{t+\Delta t}$$

$$=$$

$$\left[(1-\alpha) \frac{\lambda_{s2s3}^{t}}{S2S3} - (1-\alpha) \frac{LK_{vT\_m-s2s3}^{t}}{S2S3} \right] T_{s2}^{t}$$

$$+ \left[\frac{C_{s3}s3}{\Delta t} - (1-\alpha) \frac{\lambda_{s2s3}^{t}}{S2S3} - (1-\alpha) \frac{\lambda_{s3s4}^{t}}{S3S4} \right]$$

$$+ \left[(1-\alpha) \frac{LK_{vT\_m-s2s3}^{t}}{S2S3} + (1-\alpha) \frac{LK_{vT\_m-s3s4}^{t}}{S3S4} \right] T_{s3}^{t}$$

$$+ \left[(1-\alpha) \frac{\lambda_{s3s4}^{t}}{S3S4} - (1-\alpha) \frac{LK_{vT\_m-s3s4}^{t}}{S3S4} \right] T_{s4}^{t}$$

$$- (1-\alpha) \frac{LK_{v\psi\_m-s2s3}^{t}}{S2S3} \left(\psi_{s2}^{t} - \psi_{s3}^{t} \right) + (1-\alpha) \frac{LK_{v\psi\_m-s3s4}^{t}}{S3S4} \left(\psi_{s3}^{t} - \psi_{s4}^{t} \right)$$

$$- \alpha \frac{LK_{v\psi\_m-s2s3}^{t+\Delta t}}{S2S3} \left(\psi_{s2}^{t+\Delta t} - \psi_{s3}^{t+\Delta t} \right) + \alpha \frac{LK_{v\psi\_m-s3s4}^{t+\Delta t}}{S3S4} \left(\psi_{s3}^{t+\Delta t} - \psi_{s4}^{t+\Delta t} \right)$$

Coefficient form CV6 (S4):

$$\left[-\alpha \frac{\lambda_{s3s4}^{t+\Delta t}}{S3S4} + \alpha \frac{LK_{vT\_m-s3s4}^{t+\Delta t}}{S3S4} \right] T_{s3}^{t+\Delta t}$$

$$+ \left[\frac{C_{s4s4}}{\Delta t} + \alpha \frac{\lambda_{s3s4}^{t+\Delta t}}{S3S4} + \alpha \frac{\lambda_{s4s5}^{t+\Delta t}}{S4S5} - \alpha \frac{LK_{vT\_m-s3s4}^{t+\Delta t}}{S3S4} - \alpha \frac{LK_{vT\_m-s4s5}^{t+\Delta t}}{S4S5} \right] T_{s4}^{t+\Delta t}$$

$$+ \left[-\alpha \frac{\lambda_{s4s5}^{t+\Delta t}}{S4S5} + \alpha \frac{LK_{vT\_m-s4s5}^{t+\Delta t}}{S4S5} \right] T_{s5}^{t+\Delta t}$$

$$=$$

$$\left[(1-\alpha) \frac{\lambda_{s3s4}^{t}}{S3S4} - (1-\alpha) \frac{LK_{vT\_m-s3s4}^{t}}{S3S4} \right] T_{s3}^{t}$$

$$+ \left[\frac{C_{s4s4}}{\Delta t} - (1-\alpha) \frac{\lambda_{s3s4}^{t}}{S3S4} - (1-\alpha) \frac{\lambda_{s4s5}^{t}}{S4S5} \right]$$
$$+ \left[(1-\alpha) \frac{LK_{vT\_m-s3s4}^{t}}{S3S4} + (1-\alpha) \frac{LK_{vT\_m-s4s5}^{t}}{S4S5} \right] T_{s4}^{t}$$

$$+ \left[(1-\alpha) \frac{\lambda_{s4s5}^{t}}{S4S5} - (1-\alpha) \frac{LK_{vT\_m-s4s5}^{t}}{S4S5} \right] T_{s5}^{t}$$

$$- (1-\alpha) \frac{LK_{v\phi\_m-s3s4}^{t}}{S3S4} \left(\psi_{s3}^{t} - \psi_{s4}^{t} \right) + (1-\alpha) \frac{LK_{v\phi\_m-s4s5}^{t}}{S4S5} \left(\psi_{s4}^{t} - \psi_{s5}^{t} \right)$$
$$- \alpha \frac{LK_{v\phi\_m-s3s4}^{t+\Delta t}}{S3S4} \left(\psi_{s3}^{t+\Delta t} - \psi_{s4}^{t+\Delta t} \right) + \alpha \frac{LK_{v\phi\_m-s4s5}^{t+\Delta t}}{S4S5} \left(\psi_{s4}^{t+\Delta t} - \psi_{s5}^{t+\Delta t} \right)$$

Energy Balance CV4, CV5, CV6 Soil middle layers

□ Thermal exchanges

$$C_{s2} S2 \frac{dT_{s2}}{dt} = +\phi_{cond,s1-s2} - \phi_{cond,s2-s3} - \phi_{vap,s2-s1} + \phi_{vap,s3-s2}$$
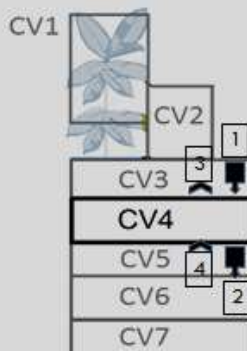
1. $\phi_{cond,s1-s2}$ conduction gain from soil upper layer
2. $\phi_{cond,s2-s3}$ conduction loss to soil lower layer
3. $\phi_{vap,s2-s1}$ latent heat loss by vapour exchange to upper layer
4. $\phi_{vap,s3-s2}$ latent heat gain by vapour exchange from lower layer

(a44)	$-\alpha \frac{\lambda_{s1s2}^{t+\Delta t}}{S1\_S2} + \alpha \frac{L\ K_{vT\_m-s1s2}^{t+\Delta t}}{S1\_S2}$ (All variables defined previously)							
Time invariant data	**Defining Equations and Remarks**	**Initial Value**	**Unit**	**Required data**			**Couple Info**
				Input	**Param eters**	**Calcul ated Variab les**	
Time variant data	**Defining Equations and Remarks**	**Initial Value**	**Unit**	**Required data**			**Couple Info**
				Input	**Param eters**	**Calcul ated Variab les**	

(a45)	$\frac{C_{s2}\ S2}{\Delta t} + \alpha \frac{\lambda_{s1s2}^{t+\Delta t}}{S1\_S2} + \alpha \frac{\lambda_{s1s2}^{t+\Delta t}}{S2\_S3} - \alpha \frac{L\ K_{vT\_m-s1s2}^{t+\Delta t}}{S1\_S2} - \alpha \frac{L\ K_{vT\_m-s2s3}^{t+\Delta t}}{S2\_S3}$							
Time invariant data	**Defining Equations and Remarks**	**Initial Value**	**Unit**	**Required data**			**Couple Info**
				Input	**Param eters**	**Calcul ated Variab les**	
Cs2	$C_s = \rho_m C_m x_m + \rho_w C_w x_w + \rho_a C_a x_a + \rho_o C_o x_o$	0.9e6	J/m3K	x_m x_a x_o	ρ_m, C_m ρ_w, C_w ρ_{ca}, C_a ρ_o, C_o	x_w $=\theta_{s2}$	
S2		0.1	m	S2			
S2S3		0.1	m	S3			
Δt		1800	s	Δt			
Time variant data	**Defining Equations and Remarks**	**Initial Value**	**Unit**	**Required data**			**Couple Info**
				Input	**Param eters**	**Calcul ated Variab les**	
λ_{s2s3}	$\lambda_{s1} = A + 2.8\ V_s \left(\frac{\theta}{\rho_w}\right)^2 + (A - B) \exp\left(-\left(\frac{C\theta}{\rho_w}\right)^4\right)$	2.62	W/mK	V_q V_m m_c	ρ_w	θ_{s2} θ_{s3}	moistu re conten

								t
	$\lambda_{s2s3} = \left(\dfrac{\lambda_{s2} + \lambda_{s3}}{2}\right)$							
$K_{vT\ m-s2s3}$	As defined for the previous CV							

(a46)	$- \alpha \dfrac{\lambda_{s2s3}^{t+\Delta t}}{S2\_S3} + \alpha \dfrac{L\, K_{vT\_m-s2s3}^{t+\Delta t}}{S2\_S3}$ (All variables defined previously)							
Time invariant data	**Defining Equations and Remarks**	**Initial Value**	**Unit**	**Required data**			**Couple Info**
				Input	**Param eters**	**Calcul ated Variab les**	
Time variant data	**Defining Equations and Remarks**	**Initial Value**	**Unit**	**Required data**			**Couple Info**
				Input	**Param eters**	**Calcul ated Variab les**	

b44 $\quad (1-\alpha)\dfrac{\lambda_{s1s2}^{t}}{S1\_S2} - (1-\alpha)\dfrac{L\, K_{vT\_m-s1s2}^{t}}{S1\_S2}$

b45 $\quad \dfrac{C_{s2}\, S2}{\Delta t} - (1-\alpha)\dfrac{\lambda_{s1s2}^{t}}{S1\_S2} - (1-\alpha)\dfrac{\lambda_{s2s3}^{t}}{S2\_S3} + (1-\alpha)\dfrac{L\, K_{vT\_m-s1s2}^{t}}{S1\_S2} + (1-\alpha)\dfrac{L\, K_{vT\_m-s2s3}^{t}}{S2\_S3}$

b46 $\quad (1-\alpha)\dfrac{\lambda_{s2s3}^{t}}{S2\_S3} - (1-\alpha)\dfrac{L\, K_{vT\_m-s2s3}^{t}}{S2\_S3}$

(c41)	$- (1-\alpha)\dfrac{L\, K_{v\psi\_m-s1s2}^{t}}{S1\_S2}(\psi_{s1}^{t} - \psi_{s2}^{t}) + (1-\alpha)\dfrac{L\, K_{v\psi\_m-s2s3}^{t}}{S2\_S3}(\psi_{s2}^{t} - \psi_{s3}^{t}) - \alpha\dfrac{L\, K_{v\psi\_m-s1s2}^{t+\Delta t}}{S1\_S2}(\psi_{s1}^{t+\Delta t} - \psi_{s2}^{t+\Delta t}) + \alpha\dfrac{L\, K_{v\psi\_m-s2s3}^{t+\Delta t}}{S2\_S3}(\psi_{s2}^{t+\Delta t} - \psi_{s3}^{t+\Delta t})$		
	(All variables defined previously)		
Time invariant data	**Defining Equations and Remarks**	**Initial** **Unit**	**Required data** **Couple**

		Value		Input	Param eters	Calcul ated Variab les	Info
Time variant data	**Defining Equations and Remarks**	**Initial Value**	**Unit**	**Required data**			**Couple Info**
				Input	**Param eters**	**Calcul ated Variab les**	

5. Soil Lower layer CV7 (S5)

Energy Balance

$$C_{s5}S5\frac{dT_{s5}}{dt} = \phi_{cond,s4-s5} - \phi_{cond,s5-x} - \phi_{vap,s4-s5}$$

C_{s5} = volumetric specific heat of soil composition

$$\phi_{cond} = \lambda\frac{dT}{dz} \; ;$$

$$\phi_{cond,s4-s5} = \lambda_{s4s5}\frac{(T_{s4}-T_{s5})}{S4S5}$$

$$\phi_{cond,s5-x} = \lambda_{s5x}\frac{(T_{s5}-T_{x})}{S5X}$$

$$\phi_{vap} = LK_{vT\_m}\frac{dT}{dz} + LK_{v\psi\_m}\frac{d\psi}{dz} \; ;$$

$$\phi_{vap,s4-s5} = LK_{vT\_m-s4s5}\frac{T_{s4}-T_{s5}}{S4S5} + LK_{v\psi\_m-s4s5}\frac{\psi_{s4}-\psi_{s5}}{S4S5}$$

Conduction on both sides of soil lower layer is considered. Vapour exchange is assumed to occur only with the soil mid layer

Coefficient form

Energy Balance CV5 Soil lower layer

| (a55) | $-\alpha \dfrac{\lambda_{s4s5}^{t+\Delta t}}{S4\_S5} + \quad \alpha \dfrac{L\, K_{vT\_m-s4s5}^{t+\Delta t}}{S4\_S5}$ (All variables defined previously) |

Time invariant data	Defining Equations and Remarks	Initial Value	Unit	Required data			Couple Info
				Input	Parameters	Calculated Variables	

Time variant data	Defining Equations and Remarks	Initial Value	Unit	Required data			Couple Info
				Input	Parameters	Calculated Variables	

| (a56) | $\dfrac{C_{s5}\, S5}{\Delta t} + \alpha \dfrac{\lambda_{s4s5}^{t+\Delta t}}{S4\_S5} + \alpha \dfrac{\lambda_{s5x}^{t+\Delta t}}{S5X} - \alpha \dfrac{L\, K_{vT\_m-s4s5}^{t+\Delta t}}{S4\_S5}$ |

Time invariant data	Defining Equations and Remarks	Initial Value	Unit	Required data			Couple Info
				Input	Parameters	Calculated Variables	
Cs5	$C_s = \rho_m C_m x_m + \rho_w C_w x_w + \rho_a C_a x_a + \rho_o C_o x_o$	0.9e6	J/m3K	x_m x_a x_o	ρ_m, C_m ρ_w, C_w ρ_{ca}, C_a ρ_o, C_o	x_w $=\theta_{s5}$	
S5X	$S5X = \left(\dfrac{S5 + X}{2}\right)$ X – thickness of roof support	0.2	m	S5 X			

Time variant data	Defining Equations and Remarks	Initial Value	Unit	Required data			Couple Info
				Input	Parameters	Calculated Variables	

λ_{s5x} thermal conductivity average value of that of S5 layer and roof support	$\lambda_{s5x} = \left(\dfrac{\lambda_{s5} + \lambda_x}{2}\right)$ (Note 1)						λ_x	

(a57)	$-\alpha\,\dfrac{\lambda_{s5x}^{t+\Delta t}}{SLX}$ (All variables defined previously)							
Time invariant data	**Defining Equations and Remarks**	**Initial Value**	**Unit**	**Required data**			**Couple Info**	
				Input	**Param eters**	**Calcul ated Variab les**		
Time variant data	**Defining Equations and Remarks**	**Initial Value**	**Unit**	**Required data**			**Couple Info**	
				Input	**Param eters**	**Calcul ated Variab les**		

b55 $\quad (1-\alpha)\dfrac{\lambda_{S4S5}^{t}}{S4\_S5} - (1-\alpha)\dfrac{L\,K_{vT\_m-s4s5}^{t}}{S4\_S5}$

b56 $\quad \dfrac{C_{S5}\,S5}{\Delta t} - (1-\alpha)\dfrac{\lambda_{S4S5}^{t}}{S4\_S5} - (1-\alpha)\dfrac{\lambda_{S5x}^{t}}{S5X} + (1-\alpha)\dfrac{L\,K_{vT\_m-s4s5}^{t}}{S4\_S5}$

b57 $\quad (1-\alpha)\dfrac{\lambda_{s5x}^{t}}{S5X}$

| (c51) | $-\ (1-\alpha)\dfrac{L\ K^{t}_{v\psi\_m-s4s5}}{S4\ S5}\left(\psi^{t}_{S4}-\psi^{t}_{S5}\right)-\alpha\dfrac{L\ K^{t+\Delta t}_{v\psi\_m-s4s5}}{S4\ S5}\left(\psi^{t+\Delta t}_{S4}-\psi^{t+\Delta t}_{S5}\right)$ (All variables defined previously) |

Time invariant data	Defining Equations and Remarks	Initial Value	Unit	Required data			Couple Info
				Input	Parameters	Calculated Variables	

Time variant data	Defining Equations and Remarks	Initial Value	Unit	Required data			Couple Info
				Input	Parameters	Calculated Variables	

Notes on soil lower layer

1. To include in the coding to read λ_x from the ESP-r for future versions of coupling by both boundary temperature and boundary flux

Appendix 3.2 Moisture model equations and coefficient tables

This appendix provides an organized documentation for all the coefficients and their derivations for the moisture domain equations in soil. Also the format of the equations for the moisture balances in each control volumes is given.

Moisture Balance Equations

Moisture exchange matrix:

$$
\begin{pmatrix}
m11 & m12 & m13 & & & \\
 & m22 & m23 & m24 & & \\
 & & m33 & m34 & m35 & \\
 & & & m44 & m45 & m46 \\
 & & & & m55 & m56 & m57
\end{pmatrix}
\times
\begin{pmatrix}
ea^{t+\Delta t} \\
\psi s1^{t+\Delta t} \\
\psi s2^{t+\Delta} \\
\psi s3^{t+\Delta t} \\
\psi s4^{t+\Delta t} \\
\psi s5^{t+\Delta t} \\
\psi x^{t+\Delta t}
\end{pmatrix}
=
\begin{pmatrix}
n11 & n12 & n13 & & & \\
 & n22 & n23 & n24 & & \\
 & & n33 & n34 & n35 & \\
 & & & n44 & n45 & n46 \\
 & & & & n55 & n56 & n57
\end{pmatrix}
\times
\begin{pmatrix}
ea^{t} \\
\psi s1^{t} \\
\psi s2^{t} \\
\psi s3^{t} \\
\psi s4^{t} \\
\psi s5^{t} \\
\psi x^{t}
\end{pmatrix}
+
\begin{pmatrix}
q1 \\
q2 \\
q3 \\
q4 \\
q5
\end{pmatrix}
=
\begin{pmatrix}
y1 \\
y2 \\
y3 \\
y4 \\
y5
\end{pmatrix}
$$

The matrix shown is for soil layers only.

Two rows representing equations for plant and canopy air CVs are absent for moisture differential equations. However the effects of precipitation through-fall, interception, canopy transpiration are included with reference to soil moisture balances.

1. Top soil layer

Moisture Balance

$$
C\theta \frac{\partial \psi}{\partial t} = \frac{\partial}{\partial z}\left[K\Psi \left[\frac{\partial \psi}{\partial z} + 1 \right] + KT \frac{\partial T}{\partial z} + P0 - Ev \right] - S
$$

ψ = soil matric potential [m = (J/kg) / g = kPa/g]
θ = soil moisture content [$m^3 m^{-3}$]
$C\theta = \dfrac{\partial \theta}{\partial \psi}$ Specific Water Content also known as Capillary Capacity or Differential Water Capacity [m^{-1}]
S = root uptake [$s^{-1} = m^3$ (water)/m^3(soil) s] which accounts for transpiration
$K\psi$ = isothermal liquid-vapour conductivity
$K\Psi = K_{L\psi} + K_{v\psi}$

$K_{L\psi}$= isothermal liquid conductivity (usually denoted as K, hydraulic conductivity)

[ms^{-1}]

$K_{v\psi}$= isothermal vapour conductivity [ms^{-1}]

KT = thermal liquid-vapour conductivity

$$KT = K_{LT} + K_{vT}$$

K_{LT}= thermal liquid conductivity [$m^2 K^{-1} s^{-1}$]

K_{vT}= thermal vapour conductivity [$m^2 K^{-1} s^{-1}$]

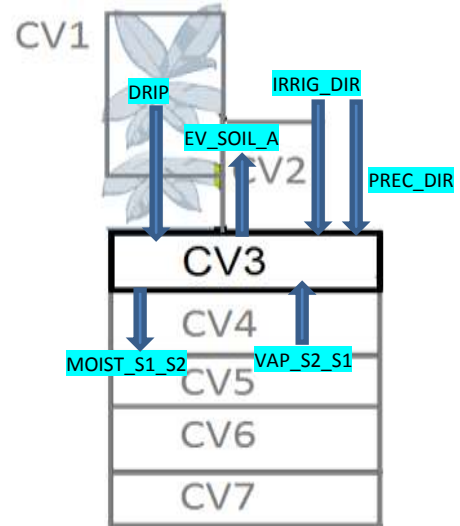P0= precipitation reaching soil top after canopy intercept

$$[ms^{-1} = m^3 \text{(water)} m^{-2} \text{(surface area) } s^{-1}]$$

Ev = soil top evaporation [$ms^{-1} = m^3$ (water)m^{-2}(surface area) s^{-1}]

Coefficient form

$$
-\left[\alpha \frac{0.622}{P\_m \left(r_{s1-a} + r_s\right)^{t+\Delta t}}\right] e_{ca\_m}^{t+\Delta t}
$$

$$
+\left[\frac{S1\, C\theta_{s1}^t}{\Delta t} + \alpha \frac{K\Psi_{s1s2}^{t+\Delta t}}{S1\_S2}\right] \psi_{s1}^{t+\Delta t}
$$

$$
-\left[\alpha \frac{K\Psi_{s1s2}^{t+\Delta t}}{S1\_S2}\right] \psi_{s2}^{t+\Delta t}
$$

$$=$$

$$
+\left[(1-\alpha) \frac{0.622}{P\_m \left(r_{s1-a} + r_s\right)^t}\right] e_{ca\_m}^t
$$

$$
+\left[\frac{S1\, C\theta_{s1}^t}{\Delta t} - (1-\alpha) \frac{K\Psi_{s1s2}^t}{S1\_S2}\right] \psi_{s1}^t
$$

$$
+\left[(1-\alpha) \frac{K\Psi_{s1s2}^t}{S1\_S2}\right] \psi_{s2}^t
$$

$$
-(1-\alpha)K\Psi_{s1s2}^t - \alpha K\Psi_{s1s2}^{t+\Delta t}
$$

$$
-(1-\alpha)\frac{KT_{s1s2}^t}{S1\_S2}\left(T_{s1}^t - T_{s2}^t\right) - \alpha \frac{KT_{s1s2}^{t+\Delta t}}{S1\_S2}\left(T_{s1}^{t+\Delta t} - T_{s2}^{t+\Delta t}\right)
$$

$$
+(1-\alpha)P0^t + \alpha P0^{t+\Delta t}
$$

$$
-(1-\alpha)\frac{0.622}{P\_m \left(r_{s1-a} + r_s\right)^t} e_{s1\_m}^t - \alpha \frac{0.622}{P\_m \left(r_{s1-a} + r_s\right)^{t+\Delta t}} e_{s1\_m}^{t+\Delta t}
$$

$$
-(1-\alpha)S1\, S_{s1}^t - \alpha S1\, S_{s1}^{t+\Delta t}
$$

CV3: Soil Upper layer

209

(m11)	$-\alpha\dfrac{0.622}{Pa\_m(r_a+r_s)^{t+\Delta t}}$							
Time invariant data	**Defining Equations and Remarks**	**Initial Value**	**Unit**	**Required data**			**Couple Info**
				Input	**Param eters**	**Calcul ated Variab les**	
Pa_m atmospheric pressure in m atmPresGR_m	Ref: [73] [116] $Pa_m = 101325 * \left(\dfrac{293 - 0.0065z}{293}\right)^{5.26} \dfrac{1}{9.81 * 1000}$ z=site altitude [m] (siteAlt)	10.13	m			z	
Time variant data	**Defining Equations and Remarks**	**Initial Value**	**Unit**	**Required data**			**Couple Info**
				Input	**Param eters**	**Calcul ated Variab les**	
r_a aerodynamic resistance in canopy air	Aerodynamic resistance as defined in thermal coefficient table a11		s/m	u L LAI dc		T(3)	
r_s surface resistance at soil	Ref [56] $rs = 100\left(0.413\dfrac{\theta_s}{\theta}\right)^{1.5}$ θs = saturated moisture content m3/m3 θ = current soil moisture content m3/m3		s/m	θ_s		θ (s1)	

(m12)	$\dfrac{S1\,C\theta_{s1}^{t}}{\Delta t} + \alpha\dfrac{K\Psi_{s1s2}^{t+\Delta t}}{S1\_S2}$							
Time invariant data	**Defining Equations and Remarks**	**Initial Value**	**Unit**	**Required data**			**Couple Info**
				Input	**Param eters**	**Calcul ated Variab les**	
S1 height of soil top layer	S1= soilHt/5 ; currently soil height (SoilHt) is divided into five equal layers S1=S2=S3=S4=S5	0.06	m	soilHt			
S1_S2 centre to centre distance	S1_S2=(S1+S2)/2	0.06	m				

between S1 and S2 layers								
Δt simulation time step	Input by user	1800	s	Δt			
Time variant data	**Defining Equations and Remarks**	**Initial Value**	**Unit**	**Required data**			**Couple Info**
				Input	**Param eters**	**Calcul ated Variab les**	
$C\theta_{s1}^{t}$ Specific Water Capacity	'Ref: [117] and Cours de Physique du sol [118] $$C\theta_{s1}^{t} = \frac{\partial \theta}{\partial \psi}$$ $$C\theta = \frac{\alpha(\theta_s - \theta_r)(n-1)(\alpha\psi)^{n-1}}{[1 + (\alpha\psi)^n]^{2-1/n}}$$ n – parameters of soil's moisture retention curve, dimensionless a curve shape factor related to soil pore-size distribution [37] currently taken as 1.56 (HyDRUS1D case studies) α- parameters of soil's moisture retention curve, $[m^{-1}]$ a scaling parameter related to the inverse of the air entry pressure currently taken as 3.6 m^{-1} θs – saturated moisture content of soil $m^3\,m^{-3}$ currently taken as 0.43 θr – residual moisture content of soil currently taken as 0.05	0.0009	m^{-1}	n α θs θr			
$K\Psi_{s1s2}^{t+\Delta t}$ Isothermal liquid vapour conductivity	Ref: [73] [60] KΨ=K$_{v\psi}$+K K$_{v\psi}$ isothermal vapour conductivity and K isothermal liquid conductivity, or simply liquid conductivity (liquid conductivity is generally pressure driven) $$K_{v\psi} = \frac{D_v}{\rho_w}\rho_{vs}\frac{Mg}{RT}h$$	6.39e-16	ms^{-1}	θs θr Ks n		T θ ψ	

211

Dv- vapour diffusivity in soil $[m^2 s^{-1}]$

$$D_v = \tau_g a_v D_a$$

Da- diffusivity of water vapour in air
It is given by:

$$Da = Do \left(\frac{T}{273.15}\right)^2$$

Do- reference value of diffusivity = 2.12e-5 $m^2 s^{-1}$
T – temperature of medium [K]

av – air filled porosity [-]
porosity can be calculated as: $a_v = \theta_s - \theta$
θ_s-saturated moisture content $[m^3 m^{-3}]$ and θ current moisture content $[m^3 m^{-3}]$

τ_g= turtosity factor[-] is given by:

$$\tau_g = \frac{(a_v)^{7/3}}{(\theta_s)^2}$$

ρ_w- density of water $[kg m^{-3}]$ at a given temperature t°C is given by:

$$\rho_w = 1000 \left(1 - 7.37e - 6\, t^2 + 3.79e - 8\, t^3\right)$$

ρ_{vs}- saturated vapour density $[kg m^{-3}]$ at a given temperature T K is given by:

$$\rho_{vs} = 1e - 3\, \frac{e^{\left(31.3716 - \frac{6014.79}{T} - 7.92495e - 3T\right)}}{T}$$

M- molar mass of water 0.018015 kg mol^{-1}
g- acceleration due to gravity 9.81 ms^{-2}
R- universal gas constant 8.314 J $moil^{-1}$ K^{-1}
T – soil temperature in K

h- relative humidity [-]
 expressing it in terms of soil matric potential ψ[m] :

$$h = e^{\left(\frac{\psi M g}{RT}\right)}$$

Liquid conductivity K is given by

$$K = K_s\, Se^L \left[1 - \left(1 - Se^{1/m}\right)^m\right]^2$$

Ks- saturation liquid conductivity $[ms^{-1}]$
Se - -effective saturation [-] given by:

212

| | $Se = \dfrac{\theta - \theta r}{\theta s - \theta r}$
 θ-current moisture content [m³m⁻³]
 θr-residual moisture content [m³m⁻³]
 θs-saturated moisture content [m³m⁻³]
 L- is a pore connectivity parameter usually taken as 0.5 [-]
 m is alternate form on soil n index :
 $m = 1 - \dfrac{1}{n}$ | | | | | | |

(m13) $\quad -\alpha \dfrac{K\Psi^{t+\Delta t}_{S1S2}}{S1\_S2}$ (all terms previously defined)

Time invariant data	Defining Equations and Remarks	Initial Value	Unit	Required data			Couple Info
				Input	Parameters	Calculated Variables	
Time variant data	**Defining Equations and Remarks**	Initial Value	Unit	Required data			Couple Info
				Input	Parameters	Calculated Variables	

'n' coefficients use time varying parameters one time step prior to that in 'm' coefficients

In addition, wherever present, multipliers α change to 1-α.

Sign change for all terms except for the one carries Δt

$$n11 = (1-\alpha)\frac{0.622}{Pa\_m(r_a+r_s)^t}$$
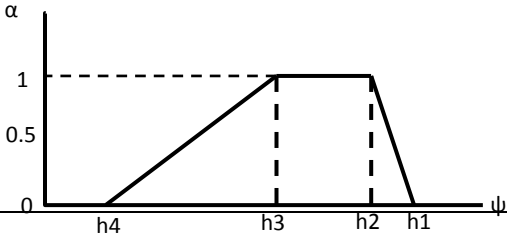
$$n12 = \frac{S1\ C\theta_{s1}^t}{\Delta t} - (1-\alpha)\frac{K\Psi_{s1s2}^t}{S1\_S2}$$

$$n13 = (1-\alpha)\frac{K\Psi_{s1s2}^t}{S1\_S2}$$

(q1)	$-(1-\alpha)K\Psi_{s1s2}^t - \alpha\ K\Psi_{s1s2}^{t+\Delta t}$ $-(1-\alpha)\frac{KT_{s1s2}^t}{S1\_S2}(T_{s1}^t - T_{s2}^t) - \alpha\frac{KT_{s1s2}^{t+\Delta t}}{S1\_S2}(T_{s1}^{t+\Delta t} - T_{s2}^{t+\Delta t})$ $+(1-\alpha)P0^t + \alpha\ P0^{t+\Delta t}$ $-(1-\alpha)\frac{0.622}{P\_m\ (r_a+r_s)^t}\ e_{s1_m}^t - \alpha\frac{0.622}{P\_m\ (r_a+r_s)^{t+\Delta t}}\ e_{s1_m}^{t+\Delta t}$ $-(1-\alpha)\ S1\ S_{s1}^t - \alpha S1\ S_{s1}^{t+\Delta t}$ -

Time invariant data	Defining Equations and Remarks	Initial Value	Unit	Required data			Couple Info
				Input	Param eters	Calcul ated Variab les	
P_m atmospheric pressure in m	P_m = P/(9.81*1000)	10.07	m				

Time variant data	Defining Equations and Remarks	Initial Value	Unit	Required data			Couple Info
				Input	Param eters	Calcul ated Variab les	
KT_{s1s2}^t Thermal liquid vapour conductivity (Non-isothermal liquid vapour conductivity)	Ref: [73] [115] [60] KT= K_{VT} + K_{LT}	Initial value not requir e as	$m^2s^{-1}K^{-1}$	fc		T θ θs ψ K	

		only used in GRq coeffs and it is calculated there.					
	K_{VT} - Thermal vapour conductivity K_{LT} - Thermal liquid conductivity $$K_{VT} = \frac{D_v}{\rho_w} \eta_e \, h \, \frac{d\rho_{vs}}{dT}$$ Dv- vapour diffusivity in soil [m²s⁻¹] ρ_w- density of water [kgm⁻³] ηe -enhancement factor [-] $$\eta_e = 9.5 + 3\frac{\theta}{\theta_s} - 8.5 \, e^{\left\{-\left[\left(1+\frac{2.6}{fc}\right)\frac{\theta}{\theta_s}\right]^4\right\}}$$ fc-clay fraction by mass [kg/kg] h- relative humidity [-] In terms of soil matric potential ψ[m] : $$h = e^{\left(\frac{\psi M g}{RT}\right)}$$ ρ_{vs}- saturated vapour density [kgm⁻³] at a given temperature T K is given by: $$\rho_{vs} = 1e-3 \, \frac{e^{\left(31.3716-\frac{6014.79}{T}-7.92495e-3T\right)}}{T}$$ $\frac{d\rho_{vs}}{dT}$is calculated as $1e-3 \, \frac{e^{\left(31.3716-\frac{6014.79}{(T+1)}-7.92495e-3(T+1)\right)}}{(T+1)} - 1e-3 \, \frac{e^{\left(31.3716-\frac{6014.79}{T}-7.92495e-3T\right)}}{T}$ $$K_{LT} = K\left(\psi \, G_{wT} \frac{1}{\gamma_o}\frac{d\gamma}{dT}\right)$$ K – isothermal liquid conductivity [ms⁻¹] ψ- matric potential [m] G_{wT}– gain factor for sand =7 [-] γ_o surface tension at 25°C = 71.89 g/s² $\frac{d\gamma}{dT} = 0.1425 - 4.76e-4\, t$ [g/s²/°c]						
$P0^t$ precipitation reaching soil after intercept	Ref: [90] $$P = a\,LAI\left[1 - \frac{1}{1+\frac{b\,P_{gross}}{a\,LAI}}\right]$$						

215

	P_i - intercepted precipitation [cm] LAI - leaf area index [m^2/m^2] P_{gross} - gross precipitation [cm] a - empirical coefficient[cm]; for agricultural crops a=0.25 cm b - soil cover fraction						
P0 alternative	Ref: [19] [119] The flow chart of precipitation interception (include precipitation and irrigation) is shown along with the notes at the end of this section. Formulae used within the routine are: 1. Canopy saturation storage height = 0.0001*LAI 2. xs -Proportion of grid area where the sum of intercepted rain and existing canopy water storage exceeds the saturation storage height $$xs = \frac{-1}{b} log \left[\frac{S_c - M_{cs} - M_{cw}}{a_p(1-\delta_p)P} - \frac{c_p}{a_p} \right]$$ a_p, c_p and b are coefficients describing special distribution of precipitation; they are taken as constants; a_p=0.0001; c_p=0.9999; b=20 S_c-canopy water saturation height M_{cs}-canopy interception snow M_{cw}-canopy interception water δ_p – canopy through fall coefficient P precipitation 3. δ_p is given by: $\delta p = 1 - V + V\, e^{-K_p L_T/V}$ V − canopy cover fraction K_p – extinction coefficient for rain fall (same as that for shortwave radiation) L_T − LAI 4. Kp is given by: $K_p = \phi_1 + \phi_2$ $\phi_1 = 0.5 - 0.633\, \chi_L - 0.33\, \chi_L{}^2$ $\phi_2 = 0.877 * (1 - 2\phi_1)$ χ_L is the leaf angle distribution factor (0 for spherical leaves, 1 for horizontal leaves and -1 for vertical leaves)		m^3/m^2 /s				

	5. direct through fall $D_d = \delta p\, P$ 6. canopy drainage through fall $$Dc = P(1 - \delta p)\frac{ap}{b}(1 - e^{-bx_s}) + c_p x_s - (S_c - M_{cs} - M_{cw})x_s$$ Input for the subroutine: • Current time precipitation (weather file), • plant LAI, • canopy water store and snow store from previous calculations, if any, • leaf angle distribution factor , • canopy cover fraction, • temperature of water precipitation (taken as ambient wet bulb temperature), • canopy plant temperature output from the sub: • intercepted water reaching soil top • a modifies value of canopy plant temperature The routine, currently do not calculate evaporation loss from the storage water on leaves as it is assumed to be very minimal during precipitation ; vapour pressure deficiency will be very small as the relative humidity is expected to be close to 100% during raining..					
S_{s1}^t root uptake	Ref: [73] [120] Root uptake calculation requires transpiration which needs to be determined in evapotranspiration calculation, prior to calling moisture coefficient routines in the program. Root uptake [$m^3/m^3/s$] or [/s] at a layer is given by: $S_p = T_p\, \alpha(\psi)\, b(z)$ Tp – transpiration rate [$m^3/m^3/s$] or [/s] $\alpha(\psi)$ - stress response function (Feddes 1978) of value between 0 and 1 and given by the current value of matric potential. 	m^3/m^3 /s	Wilt	ψ Layer #		

	h1 - oxygen deficiency limit -0.1m to -0.15 m (taken as -0.1) h2-h3 optimum no stress condition -0.25m and −3.2m (to adapt to the quick drain condition of green roof higher end of the limits as given in Feddes 1978 is taken) h4 – wilting point limit ; some draught resistant plants can have a very low limit. Published values range from -80m to -160m. If no user input a value -80m is taken b(z) – fraction of root uptake along the root zone depth A linear distribution along the top four layers is taken. A more detailed 's' shaped function is not used as the artificial conditions in a green roof is expected to produce more root densities evenly spread along the depths. b(1) = (soilHtS1 + soilHtS5 / 4) / soilHt , etc					
$e^t_{s1_m}$ soil vapour pressure in m	$e_{s1\_m} = \dfrac{e_{s1}}{9.81*1000}$ soil vapour pressure e_{s1} in Pa $e_{s1} = e_{s1\_sat} * RH$ Saturated vapour pressure [Pa] in terms of temperature t °C is given by: $e_{s1\_sat} = 610.8 * e^{\left[\frac{17.27t}{t+237.3}\right]}$ Relative Humidity RH $= e^{\left[\frac{\psi Mg}{RT}\right]}$ ψ- matric potential [m] M- molar mass of water 0.018015 kg mol^{-1} g- acceleration due to gravity 9.81 ms^{-2} R- universal gas constant 8.314 J moil^{-1} K^{-1} T – soil temperature in K		m		ψ T	
	Evapotranspiration: [45] Potential evapotranspiration by Penman-Monteith combination $ET_o = ET_{rad} + ET_{aero} = \dfrac{1}{\lambda}\left[\dfrac{\Delta(R_n - G)}{\Delta + \gamma\left(1 + \frac{r_c}{r_a}\right)} + \dfrac{\frac{\rho\,c_p}{r_a}(e_a - e_d)}{\Delta + \gamma\left(1 + \frac{r_c}{r_a}\right)}\right]$ λ-latent heat of vaporization[J/kg], given by: $\lambda = 1e6(2.501 - 2.361e - 3\ t)$		m^3/m^2/s			

	t temperature in canopy air in °C						
	Δ-slope of saturation vapour pressure curve [Pa/°C] $$\Delta = \frac{4098\ e_a}{(t + 237.3)^2}$$ e_a is saturation vapour pressure [Pa]given by: $$e_a = 610.8 * e^{\left[\frac{17.27t}{t+237.3}\right]}$$ e_d- actual air vapour pressure (canopy air)[Pa] r_c - crop canopy resistance [s m^{-1}] r_a - aerodynamic resistance [s m^{-1}] γ-thermodynamic constant gamma [Pa/°C] given by: $$\gamma = \frac{1005}{0.622} * \frac{P}{\lambda}$$ P- atmospheric pressure [Pa] cp specific heat of moist air 1013 [J/kg K] Rn – solar radiation reaching soil top [W/m^2] G – conduction heat down ward at soil surface [W/m^2] Evapotranspiration is divided into transpiration (T$_p$) and evaporation (E$_p$)as follows: $T_p = ET.SCF$ $E_p = ET.(1 - SCF)$ SCF – soil cover fraction given by: $$SCF = 1 - e^{-\frac{k}{LAI}}$$ k-extinction coefficient [-]						

Notes

1. As per definition Cθ is time varying unlike for the comparable term in thermal side, strictly speaking it should have both p-value and f-value. But only one value is used, to help cancel terms in equation manipulation. For both m coefficient and n coefficient it is calculated for time step t. To see the stability issue during code testing stage
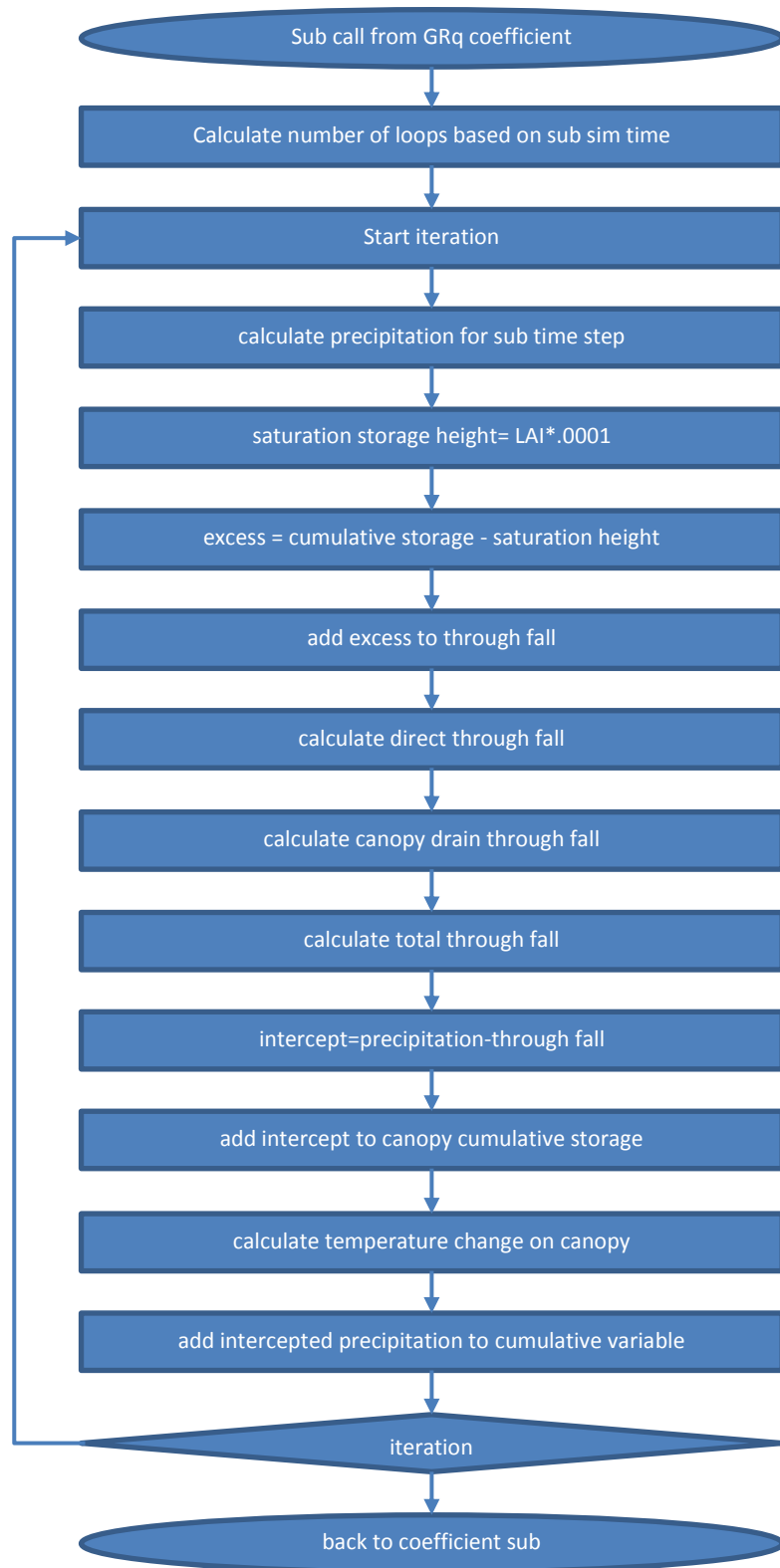
Flow chart of subroutine calculating precipitation-interception for alternative calculation of P0 (Stull 2011)

2. Soil mid layers (S2, S3, S4)

Moisture Balance

$$C\theta \frac{\partial \psi}{\partial t} = \frac{\partial}{\partial z}\left[K\Psi\left[\frac{\partial \psi}{\partial z} + 1\right] + KT\frac{\partial T}{\partial z}\right] - S$$

All terms are similar to soil top layer. Moisture exchange with air is absent.

$$-\left[\alpha\frac{K\Psi^{t+\Delta t}_{s1s2}}{S1\_S2}\right]\psi^{t+\Delta t}_{s1}$$

$$+\left[\frac{S2\,C\theta^t_{s2}}{\Delta t} + \alpha\frac{K\Psi^{t+\Delta t}_{s1s2}}{S1\_S2} + \alpha\frac{K\Psi^{t+\Delta t}_{s2s3}}{S2\_S3}\right]\psi^{t+\Delta t}_{s2}$$

$$-\left[\alpha\frac{K\Psi^{t+\Delta t}_{s2s3}}{S2\_S3}\right]\psi^{t+\Delta t}_{s3}$$

$$=$$

$$\left[(1-\alpha)\frac{K\Psi^t_{s1s2}}{S1\_S2}\right]\psi^t_{s1}$$

$$+\left[\frac{S2\,C\theta^t_{s2}}{\Delta t} - (1-\alpha)\frac{K\Psi^t_{s1s2}}{S1\_S2} - (1-\alpha)\frac{K\Psi^t_{s2s3}}{S2\_S3}\right]\psi^t_{s2}$$

$$+\left[(1-\alpha)\frac{K\Psi^t_{s2s3}}{S2\_S3}\right]\psi^t_{s3}$$

$$+(1-\alpha)K\Psi^t_{s1s2} - (1-\alpha)K\Psi^t_{s2s3} + \alpha K\Psi^{t+\Delta t}_{s1s2} - \alpha K\Psi^{t+\Delta t}_{s2s3}$$

$$+(1-\alpha)\frac{KT^t_{s1s2}}{S1\_S2}\left(T^t_{s1} - T^t_{s2}\right) - (1-\alpha)\frac{KT^t_{s2s3}}{S2\_S3}\left(T^t_{s2} - T^t_{s3}\right)$$

$$+\alpha\frac{KT^{t+\Delta t}_{s1s2}}{S1\_S2}\left(T^{t+\Delta t}_{s1} - T^{t+\Delta t}_{s2}\right) - \alpha\frac{KT^{t+\Delta t}_{s2s3}}{S2\_S3}\left(T^{t+\Delta t}_{s2} - T^{t+\Delta t}_{s3}\right)$$

$$-(1-\alpha)S^t_{s2}\,S2 - \alpha S^{t+\Delta t}_{s2}\,S2$$

CV4: Soil Middle layer

221

All terms are previously defined

(m22)	$-\alpha\frac{K\Psi_{S1S2}^{t+\Delta t}}{S1\_S2}$							
Time invariant data	**Defining Equations and Remarks**	**Initial Value**	**Unit**	**Required data**			**Couple Info**	
				Input	**Param eters**	**Calcul ated Variab les**		
Time variant data	**Defining Equations and Remarks**	**Initial Value**	**Unit**	**Required data**			**Couple Info**	
				Input	**Param eters**	**Calcul ated Variab les**		

(m23)	$\frac{S2\,C\theta_{S2}^{t}}{\Delta t}+\alpha\frac{K\Psi_{S1S2}^{t+\Delta t}}{S1\_S2}+\alpha\frac{K\Psi_{S2S3}^{t+\Delta t}}{S2\_S3}$							
Time invariant data	**Defining Equations and Remarks**	**Initial Value**	**Unit**	**Required data**			**Couple Info**	
				Input	**Param eters**	**Calcul ated Variab les**		
Time variant data	**Defining Equations and Remarks**	**Initial Value**	**Unit**	**Required data**			**Couple Info**	
				Input	**Param eters**	**Calcul ated Variab les**		

(m24)	$-\alpha\frac{K\Psi_{S2S3}^{t+\Delta t}}{S2\_S3}$							
Time invariant data	**Defining Equations and Remarks**	**Initial Value**	**Unit**	**Required data**			**Couple Info**	
				Input	**Param eters**	**Calcul ated Variab les**		

Time variant data	Defining Equations and Remarks	Initial Value	Unit	Required data			Couple Info
				Input	Parameters	Calculated Variables	

'n' coefficients use time varying parameters one time step prior to that in 'm' coefficients

In addition, wherever present, multipliers α change to 1-α.

Sign change for all terms except for the one carries Δt

$$n22 = (1-\alpha)\frac{K\Psi^t_{s1s2}}{S1\_S2}$$

$$n23 = \frac{S2\ C\theta^t_{s2}}{\Delta t} - \alpha\frac{K\Psi^t_{s1s2}}{S1\_S2} - \alpha\frac{K\Psi^t_{s2s3}}{S2\_S3}$$

$$n24 = (1-\alpha)\frac{K\Psi^t_{s2s3}}{S2\_S3}$$

(q2)	$+(1-\alpha)K\Psi^t_{s1s2} - (1-\alpha)K\Psi^t_{s2s3} + \alpha\ K\Psi^{t+\Delta t}_{s1s2} - \alpha\ K\Psi^{t+\Delta t}_{s2s3}$ $-(1-\alpha)\frac{KT^t_{s1s2}}{S1\_S2}(T^t_{s1} - T^t_{s2}) + (1-\alpha)\frac{KT^t_{s2s3}}{S2\_S3}(T^t_{s2} - T^t_{s3})$ $+\alpha\frac{KT^{t+\Delta t}_{s1s2}}{S1\_S2}(T^{t+\Delta t}_{s1} - T^{t+\Delta t}_{s2}) - \alpha\frac{KT^{t+\Delta t}_{s2s3}}{S2\_S3}(T^{t+\Delta t}_{s2} - T^{t+\Delta t}_{s3})$ $-(1-\alpha)\ S2S^t_{s2} - \alpha S2\ S^{t+\Delta t}_{s2}\quad -$

Time invariant data	Defining Equations and Remarks	Initial Value	Unit	Required data			Couple Info
				Input	Parameters	Calculated Variables	

223

3. Soil bottom layer (S5)

Moisture Balance

$$C\theta \frac{\partial \psi}{\partial t} = \frac{\partial}{\partial z}\left[K\Psi \left[\frac{\partial \psi}{\partial z} + 1 \right] + KT \frac{\partial T}{\partial z} \right] - S$$

All terms are similar to soil mid layers, except for drainage term

<p style="text-align:center;">Coefficient form for S5</p>

$$-\left[\alpha \frac{K\Psi_{s4s5}^{t+\Delta t}}{S4\_S5}\right]\psi_{s4}^{t+\Delta t}$$

$$+\left[\frac{S5\,C\theta_{s5}^{t}}{\Delta t} + \alpha\frac{K\Psi_{s4s5}^{t+\Delta t}}{S4\_S5} + \alpha\frac{K\Psi_{s5z}^{t+\Delta t}}{S5\_X}\right]\psi_{s5}^{t+\Delta t}$$

$$-\left[\alpha\frac{K\Psi_{s5z}^{t+\Delta t}}{S5\_X}\right]\psi_{z}^{t+\Delta t}$$

$$=$$

$$\left[(1-\alpha)\frac{K\Psi_{s4s5}^{t}}{S4\_S5}\right]\psi_{s4}^{t}$$

$$+\left[\frac{S5\,C\theta_{s5}^{t}}{\Delta t} - (1-\alpha)\frac{K\Psi_{s4s5}^{t}}{S4\_S5} - (1-\alpha)\frac{K\Psi_{s5z}^{t}}{S5\_X}\right]\psi_{s5}^{t}$$

$$+\left[(1-\alpha)\frac{K\Psi_{s5z}^{t}}{S5\_X}\right]\psi_{z}^{t}$$

$$+(1-\alpha)K\Psi_{s4s5}^{t} - (1-\alpha)K\Psi_{s5z}^{t} + \alpha K\Psi_{s4s5}^{t+\Delta t} - \alpha K\Psi_{s5z}^{t+\Delta t}$$

$$+(1-\alpha)\frac{KT_{s4s5}^{t}}{S4\_S5}(T_{s4}^{t} - T_{s5}^{t}) - (1-\alpha)\frac{KT_{s5z}^{t}}{S5\_X}(T_{s5}^{t} - T_{z}^{t})$$

$$+\alpha\frac{KT_{s4s5}^{t+\Delta t}}{S4\_S5}(T_{s4}^{t+\Delta t} - T_{s5}^{t+\Delta t}) - \alpha\frac{KT_{s5z}^{t+\Delta t}}{S5\_X}(T_{s5}^{t+\Delta t} - T_{z}^{t+\Delta t})$$

$$-(1-\alpha)S_{s5}^{t}\,S5 - \alpha S_{s5}^{t+\Delta t}\,S5$$

CV5: Soil Lower layer
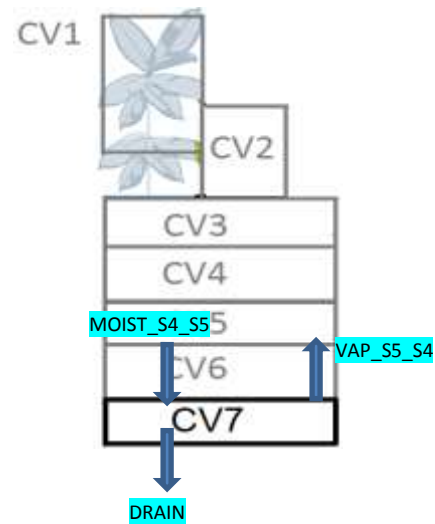
All terms are previously defined except for drainage term

| (n56) | $\frac{S5\,C\theta_{S5}^t}{\Delta t} + \alpha\frac{K\Psi_{S4S5}^{t+\Delta t}}{S4\_S5} + \alpha\frac{K\Psi_{S5\,x}^{t+\Delta t}}{S5\_X}$ | | | | | | |

Time invariant data	Defining Equations and Remarks	Initial Value	Unit	Required data			Couple Info
				Input	Parameters	Calculated Variables	
X height of drainage layer	FLL [12]recommends min aggregate layer height 6 cm	0.08	m				

Time variant data	Defining Equations and Remarks	Initial Value	Unit	Required data			Couple Info
				Input	Parameters	Calculated Variables	
$K\Psi_{S5\,x}^{t+\Delta t}$	1. Ref: [121] Example of hydraulic conductivity of sandy gravel 4.5e-4 to 5e-4 m/s 2. Ref: [122] Adapting one of many best fit equations for hydraulic conductivity [K(i)] in terms of hydraulic gradient (i) for coarse and fine aggregates. Aggregate no: 8 Type of aggregate: Gravel Size range (mm): 9.5 to 19.1 Hydraulic conductivity (m/day): $K = 9003\,i^{-0.4}$ hydraulic gradient across drainage layer is determined as i=* (Abs(matricPotGRp(5)) / SoilHtS5Gr)	0.0005	m/s				

Appendix 4: Integration of new green roof model with ESP-r; ESP-r modifications

The new green roof model is integrated with ESP-r in a manner by which it modifies, when called, the ESP-r's boundary condition of an exposed roof surface to that defined by the green roof model. Accordingly a few modifications are required at the ESP-r program. This appendix presents information in addition to the description of ESP-r integration in section 3.4

Table A4: Alterations in ESP-r facilities for green roof model integration

No	Source code location	ESP-r modules	Type of change
1	esrucom/egeometry.F	EGOMIN EMKGEO GEOREAD	EGOMIN and GEOREAD read zone geometry data from user constructed file; EMKGEO writes GEN type of geometry file; Changes involve adding "GREEN_R' as surface attributes concerning 'other sides' of surfaces in these routines;
2	esrucom/emkcfg.F	EMKCFG	This routine is to create a configuration file; it calls a routine CONXINF which return a string variable CXSTR; green roof related lines added where it identifies the concerned surface attribute
3	esrucom/emkcfgg.F	EMKCFG	GTK system related copy of the above which is for X11
4	esrucom/esru_misc.F	SURADJ	This routine return information about connection between surfaces; adding lines to return description concerning bottom of green roof temperature
5	esrucom/esystem.F	ERSYS_mmode	This routine reads a system configuration file which defines building and plant details for simulation; it calls a routine CONXINFO which return a string variable CXSTR; green roof related lines added where it identifies the concerned surface attribute

Table A4 (Contd): Alterations in ESP-r facilities for green roof model integration

6	esrudbm/esystemg.F	ERSYS_mmode CONXINFO	GTK system related copy of the above which is for X11
7	esruprj/edgeo.F	EDZONE EDSURA EZIPIN	EDZONE is the main routine for editing zone attributes and saving to a geometry file; EDSURA edits zone surface attributes in a common block G5; EZIPIN reads zip format geometry data into common blocks; in all these routines lines added to accommodate additional surface attribute namely GREEN_R
8	esruprj/edonecon.F	EDACONN CONXMENU	EDACONN edits connection attributes in variables in common block C3; CONXMENU return description of interconnection description in string variable CXITM; lines added to include green roof attribute
9	esruprj/edtopol.F	EDCONN CONFIG ESACON	These routines are part of a collection of support facilities for editing model topology lists; lines added for editing checking and clearing green roof related surface attribute

Appendix 5: Sensitivity analysis results

A sensitivity analysis was conducted for the model to evaluate the comparative influence of the model inputs on the model output, the method and the results of which are described in section 4.8, to give a comparative illustration the charts in section 4.8 have been scaled to a common y-axis size. Some of the charts presented in chapter 4, show almost no response of the output for the changes in the particular input. This appendix presents the same results of the sensitivity analysis, but without any scaling, illustrating that all input variables' variations influence the output, although in varying degrees.
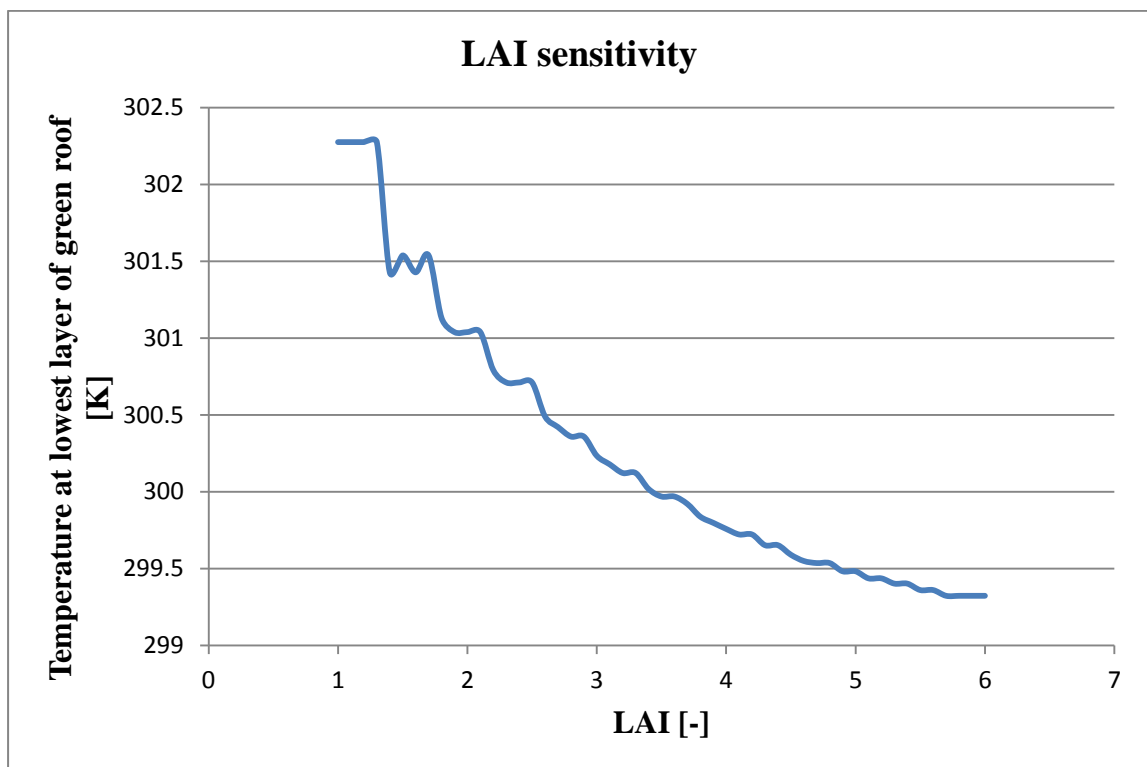
Figure A5.1: Sensitivity analysis results for LAI
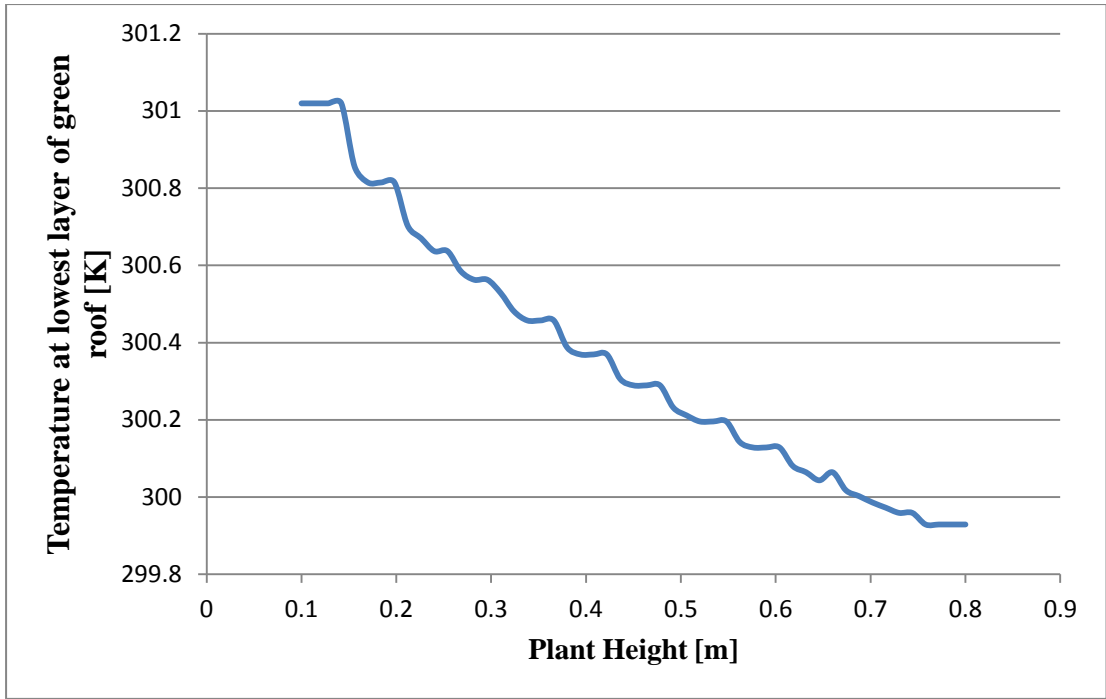
Figure A5.2: Sensitivity analysis results for plant height
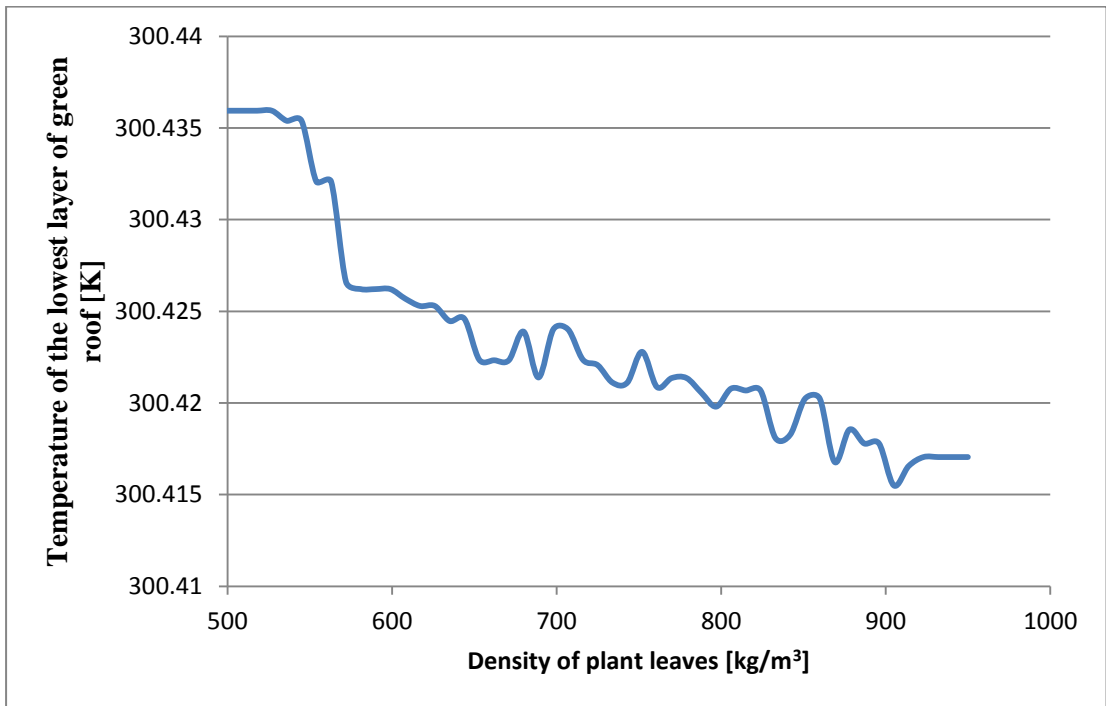
Figure A5.3: Sensitivity analysis results for density of plant leaves
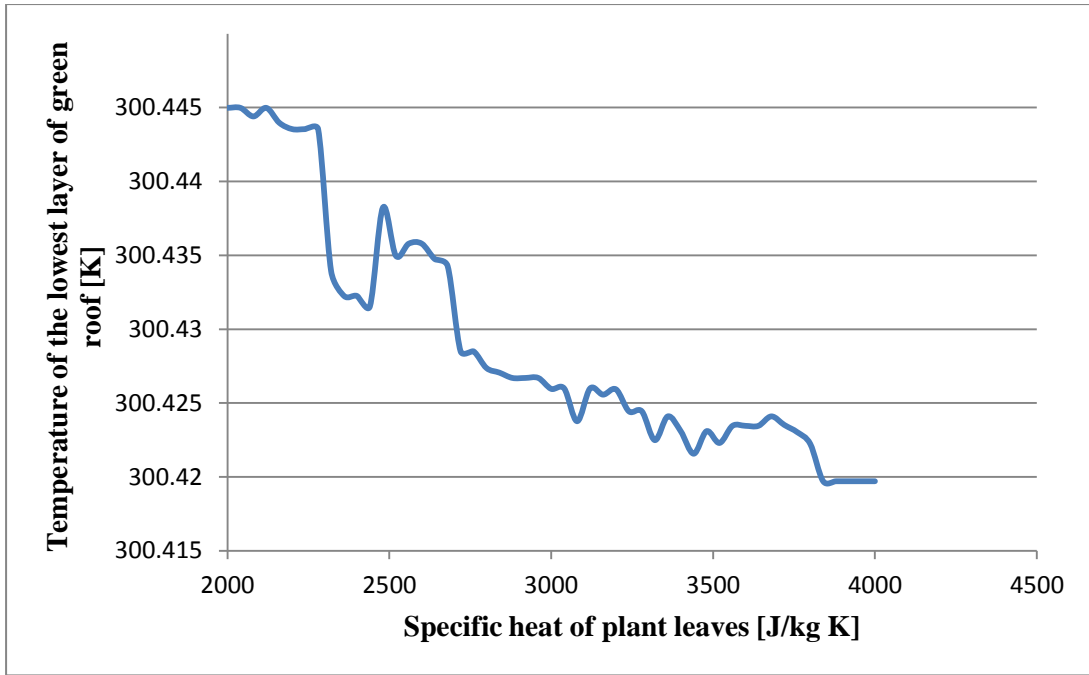
Figure A5.4: Sensitivity analysis results for specific heat of plant leaves
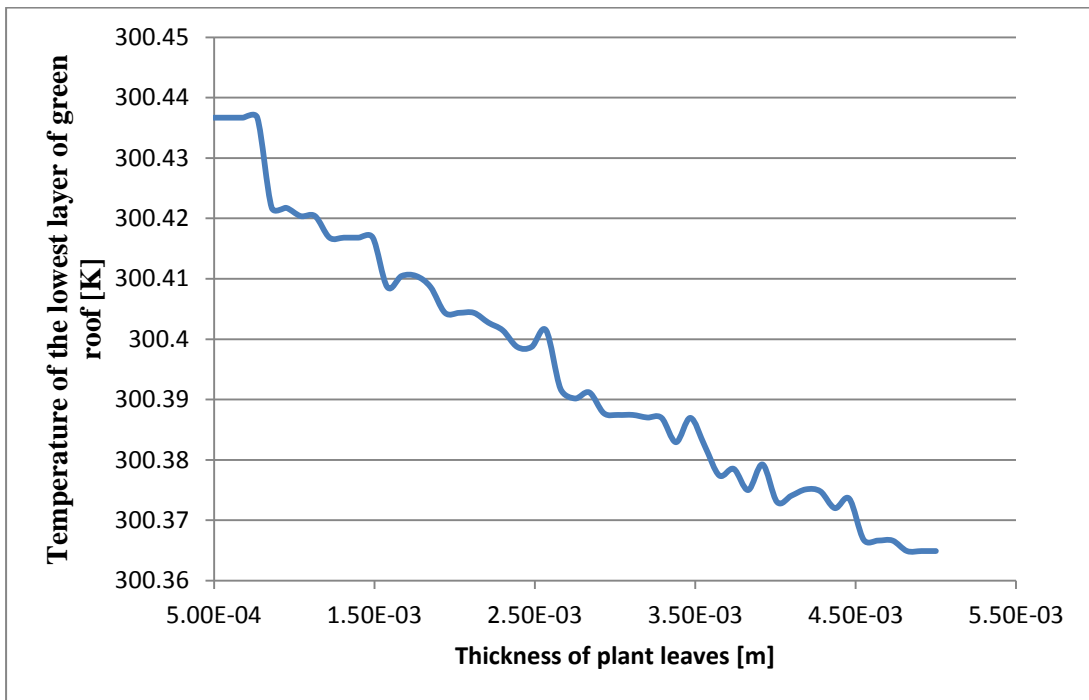
Figure A5.5: Sensitivity analysis results for thickness of plant leaves
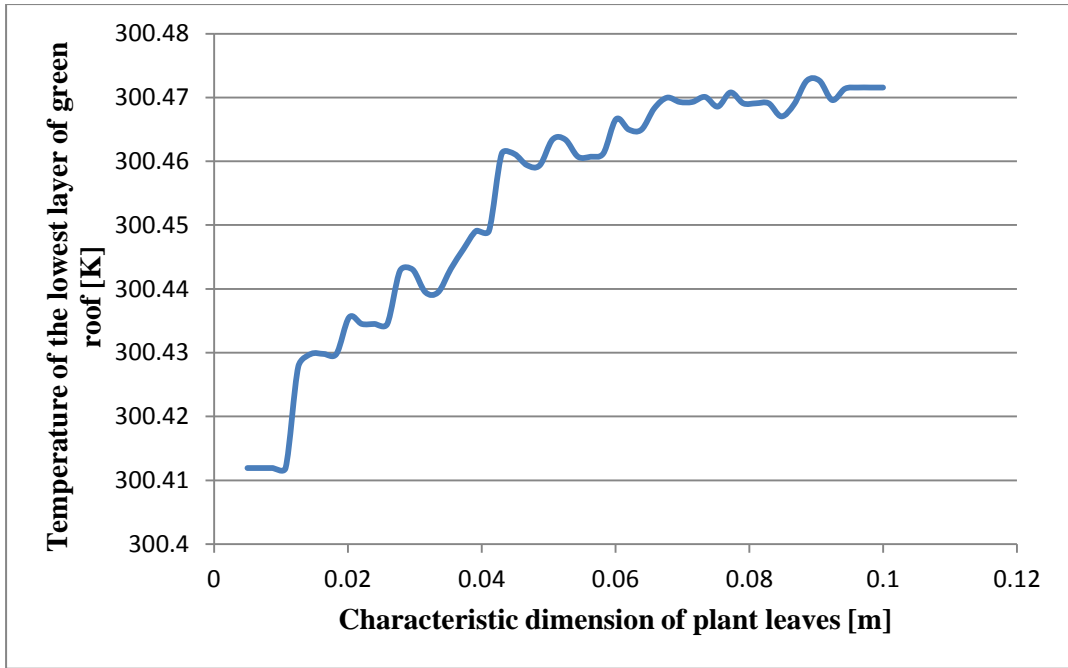
Figure A5.6: Sensitivity analysis results for width of plant leaves
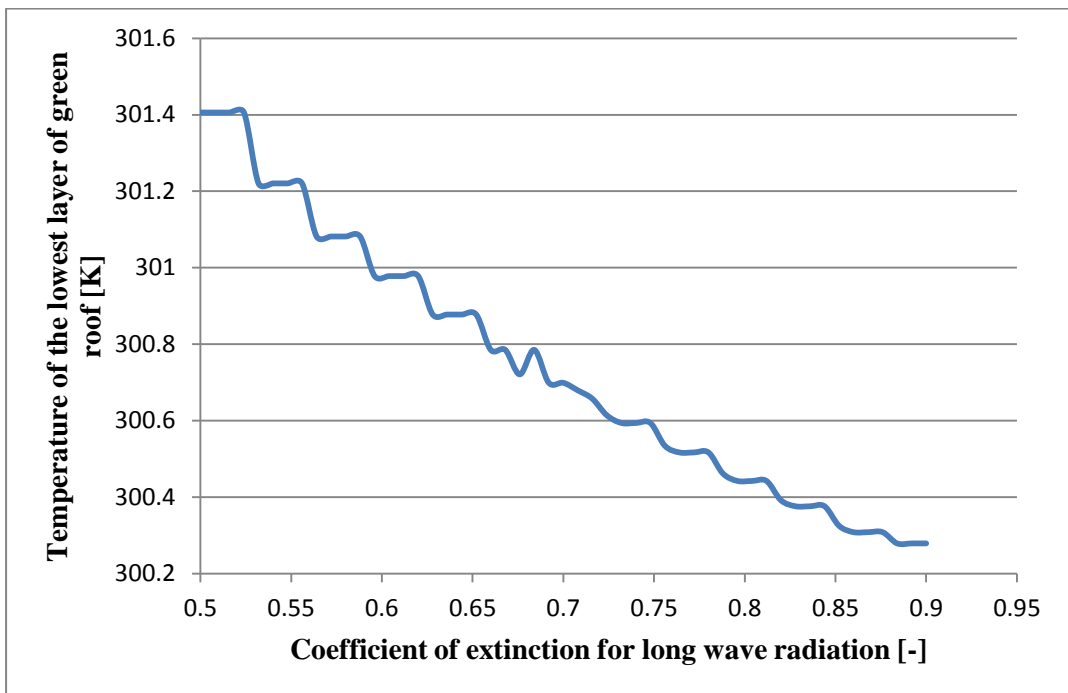
Figure A5.7: Sensitivity analysis results for coefficient of extinction for long wave radiation

231
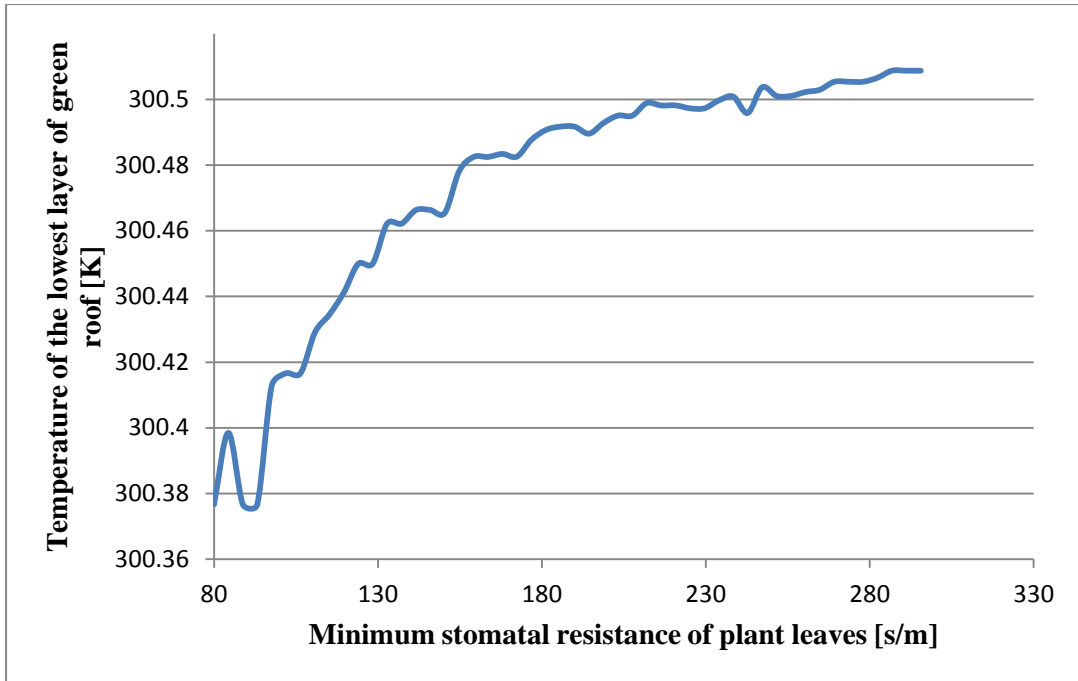
Figure A5.8: Sensitivity analysis results for minimum stomatal resistance of plant
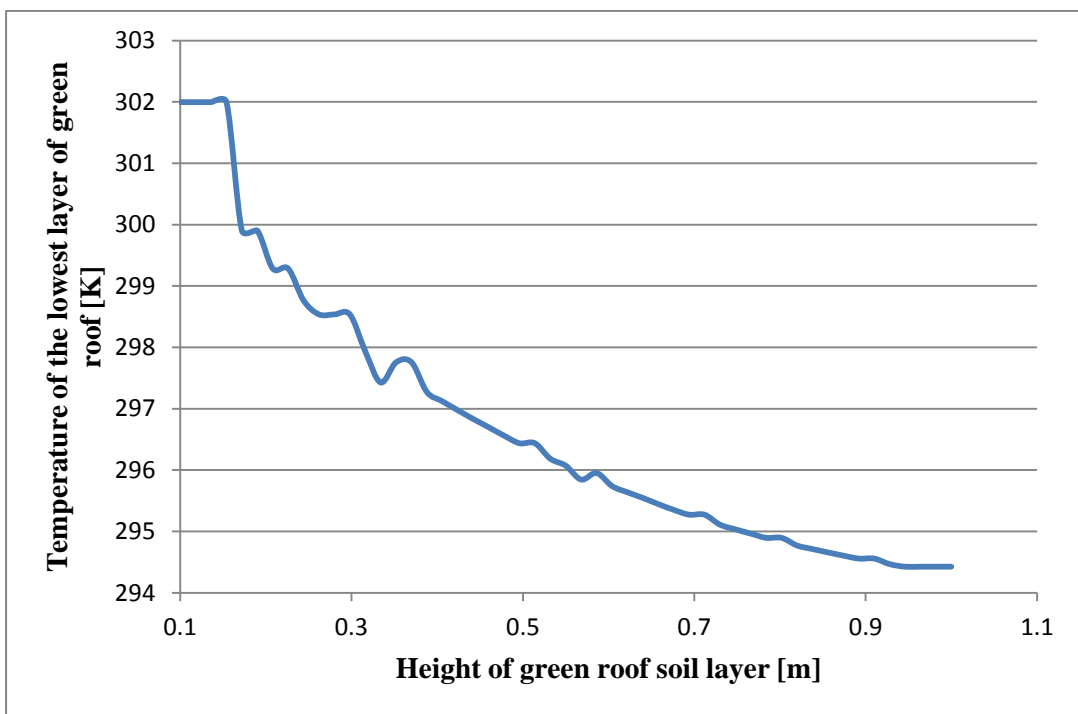
Figure A5.9: Sensitivity analysis results for soil height
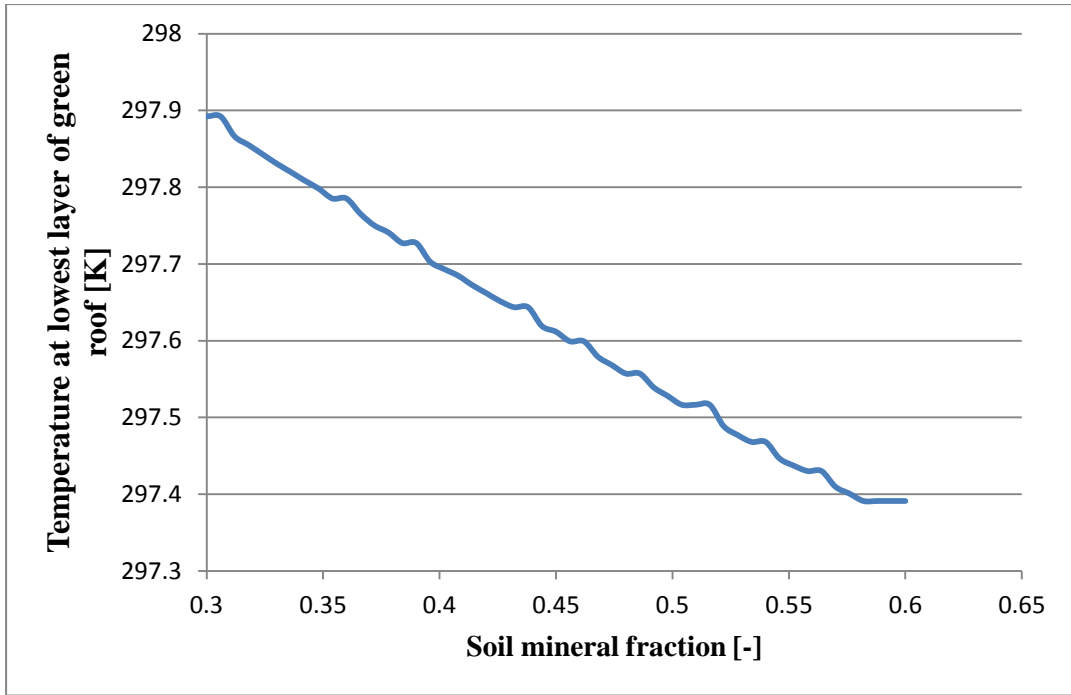
Figure A5.10: Sensitivity analysis results for soil mineral fraction
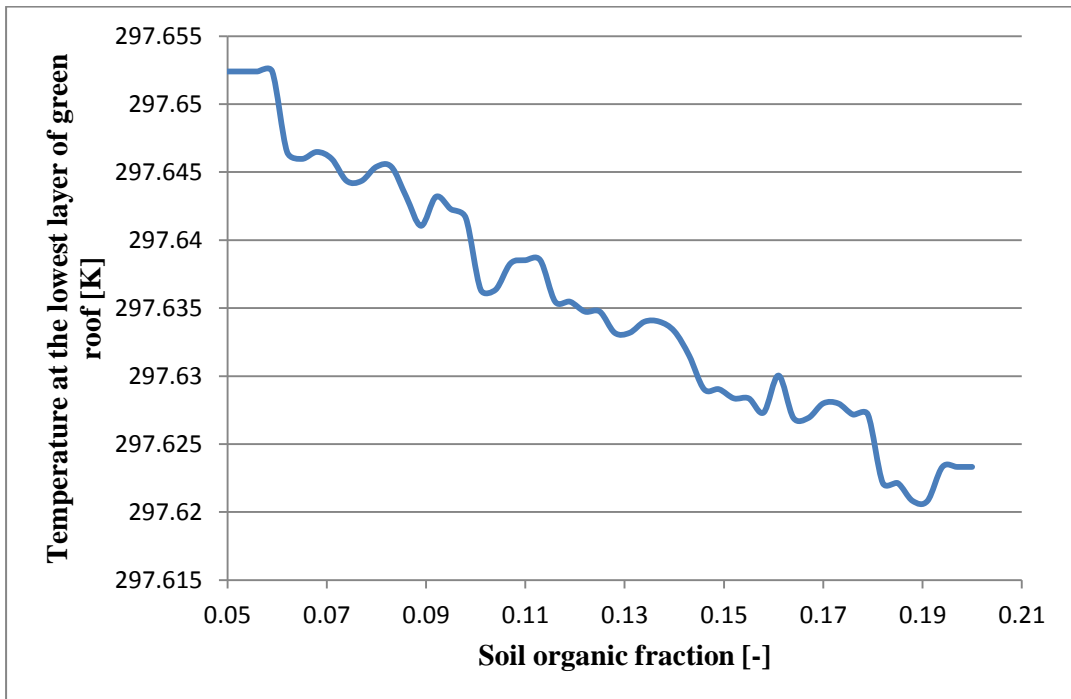
Figure A5.11: Sensitivity analysis results for soil organic fraction
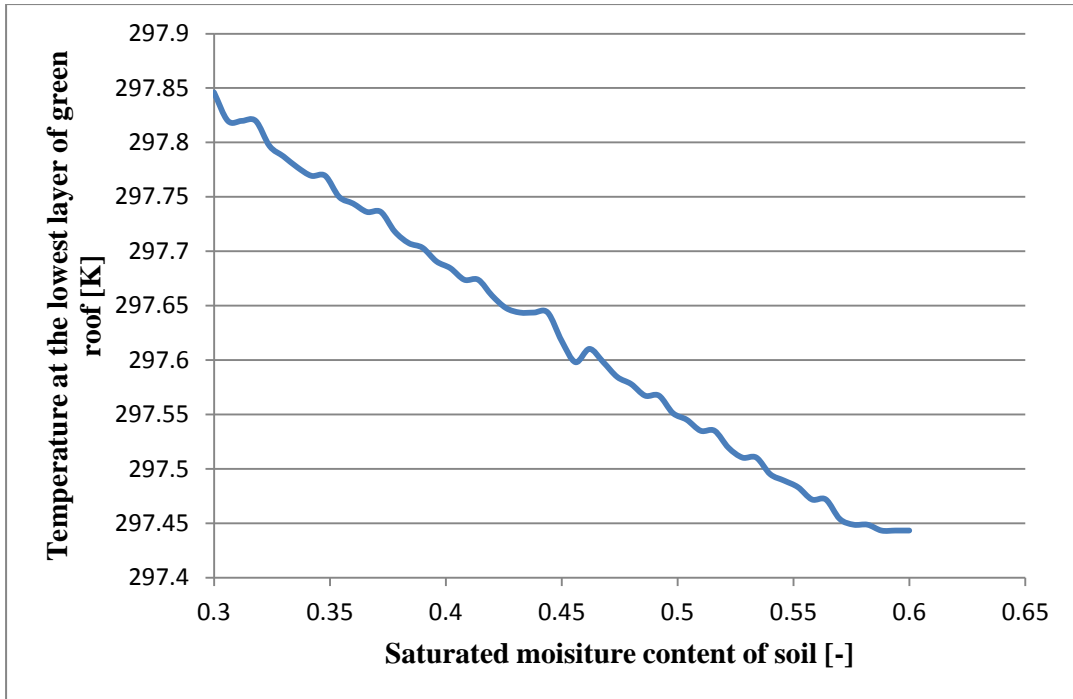
Figure A5.12: Sensitivity analysis results for soil's saturated moisture content
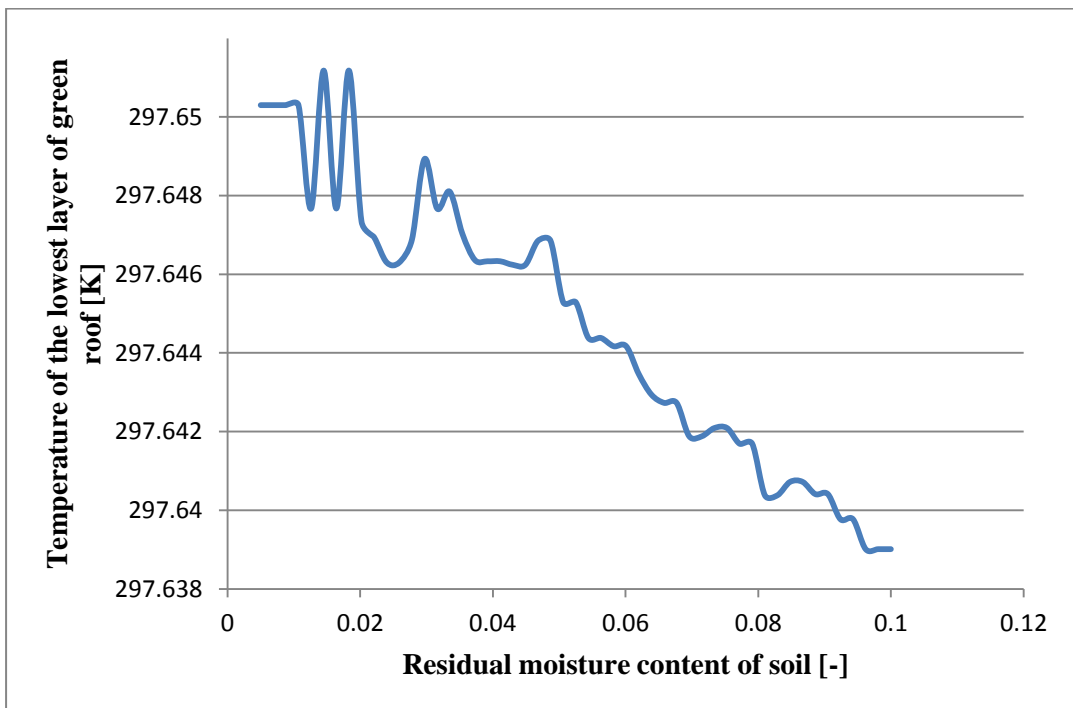
Figure A5.13: Sensitivity analysis results for soil's residual moisture content
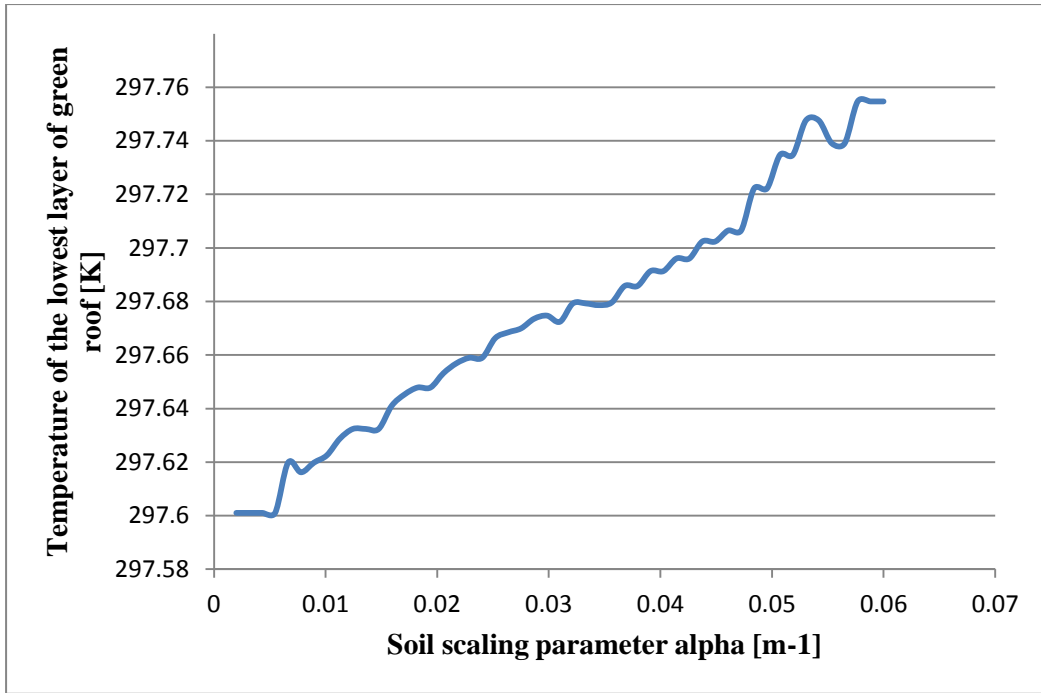
Figure A5.14: Sensitivity analysis results for soil's alpha index
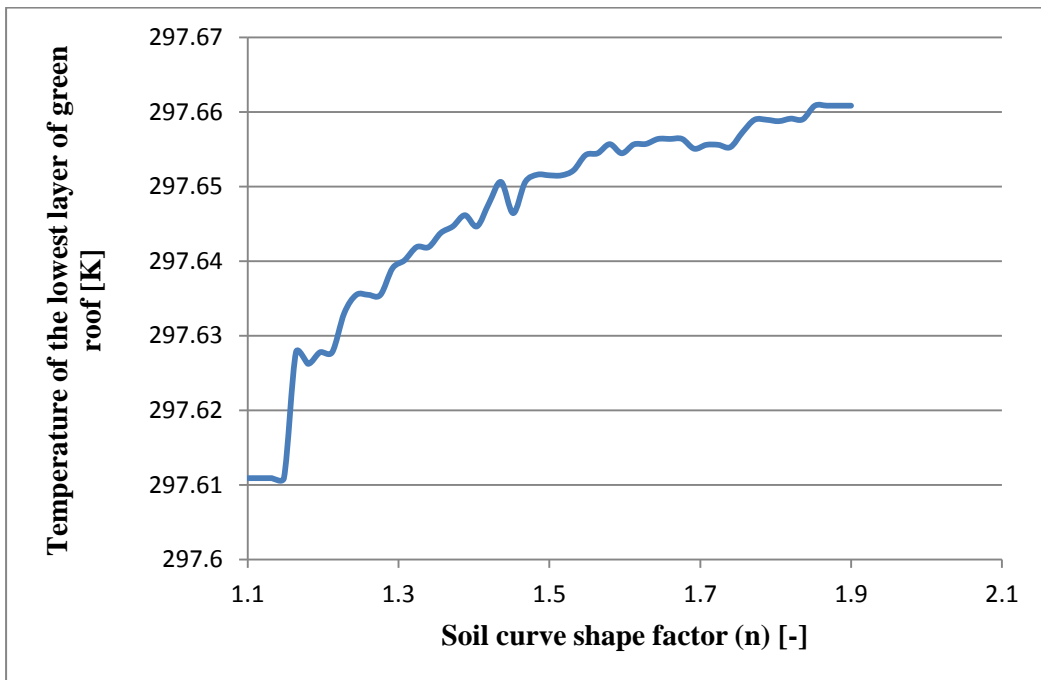
Figure A5.15: Sensitivity analysis results for soil's 'n' index
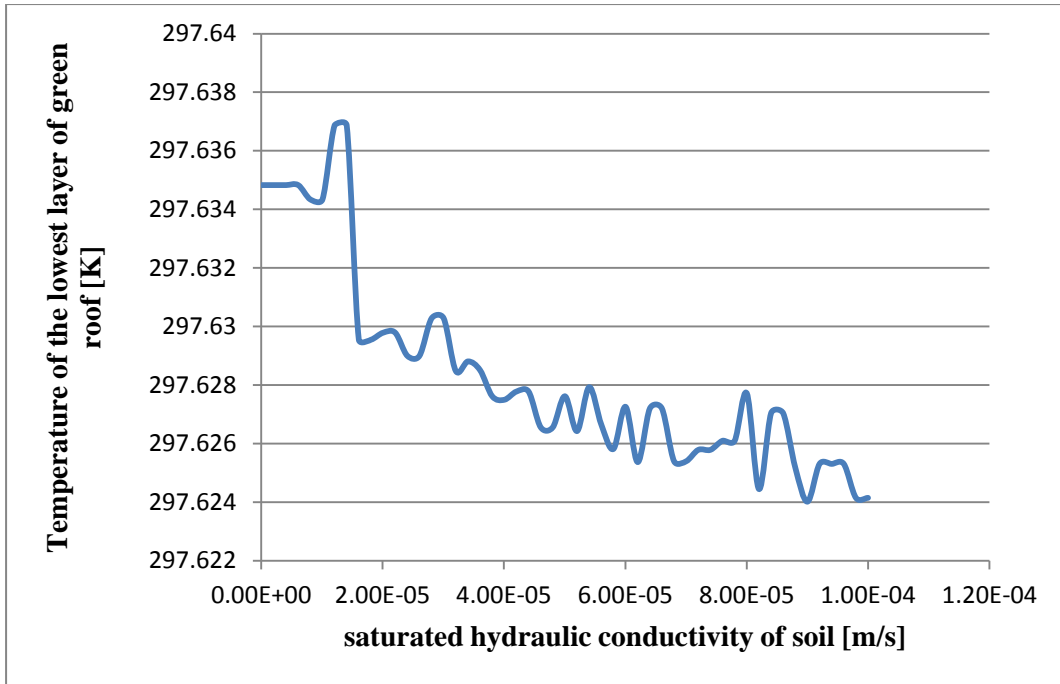
Figure A5.16: Sensitivity analysis results for saturated hydraulic conductivity of soil
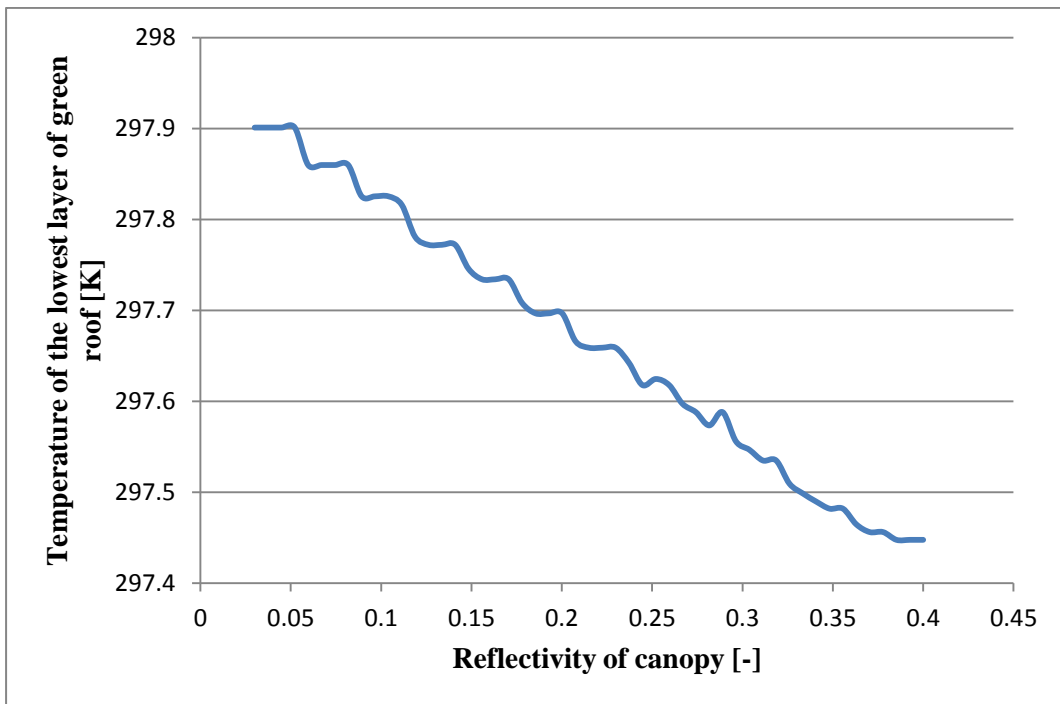
Figure A5.17: Sensitivity analysis results for reflectivity of canopy
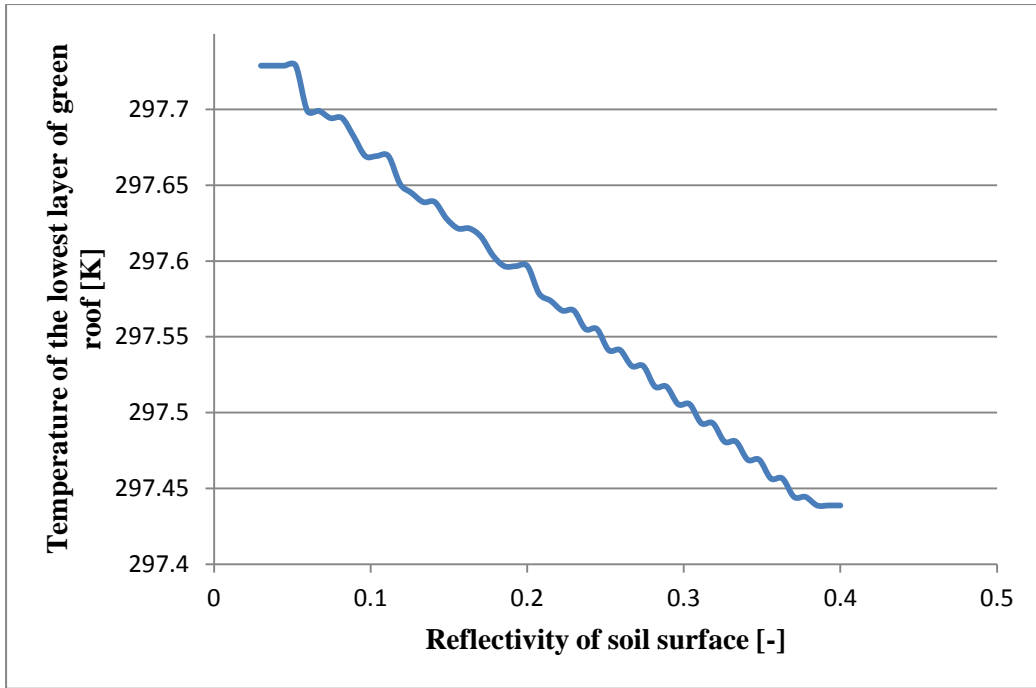
Figure A5.18: Sensitivity analysis results for soil's reflectivity
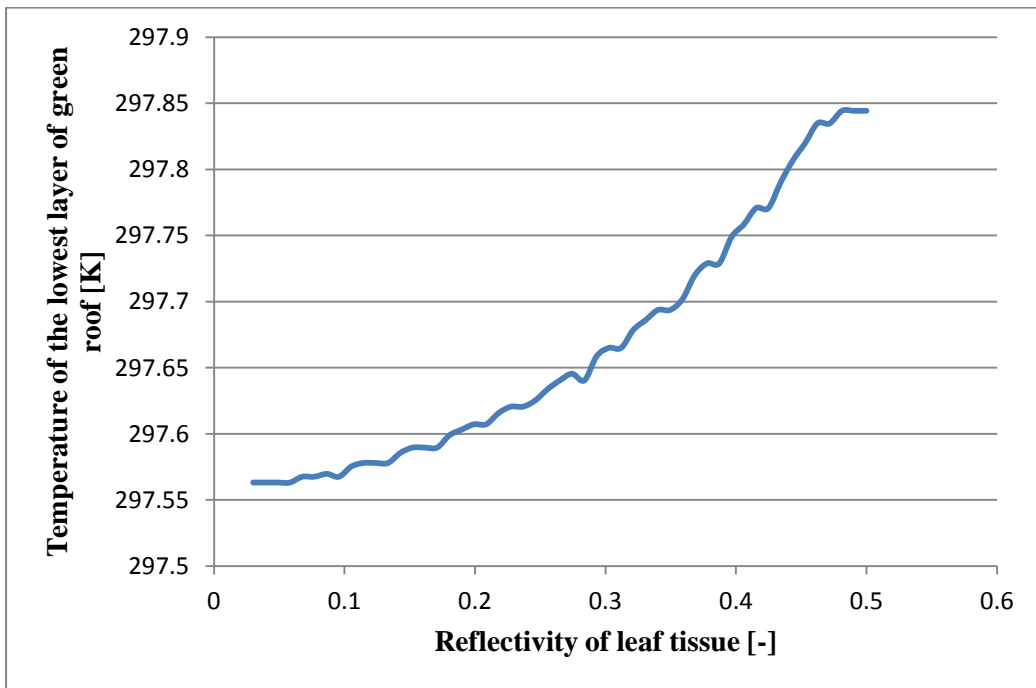
Figure A5.19: Sensitivity analysis results for leaf tissue's reflectivity
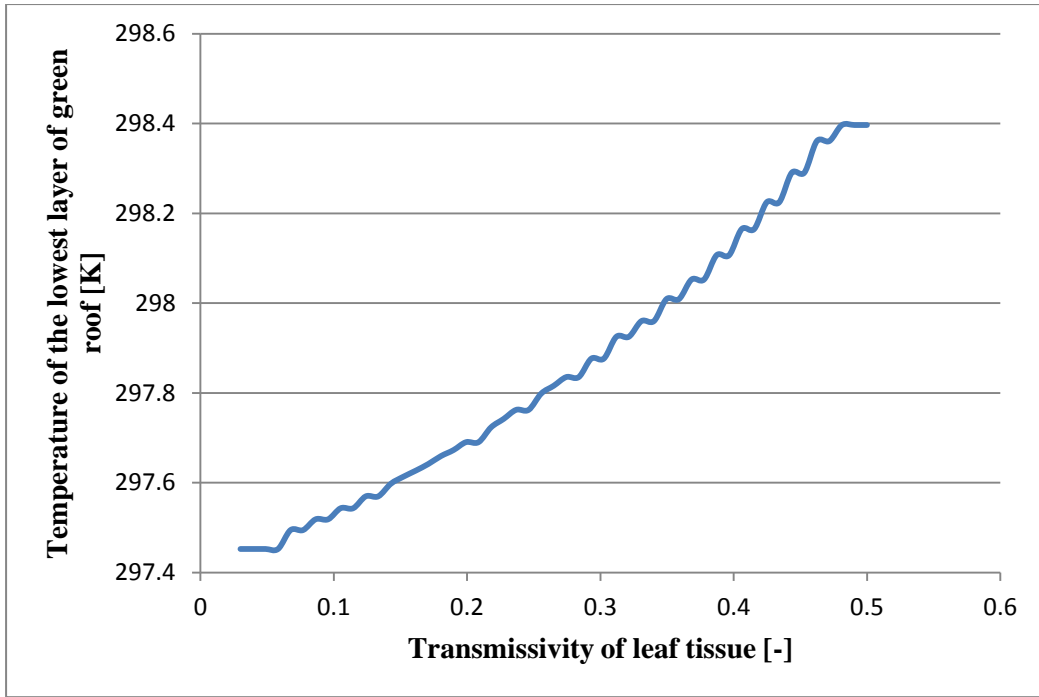
Figure A5.20: Sensitivity analysis results for transmissivity of leaf tissue
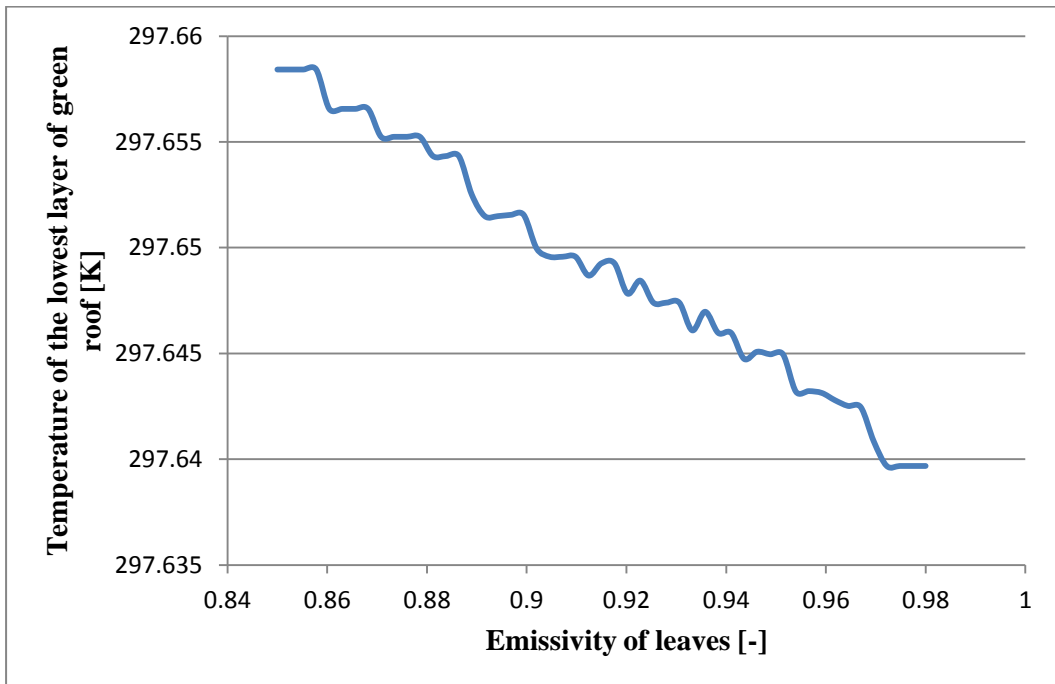
Figure A5.21: Sensitivity analysis results for emissivity of leaves
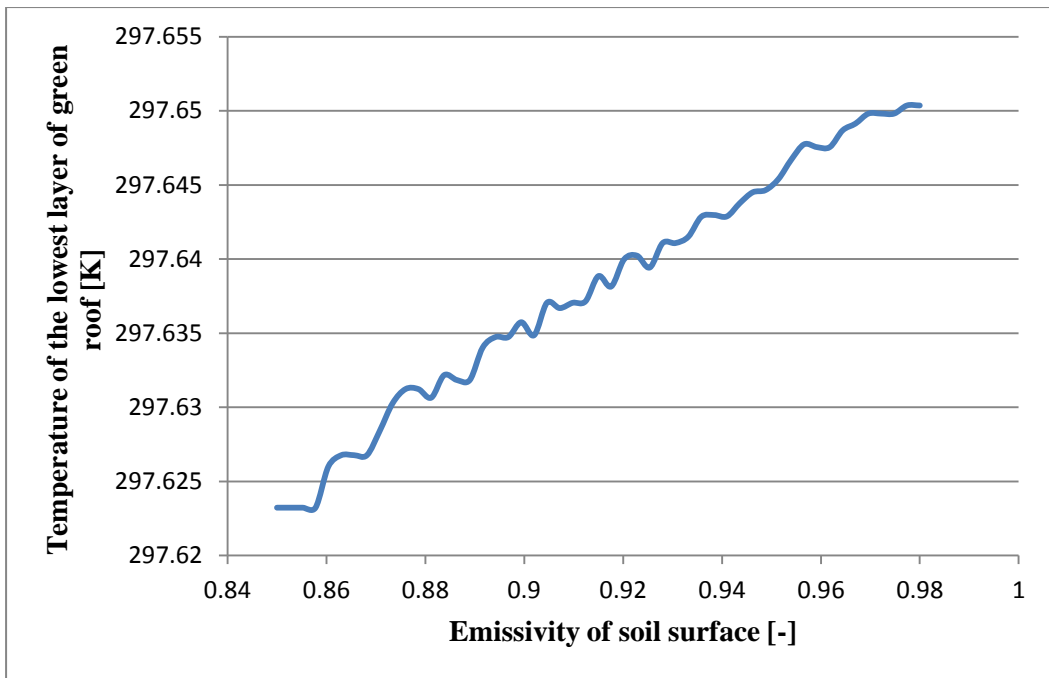
Figure A5.22: Sensitivity analysis results for emissivity of soil surface

Appendix 6: Thermal validation test1 results in detail

Thermal validation results of the new green roof model for the test dates of August 17-18, 2014 have been presented in section 5.7.1, figure 5.18,which presents the evaluation of the nine temperatures (seven control volumes and two boundary conditions). Although numerical indices such as RMSD have been provided in section 5.7 the comparison of the measured and simulated charts in figure 5.18 is not easy because of the high number of data displayed. This appendix presents the results of the same validation study in more detail for illutration purposes. For each of the control volumes, the measures and simulated temperatures are provided in separate charts.
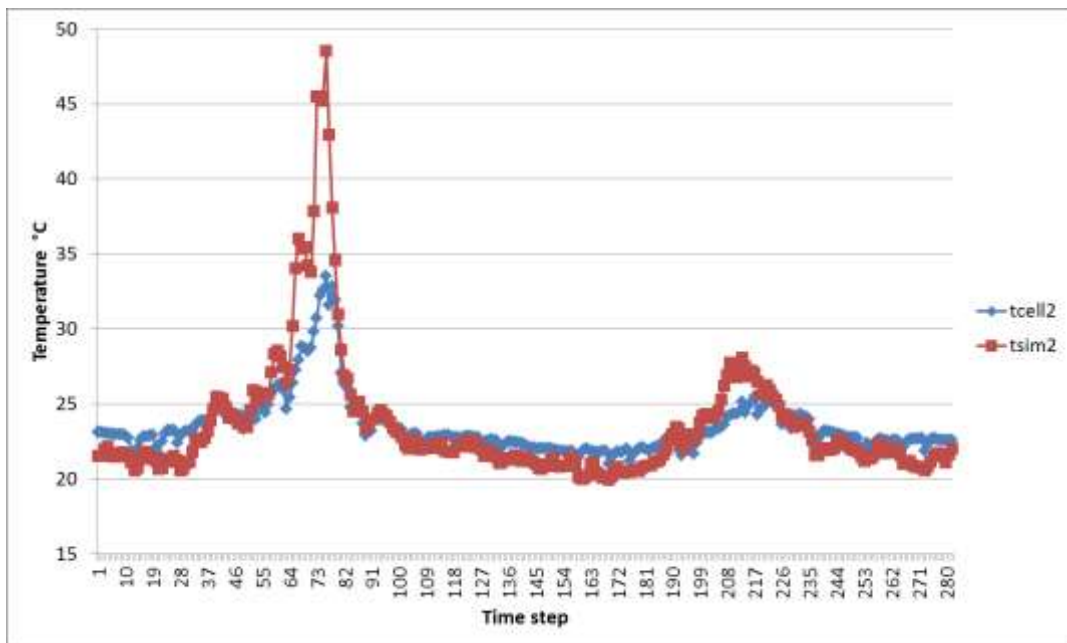
Figure A6.1: Comparison of measured and simulated temperatures of control volume 1- Plant, in the thermal validation test 1 (Aug 17-18)
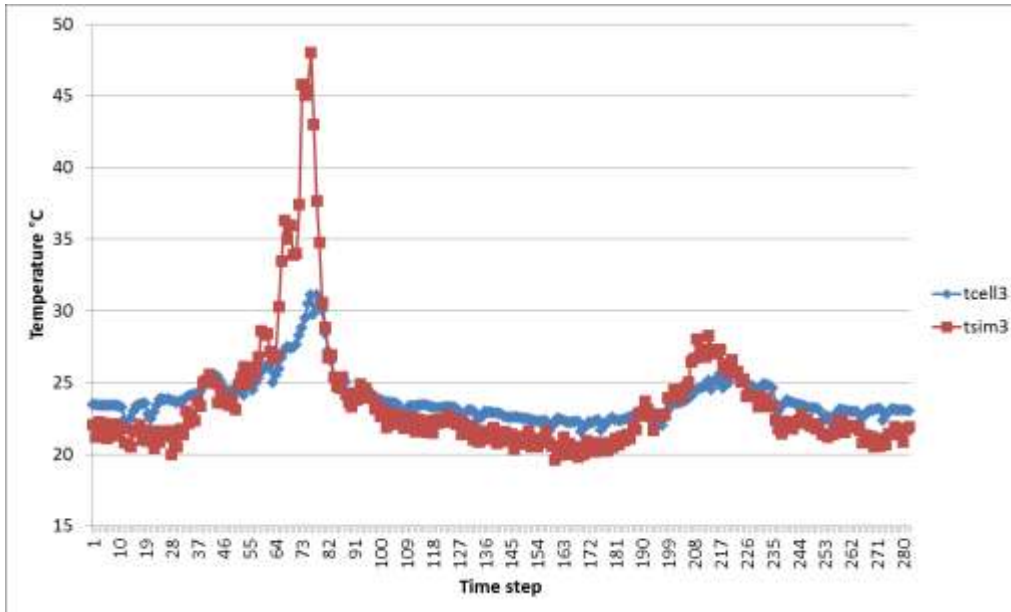
Figure A6.2: Comparison of measured and simulated temperatures of control volume 2- Canopy air, in the thermal validation test 1 (Aug 17-18)
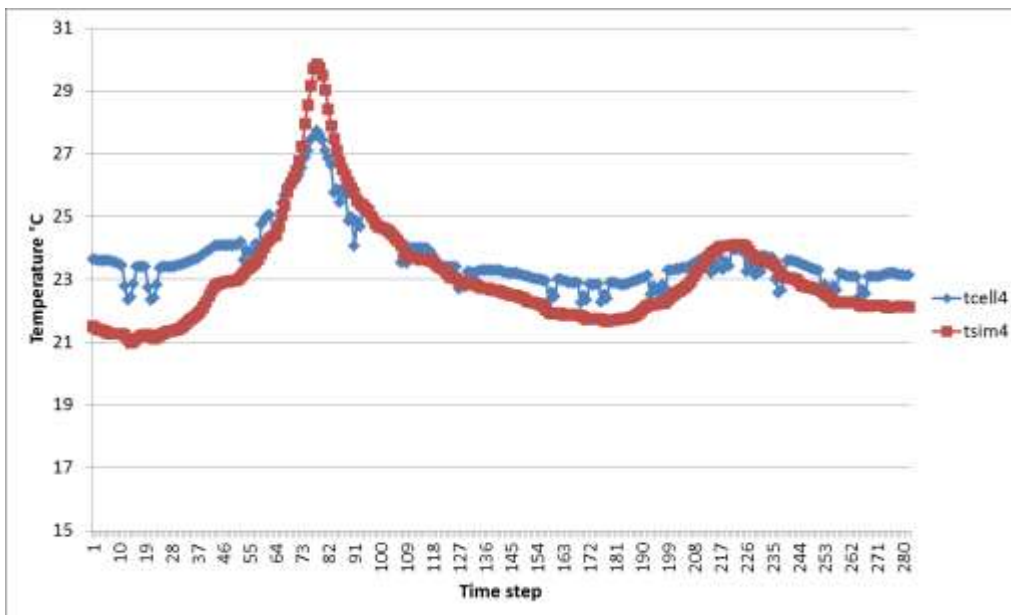

Figure A6.3: Comparison of measured and simulated temperatures of control volume 3- Soil top layer, in the thermal validation test 1 (Aug 17-18)
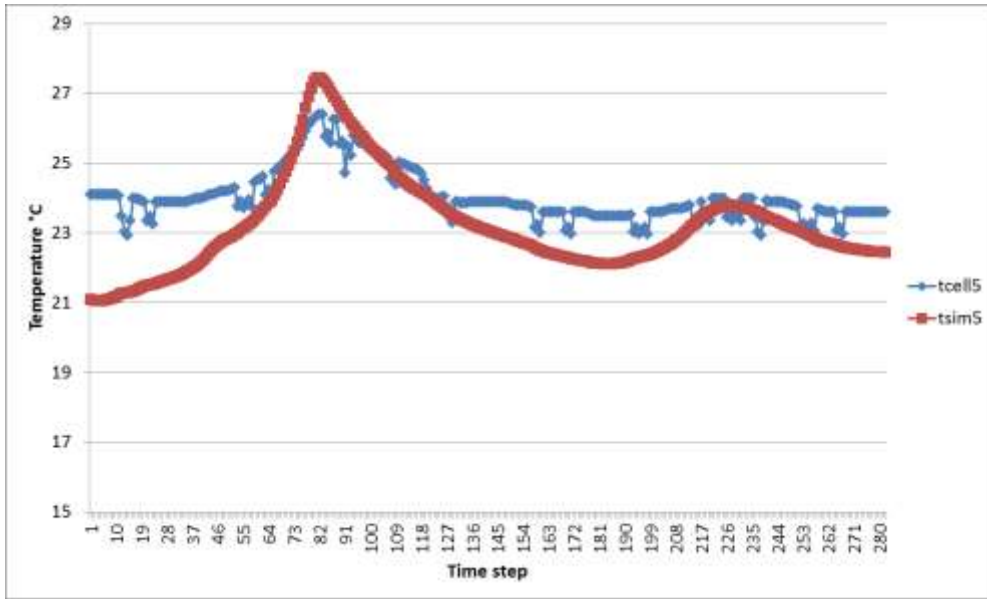
Figure A6.4: Comparison of measured and simulated temperatures of control volume 4- Soil layer 2, in the thermal validation test 1 (Aug 17-18)
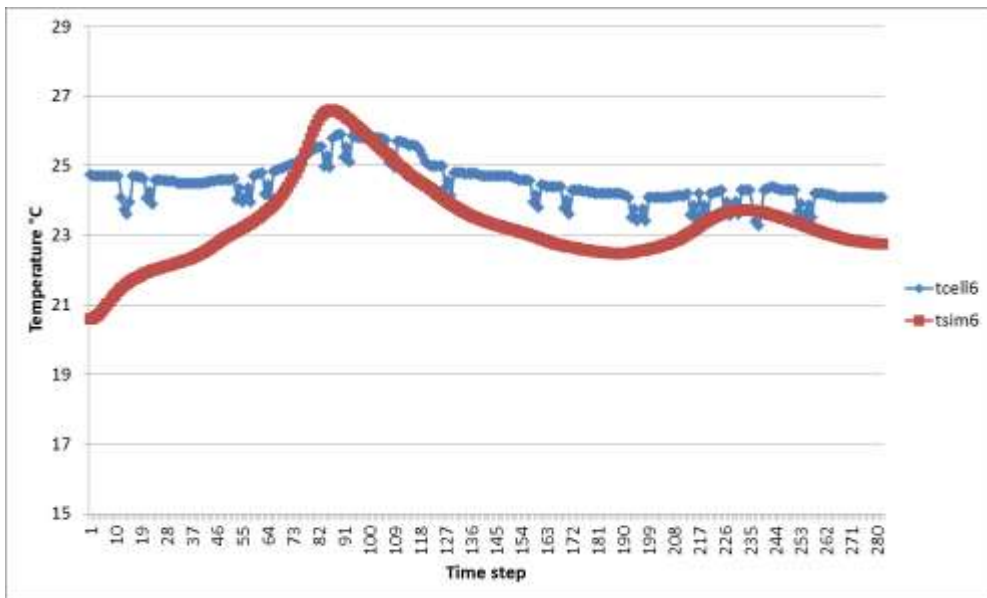

Figure A6.5: Comparison of measured and simulated temperatures of control volume 5- Soil layer 3, in the thermal validation test 1 (Aug 17-18)
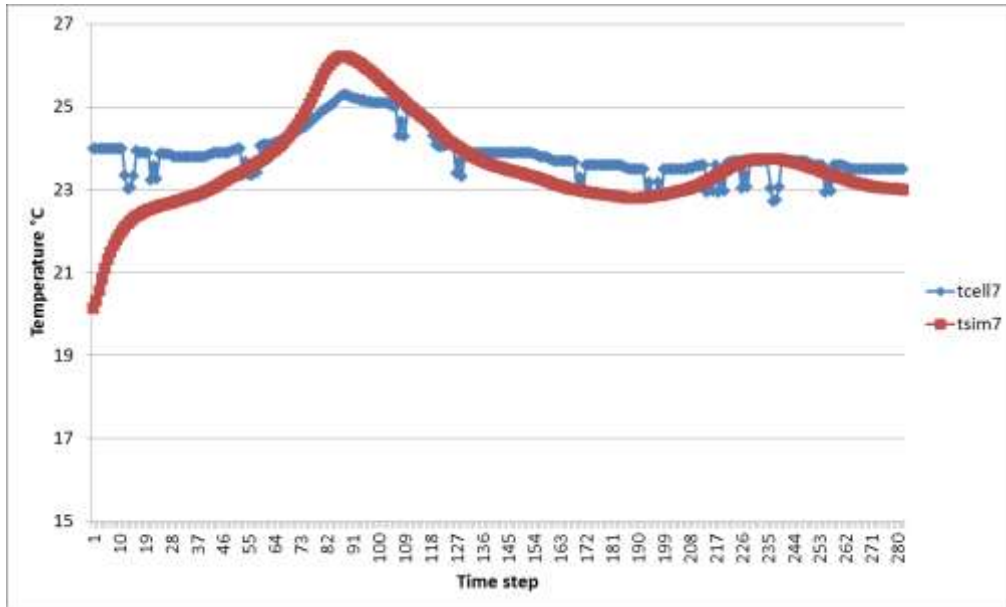
Figure A6.6: Comparison of measured and simulated temperatures of control volume 6- Soil layer 4, in the thermal validation test 1 (Aug 17-18)
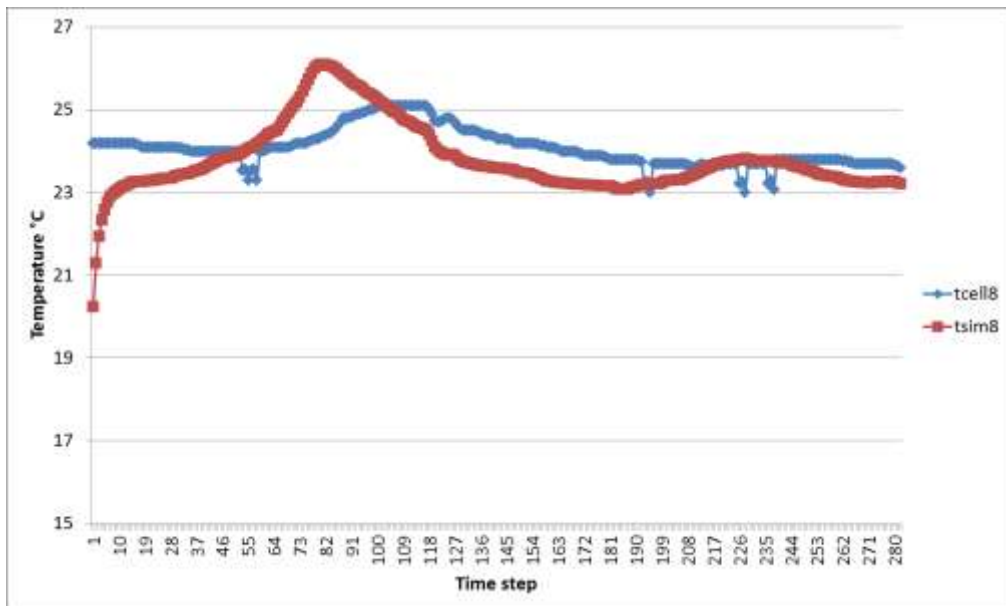

Figure A6.7: Comparison of measured and simulated temperatures of control volume 7- Soil bottom layer, in the thermal validation test 1 (Aug 17-18)

243